

Alma Mater Studiorum – Università di Bologna

DOTTORATO DI RICERCA  
Biologia e Fisiologia Cellulare

Ciclo XXI

**Settori scientifico disciplinari di afferenza:** BIO10, MED03

Molecular bases, pathogenic mechanisms and possible therapeutic  
approach in Leber's Hereditary Optic Neuropathy

**Presentata da:** Luisa Iommarini

**Coordinatore Dottorato**

**Prof.ssa Michela Rugolo**

**Relatore**

**Prof.ssa Michela Rugolo**

**Correlatore**

**Dott. Valerio Carelli**

**Esame finale anno 2008**

## Summary

<b>Introduction</b> .....	1
Mitochondria: life and death of a cell .....	2
Morphology and dynamics .....	2
The respiratory chain .....	4
Complex I structure, function and assembly .....	6
Reactive oxygen species production.....	8
Apoptosis .....	9
Mitochondrial genetics .....	17
Mitochondrial DNA variability .....	19
Mitochondrial replication, transcription and translation .....	20
Mitochondrial-nucleus communications: mitochondrial biogenesis.....	22
Mitochondrial disorders .....	33
Disorders of the mitochondrial respiratory chain .....	33
Leber's Hereditary Optic Neuropathy .....	40
Clinical features.....	40
Histopathology.....	41
Genetics .....	43
Biochemistry.....	45
Therapy and experimental treatments.....	47
<b>Aims</b> .....	49
<b>Materials and methods</b> .....	53
<b>Results</b> .....	64
1. Role of mtDNA variants in LHON: pathogenic mutations and synergistic polymorphisms ...	65
Conservation analysis and structural models of Complex I subunits.....	65
Prediction of pathogenic potential of amino acid substitutions .....	79
Identification of rare and putative new LHON pathogenic mutations .....	82
Role of mtDNA polymorphism in LHON plus myoclonus .....	92
2. Modifying factors in LHON: the role of mitochondrial biogenesis in variable penetrance.....	97
Molecular characterization of LHON mutations.....	97
Determination of mtDNA content in LHON individuals.....	98
Study of G1444A polymorphism in PGC-1 $\alpha$ gene .....	102
Gene expression assays for mitochondrial biogenesis regulators .....	104

---

3. Possible therapies for LHON: attempting to induce mitochondrial biogenesis .....	107
Cell viability and energetic competence of LHON cybrids .....	107
Titration of bezafibrate on LHON cybrids .....	110
Effect of bezafibrate on cybrids cell lines .....	111
<b>Discussion</b> .....	116
LHON pathogenic mutations are located in defined and conserved domains of mitochondrial encoded complex I subunits .....	117
Confirmation LHON rare mutations .....	121
Novel putative pathogenic LHON mutations.....	124
Rare mtDNA variants are associated to LHON plus myoclonus .....	126
Increase of mtDNA content as a compensatory mechanism in LHON.....	128
Bezafibrate does not improve the complex I impairment in LHON cybrids .....	131
<b>Conclusions</b> .....	133
<b>References</b> .....	136
<b>Appendix A</b> .....	160
<b>Appendix B</b> .....	163
<b>Appendix C</b> .....	167
<b>Appendix D</b> .....	169
<b>Candidate's publications 2005-2009</b> .....	174
<b>Acknowledgements</b> .....	175

# **Introduction**

## Mitochondria: life and death of a cell

In eukaryotes, many energetic functions, such as cellular respiration and energy production, take place in double membrane cytoplasmic organelles, containing their own genome, the mitochondria. These organelles are the main players in many cellular processes, not only the energy production, but also thermogenesis, apoptosis, reactive species of oxygen (ROS) production and calcium homeostasis. In the last 20 years several neurodegenerative diseases, aging and cancer have been associated with mitochondrial impairment and mitochondrial DNA (mtDNA) mutations.<sup>1,2</sup>

The origin of mitochondria is explained by the endo-symbiont theory, which proposes that these organelles originated from aerobic bacteria, incorporated into an oxidative proto-eukaryote host cell and maintained during evolution.<sup>3</sup>

### Morphology and dynamics

Mitochondria are delimited by two membranes, the outer mitochondrial membrane (OMM), very permeable, and the strictly selective inner mitochondrial membrane (IMM), characterized by the presence of *cristae*. These 'mitochondrial units' have a major axis of 2–5  $\mu\text{m}$ , as observed in classical electron microscopy images of isolated mitochondria. In the cytosol of a living cell, these organelles display an elongated, tubular morphology.<sup>4</sup> Mitochondria can be considered dynamic organelles in two ways: their shape is continuously remodelled by cycles of fission and fusion events and they must be strategically distributed to meet cellular needs and signals from outside.<sup>5</sup>

The fission/fusion process is regulated to respond to specific cellular needs, such as the transport of mitochondria at specific subcellular sites or the equal mitochondrial distribution between the two daughter cells during mitosis.<sup>6</sup> Moreover mitochondrial morphology changes drastically during the early steps of apoptosis (fragmentation of the reticulum and remodelling of the *cristae*) and this process is required to insure the release of apoptogenic factors and the progression of the apoptotic cascade.<sup>7</sup>

The proteins involved in the fission/fusion process are usually large GTPases belonging to the dynamin I family (Fig. 1B-C) and in mammals are known:

- Mitofusins (Mfn) 1 and 2 (fusion) are located in the OMM and are orthologs of Fzo1p (*S. cerevisiae*), which contains an NH<sub>2</sub>-terminal GTPase domain, two transmembrane domains, and two regions necessary for protein-protein interactions.<sup>8-11</sup> Mfn 1 and 2 are not redundant and are required for a proper development. Many mutations in Mfn2 have been associated with Charcot-Marie-Tooth type 2A (CMT2A) syndrome and some with HMSN6 (axonal CMT and optic atrophy).<sup>12-14</sup>
- Opa1(fusion) is an IMM protein and is mutated in Dominant Optic Atrophy (DOA), the most common inherited optic nerve atrophy.<sup>15,16</sup> Opa1 is the ortholog of Mgm1p (*S. cerevisiae*) and exists in 8 different isoforms variably expressed in all tissues, with the highest levels in retina, brain, testis, heart, and muscle. Opa1 probably has also a function in mtDNA maintenance.<sup>17,18</sup>
- Drp-1, hFis1 and endophilin B1(fission) are necessary for the control of mitochondria division.<sup>19-22</sup>

Although several components of mitochondrial morphology and dynamics have been identified, the knowledge of the mechanisms and the regulation of fusion and fission is still not completely clear.

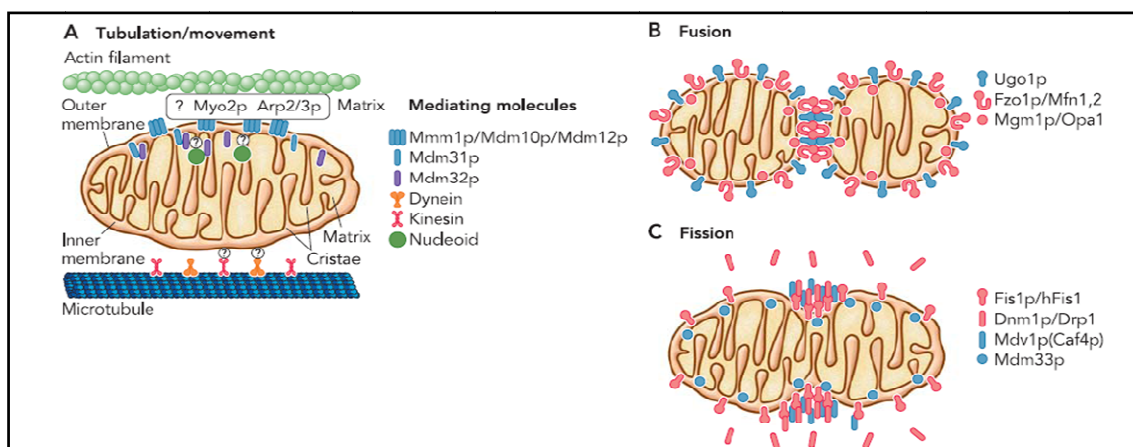


**Fig. 1** Mitochondrial dynamics, proteins involved in movement (A) and fission/fusion (B-C) mechanisms. From Dimmer KS and Scorrano L. *Physiol.* (2006) 21:233-241.

Mitochondria are travelling powerhouses that need to be located within the cytoplasm according to the local metabolic needs of the cell. Mitochondrial movements within neuronal axons occur as a bi-directional, antero-retrograde flux, traveling with the so-called “fast component” of axonal transport.<sup>23,24</sup> The mitochondrial distribution within the cytoplasm depends on their interaction with the cytoskeleton, in particular with the microtubules (MT) and the motor proteins. Thus, MT-based motility is supported by kinesin for anterograde transport, and by dynein for retrograde transport. Mitochondria can also use actin microfilaments, most likely representing an auxiliary system involved in local transport.<sup>25</sup> Both kinesin and dynein are associated with an ATPase activity that is activated by microtubule binding and so, mitochondrial axonal transport is an ATP-dependent process.<sup>26,27</sup>

### **The respiratory chain**

Mitochondrial respiration is driven by a chain of sequentially organized redox reactions fed by reducing equivalents derived from the oxidative degradation of carbon substrates. Embedded in the lipid bilayer of the IMM, the oxidative phosphorylation (OXPHOS) system is the final biochemical pathway in energy production of the cell. The respiratory chain consists of five multimeric enzyme complexes (I-V) together with two mobile electron carriers, ubiquinone (CoQ) and cytochrome *c* (cyt *c*) (Fig. 2).

Complex I (NADH:ubiquinone oxidoreductase), the first site of the respiratory chain, transfers electrons from nicotinamide adenine dinucleotide (NADH) to CoQ, generating ubiquinol (CoQH<sub>2</sub>), which then shuttles two electrons to complex III (ubiquinol:ferricytochrome *c* oxidoreductase, cytochrome *bc<sub>1</sub>* complex).<sup>28</sup> Complex I is composed approximately of 45 subunits, 7 mtDNA-encoded.<sup>29</sup> Ubiquinol is also produced by complex II (succinate:ubiquinone oxidoreductase), which, in a pathway parallel to that of complex I, transfers electrons from flavin adenine dinucleotide (FADH<sub>2</sub>) to CoQ. Complex II is the only respiratory enzyme completely encoded by nDNA (4 subunits).<sup>30</sup> A third, further source that transfers electrons to CoQ to generate ubiquinol is glycerol 3-phosphate dehydrogenase.

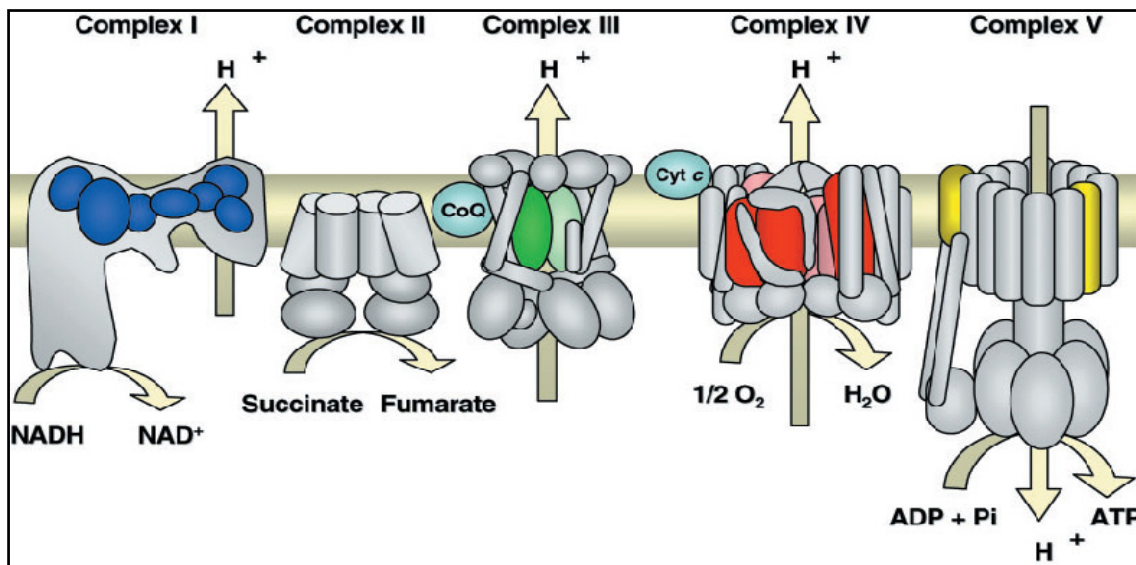


Fig. 2 Mitochondrial respiratory chain. From Zeviani M, Di Donato S. *Brain* (2004) 127:2153-2171.

Complex III has only one mtDNA-encoded subunit, cytochrome *b*; the other 10 subunits are nDNA-encoded, and at least one nDNA-encoded protein has been reported to be essential for the enzyme assembly.<sup>31,32</sup> Complex III, the middle segment of the respiratory chain, transfers two electrons from CoQH<sub>2</sub> to *cyt c*, which in turn shuttles the electrons to complex IV (ferricytochrome: oxygen oxidoreductase, cytochrome *c* oxidase). Complex IV, the terminal component of the respiratory chain, transfers electrons to molecular oxygen, the final acceptor, producing water. The three largest subunits out of the 13 that make up complex IV are encoded by mtDNA, but at least five nDNA-encoded genes have been identified as essential to the enzyme assembly.<sup>32,33</sup> All the respiratory complexes containing mtDNA-encoded subunits (complexes I, III, and IV) couple the electron transfer with the proton translocation across the inner mitochondrial membrane from the matrix side to the intermembrane space. According to the chemiosmotic theory, proposed by Mitchell,<sup>34</sup> the electrochemical gradient ( $\Delta\mu_{\text{H}}$ ) drives the reverse flow of protons back to the matrix through the membrane portion of complex V (ATP synthase, F<sub>1</sub>F<sub>o</sub>-ATPase), which then catalyzes the ATP synthesis, phosphorylating ADP to ATP. Complex V has two subunits encoded by mtDNA (ATPase6 and ATPase8), that take part to the membrane-bound portion (F<sub>o</sub>) of the enzyme, and about 13 other subunits encoded by nDNA.<sup>35</sup> The ATP synthesized in the mitochondrial matrix is transported across the inner mitochondrial membrane with an

exchange mechanism, importing cytosolic ADP by the adenine nucleotide translocator (ANT).

### **Complex I structure, function and assembly**

Complex I, the largest of the five OXPHOS complexes, binds and oxidizes NADH to free electrons via a non-covalently bound flavine mononucleotide (FMN). Then the electrons are transferred via a cascade of up to nine iron–sulfur clusters to electron acceptor ubiquinone and then through the OXPHOS system to reduce molecular oxygen at complex IV. Enzymes from different organisms have different numbers of iron–sulphur clusters, most of which share the same midpoint potential and are called “isopotential” clusters. The energy released during this process is used to drive proton translocation across the IMM. The redox reaction of complex I can be summarized in the following scheme:<sup>36,37</sup>



The way in which the electron transfer is coupled to proton translocation is still debated: it could be directly coupled via close proximity of the ubiquinone binding site to proton translocation, or indirectly via conformational changes of the enzyme. This latter hypothesis is supported by recent data obtained for bacterial and *Y. lipolytica* enzymes.<sup>38</sup>

Complex I is L-shaped, consisting of two arms: a hydrophobic membrane region which resides in the IMM and a hydrophilic peripheral or matrix region which protrudes into the mitochondrial matrix (Fig. 3).<sup>39-41</sup> Recently the crystal structure of the peripheral arm of *T. thermophilus* complex I elucidated the exact arrangement of the iron–sulfur clusters within the complex,<sup>42,43</sup> but the structure of the transmembrane arm is still unknown.

Three functional modules can be distinguished for human complex I:

1. the dehydrogenase module, which is responsible for the oxidation of NADH and consists of at least the NDUFV2, NDUFV1 and NDUFS1 subunits
2. the hydrogenase module, which guides the released electrons to ubiquinone and consists of at least the NDUFS2, NDUFS3, NDUFS7 and NDUFS8 subunits

3. the proton translocation or transporter module, which consists of at least the ND1, ND2, ND3, ND4, ND4L, ND5 and ND6 subunits.<sup>38</sup>

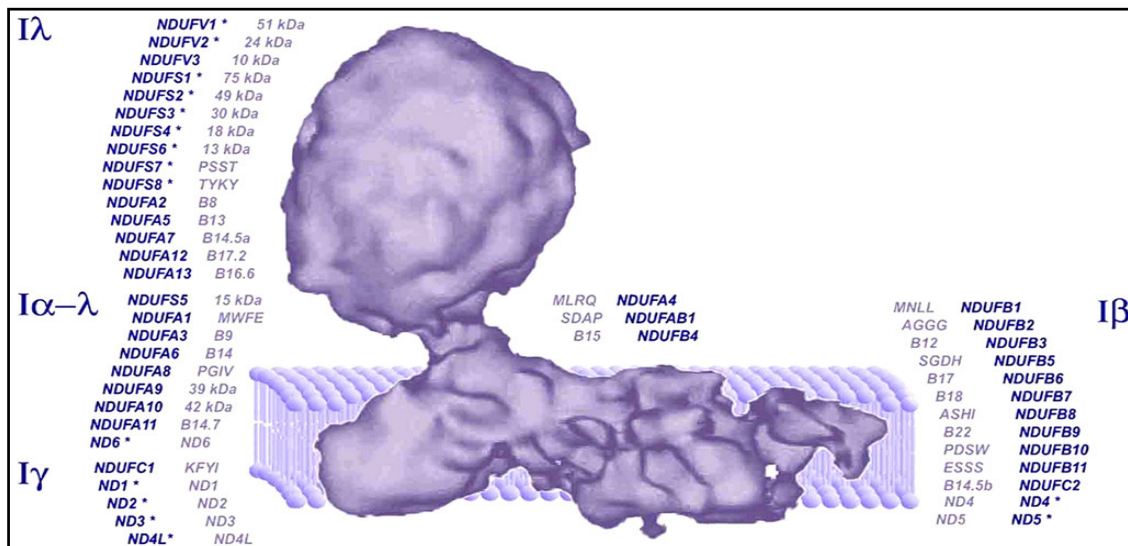


**Fig. 3** Complex I structure and protein composition. From Vogel RO et al. *Biochim Biophys Acta.* (2007) 1767:1215-1227.

The “minimal” functioning structure is considered the bacterial complex I, composed by the 14 most conserved subunits, also known as core subunits. Several phylogenetic studies have revealed a high degree of conservation of certain modules in different organisms and have led to models describing the modular evolution of complex I.<sup>38,44</sup> These models proposed that complex I is originated from an ancestral soluble nickel-iron hydrogenase (sharing homology with the NDUFS2 and NDUFS7 subunits). This hydrogenase has gained a quinone binding site and has become membrane bound upon acquisition of a protein of unknown function (NDUFS3), a ferredoxin-type (NDUFS8), ion translocating (ND5) and quinone-binding (ND1) subunits. This structure was subsequently expanded by triplication of ion translocating subunits (ND2 and ND4). Then the complex has lost its nickel-iron active site and its ability to react with molecular hydrogen, finally, membrane subunits (ND3, ND4L and ND6) and the NADH dehydrogenase module (NDUFS1, NDUFV1 and NDUFV2) are acquired.<sup>38</sup> Several subunits are necessary for a correct assembly of complex I: all the mitochondrial proteins, with the only exceptions of ND3 and ND4L, if mutated lead to many different species of subcomplexes. Moreover, mutations in many nuclear subunits, such as

NDUFA1, NDUFA6, NDUFA9, NDUFS1, NDUFS3, NDUFS4, NDUFS8 and NDUFV1, generate an incomplete assembly of complex I.<sup>38</sup>

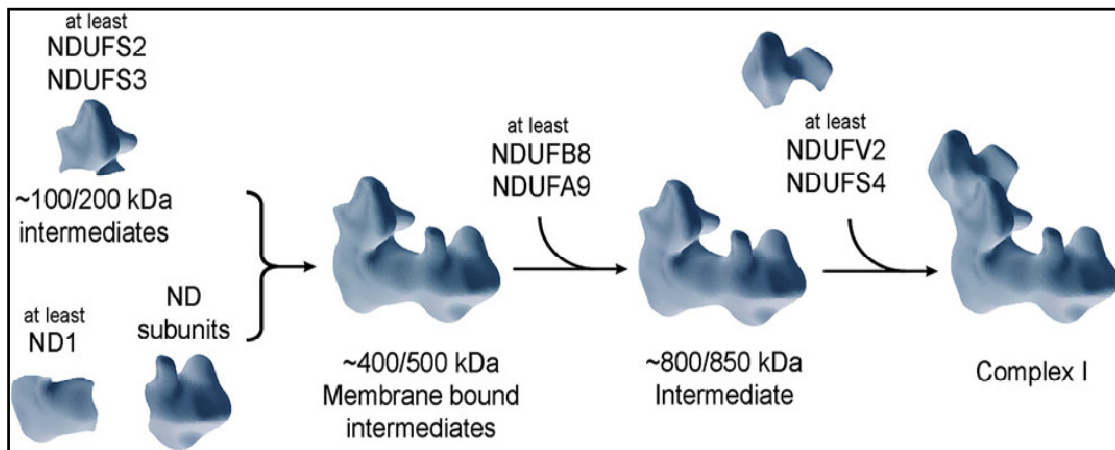


**Fig. 4** General model proposed for complex I assembly in human. From Vogel RO et al. *Biochim Biophys Acta*. (2007) 1767:1215-1227.

Four different models were proposed for the assembly mechanism in human.<sup>45-48</sup> These models agree in that 100/200kDa intermediate, containing at least NDUFS2 and NDU4S3, is anchored to the membrane by at least ND1 prior to addition of remaining membrane, hydrogenase and NADH dehydrogenase subunits (Fig. 4). This first stage is followed by the assembly of a 400/500 kDa membrane bound intermediate, probably containing NDUFS1, NDUFS7, NDUFS8, ND2, ND3 and ND6. Subsequently an 800/850 kDa intermediate is generated, most likely due to the addition of NDUFB8, NDUFA9, NDUFV1, NDUFV3 and NDUFS6. Finally the addition of at least NDUFV2 and NDUFS4 leads to a fully assembled complex I.<sup>38</sup> This extremely complex process probably regulated and coordinated by different chaperone proteins; some of them are recently identified, such as B17.2L and AIF.<sup>49-51</sup>

### Reactive Oxygen Species (ROS) production

The mitochondrial respiratory chain is also the principal cellular source of ROS. ROS are generated by loose electrons spilling from complex I and III, and reacting with molecular oxygen to form the superoxide anion ( $O_2^{\cdot-}$ ). The  $O_2^{\cdot-}$  is rapidly converted into hydrogen peroxide ( $H_2O_2$ ) by manganese superoxide dismutase (MnSOD, SOD2);  $H_2O_2$

is further metabolized by glutathione peroxidase (GPx) into H<sub>2</sub>O. Alternatively, H<sub>2</sub>O<sub>2</sub> may also generate the hydroxyl radical (OH<sup>•</sup>) in the presence of transition metals through the Fenton reaction. Furthermore, O<sub>2</sub><sup>•-</sup> may react directly with nitric oxide (NO<sup>•</sup>) to produce peroxynitrite (ONOO<sup>•</sup>). Compared to O<sub>2</sub><sup>•-</sup>, H<sub>2</sub>O<sub>2</sub> is much more stable and can diffuse through biological membranes, giving it the potential to act as a long-range signaling molecule.<sup>52-54</sup> A recent work has shown that ROS can be used by the cell as regulated and specific second messengers to propagate signals in multiple settings.<sup>55</sup>

Being the major generator of ROS, mitochondria could also be the principal target of ROS damage, which could affect DNA, proteins and/or lipids.

Oxidative damage to DNA causes modification of the bases, the deoxyribose backbone, single and double strand breaks, as well as cross-links to other molecules. DNA modifications are potentially mutagenic, contributing to cancer, premature ageing and neurodegenerative diseases.<sup>56</sup> Moreover mtDNA is especially susceptible to attack by ROS due to the close proximity to the respiratory chain and the lack of protective histones; the level of modified bases in mtDNA is 10- to 20-fold higher than that in nuclear DNA. In this way, ROS induced oxidative damage is probably a major source of mitochondrial genomic instability leading to respiratory dysfunction and this instability is thought to be one of the most important factors in ageing.<sup>57</sup>

Excessive ROS production may cause local damage to the Fe-S clusters of respiratory enzymes (complexes I, II and III), as well as to tricarboxylic acid cycle enzymes (aconitase).<sup>58,59</sup> Moreover, peroxynitrite can nitrate tyrosine residues or thiolic groups of nearby proteins and both complex I and MnSOD have been reported to be damaged by this process.<sup>60-63</sup> Oxidized proteins are recognized by proteases and degraded.

Lastly, another important damaging process is lipid peroxidation; this affects vital mitochondrial functions, such as respiration and oxidative phosphorylation, inner membrane barrier properties, maintenance of mitochondrial membrane potential ( $\Delta\Psi_m$ ), and mitochondrial Ca<sup>2+</sup> buffering capacity.<sup>64-66</sup>

## **Apoptosis**

Apoptosis is a major pathway of programmed cell death (PCD) and is extremely important in several physiological conditions, such as embryonic development, tissue generation and the immune system development. This process is involved also in many

pathological events, included neurodegenerative, cardiovascular and immunological disorders.<sup>67</sup> Apoptosis is characterized by a cascade of controlled events that leads to specific morphological changes in the cell: loss of adhesion, cell shrinkage, plasmatic membrane blebbing, chromatin condensation, DNA fragmentation, proteolytic cut of specific substrates and exposure of phosphatidylserine on the external surface of the cell.<sup>68-70</sup> The final event of this cascade is the phagocytosis of the apoptotic cell, without any release of cytoplasmic content into the extracellular matrix or inflammatory response induction.

Apart the granzyme B pathway, there are other two apoptotic cascades: the “extrinsic” or death receptor pathway, and the “intrinsic” or mitochondrial pathway (Fig. 5). The extrinsic pathway is activated by the binding of ligands to a specific death receptor, such as Fas, TNF or TRAIL receptors. This step is followed by the receptor oligomerization, which induce the recruitment of adaptor proteins and upstream procaspases. The proteolytic cut of inactive procaspases induce their direct activation and triggers the apoptotic cascade.<sup>71</sup> The mitochondrial pathway is a complex signaling cascade, regulated by the Bcl-2 family proteins, that needs the release of apoptogenic factors from mitochondria for the caspase activation. The intrinsic pathway can be divided in three well defined phases: induction, mitochondrial and execution phases.

During the induction phase external and internal stimuli activate different signaling pathways and this signal is transduced to mitochondria by Bcl-2 family proteins. This protein family includes several proteins sharing a common feature: the presence of one or more BH (Bcl-2 homology) domains. There are four different BH domains (BH1-BH4), composed by  $\alpha$ -helices, that allow the formation of homodimers and heterodimers between different members of the family.<sup>72</sup> A subgroup of these proteins, including Bcl-2, Bcl-X<sub>L</sub>, Bcl-w, Mcl-1, has an anti-apoptotic function is characterized by the BH1-2 or the BH1-4 domains and a transmembrane domain presence. Instead, there are two subgroups with pro-apoptotic functions: the Bax type proteins (Bax, Bak and Bok) with BH1-3 and transmembrane domains and the “BH-3 only” type (Bid, Bim and Bad).

The second apoptotic step is the mitochondrial phase characterized by an alteration of the OMM and the release of apoptogenic factors to the cytosol. How this happens is still debated and actually there are at least two hypothesis to explain this phenomenon, involving two distinct channels. These channels are the permeability transition pore

PTP in the inner membrane and the mitochondrial apoptosis-induced channel MAC in the outer membrane.

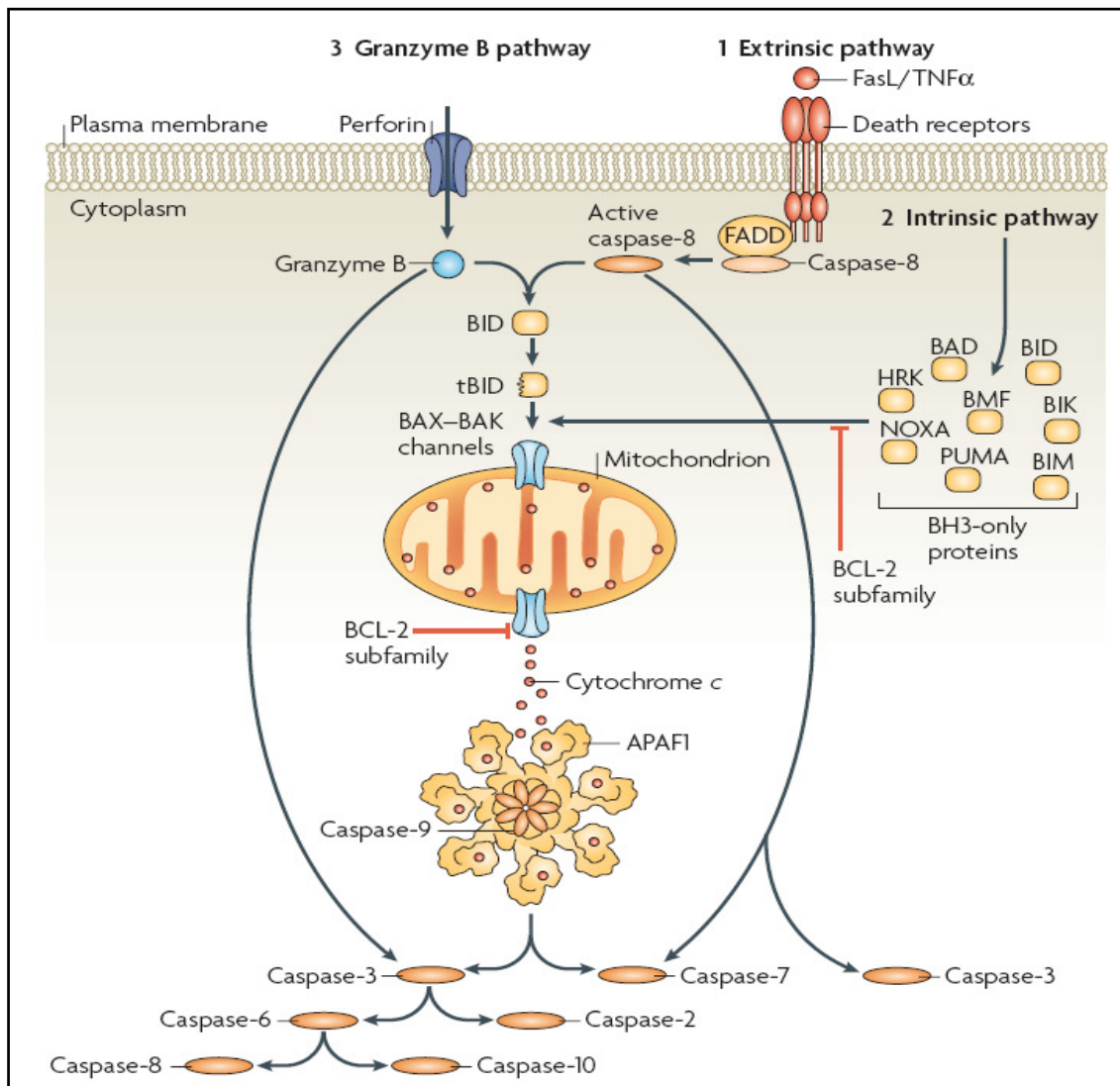


**Fig. 5** Cellular signaling pathways involved in apoptosis. From Taylor RC, Cullen SP, Martin SJ. *Nat Rev Mol Cell Biol.* 2008; 9:231-241.

The most probable model proposes that MAC is generated on the OMM thanks to the direct pore forming properties of some pro-apoptotic Bcl-2 proteins. Bax, a monomeric soluble cytosolic factor, oligomerizes, translocates, and inserts in the OMM upon induction of apoptosis.<sup>73,74</sup> Together with Bak, Bax is supposed to form tetrameric channels regulated by BH3-only proteins, such as Bid. These proteins induce the conformational change of Bax and regulates the MAC formation, functioning as sensors

for cellular integrity and activity, cytoskeleton integrity, growth factor presence, and death domain receptor signaling.<sup>75</sup> Anyway, the exact molecular composition of MAC and its regulation are still not completely explained.

The second model propose the opening of the PTP, an unselective and high conductive channel, in the IMM in response to apoptotic stimuli. This event induces an alteration of the IMM permeability, causing a depolarization of the IMM, a matrix swelling and OMM break.<sup>76</sup> Recent studies demonstrates that the first step of mitochondrial permeabilization could be the transient opening of MAC, and that PTP has a role in the amplification of the apoptotic signaling. Whatever is the mechanism of the mitochondrial permeabilization, the final result is the release of apoptogenic factors (cytochrome *c*, AIF, endonuclease G, Smac/DIABLO and Omi/HtrA2). (Fig. 6)

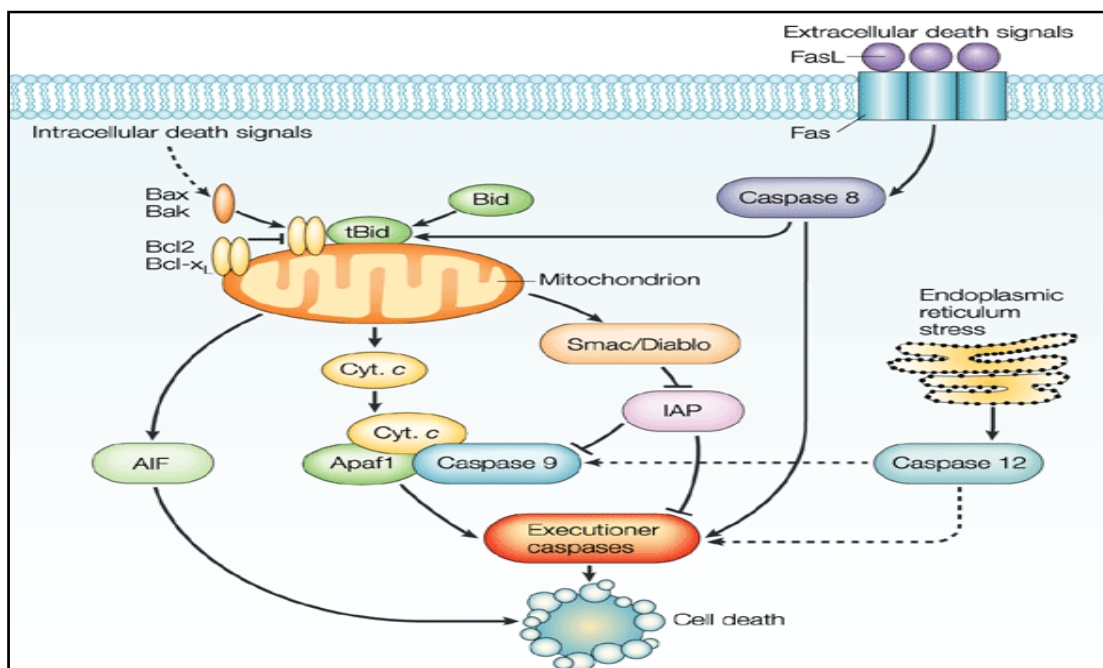


**Fig. 6** Apoptogenic factors released from mitochondria during apoptosis. From Vila M, Przedborski S. Nat Rev Neurosci. 2003; 4:365-375.

The most important and well known apoptotic factor is *cytochrome c* (12.3 kDa) that is able to trigger the assembly of the apoptosome. The apoptosome is a complex composed of *cyt c*, Apaf-1, and dATP. *Cyt c* binds Apaf-1 at WD-40 repeats domain in the presence of ATP, and allows the conformational change of Apaf-1 from a closed monomeric configuration to a platform for procaspase-9 assembly (Fig. 7). Procaspase-

9 binds Apaf-1 at a conserved amino acid sequence called the caspase recruitment domain or CARD, leading to the activation of procaspase-9.<sup>77</sup>

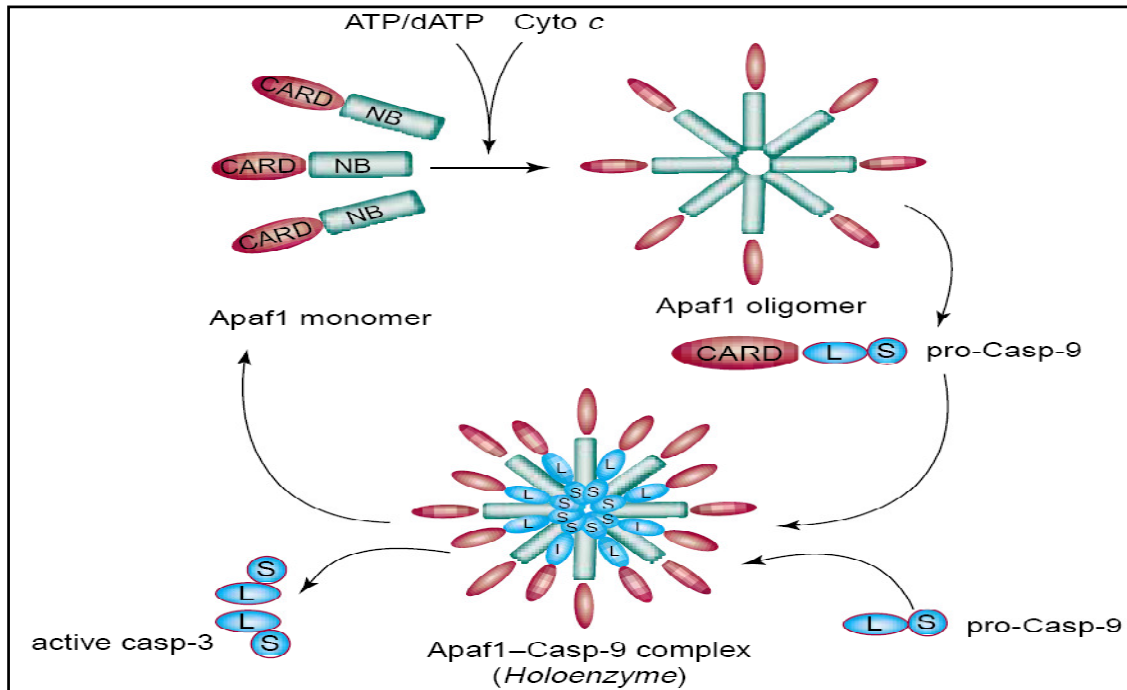


**Fig. 7** Apoptosome assembly and caspase-9 activation. From Reed JC. Trends Mol Med. 2001; 7:314-319.

AIF (Apoptosis Inducing Factor, 57 kDa) is a flavoprotein confined to the mitochondria in normal conditions but able to translocate to the nucleus in response to apoptogenic stimuli.<sup>76</sup> The exact function of AIF under normal physiological conditions is still not clear, but it has been reported to be an important part of the antioxidant machinery. Overexpression of AIF induces chromatin condensation, dissipation of the mitochondrial transmembrane potential, exposure of phosphatidylserine on the plasma membrane, and high molecular weight (50 kbp) DNA fragmentation.<sup>78</sup> The molecular mechanism of AIF functioning in apoptosis is also unknown. It has no intrinsic nuclease activity and its oxidoreductase activity is not required for its apoptogenic function. Probably AIF acts together with endonuclease G in a caspase-independent apoptotic mechanism.<sup>79,80</sup>

Endonuclease G (endoG, 30 kDa) is a non-specific nuclease released from mitochondria in apoptotic cells. Probably this endonuclease has a role in the normal mitochondrial

nucleic acid metabolism, but this role is still unclear. During apoptosis in mammalian cells, endoG translocates to the nucleus and digests nuclear DNA in the absence of caspase activity or the caspase-activated deoxyribonuclease CAD/DFF. Probably endoG acts in concert with both exonucleases and DNase I in the nucleus to generate DNA cleavage products.<sup>76</sup>

Recently, a new protein, Smac/DIABLO (23 kDa) has been discovered.<sup>81,82</sup> This protein is released from the mitochondria along with *cyt c* during apoptosis and promotes caspase activation by associating with the apoptosome and by inhibiting IAPs. Smac/DIABLO relieves the inhibition on caspases by binding to the BIR domains (Baculovirus IAP Repeats) of IAPs proteins (Inhibitors of Apoptosis Proteins) and by disrupting their association with caspase-9. In this way, Smac/DIABLO allows caspase-9 to activate caspase-3, causing apoptosis.<sup>83</sup>

Omi/HtrA2 (37kDa) is a serine protease identified because of its homology to the bacterial endoprotease HtrA (high-temperature requirement). Omi/HtrA2 seems to be upregulated in conditions of cellular stress.<sup>83,84</sup> The proapoptotic feature of Omi/HtrA2 was first identified through its ability to bind and antagonize IAPs, similar to Smac/DIABLO.<sup>85,86</sup> Omi/HtrA2 is released from mitochondria during apoptosis and contributes to caspase-dependent and independent PCD.<sup>76</sup>

The last step in apoptosis is the executive phase and the major players are specific proteases called caspases (cysteine aspartyl-specific proteases) that cleaves their substrates at aspartic acid (Asp) residues.<sup>87,88</sup> This family of intracellular proteases is composed in human at least of 12 members, even if not all directly involved in apoptosis, sharing an high sequence homology and substrates specificity. (Fig. 8)

Caspases are produced as inactive zymogens with three domains: a regulatory N-term, and two highly conserved catalytic domains. They can be activated by proteolytic cleavage at conserved Asp residues and can collaborate in proteolytic cascades, where caspases activate themselves and each other, and finally cleave their substrates. Caspases are often divided in upstream 'initiator' caspases or downstream 'effector' caspases.<sup>89</sup> The upstream pro-caspases have long N-terminal pro-domains that function as protein interaction modules, by associating with proteins that trigger caspase activation. By contrast, downstream effector caspases contain short N-terminal pro-domains, and are largely dependent on upstream caspases for their proteolytic

processing and activation. Upstream pro-caspases are not completely inactive and, if brought into close apposition through protein interactions, they can trans-process each other, producing fully active proteases (induced proximity mechanism).<sup>90</sup>

Caspases have as substrates several proteins with structural and enzymatic functions (collected in caspase substrates database, <http://www.casbah.ie>) that have to be cleaved to continue the apoptotic process.<sup>91</sup>

1. the cell cytoskeleton is degraded causing rounding of cells and membrane blebbing; caspases' substrates are proteins involved in microfilaments, microtubules and intermediates filaments formation, such as actin, myosin, spectrins, gelsolin, filamin, tubulin, vimentin, keratins.
2. nuclear envelope and fragmentation is mainly due to degradations of laminins.
3. loss of adhesion is caused by dismantling of cell-matrix focal adhesion sites, cell-cell adhesion complexes and desmosomes (substrates are focal adhesion kinase FAK, p130<sup>cas</sup>, tensin, catenins and cadherins)
4. mitochondrial, Golgi and endoplasmic reticulum fragmentation is actuated in order to block any cellular function and metabolism
5. DNA condensation and fragmentation is necessary to prevent any replication or transcription, to block the immune response and any kind of possible rescue mediated by new protein synthesis. The fragmentation process is mainly due to activation of CAD endonuclease, through degradation of its inhibitor ICAD, while the condensation mechanism is mediated by degradation of MST1 kinase (mammalian sterile-20), that prevent the histon H2B phosphorylation.

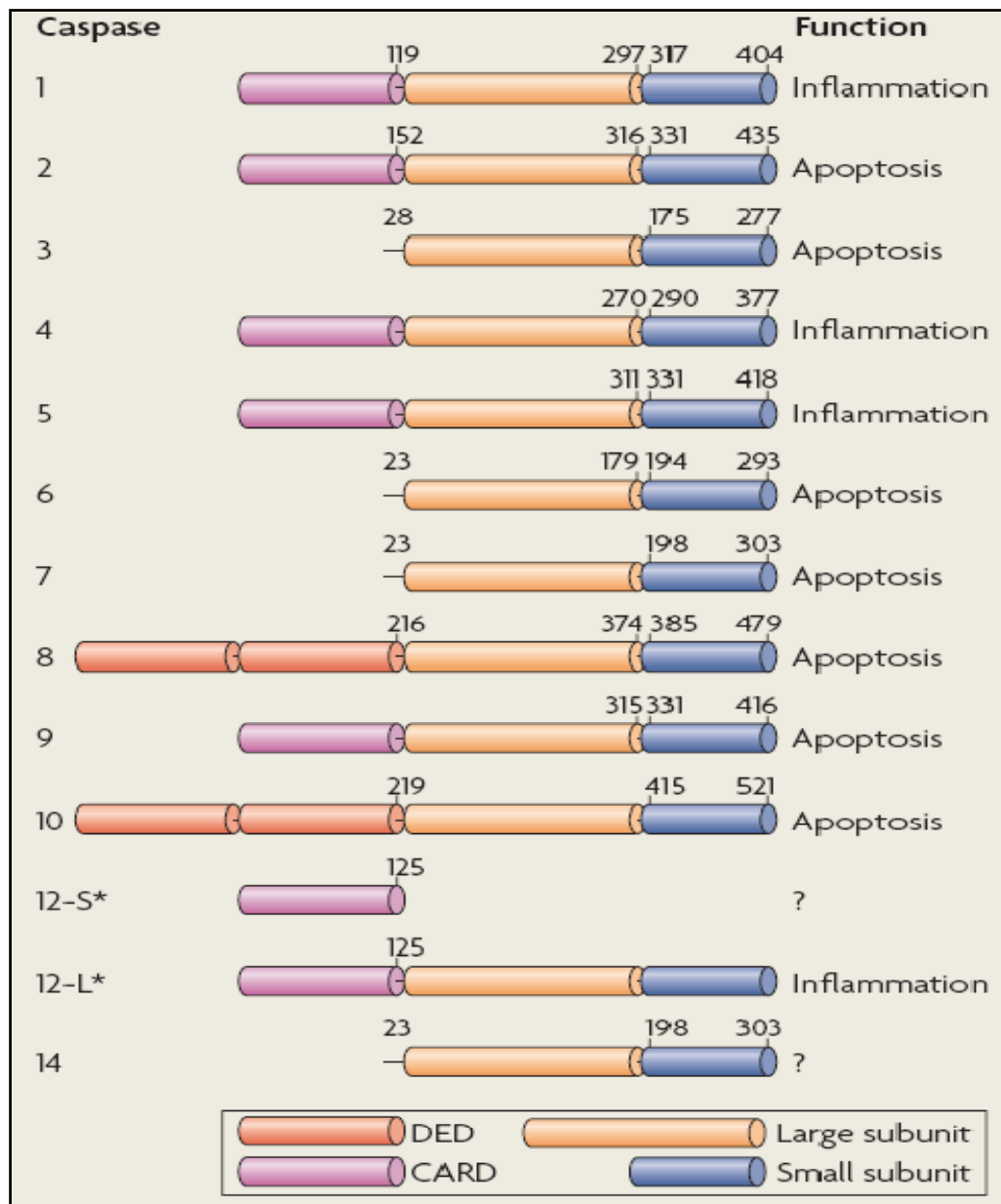


**Fig. 8** Mammalian caspases: function and structure. From Taylor RC, Cullen SP, Martin SJ. *Nat Rev Mol Cell Biol.* 2008; 9:231-241.

### **Mitochondrial genetics**

Human mtDNA is a double-stranded, circular molecule of 16569bp, completely decoded,<sup>92</sup> containing 37 genes: 13 genes encoding for subunits of the respiratory chain and 22 tRNA and 2 rRNA necessary for translation of these proteins (Fig. 9). Based on their nucleotide composition, the two strands are distinct in heavy (H), rich in guanine, and light (L), rich in cytosine.

The mammalian mtDNA shows a high level of economy, in terms of sequence organization. In fact, there are essentially no repetitive sequence families, introns or intergenic regions. Some respiratory protein genes overlap, and protein coding and rRNA genes are interspersed with tRNA genes, that represent the signal for cleavage sites of RNA processing. The major non-coding region is the D-loop (displacement loop), characterized by the presence of a triple strand structure due to the association of the new H-strand in this region. The D-loop contains the origin of H-strand DNA replication and is also the site of transcription from opposing heavy and light strand promoters.<sup>93,94</sup> The second non-coding region is composed by 30 nucleotides and represent the replication origin for the L-strand. (Fig. 9)

Mitochondrial genetics follows its specific rules and differs from mendelian genetics at least in three main aspects:<sup>95</sup>

1. Heteroplasmy and threshold effect. A somatic mammalian cell contains 1000-10000 mtDNA copies; if all mtDNA molecules are identical (*wild type* or mutant), this condition is called homoplasmy, whereas if different molecules coexist, this condition is known as heteroplasmy. In case of heteroplasmic pathogenic mutations, a minimal critical load of mtDNA molecules have to be mutated to exert the pathogenic effect of the mutation (threshold effect). This threshold is also dependent on the tissue energy requirement. Thus, the threshold is unsurprisingly lower in high energy demand tissues and they are more vulnerable to mtDNA mutations.
2. Maternal inheritance. Every mitochondrion and so, every mtDNA molecule, in the zygote derives from the oocyte, because after the fecundation process all mitochondria from the spermatocytes are degraded in a ubiquitin-dependent fashion.<sup>96,97</sup> Thus, mtDNA molecules and, if present, mtDNA mutations are transmitted in the progeny, along the maternal lineage. Anyway, a heteroplasmic

mutation can be transmitted with different mutation load, because during the oogenesis there is a preferential amplification of only few mtDNA molecules (bottleneck).<sup>98</sup> The bottleneck phenomenon explain the rapid shift of some heteroplasmic mutation to homoplasmy, in few generations.

3. Mitotic segregation. During the cellular division, the proportion of mutated mtDNA may vary with time, because the replication of mtDNA and nDNA are not coordinated and the distribution of mitochondria during the mitotic process is casual. Segregation of heteroplasmic mutations may occur during the cell division or during the mtDNA content of a post mitotic cell is renewed. This phenomenon explains the mosaic distribution of mutated mtDNAs and the reaching of a certain mutation load in some tissues.

These rules are complicated by the different tendency of certain mutations to be transmitted (heteroplasmic point mutation are frequently transmitted, whereas deletions are rare) and by the mutation levels in the maternal germ line.<sup>99</sup>

The distribution of mtDNA molecules in the progeny depends on a bottleneck mechanism during oogenesis. A mammalian oocyte contains many copies of mtDNA, probably derived by just a few mtDNA molecules in a precursor cell. How this mechanism is actuated and regulated is still unexplained, but it seems like its purpose is to reset the mtDNA mutation rate between generations.<sup>99</sup>

Mitochondrial DNA molecules are organized, in association with several proteins, in distinct particles, called nucleoids. These particles are dynamic structures able to divide and redistribute in the mitochondrial network and may be single units of inheritance.<sup>100</sup> Their distribution could be important for the mitotic segregation of certain genomes in heteroplasmy condition and explain why the segregation of mtDNA mutants is faster than expected, with so many mtDNA genomes per cell. The major nucleoid component is Tfam, that acts probably as a key regulator of the mtDNA copy number, but many other proteins were identified, such as mtSSB, TWINKLE, ANT1 and prohibitin.<sup>99</sup>

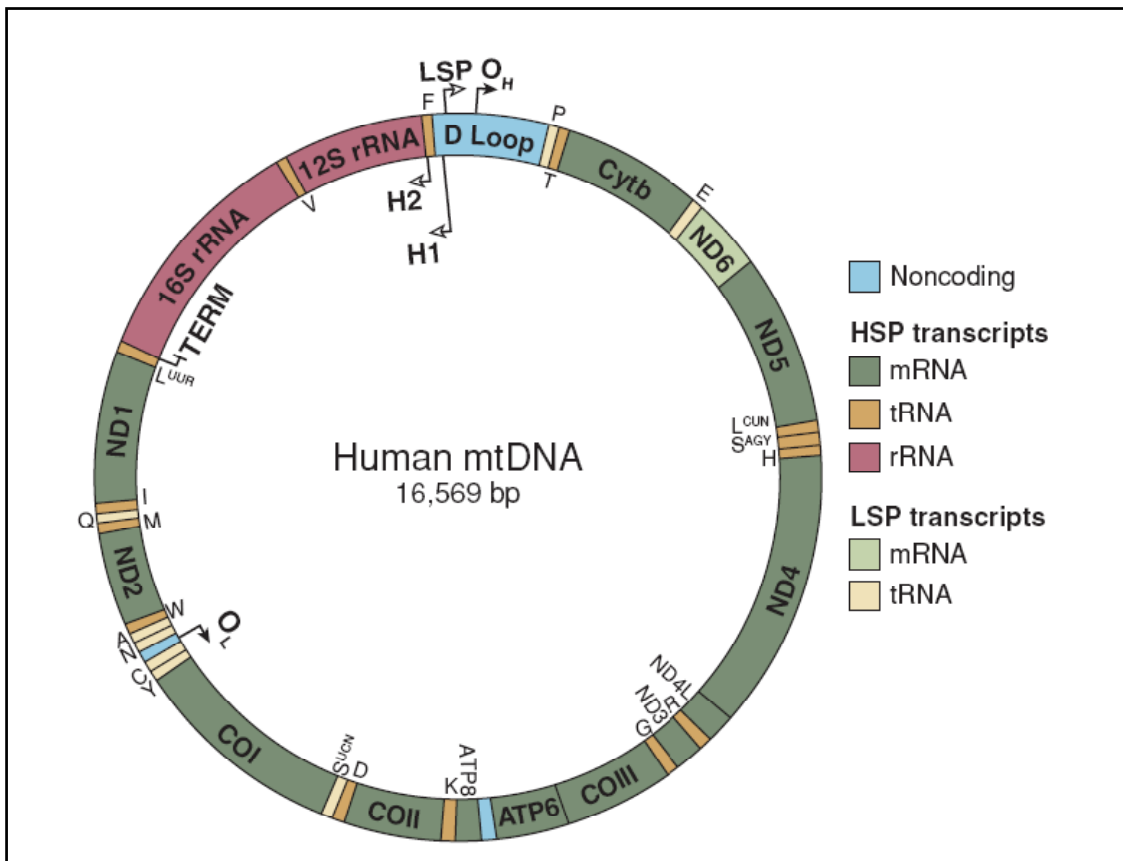


**Fig. 9** Map of human mtDNA. From Falkenberg M, Larsson NG, Gustafsson CM. *Annu Rev Biochem.* 2007; 76:679-699.

### Mitochondrial DNA variability

Due to its peculiar uniparental maternal inheritance, mtDNA has been extensively used to study population genetics by phylogenetic analysis. Moreover, mtDNA recombination in identical molecules does not influence the genetic assessment and is able to accumulate mutation at higher rate, compared to nuclear DNA.<sup>101-103</sup> Thus, a great number of mtDNA variants have been fixed and accumulated characterizing different maternal lineages. These mtDNA lineages have diverged from the first 'Eve' and colonized different geographical regions. Based on different clusters of population-specific polymorphisms, present both in coding and control regions, we can now define the mitochondrial haplogroups. Many phylogenetic studies defined the occurrence of specific haplogroups in the different continents. In Africa, haplogroup L is present in 80-100% of mtDNAs; in Asia the most representative haplogroups are A, B, F and M, divided in sub-classes C, D, E and G.<sup>102-104</sup> Asian haplogroups are also present in Native

Americans populations, whereas four European haplogroups (H, J, K and I) are the most representative in the general northern American population.<sup>105</sup>

Among Europeans, 95% of the population belongs to 1 of 10 haplogroups: H, I, J, K, M, T, U, V, W, and X.<sup>106</sup> Given the central role of mitochondria in cellular metabolism, many studies have investigated the association between mtDNA haplogroups and sub-haplogroups and multifactorial diseases and aging, based on the assumption that the many non-synonymous variants may have functional relevance.

### **Mitochondrial replication, transcription and translation**

Mitochondrial DNA replication is independent from cell cycle (the so called relaxed replication) and some mtDNA molecules are preferentially replicated while others do not replicate at all.<sup>107,108</sup>

The enzyme responsible for mtDNA replication is polymerase  $\gamma$  (POL $\gamma$ ), an RNA dependent DNA polymerase, discovered in human HeLa cells.<sup>109</sup> In human this enzyme is a heterotrimer composed by a catalytic subunit (POL $\gamma$ A, 140kDa), with polymerase, 3'-5' exonuclease, and 5'-deoxyribose phosphate lyase activities, and two smaller accessory subunits (POL $\gamma$ B, 55kDa), able to increase the catalytic activity of POL $\gamma$ A.<sup>110-113</sup> Other two proteins are necessary for mtDNA replication: the helicase TWINKLE and the mitochondrial single-stranded DNA-binding protein (mtSSB). Together with POL $\gamma$ , they form a processive replisome, able to replicate the entire mtDNA.<sup>99</sup>

The mtDNA replication mechanism is still unclear and at least two models has been proposed and currently debated. The first model proposes a strand-asymmetric and asynchronous replication, in which the primers for the H-strand (leading strand) replication are provided by the transcription mechanism.<sup>114</sup> When H-strand synthesis has reached 2/3 of the DNA molecule, it exposes the origin of L-strand DNA replication (O<sub>L</sub>), and lagging-strand DNA synthesis then initiates in the opposite direction. New complete mtDNA molecules are finally ligated.<sup>99</sup>

Another model has been more recently proposed and suggests that mtDNA replicates symmetrically, with leading and lagging strands synthesis progressing from multiple, bidirectional replication forks, in a precise initiation zone that includes *cyt b* and ND5-6 genes.<sup>115-117</sup>

Moreover, a novel major replication origin has been found at position 57 in the D-loop region, probably responsible for mtDNA maintenance under steady-state conditions. In this paper the authors suggested that the previously characterized origins may be more important for recovery after mtDNA depletion and to improve the DNA synthesis in response to certain stimuli.<sup>118</sup>

Mitochondrial transcription starts from three different transcription origins, one for the L-strand and two for the H-strand (H1 and H2), producing three polycistronic molecules.<sup>119</sup> The H1 site (nt 561) is the most frequently used and is responsible for the synthesis of the two rRNAs, tRNA<sup>Phe</sup> and tRNA<sup>Val</sup>. The second transcription unit is less frequently used than the previous one, starts at the initiation site H2 (position 646) and produces a polycistronic molecule, that is subsequently processed in 12 mRNAs and 14 tRNA.<sup>114</sup> The L-strand generates a single polycistron starting at position 407, from which 8 tRNAs and the ND6 mRNA are derived.<sup>119</sup>

The primary transcripts are processed, according to the “tRNA punctuation” model, to generate the mature RNAs after an endonucleolytic cleavage, triggered by the maturation of tRNAs secondary structure.<sup>120,121</sup> The 5'- cleavage occurs first, by a mitochondrial RNaseP, then the 3'- end is cleaved by a tRNAase Z.

The minimal machinery required for mtDNA transcription includes the RNA polymerase mtRPOL (similar to that from T7 and T3 bacteriophages), the initiation factors Tfam, TFB1M, and TFB2M and the termination factor mTERF (Fig. 10). The human mtRPOL gene encodes a protein of 1230 amino acid residues with a series of conserved motifs in the C-term (520-1230 aa).<sup>122</sup>

Tfam (10q21, 202 aa) was the first mitochondrial transcription factor identified and contains two HMG-boxes (High Mobility Group) with DNA binding activity, separated by a linker region and a basic C-terminal tail required for promoter-specific transcription.<sup>123</sup> Tfam is able to wrap, bend and unwind DNA in vitro with a low sequence specificity.<sup>124,125</sup> Moreover, Tfam is also able to bind mtDNA in a nonspecific manner, and probably is responsible for its stabilization and maintenance.<sup>125,126</sup> Interestingly, Tfam levels correlate well with mtDNA copy number, suggesting that this protein can function as a limiting determinant of mtDNA abundance.<sup>94</sup>

Two isoforms of human mt-TFB, named TFB1M and TFB2M, have been identified but the first one exhibits about 1/10 the transcriptional activity of TFB2M. Both factors

seem to interact directly with the RNA polymerase forming a heterodimer, and, in addition to TFAM, are required for the accurate initiation from H- and L-strand promoters in vitro.<sup>119</sup>

Mitochondrial encoded mRNAs are translated in the matrix with a specific translational machinery, represented by the mitoribosomes. These ribosomes are particular being composed by two mitochondrial rRNAs (12s and 16s) and nuclear encoded proteins. The genetic code of mtDNA is also slightly different. Thus, UGA in mitochondrial translation does not specify for a tryptophan amino acid, but a stop codon; moreover AUA represent an isoleucine and not a methionine and AGA/AGG are not stop codons but specify for arginine. Moreover, mitochondrial translation has a more simplified codon-anticodon recognition mechanism (22 tRNAs are sufficient to specify for all the amino acid, a single tRNA specifies for both methionine and N-formyl methionine and AUA/AUU codons are often used as a start signal).<sup>127</sup>

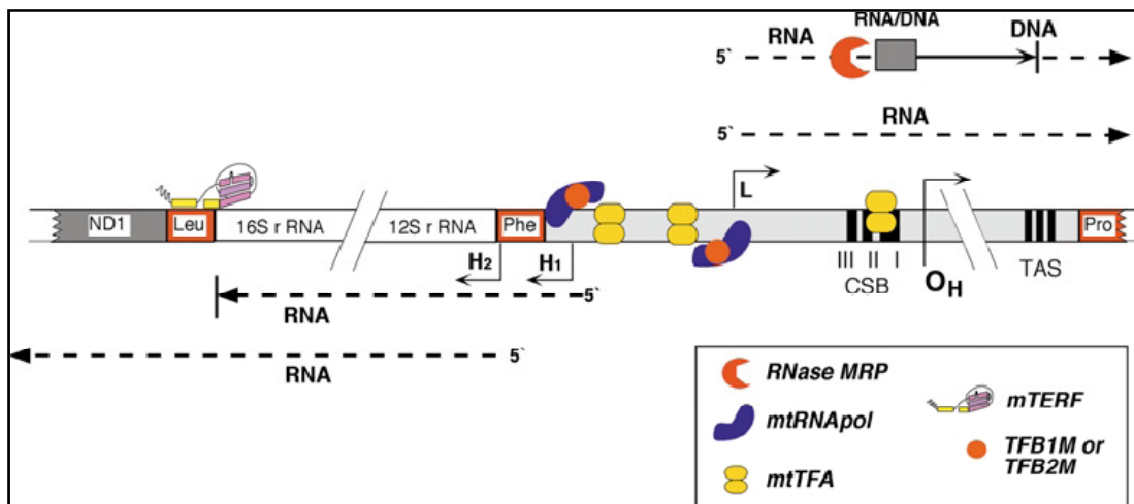


**Fig. 10** Schematic representation of the mammalian D-loop and transcription termination regions, showing the main elements and factors involved in transcription and in replication initiation. From Fernandez-Silva P, Enriquez JA, Montoya J. *Exp Physiol.* 2003; 88:41-56.

### Mitochondrial-nucleus communications: mitochondrial biogenesis

Mitochondrial biogenesis is a complex and regulated process that involves the coordinated expression of mitochondrial and nuclear genes. This process has been intensively studied in the last 20 years and it is now known that mitochondrial biogenesis is finely tuned by different signaling cascades that involve transcription

factors and coactivators that regulate the expression of genes coding for mitochondrial components.<sup>128</sup>

These include nuclear encoded mitochondrial proteins participating in OXPHOS, heme biosynthesis, mitochondrial protein import, and mtDNA transcription and replication. The most important transcription factors activating promoters of mitochondrial genes are Tfam, NRF-1, NRF-2 and ERR $\alpha$  (estrogen related receptor), together with transcriptional coactivators belonging to the peroxisome proliferator-activated receptor  $\gamma$ -coactivator-1 (PGC-1) family (Fig. 11).<sup>129-131</sup>

### ***PGC-1 protein family***

This family is composed by at least three members sharing a sequence homology and regulating several metabolic pathways such as cellular respiration, adaptive thermogenesis and hepatic glucose metabolism. These coactivators stimulate the mitochondrial biogenesis in general, even if PGC-1 $\alpha$  is mainly involved in the regulation of gluconeogenesis, PGC-1 $\beta$  in the regulation of fatty acid oxidation and PRC seems to be responsible for the coordination of nuclear and mitochondrial DNA replication during the cell cycle progression.<sup>132,133</sup>

These proteins have conserved domains with well characterized features (Fig. 11):

- the N-terminus contains a transcriptional activation domain, includes the major nuclear hormone receptor-interacting motif (LXXLL), and is important for interactions with proteins capable of remodeling chromatin.
- the C-terminal contains an RNA-binding motif (RMM), that enhances the RNA splicing, and a serine-arginine-rich (RS) domain.

These domains are extremely conserved from fish to mammals, suggesting that these coactivators play a major role by regulating some important functions in eukaryotes.<sup>134</sup>

It is still unclear if the biological functions of PGC-1 $\alpha$  are overlapped with the functions of the other two family members, and further studies are necessary.

The first member of this family, PGC-1 $\alpha$  (92 kDa), was discovered as an interacting partner of the adipogenic nuclear receptor PPAR $\gamma$  in brown adipose tissue (BAT) where is responsible for the regulation of adaptive thermogenesis and adipocyte differentiation.<sup>135</sup>

The N-terminal 200 amino acids of PGC-1 $\alpha$  contain a powerful transcriptional activation domain, rich in acidic amino acids (Fig. 11). Even if this protein lacks an intrinsic histone-modifying activity, this domain allows PGC-1 $\alpha$  to recruit several cofactors with chromatin remodeling functions, such as p300/CBP (CREB Binding Protein) or SRC-1.

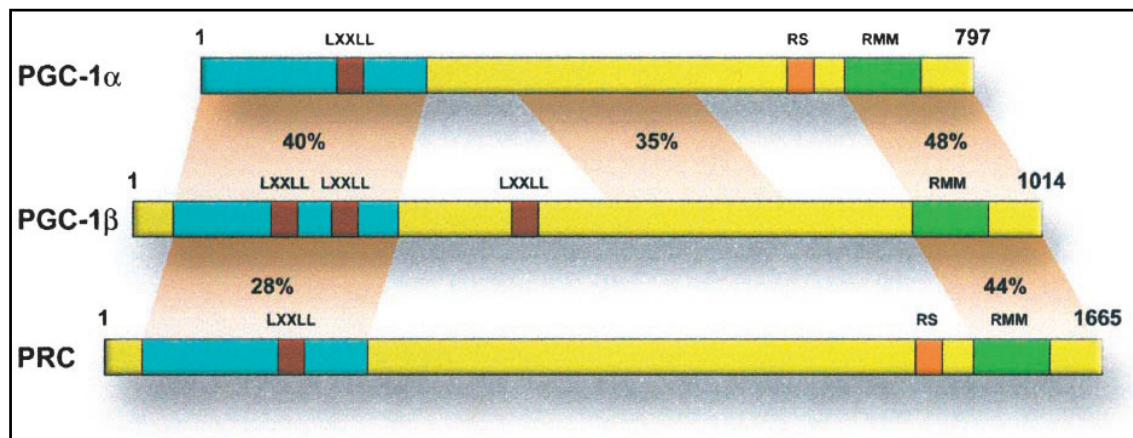


**Fig. 11** The PGC-1 protein family, conserved domains and protein homology. From Puigserver P and Spiegelman BM. *Endocrinol Rev.* 2003; 24:78-90.

Moreover, in this region there is an LXXLL sequence (amino acids 142–146), responsible for ligand-dependent interaction of other coactivators with nuclear hormone receptors.<sup>134,136</sup> The presence of this motif on PGC-1 $\alpha$  is necessary for the ligand-dependent interaction with ER, PPAR $\alpha$ , RXR $\alpha$ , glucocorticoid receptor, and probably other nuclear hormone receptors.<sup>134</sup> PGC-1 $\alpha$  also uses different non-LXXLL domains to interact with certain other transcription factors: a domain between amino acids 200 and 400 interacts with PPAR $\alpha$  and NRF-1 and a region between amino acids 400 to 500 that interacts with MEF2.<sup>136</sup> The binding of proteins with HAT (histone acetyl transferase) activity is driven by the presence of a specific association with a transcription factor (for example PPAR $\gamma$  or NRF-1).<sup>137</sup> This event induces a conformational change in PGC-1 $\alpha$  structure that recruits SRC-1 and CBP/p300 into the transcriptional complex. Moreover, the C-terminal domain is the docking site of a second activating complex formed by TRAP/DRIP.<sup>138</sup>

The C-terminal region contains also the RS domain (aa 565-631), that has been shown to interact with the C-terminal of RNA polymerase II,<sup>139</sup> and the RMM domain (aa 677-

709). This region is also involved in the recruitment and the docking of several splicing factors, such as SC35, SRp75, 55 and 40, suggesting that PGC-1 $\alpha$  can participate in the RNA splicing process.<sup>134</sup>

In general transcriptional coactivators are expressed in a stable manner and their activation depends on the associated transcription factor. Indeed, PGC-1 $\alpha$  is strongly induced by cold exposure and prolonged exercise.<sup>135,140,141</sup>

Ectopic overexpression of PGC-1 $\alpha$  causes the increase of mtDNA content at the steady state and transcriptional activation of several genes involved in respiration, ROS detoxification machinery, energy metabolism, fatty acid  $\beta$ -oxidation and glucose uptake.<sup>142,143</sup> During mitochondrial biogenesis the most important action of this protein probably is the transcriptional activation of NRF1 and 2 and its interaction with the same proteins that leads the transcription of many nuclear encoded mitochondrial genes, especially Tfam, TFB1M and TFB2M. PGC-1 $\alpha$  is also able to interact with PPAR $\alpha$ , causing the stimulation of fatty acid  $\beta$ -oxidation, with PPAR $\gamma$ , inducing UCP-1 and the adaptative thermogenesis, and many other nuclear transcription factors (HNF4, FOXO1, MEF2, SRBP1, SOX9).<sup>135,144-149</sup> A list of transcription factors activated by this coactivator is provided in table 1.

PGC-1 $\alpha$  gene expression can be modulated by several mechanisms in response to different stimuli and cell type (Fig. 12).

1. In adipocyte, in response to cold exposure,  $\beta$ -adrenergic receptors are activated. This causes the signal transduction via protein G<sub>s</sub> (a subtype of protein G) and adenylate cyclase, associated with an increase of cAMP concentration. The subsequently PKA (Protein Kinase A) activation induces the phosphorylation of CREB or ATF2 (Activating Transcription Factor 2), factors able to stimulate PGC-1 $\alpha$  transcription.
2. During fasting, the activation of CREB and the subsequent PGC-1 $\alpha$  increase, can induce the gluconeogenic pathway in mouse liver.<sup>150</sup>
3. It also has been shown a strong activation of PGC-1 $\alpha$  transcription after a prolonged exercise *in vivo* or an increase in Ca<sup>2+</sup> levels in myotubules. In the first case, a chronic energy deficit is associated with an increase in AMP/ATP ratio and the activation of AMPK.<sup>151</sup> The same kinase can be activated by CamK (Ca<sup>2+</sup>/calmodulin dependent protein kinase) as a consequence of the intracellular

Ca<sup>2+</sup> levels increase. AMPK is involved in CREB phosphorylation and/or direct PGC-1 $\alpha$  transcriptional activation. Lastly, MEF2 induction via calcineurin A is also involved in PGC-1 $\alpha$  activation in skeletal muscle.<sup>152</sup>

- Another signaling pathway is mediated by NO generation and involves the cGMP signaling. The final event is the increase in coupled respiration mediated by PGC-1 $\alpha$  transcription.<sup>153,154</sup>

Transcription Factor	Function	PGC-1 $\alpha$	PGC-1 $\beta$
NRF1	Mitochondrial genes	+	+
NRF2	Mitochondrial genes	+	ND
PPAR $\alpha$	Fatty acid oxidation	+	+
PPAR $\beta/\delta$	Fatty acid oxidation	+	ND
PPAR $\gamma$	UCP1/GyK induction adaptative thermogenesis	+	+
ERR $\alpha,\beta,\gamma$	Mitochondrial genes	+	+
TR $\beta$	Cpt-1 induction	+	+
LXR $\alpha,\beta$	Lipoprotein secretion	+	+
FXR	Triglyceride metabolism	+	ND
GR	Gluconeogenesis	+	-
ER $\alpha,\beta$	Unknown	+	+
PXR	Unknown	+	ND
Sox9	Chondrogenesis	+	ND
MEF2	Slow fiber genes	+	ND
FOXO1	Gluconeogenesis	+	-
HNF4 $\alpha$	Gluconeogenesis	+	+/-
SREBP1a, 1c, 2	Lipogenesis, lipoprotein secretion	-	+

**Tab. 1** Transcriptional partners of the PGC-1 coactivators. Modified from Lin J, Handschin C, Spiegelman BM. Cell Metab. 2005; 1:361-370.

PGC-1 $\alpha$  exhibits a very short half life (2-3 hours),<sup>155</sup> but it can be increased by p38 mediated phosphorylation in three sites (Thr262, Ser265, Thr298).<sup>156</sup> This process causes also the dissociation of the transcriptional repressor p160 myb-binding protein.<sup>157</sup> Lastly, PGC-1 $\alpha$  presents also 13 Lys that can be deacetylated by Sirt1, in fasting conditions, in a NAD<sup>+</sup> dependent reaction. In this pathway PGC-1 $\alpha$  is able to

switch on the hepatic glucose production without affecting mitochondrial protein content.<sup>158</sup>

The second family member, PGC-1 $\beta$ , is larger but shares sequence similarity with PGC-1 $\alpha$  along its entire length. Like its homolog, the protein is particularly expressed in tissue with high energy demand, such as brown fat, heart and skeletal muscle, where is able to coordinate mitochondrial biogenesis, inducing NRF1-target genes.<sup>131,159</sup> In contrast with PGC-1 $\alpha$ , PGC-1 $\beta$  is not induced in BAT after cold exposure and is a poor inducer of gluconeogenesis in liver, due to the lack of interaction with HNF4 and FOXO1.<sup>160</sup>

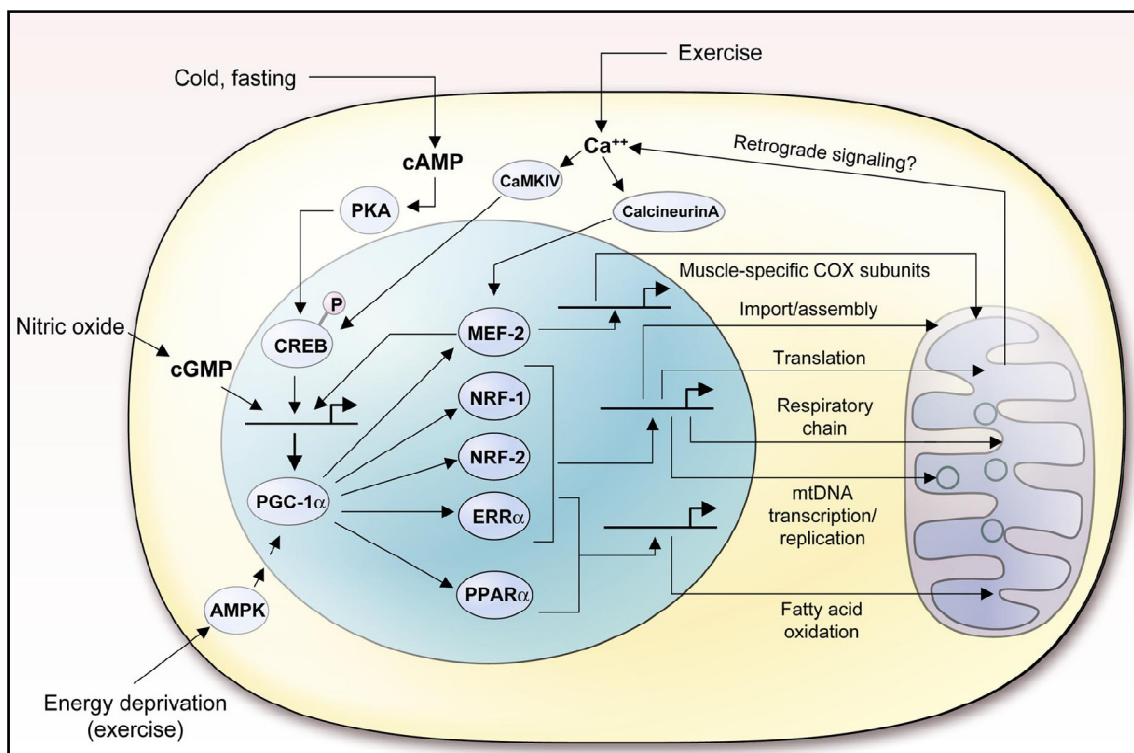


**Fig. 12** Integration of different signaling pathways in mitochondrial biogenesis regulated by PGC-1 $\alpha$ .

From Scarpulla RC. *Physiol Rev.* 2008; 88:611-38.

Another homologue is PRC (PGC-1 $\alpha$  Related Coactivator), identified through a database search for sequence similarities. PRC is significantly longer than PGC-1 $\alpha$ , and the protein contains an LXXLL consensus, an acid N-terminal activation domain and a C-terminal RS domain.<sup>161</sup> The main difference with the other two family members is the low expression of PRC in tissues with high energy demand.<sup>94</sup> However, PRC is rapidly

induced after serum treatment of quiescent fibroblasts and is expressed more abundantly in proliferating cells compared with growth-arrested cells. The transcription pathway is similar to that previously described, involving the induction of NRF-1, NRF-2, Tfam, TFB1M and TFB2M, as well as genes encoding for nuclear and mitochondrial respiratory subunits.<sup>94</sup>

### ***Nuclear respiratory factors (NRF1 and NRF2)***

NRF1 is a transcription factor that recognizes directly a palindromic sequence (5'-YGC GCAYGCGCR-3') in the promoter of several nuclear encoded mitochondrial genes.<sup>162,163</sup> This transcription factor binds the recognition site as an homodimer and is a protein of 503 amino acids, with a N-terminal Ser-phosphorylation domain, a central DNA binding domain and a C-terminal transactivation domain.<sup>94</sup> NRF-1 has been associated with the expression of many genes required for mitochondrial respiratory function, including the vast majority of nuclear genes that encode subunits of the five OXPHOS complexes.<sup>94</sup> Moreover, there are several evidences supporting the idea that NRF1 could be an integrative factor that coordinates respiratory subunit expression with the mitochondrial transcriptional machinery.<sup>94</sup> NRF-1 binds and activates not only the promoters of Tfam and TFB, but also genes of the respiratory chain complexes, heme-biosynthesis, mitochondrial transmembrane transporters.<sup>94</sup>

Human NRF2 is comprised of five subunits, a DNA-binding  $\alpha$  subunit and four others accessory subunits ( $\beta_1$ ,  $\beta_2$ ,  $\gamma_1$  and  $\gamma_2$ ) that form a complex with  $\alpha$  subunit do not bind DNA alone. All the accessory subunits contain a transcriptional activation domain. NRF2 binding sites contain the GGAA core motif, found in many mitochondrial genes promoters, such as all 10 nucleus encoded cytochrome oxidase subunits, Tfam, the two isoforms of TFB and three subunits of SDH.<sup>94,164-166</sup>

### ***Nuclear receptors***

There are several nuclear receptors involved in mitochondrial biogenesis, such as PPARs (peroxisome proliferator associated receptors) and ERRs (estrogen related receptors). Nuclear hormone receptors generally function as ligand-activated transcription factors that regulate the expression of specific genes and they usually share

conserved functional domains (the DNA binding domain, the ligand binding domain and the N- and C-terminal transcriptional activation domains).<sup>167</sup>

Many mitochondrial oxidative pathways converge into the respiratory chain, and one of the most important is the fatty acid oxidation pathway, which consists of a series of reactions that oxidize fatty acids to acetyl-CoA, due to mitochondrial enzymes. PPARs have been implicated as transcriptional regulators of this metabolic pathway. This family of adopted orphan receptors consists of three isoforms: PPAR $\alpha$ , PPAR $\beta/\delta$  and PPAR $\gamma$ , sharing a highly conserved structure and mode of action. They act as transcriptional regulators through their direct binding to specific nucleotide sequences (PPREs, peroxisome proliferator response elements), present in the promoter or, sometimes, in an intron, of target genes.<sup>168</sup>

Their transcriptional activity is expressed only after the binding of their ligands; some of them are shared by the three isoforms, such as polyunsaturated and oxidized fatty acids. Other ligands, specific for PPAR $\alpha$ , are long-chain unsaturated, branched, conjugated and oxidized fatty acids (linoleic acid, phytanic acid, eicosanoids and leukotrienes), while some prostaglandins are specific ligands of PPAR $\gamma$ .<sup>169</sup> Moreover PPARs are activated by two classes of agonists, the thiazolidinediones for PPAR $\gamma$  (TZDs) and the fibrates for PPAR $\alpha$ . TZDs are mainly used in the treatment of diabetes mellitus type 2 and related diseases; activating PPAR $\gamma$ , they cause a decrease in insulin resistance and in VEGF induced angiogenesis and changes in adipocyte differentiations. Instead, fibrates are hypolipidemic agents, commonly used in the therapy of metabolic disorders coupled with hypercholesterolemia. Interestingly, one of those drugs, bezafibrate, is a well known PPARs pan-activator, and is also used as treatment against insulin resistance.<sup>167</sup> PPARs bind the promoter only as a heterodimer with the receptor for 9-*cis* retinoic acid, RXR (retinoid X receptor).<sup>170,171</sup> This heterodimer can be activated by the PPARs ligand alone, but the coordinated binding of both ligands is much more potent.<sup>169</sup>

PPAR $\alpha$  controls the expression of several genes involved in fatty acid metabolism. After fasting, when fatty acids are more used for energy production, PPAR $\alpha$  expression and activity increase, inducing the  $\beta$ -oxidation. Furthermore, PPAR $\alpha$  is induced, coordinating its target genes, in skeletal muscle after exercise<sup>172</sup> and also in the heart,

where the main energy source derives from lipids, especially during the fetal-adult transition.<sup>173</sup>

Whereas PPAR $\alpha$  is the main player in the catabolism of fatty acids in the liver, PPAR $\gamma$  influences their storage in adipose tissue and is essential for adipocyte survival. There are two isoforms of PPAR $\gamma$ : PPAR $\gamma$ 1 mainly expressed in colon, spleen, blood cells, liver, skeletal muscle and retina, and PPAR $\gamma$ 2 expressed in the adipose tissue. Both these isoforms respond to the same stimuli and activate the same target genes.<sup>167</sup>

Lastly, PPAR $\beta/\delta$  is linked to colon cancer and regulates the expression of acyl-CoA synthetase 2 in the brain, but this member received only little attention to date, probably because no diseases seem associated with this factor.<sup>169</sup>

Another family of nuclear receptor involved in the regulation of mitochondrial biogenesis and oxidative metabolism is the estrogen-related receptor family (ERRs).

This is a family of orphan nuclear receptors resembling the estrogen receptor without binding estrogens or other ligands.<sup>167</sup> The three family members (ERR $\alpha$ ,  $\beta$  and  $\gamma$ ) have the typical structure of nuclear receptors, as PPARs. The central zinc finger DNA-binding domain recognizes the response element (ERREs) characterized by the nucleotide sequence 5'-TNAAGGTCA-3'.<sup>174</sup> The conserved C-term domain should be the one responsible for interactions with corepressors and/or coactivators and for the ligand binding, but putative ligands are still unknown. These receptors are constitutively present in an active conformation, even in the absence of ligand.<sup>175-177</sup>

ERR $\alpha$ , the most extensively studied, is ubiquitously expressed and is more abundant compared to the other two family members, reaching the highest levels in tissues with high metabolic needs (heart, skeletal muscle, kidney, BAT and central nervous system). Several studies have revealed the strict connection between ERRs and PGC-1 $\alpha/\beta$  in the regulation of energy metabolism genes.<sup>178-181</sup> These two proteins interact directly through their specific domains: in PGC-1 $\alpha$  there are three nuclear hormone receptor-interacting motifs and one of these (L3) is exclusively used for the interaction with ERR $\alpha$  ligand binding domain. This interaction improves dramatically the transcriptional activity of ERR $\alpha$ , suggesting that PGC-1 $\alpha/\beta$  could be a “protein ligands” of ERRs.<sup>174</sup> Furthermore, PGC-1 $\alpha$  regulates not only the activity, but also the expression of ERR $\alpha$  in an auto-regulatory loop, in which high levels of PGC-1 $\alpha$  induce the increase of ERR $\alpha$  transcriptional activity at the level of its promoter.<sup>182-184</sup> Taken together, the coactivator

and the nuclear receptor coordinate the expression of several genes involved in fatty acid oxidation, tricarboxylic acid cycle, oxidative stress defense, mitochondrial biogenesis and dynamics and oxidative phosphorylation.<sup>174</sup> A list of genes probably regulated by the complex PGC-1/ERRs is reported in table 2.

***Other nuclear factors***

Many other nuclear factors have been implicated in the expression of respiratory genes and in the control of mitochondrial biogenesis. For example, the cytochrome *c* promoter contains *cis*-elements that recognize transcription factors ATF/CREB, c-Myc and Sp1, while muscle-specific complex IV subunits are regulated by MEF-2 and/or YY1 (YingYang1).<sup>167</sup>

Gene	Function	ERRE	Position	Dir	Gene	Function	ERRE	Position	Dir
<i>Acadm</i>	Fatty acid oxidation	TAAAGGTCA	-557	F	<i>Iscu</i>	Respiratory chain	GGAAGGTCA	-845	F
<i>Aco2</i>	TCA	TCAAGGTCA	-225	R	<i>Me3</i>	Tricarboxylic acid cycle	TGAGGGTCA	-559	R
<i>Atp5b</i>	ATP synthesis	CCAAGGACA	-325	F	<i>Mtx2</i>	Protein transport Translation	CCAAGGTCA	+61	R
					<i>Mrpl11</i>		TTTGGGTCA	+14	R
<i>Atp5e1</i>	ATP synthesis	TCAAGGTCA	+198	R	<i>Mrpl19</i>	Translation	ACAAGGACA	+314	R
		ACAAGGTCA	+246	F	<i>Mrpl34</i>	Translation	TTTAGGTCA	-546	R
<i>Atp5d</i>	ATP synthesis	CACGGGTCA	+291	R	<i>Mrpl47</i>	Translation	TCCGGGTCA	+1	R
		ATTAGGTCA	+308	F			GGCGGGTCA	+22	R
<i>Atp5f1</i>	ATP synthesis	TCGGGGTCA	-1	F	<i>Mrps18b</i>	Translation	CCAAGGTCA	-490	F
							ACGAGGTCA	+4	R
<i>Atp5g1</i>	ATP synthesis	ACAGGGACA	+7	F	<i>Mech2</i>	Transport	GCAAGGTCA	-188	R
		AGAAGGACA	-208	R	<i>Mfn2</i>	Mitochondrial fusion	TCAGGGTCA	-179	F
							TGAAGGACA	-559	F
							ACAGGGTCA	-461	F
					<i>Mlycd</i>	Fatty acid oxidation	TCAAGGTCA	+923	F
					<i>Ndufa4</i>	Respiratory chain	CCAGGGTCA	-284	R
<i>Atp5g3</i>	ATP synthesis	AGAAGGACA	-156	R					
		AAAAGGTCA	+267	R	<i>Ndufa5</i>	Respiratory chain	ATGAGGTCA	-387	R
		TCAAGGTCA	-75	R					
<i>Atp5k</i>	ATP synthesis	TTAAGGTCA	+215	R	<i>Ndufa8</i>	Respiratory chain	TGGAGGTCA	+172	F
		CGAAGGTCA	+1	F	<i>Ndufa9</i>	Respiratory chain	TCAAGGTCA	-980	R
<i>Cabc1</i>	Electron transfer	TTAAGGACA	-48	F					
<i>Ccdc90b</i>	Unknown	CTAGGGACA	-792	R	<i>Ndufb2</i>	Respiratory chain	AAAGGGTCT	-301	F
		CGCAGGTCA	-7	R					
<i>Ckmt2</i>	Phosphocreatine metabolism	TCAAGGTCA	+60	F					
		TAAAGGACA	+97	F	<i>Ndufb1</i>	Respiratory chain	GCGGGTCA	-38	R
<i>Clybl</i>	Hydrocarbon metabolism	CAGAGGTCA	+176	R					
<i>Cog7</i>	Ubiquinone biosynthesis	TCAGGGTGA	+9	R					
		TGGAGGTCA	+195	F					
<i>Cox5b</i>	Respiratory chain	TAAAGGTCA	-553	F	<i>Ndufb5</i>	Respiratory chain	TCAAGGTCA	-379	R
		CCAAGGTCA	+353	R					
<i>Cox6c</i>	Respiratory chain	TCAAGGTCA	+440	R					
<i>Cox7a2</i>	Respiratory chain	GGAGGGTCA	+258	F					
<i>Cox7b</i>	Respiratory chain	TATAGGTCA	-26	F	<i>Ndufs1</i>	Respiratory chain	ACGAGGTCA	-290	F
		ACAAGGACA	+371	R					
<i>Cox7c</i>	Respiratory chain	TGAAGGTCA	+413	F					
<i>Cox8a</i>	Respiratory chain	TCAAGGTCA	-834	F	<i>Ndufs2</i>	Respiratory chain	CATAGGTCA	+196	F
		CCAAGGTCA	+71	R					
<i>Cox8b</i>	Respiratory chain	AGAAGGACA	-872	F					
		AGAAGGACA	-664	F					
<i>Cpt1b</i>	Fatty acid metabolism		-754	F	<i>Ndufs3</i>	Respiratory chain	GGGAGGTCA	-91	R
<i>Cpt2</i>	Fatty acid metabolism	TAGAGGACA	-896	F					
<i>Cyts</i>	Respiratory chain	TAAAGGTCA	-494	F					
<i>Cyp27a1</i>	Cholesterol metabolism	TGAGGGACA	-363	F	<i>Ndufs7</i>	Respiratory chain	CAGGGTCA	+206	R
<i>D10Ert322e</i>	Translation	TGCAGGTCA	-339	F					
		GCAAGGTCA	+236	R					
<i>Endog</i>	DNA metabolism	CTAGGGTCA	-307	R	<i>Ndufv1</i>	Respiratory chain	CCTGGGTCA	+224	R
		CTAGGGTCA	+82	R					
<i>Etfb</i>	Fatty acid catabolism	AGAGGGTCA	+37	F	<i>Ddk4</i>	Glucose metabolism	GCACGGTCA	-336	R
<i>Etfih</i>	Fatty acid catabolism	GTCGGGTCA	+188	R	<i>Rtn4ip1</i>	Metabolism	GACGGTCA	+65	F
		TCCGGGTCA	-69	R					
					<i>Sdha</i>	Tricarboxylic acid cycle	CCCGGGTCA	-263	R
<i>Ph1</i>	Tricarboxylic acid cycle	CAAAGGTCA	+326	F					
<i>Got2</i>	Amino acid metabolism	TGAAGGTCA	+172	R	<i>Sdhb</i>	Tricarboxylic acid cycle	CCTAGGTCA	+74	R
		ACAGGGACA	-451	F					
					<i>Sdhc</i>	Tricarboxylic acid cycle	CGAAGGTCA	+202	F
<i>Hdh3</i>	Metabolism	CTCGGGTCA	-345	F	<i>Slc25c4</i>	Transport	TCAAGGTCA	+13	R
		CGGAGGTCA	-162	R					
<i>Hk2</i>	Glucose metabolism	TTAAGGTCA	-195	R					
<i>Hspa9a</i>	Protein folding	CCAAGGTCA	-587	R					
<i>Idh3a</i>	Tricarboxylic acid cycle	ACTGGGTCA	+177	R					
		TCAAGGTCA	-292	R	<i>Slc25c29</i>	Transport	AGAGGTCA	+176	F
		TCAAGGTCA	+221	F					
<i>Isc1</i>	Respiratory chain	TGAGGGTCA	+304	F					
		GCAAGGTCA	-141	F	<i>Suclg1</i>	Tricarboxylic acid cycle	TGAGGGTCA	+214	F
<i>Supv3l1</i>	Helicase	CACAGGTCA	-133	F					
<i>Tfb2m</i>	Transcription	GAAAGGTCA	+354	F	<i>Timm17a</i>	Protein transport	TGAGGGTCA	-240	R
		GGGAGGACA	-446	F					
<i>Timm8b</i>	Protein transport	GAATGGTCA	-767	F					
		GGGAGGACA	-446	F					
<i>Timm9</i>	Protein transport	TCAAGGTCA	-104	F					
					<i>Txn2</i>	Redox homeostasis	ACAAGGTCA	+233	R
					<i>1110020P15Rik</i>	Electron transfer	CTAGCGTCA	+2	R
							CCAAGGTCA	+200	R
<i>Timm10</i>	Protein transport	TCAAGGTCA	+410	R					
		TCTAGGTCA	-585	F					

**Tab. 2** Genes encoding mitochondrial proteins with ERREs in their promoter, probably regulated by ERRs. Modified from Giguere V. *Endocr Rev.* 2008; 29:677-696.

## **Mitochondrial disorders**

The term “mitochondrial medicine” was introduced for the first time by Rolf Luft in 1994 and now is commonly used to indicate that branch of medicine interested in studying mitochondrial dysfunctions.<sup>185</sup> Historically, the first mitochondrial patient is considered to be a woman described by Luft in 1962, suffering of severe hypermetabolism, heat intolerance, profuse perspiration, muscular wasting and weakness, polyphagia and resting tachycardia.<sup>186</sup> This phenotype, now known as Luft’s syndrome, is caused by a deregulated mitochondrial respiration, consuming an excess of energy, possibly due to a profound uncoupling, even if the molecular cause is still unknown.<sup>186</sup> In 1988, 25 years later, the first pathogenic mtDNA point mutations and deletions were reported in association with Leber’s hereditary optic neuropathy (LHON) and mitochondrial myopathies.<sup>187,188</sup> After these seminal reports, a multitude of mtDNA mutations were discovered associated with several maternally inherited and sporadic disorders, most of them affecting the central and peripheral nervous system, as well as skeletal and cardiac muscle.

Mitochondrial disorders can be divided in two classes: the first is due to mtDNA mutations or rearrangements, whereas the second comprise Mendelian diseases associated with nuclear DNA mutations or rearrangements in genes encoding mitochondrial proteins.<sup>189</sup> Moreover, mitochondrial disorders can be also classified in those affecting the respiratory chain function (directly, OXPHOS subunits, or indirectly, affecting ancillary proteins, lipid milieu, and mitochondrial translation) and those affecting mitochondrial dynamics. Furthermore, a mitochondrial involvement has been proposed for several neurodegenerative diseases, such as Parkinson and Alzheimer disease.<sup>189</sup>

### **Disorders of the mitochondrial respiratory chain**

In figure 13 is shown the mitochondrial respiratory chain, depicted with the major mitochondrial disorders affecting directly the respiratory chain and the genes involved.<sup>189</sup>

To date, about 200 mtDNA mutations and several single and multiple deletions have been associated with human diseases, and novel mutations are still being reported. Due

to the very peculiar characteristics of mitochondrial genetics, these disorders show often a phenotypic heterogeneity.

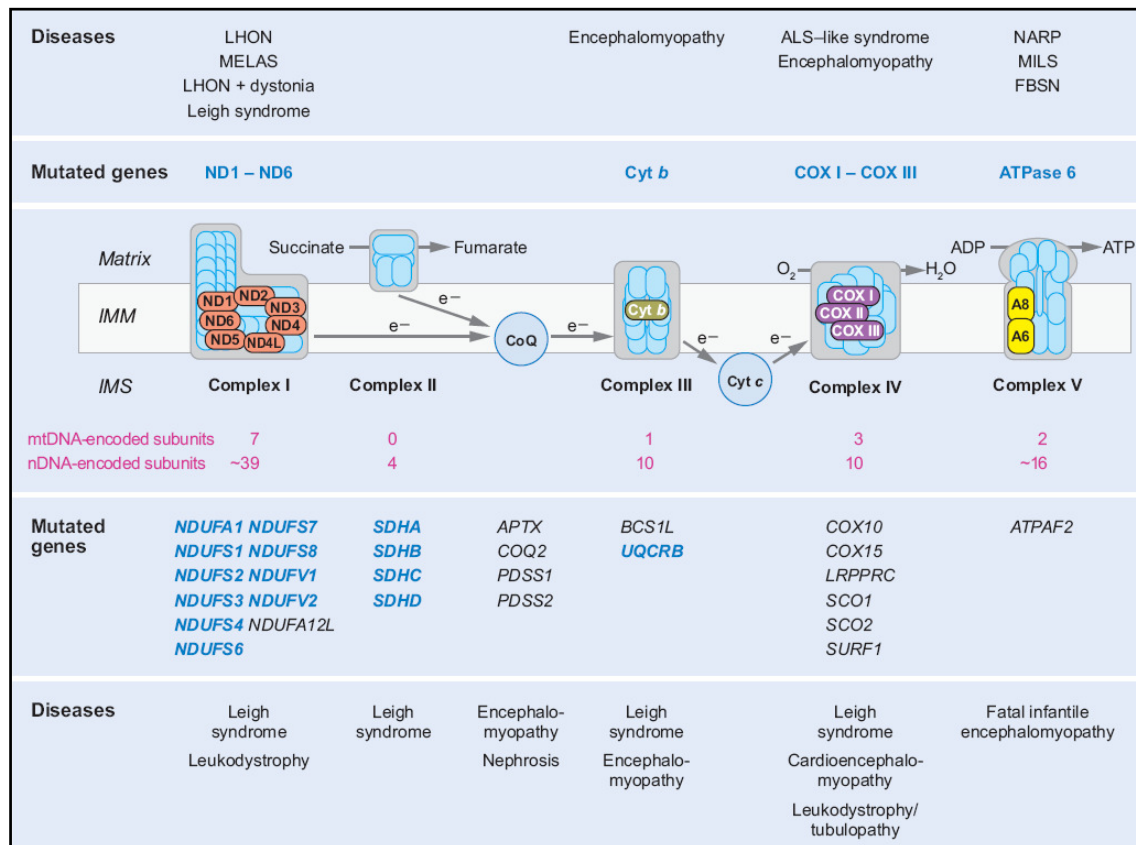


**Fig. 13** The mitochondrial respiratory chain: diseases associated with respiratory chain defect and relative mutated genes. From DiMauro S and Schon EA. *Annu Rev Neurosci.* 2008;31:91-123.

The same genetic defect may result in different phenotypes in different individual belonging to the same family, and/or in different families. On the other hand the same phenotype can be associated with several different mutations.<sup>190</sup> Furthermore, the threshold effect is generally critic for the expression of the pathology, but in some cases, such as LHON, homoplasmic mutations may have variable penetrance and different clinical severity, often within the same family. A related question concerns the functional significance of mtDNA background. It has been shown that different haplogroups may modulate the oxidative phosphorylation and the complex I assembly, predisposing or protecting individuals to/from certain disorders.<sup>191,192</sup>

Major rearrangements of mtDNA usually comes as deletions or duplications, even if deletions are most common. Multiple deletions are caused by defects in nuclear genes encoding for enzymes involved in mtDNA maintenance and nucleotide metabolism, whereas single deletions are usually sporadic.<sup>189</sup> The main syndromes associated with single sporadic deletions are Kearns-Sayre Syndrome (KSS), Pearson marrow-pancreas Syndrome (PS) and some forms of Chronic Progressive External Ophthalmoplegia (CPEO).

PS is a fatal sideroblastic anemia complicated by the involvement of exocrine pancreas. Usually the patients die around 4 years of age, but in case of survival deletions are associated with the development of KSS.<sup>190</sup>

KSS is characterized by retinitis pigmentosa, external ophthalmoplegia and onset before age 20. Other symptoms are variously reported, such as cardiac conduction block, cerebellar ataxia, short stature, cerebrospinal fluid proteins greater than 100mg/dL, hearing loss and muscle weakness.<sup>190</sup>

CPEO (widely reviewed by Spinazzola and Zeviani)<sup>193,194</sup> is clinically defined by palpebral ptosis, generalized weakness and progressive limitation of ocular movements. Additional symptoms can be ataxia, sensorineural hearing loss, cataracts, parkinsonism and peripheral polyneuropathy. Skeletal muscle histological analysis, with modified Gomori trichromic stain, shows the presence of ragged-red fibers (RRFs) due to accumulation of aberrant mitochondrial. Biochemically, it has been shown a moderate reduction in the activity of respiratory chain complexes.<sup>195,196</sup> Sporadic forms are reported but there are also inherited CPEO, that can be autosomal dominant (adCPEO), autosomal recessive (arCPEO) and maternally inherited.<sup>189</sup> Maternally inherited forms are caused by point mutations in mitochondrial tRNA genes specifying for leucine, isoleucine and alanine, whereas autosomal forms are caused by mutations in POLG1, POLG2, Twinkle and ANT-1 (Fig. 14), all genes involved in mtDNA replication or nucleotide metabolism, and leading to multiple deletions.<sup>197-200</sup>

Recently a new syndrome, characterized by dominant optic atrophy, sensorineural deafness, ataxia, axonal sensory-motor polyneuropathy, CPEO and mitochondrial myopathy with cytochrome c oxidase negative and RRFs, has been described.<sup>17,18,201</sup> These patients harbour missense mutations in the OPA1 GTPase domain and multiple deletions of mitochondrial DNA (mtDNA) in skeletal muscle, revealing an

unrecognized role of the OPA1 protein, previously known only as a regulator of mitochondrial fusion, in mtDNA stability.<sup>17,18,201</sup>

A more complex syndrome is MNGIE (Mitochondrial NeuroGastroIntestinal Encephalomyopathy), an autosomal recessive disorder affecting young adults. This syndrome is characterized by CPEO, peripheral neuropathy, leukoencephalopathy and gastrointestinal dysmotility.<sup>202</sup> The gastrointestinal symptoms include gastroparesis, frequent diarrhea and intestinal pseudo-obstruction, that lead to cachexia and early death.<sup>18</sup> MNGIE is caused by different mutations in the gene TP, encoding the enzyme thymidine phosphorylase (Fig. 14).<sup>203</sup> This enzyme is necessary in the thymine metabolism, acting in the thymine recycle pathway. Mutations in this gene cause the lack of enzyme activity, inducing an accumulation of thymidine, that is promptly transformed in deoxythymidine triphosphate, by the enzyme TK2 (Thymidine Kinase 2). This process causes an unbalancing in the nucleotide pool which interferes with mtDNA replication, and consequently induces mtDNA depletion and accumulation of multiple deletions and point mutations.<sup>202</sup>

Other recessive disorders leading to mtDNA depletion and multiple deletions are Sensory-Ataxia Neuropathy, Dysarthria and Ophthalmoplegia (SANDO), spinocerebellar ataxia epilepsy syndrome and Alpers' syndrome, all associated with recessive mutations in POLG1 gene.<sup>194</sup>

Mitochondrial DNA depletion syndromes are also recessive traits with various phenotypical expression, which are caused by mutations in several genes (Fig. 14). The degree of depletion may vary in different tissues.<sup>189,194</sup> The two major syndromes are:

- Hepatocerebral syndrome, caused by mutations in POLG1 (Alpers' syndrome), DGUOK (deoxyguanosine kinase, involved in nucleotide metabolism) and MPV17 (an IMM protein with unknown function)<sup>189,194,204</sup>
- Pure myopathic syndromes, due to mutations in TK2, SUCLA2 (encoding the  $\beta$ -subunit of succinylCoA synthetase) and RRM2B (p53 inducible ribonucleotide reductase small subunit)<sup>189,205,206</sup>

Mitochondrial DNA is also an hot spot for pathogenic point mutations accumulation, causing different pathologies. One of the most common disorder is MELAS (Mitochondrial Encephalomyopathy Lactic Acidosis and Stroke-like

episodes), a multisystem disorder characterized by stroke-like episodes in young age, encephalopathy with seizures and/or dementia and mitochondrial myopathy with lactic acidosis and RRFs.<sup>207</sup> Additional features are myoclonus, ataxia, basal ganglia calcifications, pigmentary retinopathy, optic nerve atrophy, short stature, hearing impairment and cardiomyopathy.<sup>207</sup> At least 15 different mtDNA mutations have been associated with MELAS, but more than 80% of the patients harbour the common mutation A3243G in the tRNA<sup>Leu</sup> gene. Other reported mutations affect other positions in the tRNA<sup>Leu</sup> gene and other tRNA genes, but mutations in structural genes, such as COIII, ND1, ND5 and ND6, have been also reported.<sup>208</sup> The phenotype of these mutations is usually heterogeneous, and individuals belonging to the same family are often oligosymptomatics, and manifest only some features of MELAS.<sup>209</sup> Mutations in tRNA cause an impaired protein synthesis and a generalized respiratory chain biochemical defect.<sup>210</sup>

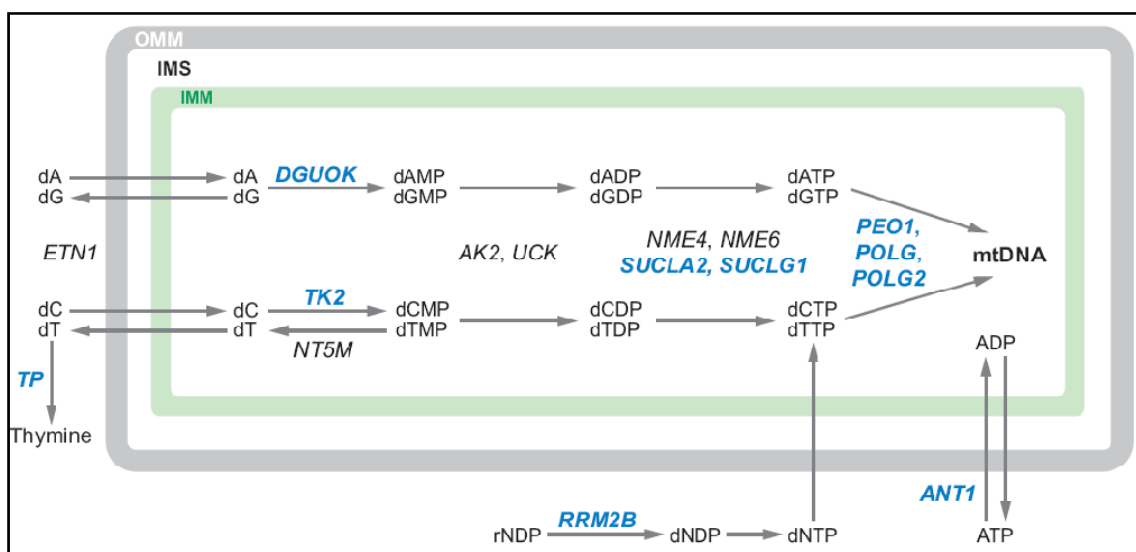


**Fig. 14** Nucleotide metabolism for mtDNA synthesis and replication: genes in bold have been associated with diseases, mtDNA multiple deletions and/or depletion syndromes. From DiMauro S and Schon EA. *Annu Rev Neurosci.* 2008;31:91-123.

Mitochondrial DNA is also an hot spot for pathogenic point mutations accumulation, causing different pathologies. One of the most common disorder is MELAS (Mitochondrial Encephalomyopathy Lactic Acidosis and Stroke-like episodes), a multisystem disorder characterized by stroke-like episodes in young age,

encephalopathy with seizures and/or dementia and mitochondrial myopathy with lactic acidosis and RRFs.<sup>207</sup> Additional features are myoclonus, ataxia, basal ganglia calcifications, pigmentary retinopathy, optic nerve atrophy, short stature, hearing impairment and cardiomyopathy.<sup>207</sup> At least 15 different mtDNA mutations have been associated with MELAS, but more than 80% of the patients harbour the common mutation A3243G in the tRNA<sup>Leu</sup> gene. Other reported mutations affect other positions in the tRNA<sup>Leu</sup> gene and other tRNA genes, but mutations in structural genes, such as COIII, ND1, ND5 and ND6, have been also reported.<sup>208</sup> The phenotype of these mutations is usually heterogeneous, and individuals belonging to the same family are often oligosymptomatics, and manifest only some features of MELAS.<sup>209</sup> Mutations in tRNA cause an impaired protein synthesis and a generalized respiratory chain biochemical defect.<sup>210</sup>

Another syndrome characterized by the presence of mitochondrial tRNAs point mutations is MERRF (Myoclonus, Epilepsy and Ragged-Red Fibers). The clinical manifestation of this disorder includes myoclonus, epilepsy, ataxia and RRFs in muscle biopsies.<sup>207</sup> In many patients were also reported hearing loss, dementia, short stature, lactic acidosis, peripheral neuropathy and exercise intolerance.<sup>207</sup> In literature are described at least 6 different mutations in mitochondrial tRNAs genes, especially in tRNA<sup>Lys</sup> (the most common A8344G, 80% of cases, T8356C, G8363A, G8361A), a mutational hot spot for MERRF. Other genes involved are tRNA<sup>Phe</sup>, tRNA<sup>Ser</sup> and tRNA<sup>His</sup>.<sup>211</sup>

Mutations can also occur in structural mitochondrial genes and the major disorders associated with these mutations are LHON (Leber's Hereditary Optic Neuropathy, that will be extensively described in the next section), NARP (Neuropathy, ataxia, retinitis pigmentosa) and MILS (Maternally Inherited Leigh Syndrome).

NARP is a multisystem disorder affecting young adults. The main symptoms are sensory neuropathy, ataxia, dementia, seizures and retinitis pigmentosa.<sup>207</sup> A single heteroplasmic point mutation in ATPase6 gene (T8993G/C) is the molecular cause of the pathology.<sup>208,212</sup> The same mutations, at high levels of mutational load may be associated with mild forms of MILS.<sup>213</sup>

Lastly, Leigh syndrome is a complex, early-onset, disease with a heterogeneous clinical manifestation, due to different mutations in several genes (nuclear and mitochondrial),

to difference in age of onset, progression and the frequency of epilepsy.<sup>207</sup> The wide variety of symptoms includes developemental regression, hypotonia, CPEO, hearing loss, optic neuropathy or pigmentary retinopathy, nystagmus, ataxia, seizures. Other symptoms may involve respiratory and cardio circulatory apparatus.<sup>207</sup> Mutations were discovered in several genes, both structural and assembly genes, essential for the respiratory chain function. The inheritance may be autosomal recessive, X-linked and maternal (MILS), with several mutations reported in the following genes:<sup>213-216</sup>

- Complex I: mitochondrial structural genes ND1-ND6, with the only exception of ND4L
- Complex II: nuclear structural gene SDHA
- Complex III: BCS1L
- Complex IV: mitochondrial structural gene COIII and nuclear asseblly factors COX10, COX15, SCO2 and SURF1
- Complex V: mitochondrial structural gene ATPase6.

Moreover, LRPPRC mutations have been found in the French Canadian variant of Leigh syndrome.<sup>207</sup> LS may be a feature of a deficiency of any of the mitochondrial respiratory chain complexes, but also of pyruvate dehydrogenase complex (PDCH), leading to an inappropriate ATP production and cellular energy impairment.

## **Leber's hereditary optic neuropathy**

LHON is a maternally inherited form of acute or subacute loss of central vision affecting predominantly young males.<sup>217</sup> This usually monosymptomatic disease was clinically defined by Leber and is now recognized as the most frequent mitochondrial disease.<sup>218</sup>

### **Clinical features**

Clinically, LHON is characterized by rapid loss of central vision in one eye, followed by similar involvement of the other eye, usually in a short time laps.<sup>219,220</sup> This condition is usually painless and associated with dyschromatopsia. Visual acuity reaches stable residual values at or below 20/200 within a few months, and the visual field defect involves the central vision in the form of a large centro-cecal absolute scotoma. Fundus examination during the acute/subacute stage reveals circumpapillary telangiectatic microangiopathy, swelling of the nerve fiber layer around the disc (pseudoedema), absence of leakage on fluorescein angiography.<sup>221,222</sup> The microangiopathy may be present in a number of asymptomatic at-risk family members along the maternal line, in whom it may remain stable over the years.<sup>223</sup> In the acute phase, axonal loss in the papillomacular bundle leads to temporal atrophy of the optic nerve, and the endpoint of the disease is generally, a full optic atrophy with permanent severe loss of central vision but with relative preservation of pupillary light responses.<sup>220</sup> However, spontaneous recovery of visual acuity has occasionally been reported even years after onset.<sup>220, 224-226</sup> A young age of onset is a favorable prognostic factor, and the rate of visual recovery is more frequent in the patients bearing the 14484/ND6 mutation.<sup>220</sup> Visual function may improve progressively or suddenly, with contraction of the scotoma or reappearance of small islands of vision within it (fenestration).<sup>220</sup> In long-lasting LHON, cupping of the optic disc has frequently been reported as a sign of the chronic stage of the pathological process.<sup>227-229</sup>

A recent study from our group has demonstrated that the optic disc area can be a prognostic marker for LHON patients, because LHON carriers (harboring the mutation, but unaffected) display a greater optic disc area and higher vertical disc diameter, compared to controls and affected LHON. Thus, the optic nerve head morphology may

have a protective role. Our hypothesis is reinforced by the observation that, among the LHON-affected, larger discs were correlated with visual recovery and better visual outcome.<sup>230</sup>

Even if LHON is usually a monosymptomatic disorder, a subset of patients has a syndromic form of optic atrophy frequently referred as “Leber’s plus”,<sup>231,232</sup> which may include central nervous system involvement and movement disorders frequently associated with basal ganglia lesions, Leigh-like syndrome, cerebellar atrophy, migraine, epilepsy and peripheral neuropathy, and also cardiac involvement with conduction abnormalities or skeletal deformities.<sup>232,233-237</sup>

In some cases, the occurrence of “Leber’s plus” has been related to specific mtDNA mutations, different from the primary LHON mutations and expressing a syndromic form of LHON, such as 14459/ND6 which is associated with LHON and dystonia.<sup>238</sup>

Recently, several mutations have been described in the ND1, ND6, and ND5 genes of complex I associated with syndromic forms of LHON (from Leber’s like optic atrophy to MELAS or MILS).<sup>239-241</sup> In other cases the “Leber’s plus” phenotype has been linked to a combination of different mtDNA mutations, including the association of one primary LHON mutation and other putative pathogenic changes, multiple putative pathogenic mutations, and the co-occurrence of two primary LHON mutations.<sup>242-244</sup>

## **Histopathology**

LHON is characterized by a very selective degeneration of a single cell type, the retinal ganglion cells (RGCs). Thus, RGCs are somehow particularly sensitive to the mitochondrial energy defect due to the presence of LHON pathogenic mutations. All 1.2 million fibers of the optic nerve derive from the retinal ganglion cells (RGC) of the inner retina.<sup>220,245,246</sup> These cells have to transmit under all optical conditions and ensure axoplasmic transport all the way to distant primary visual nuclei.<sup>245,247</sup> Moreover, the retinal nerve fibers run a long course without the myelin sheath, so that there is not saltatory conduction of action potential until past *lamina cribrosa*. In order to maintain the optical transparency and the consequently good visual resolution, these axons become myelinated only after they have exited the eye and formed the optic nerve (Fig. 15).<sup>244</sup> Thus, the high dependence of these cells on mitochondrial oxidative

phosphorylation may explain the particular sensitivity of RGCs and the related visual loss due to mitochondrial dysfunction. In the perifoveal macula, the RGCs are concentrated, then from the fovea, the number of RGCs decreases, becoming relatively sparse in the periphery.<sup>220,245,246</sup> In addition there are two different classes of RGCs: the magno (M)-cells and the parvo (P)-cells, probably belonging to different class of neurons.<sup>248</sup> Recent studies of the intraretinal ganglion cell axons have shown that varicosities, very rich in mitochondria and in desmosome- and hemidesmosome-like junctions, are present in single axons.<sup>248</sup> Probably, these are functional sites, with high energy demand, important for signal transmission.<sup>249</sup> Only a few LHON cases have been studied histopathologically, none during the acute stage of the disease and only three were molecularly defined and studied by both light and electron microscopy.<sup>220</sup> A drastic loss of RGC and NFL was reported in all cases (one 11778/ND4, one 14484/ND6 plus 4160/ND1, and one 3460/ND1, reviewed by Carelli et al., 2004).<sup>220</sup> The 11778/ND4 and 3460/ND1 cases displayed a complete loss of central fibers with various degrees of axonal sparing in the periphery and absence of inflammatory signs.<sup>250-252</sup> A diffuse axons demyelination, accumulation of mitochondria, cellular debris and cytoskeleton rearrangements were found in both cases. Some evidence of remyelination was also observed, suggestive of a still ongoing low-grade degenerative process long after the clinical onset of LHON.<sup>220</sup> The 14484/4160 case, a “LHON plus” patient, displayed some residual RGC with swollen mitochondria and double-membrane bodies with calcium inclusions.<sup>253</sup> This case is peculiar because of the double mutation and the clinical phenotype, characterized by LHON and MELAS overlap syndrome.<sup>242,254</sup>

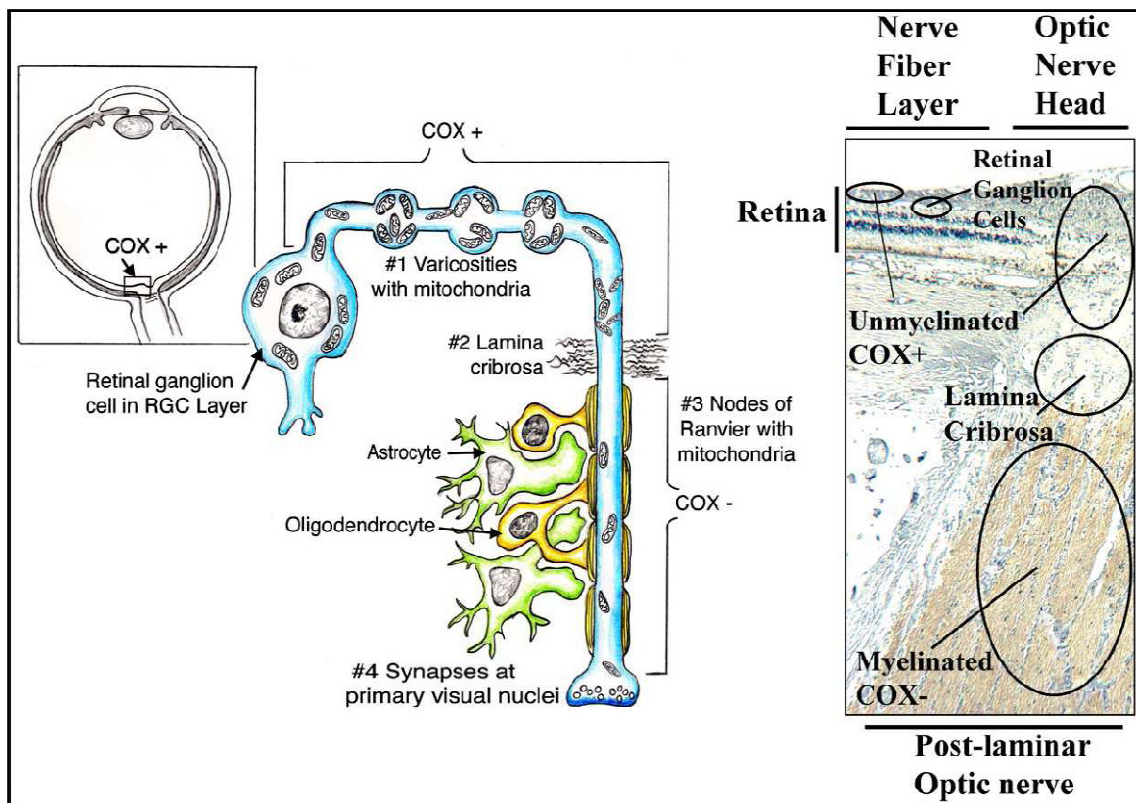


**Fig. 15** Mitochondria distribution within the optic nerve. From Carelli V, Ross-Cisneros FN, Sadun AA. *Prog Retin Eye Res.* 2004; 23:53-89.

## Genetics

LHON is transmitted with a maternal pattern of inheritance, due to the presence of point mutations on mtDNA. The most common pathogenic mutations are 11778/ND4, 3460/ND1, and 14484/ND6, characterizing about 90% of LHON cases. Several putatively pathogenic mutations have also been reported in single cases or families and still need a confirmation. In table 3 are reported all the LHON pathogenic, confirmed and putative, mutations. All LHON reported mutations have been identified in mitochondrial genes encoding complex I subunits. Other mitochondrial polymorphisms, either common or rare, have been associated with LHON and are defined as “secondary mutations” by some authors.<sup>255</sup> Their role is still debated, but recent findings demonstrated definitively that both 11778/ND4 and 14484/ND6 mutations are associated respectively with mitochondrial subhaplogroup J2b and J1c, and that the 3460/ND1 mutation is associated with haplogroup K.<sup>191</sup> Probably, accumulation of non

synonymous polymorphisms in ND subunits and the *cytb*, most of them being the previously defined secondary mutations, gene can increase the penetrance of LHON.<sup>191</sup> Other studies confirm that one particular sub-branch of haplogroup J is associated with a unique, very old founder event for the 14484/ND6 mutation.<sup>256</sup> This founder is responsible for their tight association in some specific populations, such as the French-Canadians and the Dutch.<sup>220,256,257</sup> This combination seems to induce a very low penetrance in females (male-female ratio 8:1, compared to other mutations 4-6:1) and could be an explanation for the tendency of 14484/ND6 and 11778/ND4 mutations to persist longer within a population when associated with haplogroup J.<sup>220</sup>

Mutation	Frequency	Gene	Amino acidic change	Heteroplasmy	Homoplasmy
G11778A	Frequent	ND4	R340H	+	+
G3460A	Frequent	ND1	A52T	+	+
T14484C	Frequent	ND6	M64V	+	+
A14495G	Rare	ND6	L60S	+	-
T14482A/G	Rare	ND6	M64I	+	+
T10663C	Rare	ND4L	V65A	-	+
C4171A	Rare	ND1	L289M	+	+
C14568T	Rare	ND6	G36S	-	+
G3700A	Rare	ND1	A132T	-	+

**Tab. 3** LHON pathogenic mutations, with corresponding genes, amino acidic change and heteroplasmy/homoplasmy detection.

However, this aspect does not explain completely the variable penetrance and the male prevalence, two LHON features that remain still unclear. Even if the majority of LHON families carry the mtDNA pathogenic mutation in the homoplasmic condition, many individuals belonging to the maternal lineage are not clinically affected. Thus, the existence of other genetic determinants, such as nuclear modifying genes, has been suggested and widely debated.<sup>258</sup>

Chromosome X has been extensively investigated, but to date no modifying gene has been identified yet.<sup>258,259</sup> Several approaches have been tried unsuccessfully, in order to find a modifying gene, such as linkage analysis, X-inactivation pattern analysis, or by directly sequencing of candidate genes.<sup>260-266</sup> Only recently, two different loci have been identified on chromosome X.<sup>267,268</sup>

Another factor that may influence LHON penetrance, triggering the pathological

features in previously unaffected mutation carriers, is the exposure to certain environmental factors. These includes not only tobacco smoking and alcohol consumption, but also exposure to n-hexane and other solvents, head trauma, non-controlled diabetes, ethambutol, and antiretroviral therapy in HIV patients.<sup>220,269</sup>

### **Biochemistry**

Primary LHON mutations generally induce moderate changes in the catalytic function of complex I, with the only exception of 3460/ND1 mutation, the most severe, which has been shown to decrease the electron transport activity of complex I.<sup>270,271</sup> Different studies, based on the investigation of complex I specific activity on different tissue of LHON patients and cell lines, do not shown a visible reduction in complex I activity, at least with 11778/ND4 and 14484/ND6 mutations.<sup>270-273</sup> Interestingly, these mutations affect the overall mitochondrial respiration, driven by complex I substrates, and different percentages of reduction have been reported. Moreover, mitochondria carrying the three common LHON mutations show a decreased sensitivity to rotenone, a powerful complex I inhibitor, and the 14484/ND6 and 3460/ND1 mutations induce an increase sensitivity of complex I to myxothiazol and nonyl-benzoquinol.<sup>274,275</sup> These results suggest that LHON mutations may influence the interaction between complex I and ubiquinone, and that the three subunits affected by LHON mutations may constitute part of the ubiquinone binding site.<sup>273</sup>

Several biochemical analyses have been carried out on cellular model, mainly primary cultures of patients' fibroblasts and transmitochondrial cytoplasmic hybrids (cybrids, Fig. 16). Cybrids are generated from human immortalized cell lines, lacking their mtDNA (the so called Rho<sup>0</sup>), and repopulated with patients mitochondria, harboring mtDNA mutations.<sup>276</sup> The result is a transmitochondrial cell line in which only the features dependent on the patient mtDNA are co-transferred, dissected from the original nuclear genome and placed in a "neutral" nuclear background. In this widely used cellular model the main biochemical features of LHON mutations have been reproduced.<sup>272</sup>

The impairment of complex I may induce a partial decrease of net energy production and a slight chronic increase of oxidative stress. Both hypotheses have been tested and many evidences have been found. Baracca and coll., 2005, showed that complex I-driven ATP synthesis is consistently reduced with all three common LHON mutations, even though

cells may compensate this energy impairment by alternative pathways, such as glycolysis and complex II/glycerol 3-phosphate dehydrogenase.<sup>277</sup> These results fit with the <sup>31</sup>P magnetic resonance spectroscopy (MRS) results in LHON patients, indicating a defective ATP synthesis in skeletal muscle and/or brain.<sup>278,279</sup>

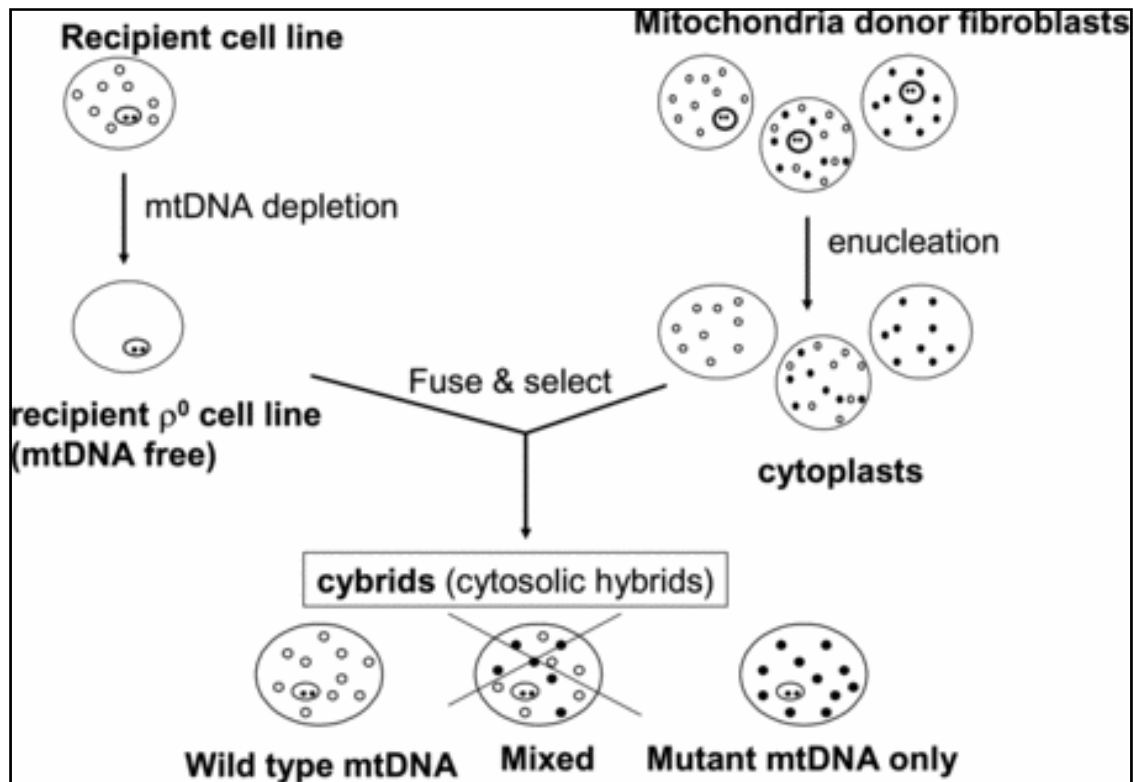


**Fig 16** Scheme of cybrids generation process. From Maechler P, de Andrade PB. *Biochem Soc Trans.* 2006; 34:824-827.

On the other hand, an increased ROS production and chronic oxidative stress may be relevant for LHON pathophysiology. A significant increase in ROS generation and glutathione depletion, have been indeed observed in NT2 neuronal differentiated LHON cybrids carrying the 11778/ND4 and 3460/ND1 mutations and in osteosarcoma cybrids.<sup>280-282</sup> Drastic changes in the mitochondrial antioxidant enzymatic machinery were also observed culturing cells in glucose free/galactose medium, suggesting a possible burst of oxidative stress, which may be implicated in the apoptotic cell death observed in LHON cybrids under these conditions of forced oxidative metabolism.<sup>283,284</sup> Using a medium without glucose and containing only galactose, the slow metabolism of

galactose to glucose-1-phosphate is not sufficient for the cells to synthesize the ATP necessary by glycolysis, and cells are forced to rely on respiratory chain for ATP synthesis. Thus, cells with a respiratory chain defect are not able to grow in similar conditions. In fact, incubation of LHON cybrids in galactose medium cause cell death characterized by the typical apoptotic hallmarks, including changes in nuclear morphology, chromatin condensation and fragmentation of chromosomal DNA.<sup>285</sup> The cell death characterization study revealed that, even if there was a significant release of cytochrome c from mitochondria, the galactose-induced death process was caspase-independent, and involved AIF and EndoG.<sup>286,287</sup> The early reduction of ATP levels observed under the galactose conditions possibly prevents the execution of apoptosis through the “classical” cytochrome c-mediated caspase-dependent pathway, whereas AIF and EndoG, once translocated to the nucleus, may account for the cell death process.<sup>287</sup> Moreover, an increased sensitivity to cell death was also reported in LHON cybrid after treatment with Fas, a well-known activator of the extrinsic apoptotic pathway.<sup>288</sup> Only recently it has been demonstrated that, even if the LHON mutations do not affect the steady state levels of respiratory chain complexes, an accumulation of low molecular weight subcomplexes is evident in LHON cybrids. Moreover, LHON mutants belonging to different haplogroups shows a differentially delayed assembly rates of complexes I, III and IV, revealing that specific mtDNA polymorphisms may modify the pathogenic potential of LHON mutations.<sup>192</sup>

### **Therapy and experimental treatments**

Currently, none of the proposed treatments, such as vitamins, cofactors, steroids and surgical treatment, is effective.<sup>220,245</sup> The clinical trial of the neuroprotective agent brimonidine, during the acute phase of LHON, did not reveal any protective effect in the involvement of the second eye, during the disease progression.<sup>289</sup>

A partial improvement of visual recovery and of neurological symptoms have been described with the treatment with idebenone, a coenzyme Q analogue.<sup>290,291</sup>

Another approach recently proposed is based on allotopic expression of corrected mitochondrial genes transferred to the nucleus and targeted to mitochondria. This approach has been used to rescue the biochemical defect, due to mutations 8993 in ATPase 6 gene (NARP/MILS) and 11778 in ND4 gene (LHON).<sup>292,293</sup> However, the

use of this approach is still controversial, especially because of the lacking of complete and long-lasting rescue.<sup>294,295</sup> Recently, an optimization of allotopic expression for mitochondrial genes ATPase6, ND1 and ND4 has been developed, obtaining a complete restoration of mitochondrial activity in mutated human fibroblasts.<sup>296,297</sup> The same authors also demonstrated that the allotopic expression of the human mitochondrial ND4 prevents blindness in a LHON rat model. The LHON 11778/ND4 mutation was introduced in rat eyes in vivo by electroporation causing the RGCs degeneration. Subsequent electroporation with the wild-type ND4 gene prevented the degeneration and the impairment of visual function.<sup>298</sup> Another similar approach, consists to complement the mitochondrial defect through the expression of a transgene with ND subunits from other species. This approach has been applied on human cybrids bearing the 11778/ND4 mutation, using the nuclear protein Ndi1, a rotenone sensitive NADH-quinone oxidoreductase, from *S.cerevisiae*.<sup>299</sup> Mutant cells expressing Ndi1 show a recovery in complex I specific activity and in complex I driven respiration, a partial increase in ATP synthesis, a decrease in ROS production and are able to grow in galactose medium.<sup>299</sup>

The biochemical phenotype of LHON mutations includes an increase of cellular oxidative stress, due to the “electron leaking” of impaired complex I. Different strategies have been tested in order to reduce the chronic oxidative condition. Ghelli et al., 2008, demonstrated that exogenous glutathione is the only one, in a variety of antioxidant and antiapoptotic compounds, able to reduce the cell death induced by the exposure of LHON cybrids to oxidative stress.<sup>300</sup> Moreover, the overexpression of human MnSOD is able to rescue the apoptotic cell death induced by galactose medium in mutant cells 11778/ND4.<sup>301</sup>

# **Aims**

Leber's hereditary optic neuropathy (LHON) is one of the most common mitochondrial diseases, characterized by a very rapid loss of central vision and optic atrophy, due to the selective degeneration of retinal ganglion cells. The age of onset is around 20, and the degenerative process is fast and usually the second eye becomes affected in weeks or months. Even if this pathology is well known and has been well characterized, there are still open questions on its pathophysiology, such as the male prevalence, the incomplete penetrance and the tissue selectivity.

Most, but not all the patients clinically characterized as LHON have a molecular diagnosis. This is due to the fact that the 90% of LHON cases are caused by one of the three common mtDNA mutations (11778/ND4, 14484/ND6 and 3460/ND1), but the remaining 10% is caused by rare pathogenic mutations, reported in literature in one or few families. Moreover, there is also a small subset of patients reported with new putative pathogenic nucleotide changes, which awaits to be confirmed.

The first aim of this research project was the identification of new pathogenic mutation or the validation of rare known mutations in families with a clear clinical diagnosis of LHON, but negative at the screening for the three classic mutations. The assessment of pathogenicity for a mitochondrial mutation is still debated. Mitchell and coll., 2006, proposed a new score system for the assignment of pathogenic value of mtDNA mutations.<sup>302</sup> This score system considers as parameters the presence of a biochemical defect in affected and non affected tissues, functional studies, the independent identification of the same mutation in unrelated cases, the heteroplasmy and the conservation through different species. Thus, our purpose was the generation of a complete alignment of ND1-ND6 and ND4L subunits of complex I and, being the structure of the hydrophobic core of this enzyme still not known, the elaboration of new models for the secondary structure of these proteins. Both these *in-silico* analysis may help us to better understand the possible impact of a non-synonymous nucleotide change on protein structure and function. Furthermore, these models may suggest a recurrent pattern of pathogenic mutations and clarify their genotype-phenotype correlation. Furthermore, they may be useful for the identification of a functional role for polymorphic variants fixed during evolution in different mtDNA haplogroups.

LHON is usually a monosymptomatic disorder, but there is a subset of patients with a syndromic form of optic atrophy referred as "Leber's plus", which may include central

nervous system involvement with frequent movement disorders.<sup>231,232</sup> The occurrence of “Leber’s plus” in certain cases has been related to specific mtDNA mutations, different from the common LHON mutations or has been linked to a combination of different mtDNA mutations, including the association of one primary LHON mutation and other putative pathogenic changes or the co-occurrence of two primary LHON mutations. The second aim of this research project was to understand if some particular polymorphisms of mtDNA may have a functional role in Leber’s plus cases, influencing the clinical expression of the primary mutations. In particular we analyzed the mtDNA sequence in two unrelated Italian families with LHON plus myoclonus, and evidence of maternal transmission.

Probably, one of the most interesting and unclear aspect of LHON is the variable penetrance. This phenomenon is common in LHON families, most of them being homoplasmic mutant. Inter-family variability of penetrance may be caused by nuclear or mitochondrial ‘secondary’ genetic determinants or other predisposing factors. However, within-family variability of penetrance in pedigrees with homoplasmic mutation harbored by all maternal related individuals remains unexplained. Thus, our third aim was to identify some molecular markers that may clearly differentiate affected individuals from carriers. In several mitochondrial disorders, the respiratory chain impairment is followed by an increase in mitochondrial mass, a common cellular strategy to compensate the energy defect. The compensatory activation of mitochondrial biogenesis is particularly evident in MELAS and MERRF, in which there is a massive subsarcolemmal accumulation of aberrant mitochondrial (RRFs) in patients’ skeletal muscle fibers. In LHON this accumulation is less evident, but an increase in SDH staining in skeletal muscle has been shown. Thus, the focus of this part of the project was the investigation of mitochondrial biogenesis in LHON patients. This part of the project was carried out in collaboration with Dr. Carla Giordano and Prof. Giulia d’Amati, at the University La Sapienza, Roma.

To date, there is no therapy for LHON and many approaches have been tried to rescue the energetic defect in LHON cell lines. The last aim of this project was to analyze the potential therapeutic role of molecules reported in literature able to induce mitochondrial biogenesis. To this end, we investigated in a cellular model the

biosynthetic pathway driving mitochondrial biogenesis, and how its activation may rescue the pathologic cellular phenotype of LHON.

# **Materials and methods**

### **Sequence alignment and conservation analysis**

The protein sequences of ND1-ND6, ND4L, ATPase6 and COII genes were obtained from the non-redundant SwissProt database (<http://www.expasy.org/sprot>). All the available complete mitochondrial sequences were downloaded and three sequence sets were created, corresponding to eukaryotes, vertebrates and mammals. These data sets were aligned with ClustalX ver. 2.1 maintaining the default parameters.<sup>303</sup> The analysis of amino acid conservation of the aligned sequences was carried out by GeneDoc, a sequence editor able to calculate the percentage of amino acid conservation for each position in the query alignment.<sup>304</sup> In this way we also identified the most representative amino acidic residues and calculates their prevalence at each position within the alignment, setting the value of 70% as conservation threshold. For *cytochrome b* protein we used the alignment from Degli Esposti M. available on-line in the “The bc<sub>1</sub>-complex” home page ([http://www.life.uiuc.edu/crofts/bc-complex\\_site/](http://www.life.uiuc.edu/crofts/bc-complex_site/)).

### **Prediction analysis of pathogenicity of amino acid substitutions**

PolyPhen, SIFT and PMut (<http://tux.embl-heidelberg.de/ramensky/polyphen.cgi>, <http://blocks.fhcrc.org/sift/SIFT.html>, <http://mmb2.pcb.ub.es:8080/PMut/>) were used to predict the possible impact of amino acid substitutions on the protein.

PolyPhen is a program based on sequence comparison with homologous proteins; profile scores (PSIC, Position-Specific Independent Counts) are generated for the allelic variants and represent the logarithmic ratio of the likelihood of a given amino acid occurring at a particular site relative to the likelihood of this amino acid occurring at any site. PSIC score differences above 2 indicate a damaging effect; scores between 1.5 and 2 suggest that the variant is possibly damaging, whereas scores below 1.5 indicate that the variant is benign.<sup>305</sup>

SIFT is a sequence homology-based tool that sorts intolerant from tolerant amino acid substitution, based on the premise that protein evolution is correlated with protein function. Positions important for function should be conserved in an alignment of the protein family, whereas unimportant positions should appear diverse in an alignment.<sup>306</sup>

SIFT follows a multistep procedure that searches for similar sequences, chooses related sequences, obtains the alignment of these sequences, and calculates normalized probabilities for all possible substitutions from the alignment. Positions with normalized

probabilities less than 0.05 are predicted to be not tolerated, those greater than or equal to 0.05 are predicted to be tolerated.

Also PMut is a tool for the prediction of disease-associated amino acid mutations, which uses only sequence-based information (amino acid properties, evolutionary information, secondary structure and accessibility predictions, and database annotations) but is based on neural networks.<sup>307</sup> Mutations are predicted to be either pathological or neutral. The overall success rate is 83.5 %, with a 66.5 % improvement over random when only sequence-derived information is included, while when structure is available the success rate increases to 87.0 % and the improvement over random to 73.0%. Thus, this program has the best success rate compared to the other two (SIFT 70.3 % overall success rate and 37.0 % improvement over random, PolyPhen 73.5% success rate with 41.4 % improvement over random).

### **Generation of ND1-ND6 subunit structural models**

The alignments produced for ND1-ND6 subunits were used to generate a consensus sequence for each gene. The hydrophobicity profile of these sequences and the average hydrophobicity along each position in the alignments was generated using three different hydropathy scales: RAO-AR, based on membrane-buried-helix parameters, MPH, based on membrane propensity for haemoproteins, and AMP07, based on the average of seven different hydrophobicity scales, including RAO-AR and MPH. These scales have been widely described and validated by Degli Esposti and coll., 1989 and 1990.<sup>308,309</sup> The resulting hydrophobicity profiles define for each subunits the number of transmembrane helices (TMH). When helices were predicted at least 5/6 times they were considered reliable. The transmembrane models topology was assessed based on the net charge and positioning the positive side in the mitochondrial matrix and the negative side in the mitochondrial intermembrane space.

### **Cell lines and cultures conditions**

Human transmitochondrial hybrids (cybrids) were grown in DMEM added with 10% fetal bovine serum (FBS), 2 mM L-glutamine, 100 units/mL penicillin, and 100 µg/mL streptomycin and 0.1 mg/mL bromodeoxyuridine (complete medium). Cell lines were grown in a humidified incubator at 37°C with 5% CO<sub>2</sub>. For incubations in galactose

medium it has been used DMEM glucose-free medium supplemented with 5mM galactose, 2 mM L-glutamine, 5 mM Na-pyruvate and 10% FBS (galactose medium). For incubations with bezafibrate (BF), complete medium was supplemented with BF 100  $\mu$ M (diluted in DMSO, stock 20 mM), or the corresponding volume of DMSO.

### **Growth curve in galactose or bezafibrate medium**

Cells ( $3 \times 10^4$ ) were seeded into 24-well plates and, after 24 hours, were washed twice with PBS and incubated with galactose medium, or in complete medium with bezafibrate or DMSO. At the end of incubation cells were harvested and counted using the Z1 COULTER COUNTER<sup>®</sup> Cell and Particle Counter (Beckman Coulter).

### **Cell viability measurements**

Cells ( $3 \times 10^4$ ) were seeded into 24-well plates and, after 24 hours, were washed twice with PBS and preincubated 24 hour in complete medium with bezafibrate or DMSO, and then incubated in galactose medium supplemented with bezafibrate or DMSO. The sulforodhamine B (SRB) assay was performed following the manufacturer's conditions. Briefly, at the end of incubation time, cells were fixed with 50% trichloroacetic acid (TCA) for 1 hour at 4°C, washed 5 times with H<sub>2</sub>O and finally dried for 1 hour at room temperature. Cells were then stained with SRB 0.4% diluted in 1% acetic acid for 1 hour at room temperature, washed 4 times with 1% acetic acid, and disrupted with 10 mM Tris-HCl pH 9.8. The absorbance of SRB was detected with Victor3 plate reader (Perkin Elmer) at the wavelength of 560 nm.

### **Total cellular lysates preparation**

Cells were seed into 78 cm<sup>2</sup> dishes in complete medium, after 24h, cells were washed in PBS and incubated for 72h in medium with bezafibrate 100  $\mu$ M or DMSO. At the end of incubation time cells were scraped in 100  $\mu$ L of RIPA lysis buffer [PBS, 1% Triton X-100, 0.5 mM EDTA, 0.6 mM PMSF and 100  $\mu$ L/mL protease inhibitors]. The lysate was incubated in ice for 15', frozen and thawed in liquid nitrogen twice, sonicated in waterbath for 2' and centrifuged at 12000rpm for 10' at 4°C. The supernatant was then collected and protein content was assessed according to Bradford.<sup>310</sup>

### **Western blotting of mitochondrial proteins**

Total cellular lysates were resuspended in Laemmli buffer (20% glycerol, 4% SDS, 125 mM Tris-HCl pH 6.8, 10%  $\beta$ -mercaptoethanol, 0.004% bromophenol blue). Samples were denatured at 100°C for 5' before loading on the polyacrilamide gel. Fifty micrograms of protein were separated by SDS-PAGE (10% acylamide/bis-acrylamide) electrophoresis and transferred onto nitrocellulose membrane (BioRad). Antibodies used were: mouse antibodies for complex I, IV and V subunits, purchased in cocktails from MitoSciences; goat polyclonal antibody for  $\beta$ -actin purchased from Santa Cruz Biotechnology. Mouse antibodies for complex I, IV and V subunits were used according to the manufacturer's instructions. Goat polyclonal antibody for  $\beta$ -actin was used at 1:1000 dilution. Incubation with secondary antibodies (dilution 1:5000) and subsequent detection by chemiluminescence were done with SuperSignal West Pico Chemiluminescent Substrate (Thermo Scientific) according to the manufacturer's instructions.

### **Spectrophotometric assays for respiratory chain complexes and citrate synthase activity.**

Spectrophotometric assays for OXPHOS complexes and citrate synthase activity were performed using a double wavelength spectrophotometer (Jasco V550), under stirring and controlled temperature.

Respiratory chain complexes activity (I, II+III, III and IV) were evaluated in platelet homogenate freshly prepared from 100 mL of venous blood as described by Carelli et al., 1997, and Degli Esposti et al., 1994.<sup>271,273</sup>

Specific NADH ubiquinone oxidoreductase and cytochrome *c* oxidase activities were determined in cells grown in complete medium according to Benit et al., 2006.<sup>311</sup> with minor modifications. Briefly, small aliquots of cells were deep-frozen in 50  $\mu$ L PBS and then thawed in 1 mL of ice-cold medium 1 [0.25 M sucrose, 20 mM Tris (pH 7.2), 40 mM KCl, 2 mM EGTA, 1 mg/mL BSA, 0.01% digitonin (w/v), 10% Percoll (v/v)]. Cells were incubated 10 minutes in ice, centrifuged for 5 min at 5000rpm and the supernatant was discarded. The pellet was then washed with 1mL of medium 1 devoid of digitonin and Percoll and centrifuged for 5 min at 8000rpm. Finally, the pellet was resuspended in 30  $\mu$ L of medium 1 devoid of digitonin and Percoll. Complex IV activity

was determined following the absorbance of reduced cytochrome *c* at wavelengths 550 nm and 540 nm ( $\epsilon = 19.1 \text{ mM}^{-1} \text{ cm}^{-1}$ , 37°C). The assay was performed in 1 mL of medium A [10 mM  $\text{KH}_2\text{PO}_4$  (pH 7.2), 1 mg/mL BSA] and the reaction was blocked by addition of 0.3 M KCN. Complex I specific activity was determined following the absorbance of NADH at wavelengths 340 nm and 380 nm ( $\epsilon = 4.87 \text{ mM}^{-1} \text{ cm}^{-1}$ , 37°C). The assay was performed in 1 mL of medium B [50 mM Tris (pH 8.0), 5 mg/mL BSA] and the reaction was blocked by addition of 8  $\mu\text{M}$  rotenone. Citrate synthase activity was determined as described by Trounce et al., 1996.<sup>312</sup> and protein content was assessed according to Bradford.<sup>310</sup>

### **ATP synthesis assay**

The measurements of mitochondrial ATP synthesis were done in cells grown in DMEM-glucose according to Manfredi et al. 2002.<sup>313</sup> with minor modifications. Briefly, after trypsinization, cells were resuspended ( $7 \times 10^6/\text{mL}$ ) in buffer A [10 mM KCl, 25 mM Tris-HCl, 2 mM EDTA, 0.1% bovine serum albumin, 10 mM potassium phosphate, 0.1 mM  $\text{MgCl}_2$  (pH 7.4)], kept for 15 minutes at room temperature, and then incubated with 50  $\mu\text{g}/\text{mL}$  digitonin for 1 minute. After centrifugation, the cells pellet was resuspended in buffer A and aliquots were taken to measure ATP synthesis, protein content, and citrate synthase activity. Aliquots of cells were incubated with 5 mM malate plus 5 mM pyruvate (complex I-driven substrates) in the presence or absence of 10  $\mu\text{g}/\text{mL}$  oligomycin, or with 10 mM succinate plus 2  $\mu\text{g}/\text{mL}$  rotenone (complex II-driven substrate), and 0.2 mM ADP for 1 and 3 minutes. The amount of ATP was measured as described.<sup>287</sup> Adenosine 5'-triphosphate (ATP) Bioluminescent Assay Kit was from Sigma Aldrich. The rate of ATP synthesis was expressed as a ratio of citrate synthase activity.<sup>312</sup> Protein concentration was determined according to Bradford.<sup>310</sup>

### **Nucleic acid extraction**

DNA samples were extracted from different tissues (whole blood, skeletal muscle, urinary epithelium, platelet fraction and hair) using the standard phenol-chloroform method, resuspended in MilliQ water and stored at -20°C. Cells from a confluent 75  $\text{cm}^2$  flask were pelleted and washed once in PBS. PBS was removed and DNA extracted with the standard phenol-chloroform method.

Total RNA was extracted from human skeletal muscle bioptic fragments and cultured cells (cybrids). Approximately, 50 sections of 20  $\mu\text{m}$  were obtained from frozen tissue samples and total RNA was extracted using the RNeasy Micro Kit (Qiagen) following the manufacturer protocol. Briefly, sections were disrupted with 150 $\mu\text{L}$  RLT buffer plus 143 mM  $\beta$ -mercaptoethanol and vortexed. The lysis buffer is then diluted with 290  $\mu\text{L}$  RNase-free water and treated with 10  $\mu\text{L}$  of Proteinase K (10 mg/mL) at 55°C for 10 minutes. The homogenate was subsequently centrifuged for 3 minutes at 10000g at room temperature with the purpose to eliminate any eventually present tissue debris. The sample was transferred in a new tube and 0.5 volumes of ethanol 100% were added and loaded in a MinElute Spin Column (Qiagen). After a series of washes the total RNA is finally eluted with 14  $\mu\text{L}$  of RNase-free water.

Cybrids were grown in a 78  $\text{cm}^2$  cell culture dish; when the cells were confluent, total RNA was extracted with TRIzol (Invitrogen) following the manufacturer suggested protocol. RNAs samples were precipitated with isopropanol followed by centrifugation for 10 minutes at 4°C at 12000g, and then the pellets were washed, dried and resuspended in RNase-free water. All the RNA samples were treated with DNase I (Promega), to avoid any contamination with genomic DNA, at 37°C for 30 minutes, followed by enzyme inactivation at 65°C for 10minutes.

Nucleic acid concentration and purity was evaluated measuring 1  $\mu\text{L}$  of sample with Nanodrop 1000 Spectrophotometer (Thermo Scientific), at the wavelengths 260 nm and 280 nm.

### **Identification of LHON common mutations**

The PCR mixture contained 2 ng of DNA, 0.2 U Taq DNA Polimerase (Eppendorf), 1x Buffer Advanced (Eppendorf), 200  $\mu\text{M}$  PCR nucleotide Mix (Roche), 200  $\mu\text{M}$  each primer (Invitrogen), in a final volume of 25  $\mu\text{L}$ .

For the PCR reaction we used a GeneAmp PCR System 2700 (Applied Biosystems) thermal cycler. Primers sequences and PCR conditions are reported in appendix B. The PCR reaction was checked with an electrophoresis on agarose gel and ethidium bromide staining. The PCR fragments were of 119 bp (11778/ND4), 75 bp (14484/ND6) and 398 bp (3460/ND1).

The PCR products were subsequently digested with the following restriction enzymes LweI (Fermentas) for the G11778A mutation, Bsp143I (Fermentas) for the G14484A mutation and Hin1I (Fermentas) for the T3460A mutation. LweI recognize a restriction site in the *wild type* DNA and generates two fragments of 64 bp and 55 bp; Bsp143I recognize a restriction site in the *wild type* DNA and produce two fragments of 64 bp and 21 bp; Hin1I recognize a restriction site in the mutant DNA and produce two fragments of 298 bp and 91 bp.

The digestion mixture was composed by 5 or 8  $\mu\text{L}$  of PCR product, 1 U/ $\mu\text{L}$  of restriction enzyme, 1x suggested Buffer, in a final volume of 10  $\mu\text{L}$ , and was incubated for 16 hours at 37°C. Subsequently the fragments were separated with electrophoresis on Metaphor (BioSpa) gel at 3% or 4% and displayed with ethidium bromide staining.

### **Mitochondrial DNA complete sequencing**

The complete mtDNA sequencing was carried out on DNA samples extracted from venous blood, in the Laboratory of Genetics, Dipartimento di Genetica e Microbiologia, Università di Pavia (Prof. Antonio Torroni), as previously described.<sup>314</sup>

### **Restriction fragment length polymorphism (RFLP) assay for LHON rare mutations**

The PCR mixture contained 2 ng of DNA, 0.2 U Taq DNA Polimerase (Eppendorf), 1x Buffer Advanced (Eppendorf), 200  $\mu\text{M}$  PCR nucleotide Mix (Roche), 200  $\mu\text{M}$  each primer (Invitrogen), in a final volume of 25 $\mu\text{L}$ .

For the PCR reaction we used a GeneAmp PCR System 2700 (Applied Biosystems) thermal cycler. Primers sequences and PCR conditions are reported in appendix B. The PCR reaction was checked with an electrophoresis on agarose gel and ethidium bromide staining.

The digestion mixture was composed by 5 or 8  $\mu\text{L}$  of PCR product, 1 U/ $\mu\text{L}$  of restriction enzyme, 1x suggested Buffer, in a final volume of 10  $\mu\text{L}$ , and was incubated at the suggested temperature. The enzyme list, digestion conditions and fragment length are shown in table 4. Subsequently the fragments were separated with electrophoresis on Metaphor (BioSpa) gel at 3% or 4% and displayed with ethidium bromide staining.

Mutation	Enzyme	Temperature/Time	Mutant fragments size (bp)	Wild type fragments size (bp)
14258	BamHI	37°C / 16h	575	446, 129
14495	NlaIII	37°C / 3h	102, 98	130
14459	MaeIII	55°C / 16h	139, 25	164
3700	HhaI	37°C / 16h	479	258, 221
14568	AciI	37°C / 16h	298	160, 138
14568	BcgI	37°C / 16h	160, 138	298
4172	BseMI	55°C / 16h	130, 20	150

**Tab. 4** LHON candidate pathogenic mutation, digestion conditions, enzyme list (Fermentas) and digestion fragment length.

#### RFLP assay for rare polymorphisms

The PCR mixture contained 2 ng of DNA, 0.2 U Taq DNA Polimerase (Eppendorf), 1x Buffer Advanced (Eppendorf), 200 µM PCR nucleotide Mix (Roche), 200 µM each primer (Invitrogen), in a final volume of 25 µL.

For the PCR reaction we used a GeneAmp PCR System 2700 (Applied Biosystems) thermal cycler. Primers sequences and PCR conditions are reported in appendix B. The PCR reaction was checked with an electrophoresis on agarose gel and ethidium bromide staining.

The digestion mixture was composed by 5 or 8 µL of PCR product, 1 U/µL of restriction enzyme, 1x suggested Buffer, in a final volume of 10µL, and was incubated at the suggested temperature. The enzyme list, digestion conditions and fragment length are shown in table 5. Subsequently the fragments were separated with electrophoresis on Metaphor (BioSpa) gel at 3% or 4% and displayed with ethidium bromide staining.

Polymorphism	Enzyme	Temperature/Time	Mutant fragments size (bp)	Wild type fragments size (bp)
4136	NlaIII	37°C / 3h	74, 26	100
9319	TaaI	65°C / 16h	380, 139	519
15773	BsrI	65°C / 16h	1709	480, 1229

**Tab. 5** LHON candidate pathogenic mutation, digestion conditions, enzyme list (Fermentas) and digestion fragment length.

### **Analysis of the functional polymorphism G1444A in the PGC-1 $\alpha$ gene**

The PCR mixture contained 2 ng of DNA, 0.2 U Taq DNA Polimerase (Eppendorf), 1x Buffer Advanced (Eppendorf), 200  $\mu$ M PCR nucleotide Mix (Roche), 200  $\mu$ M each primer (Invitrogen), in a final volume of 25  $\mu$ L.

For the PCR reaction we used a GeneAmp PCR System 2700 (Applied Biosystems) thermal cycler. Primers sequences and PCR conditions are reported in appendix B. The PCR reaction was checked with an electrophoresis on agarose gel and ethidium bromide staining.

The PCR product (260 bp) was subsequently digested with the restriction enzyme HpaII (Fermentas). This enzyme recognize the palindromic sequence 5'-CCGG-3', and is able to cut the allele G, producing two fragments of 111 and 149 bp, while the allele A remains uncut. The digestion mixture was composed by 5 or 8  $\mu$ L of PCR product, 1 U/ $\mu$ L of restriction enzyme, 1x suggested Buffer, in a final volume of 10  $\mu$ L, and was incubated for 16 hours at 37°C. Subsequently the fragments were separated with electrophoresis on Metaphor (BioSpa) gel at 4% and displayed with ethidium bromide staining.

### **Mitochondrial DNA copy number evaluation**

Absolute quantification of mtDNA relative to nuclear DNA (nDNA) was performed by a real-time PCR based method using the LightCycler480 (Roche). This method is a multiplex assay based on hydrolysis probe chemistry. A mtDNA fragment (ND2 gene) and a nDNA fragment (FasL gene) were co-amplified by multiplex polymerase chain reaction according to the primers, probes and conditions previously published.<sup>315</sup> These two fragments were cloned tale to tale in a vector and serial dilutions were used to construct a standard curve, obtaining a ratio of 1:1 of the reference molecules. Primers and probes sequences and PCR conditions are available on request.

### **Reverse transcription**

Reverse transcription was performed on extracted RNA, using Transcriptor First Strand cDNA Synthesis Kit (Roche) and following the manufacturer's protocol. The cDNA was generated performing a reverse transcription of 2  $\mu$ g of total RNA using random hexameric primers.

### **Relative quantitative PCR assays for mitochondrial biogenesis related genes**

Relative mRNA quantification was performed by a real-time PCR based method using the instrument LightCycler480 (Roche). This method is a singleplex assay based on SybrGreen I chemistry. The mRNAs amount relative to target genes (PGC-1 $\alpha$ , PGC-1 $\beta$ , PRC and Tfam) was determined using the human  $\beta$ -actin as reference. Primer sequences and PCR conditions are reported in appendix B.

### **Statistical analysis**

Statistical analysis was performed using the SigmaStat ver.3.5 software package, choosing the most appropriate test. For mtDNA copy number analysis within the Brazilian family, ANOVA Dunn's test or Mann-Whitney test were performed, being the values from these samples not normally distributed. Linear regression analysis was performed to correlate mtDNA copy number and age. For mtDNA copy number analysis in Italian families paired t-test was used for blood and ANOVA Holm-Sidak test for skeletal muscle. For analysis of PGC-1 $\alpha$  genotypes,  $\chi^2$  or Fisher's exact tests were performed. For correlation of mtDNA copy number and PGC-1 $\alpha$  genotypes, ANOVA was performed. For relative gene expression analyses paired t-test was used on raw  $\Delta$ Ct data. For cellular analyses t-test or ANOVA were performed. Data were considered significantly different for p-values < 0.05.

# **Results**

## Part 1 - Role of mtDNA variants in LHON: pathogenic mutations and synergistic polymorphisms

### Conservation analysis and structural models of complex I subunits

In order to establish the pathogenic potential of mtDNA mutations and the possible functional role of some common polymorphic variants, a conservation analysis on ND1-ND6 and ND4L protein sequences has been carried out. The number of complete sequences, for each protein, downloaded from the non-redundant SwissProt database is reported in table 6. Moreover, we have downloaded, aligned and analyzed complete protein sequences of COX2 and ATPase6 subunits (Tab. 6). These sequences have been divided in three subsets, corresponding to eukaryotes, vertebrates and mammals, and used to generate global alignments.

Subunit	Eukaryotes	Vertebrates	Mammals
ND1	140	106	81
ND2	119	88	62
ND3	137	89	67
ND4	88	51	38
ND4L	90	63	55
ND5	96	51	38
ND6	86	75	41
ATP 6	97	58	38
COX2	286	184	162

**Tab. 6** Number of complete mitochondrial protein sequences used for the generation of ND1-6, ND4L, COX2 and ATPase6 global alignments.

For each position, the percentage of amino acid conservation has been calculated and a consensus sequence has been generated, identifying the most prevalent amino acid along each alignment. The average of protein conservation and the percentage of conserved amino acids have been calculated and reported in table 7. Considering both parameters, the most conserved ND subunit is invariably ND1 (average conservation from 70.95% in eukaryotes to 84.90% in mammals), whereas the less conserved is ND6 (average conservation from 55.89% in eukaryotes to 71.15% in mammals). The conservation among the other subunits varies in the three different data sets. As

expected, the average conservation and the percentage of conserved amino acid increase with the reduction of evolutionary distances, independently from the protein. However, considering each single amino acid position, this is not a general rule, being some amino acid position more conserved in eukaryotes and vertebrates than in mammals.

Complex I subunit	Eukaryotes		Vertebrates		Mammals	
	Average conservation (%)	Conserved amino acid (%)	Average conservation (%)	Conserved amino acid (%)	Average conservation (%)	Conserved amino acid (%)
<b>ND1</b>	70.95	58.81	81.72	72.33	84.90	76.73
<b>ND2</b>	57.55	33.43	67.27	45.82	75.01	59.65
<b>ND3</b>	62.18	46.96	75.12	60.00	79.71	67.83
<b>ND4</b>	60.30	34.86	76.83	63.18	82.68	74.73
<b>ND4L</b>	60.03	38.78	72.33	55.10	80.24	66.33
<b>ND5</b>	55.69	26.70	73.16	56.55	79.38	68.66
<b>ND6</b>	55.89	28.16	60.05	29.31	71.15	54.02

**Tab. 7** Percentages of average conservation and conserved amino acids in the ND1-6 and ND4L alignments, for each data set.

The analyses of consensus sequences hydrophobicity and average hydropathy along the alignments allow us to identify the putative transmembrane segments, characterized by  $\alpha$ -helix secondary structure (TMH), and to generate a structural model for each ND subunit.

The scales AMP07 and RAO-AR predict the same number of TMHs, for ND1, ND2, ND3, ND4L and ND6 subunits, considering the average or consensus sequences hydrophobicity. In the case of ND4 and ND5, the same TMHs are predicted for both scales, but this number varies if we consider average or consensus sequences hydropathy.

MPH scale recognizes different TMHs using average or consensus sequences hydrophobicity and predicts an equal number or less  $\alpha$ -helix compared to AMP07 and RAO-AR. This is due to the more restrictive assignment of hydrophobicity to each amino acid and to the higher MPH threshold of hydrophobicity (1.1 for MPH versus 1.0 for AMP07 and RAO-AR). In order to consider the influence in the prediction analysis of each scale, each transmembrane domain has to be predicted at least by 5 analyses on

a total of 6 (considering the three scales for average and consensus sequences hydrophathies).

### ***ND1 subunit***

In the ND1 subunit AMP07 and RAO-AR clearly predict 8 TMHs, whereas MPH predicts 7  $\alpha$ -helices using the average hydrophathy and 6  $\alpha$ -helices using the consensus sequence. Figure 17A shows the hydrophathy profile generated with MPH scale on the consensus sequence obtained from eukaryotes global alignment. Our model represents ND1 with 6 TMHs and 1 amphipathic helix (named helix E in figure 17) protruding in the mitochondrial intermembrane space. The boundaries of helix E are the amino acid positions 220-240 and this helix shows a peculiar double peak hydrophathy plot, with a very profound decrease of hydrophobicity in the middle of the helix. The conservation analysis reveals that ND1 is extremely conserved in mammals (Tab. 7), presenting 115 invariant residues (36% of the protein) and 8 invariant zones corresponding to extra-membrane loops AB, CD, DE and FG. In vertebrates there are 77 invariant amino acids (24% of the protein) and 5 invariant regions in the previously cited loops. The alignment of eukaryotes sequences reveals the lack of invariant zones and only three invariant residues (Arg-134, Pro-197 and Phe-198), probably the most important for ND1 function.

Mitomap reports 12 nucleotide changes associated with LHON or LHON plus other mitochondrial diseases in ND1 subunit (Fig. 17B). Only one of these is defined as confirmed (G3460A), whereas 2 are reported as unclear (G3316A and T3394C), 8 as reported (G3376A, G3496T, C3497T, G3635A, G3700A, G3733A, T4160C, C4171A) and one as possibly synergistic (A4136G). According to our model, ten of the reported variants are located in extra-membrane loops (AB, CD, and FG) on the membrane side facing the mitochondrial matrix. These loops are very conserved regions of ND1 subunit and the presence of pathogenic mutations may underlie the importance of these regions for ND1 function. The nucleotide change G3316A, reported as unclear, is located in the N-terminal of the protein, whereas the possibly pathogenic mutation G3635A is located inside the TMH C. Common non-synonymous polymorphisms, associated with mtDNA haplogroups, are also present in ND1 gene (T3394C/J1c1,

---

A3505G/W, A3796G/H1b, C3992T/H4, A4024G/H4a and T4216C/R2-JT), affecting different positions of the polypeptide chain.

### ***ND2 subunit***

In the ND2 subunit AMP07 and RAO-AR predict 9 TMHs, whereas MPH predicts 8  $\alpha$ -helices with average hydrophathy and 7  $\alpha$ -helices with the consensus sequence. In figure 18A is shown the hydrophathy profile generated with MPH scale on the consensus sequence. In this model we propose 8 TMHs and a  $\alpha$ -helix in the C-terminal of the polypeptide chain (helix I) that can be either amphipathic or embedded in the membrane (Fig. 18). ND2 is a moderately conserved protein. Along mammalian sequences alignment there are 73 invariant residues (21% of the protein) and two hyper-conserved regions (130-135 and 169-173). In vertebrates and eukaryotes there are no invariant regions and respectively 37 and 6 invariants amino acid positions (10% and 1% of the protein). Only one nucleotide change may have a pathogenic potential for LHON (G5244A), and affect an amino acid position located in the loop GH, facing the intermembrane space. Conversely, several haplogroups defining non-synonymous polymorphisms have been accumulated in the ND2 gene (T4561C/K2a, T4639C/V1, C4640A/U3b-K1a5, A4917G/R1-T, 4960/N1b, G5046A/N2, C5263T/V1a, G5460A/W-J1b) affecting residues located both in extra-membrane loops and in membrane spanning regions.

### ***ND3 subunit***

This very small protein is predicted to fold in 3 TMHs by all the scales used in this study, corresponding to three wide hydrophobic regions (Fig. 19). ND3 shows a high overall conservation along mammals (Tab. 7), with 37 absolutely conserved amino acids (32% of the protein) and two hyper-conserved regions in helix A (aa 22-25) and helix B (aa 54-57). In vertebrates the invariant residues represent the 20% of the entire protein (23 amino acids), but no invariant regions can be defined. The overall conservation decrease in eukaryotes and only two residues are absolutely conserved Gly-40 and Glu-68, both located in extra-membrane loops (respectively AB and BC). Even in the absence of invariant zones, a large region with high local conservation can be observed from amino acid 32 to 77, representing the subunit core and covering part

of loops AB and BC and the entire helix B. In this region resides the only one reported mutation associated with LHON (T10237, Ile60Thr), whereas the population non-synonymous polymorphism A10398G, defining haplogroups L3, N1a, K1 and J, affects position 114 in the C-terminal of the protein.

#### ***ND4L subunit***

Similar to ND3, ND4L is a very small protein in which three TMHs are recognized by every hydrophobicity scale. Moreover, this protein presents three wide hydrophobic regions and consequently the TMHs boundaries cannot be clearly defined (Fig. 20). In mammals 29% of the polypeptide chain is represented by absolutely conserved amino acids and there is an invariant region corresponding to helix B. In vertebrates this percentage decreases at 10% and there is only one invariant amino acid (Glu-34) in eukaryotes. Three LHON possibly pathogenic mutations are reported on Mitomap (A10543G, T10591G and T10663C), affecting helices B and C. A single non-synonymous variant (A10506G) is associated with haplogroup U3a and hits Thr-13 in helix A.

#### ***ND4 subunit***

The hydrophobicity analysis of ND4 consensus sequence using AMP07 and RAO-AR scales reveals the presence of 14 hydrophobic segments, whereas for analysis conducted on average hydrophobicity only 13 TMHs are recognized. The more restrictive MPH scale predicts only 9 and 8  $\alpha$ -helices, respectively for average and consensus hydrophobicity. We here propose a model of ND4 with 10 defined TMHs and 2 helices (named in figure 21 A and J) with a controversial hydrophobicity plot that can be either membrane spanning or protrude in the intermembrane space. Moreover, the assignment of ND4 topology across the membrane is controversial, being both sides positively charged. In mammals 39% of amino acids results invariant and 8 hyper-conserved regions are present, including a very long stretch of 16 amino acids, from 214 to 229. This stretch corresponds to the loop EF, facing the intermembrane space where mutations or polymorphisms have never been reported. Along vertebrates' alignment, 106 amino acids (23% of the chain) and 3 extremely conserved regions can be identified. These regions include the previously reported long stretch divided in two zones (214-224 and 226-229). Finally,

in eukaryotes there are 13 invariant residues (3% of the protein), including 4 from the long hyper-conserved stretch (Trp-215, Leu-216, Hys-220 and Ser-228). At least 4 nucleotide changes are reported in Mitomap to be associated with LHON, but only G11778A is confirmed. This mutation induces the amino acid substitution Arg340Hys, an extremely conserved position in the intermembrane space loop IJ. Another reported mutation, C11874A, affects the loop JK on the same membrane side, whereas mutations T11253C and G11696A affect respectively loop DE and helix I. Moreover, two polymorphic variants of haplogroup K2c (A11015G and A11172G) hit ND4 subunit, precisely in loops BC and CD.

### ***ND5 subunit***

The largest mitochondrial-encoded complex I subunit is ND5. This protein shows 13 hydrophobic segments, considering the hydrophobicity of the consensus sequence, independently from the used hydropathy scale. If average hydrophobicity is considered, AMP07 and RAO-AR predict 15 TMHs, whereas MPH predicts only 13 TMHs. The proposed model represents ND5 with 13 membrane spanning segments (Fig. 22). Moreover, another hydrophobic region can assume a TMH structure or be an amphipathic helix outside the membrane on the matrix side (Fig. 22, helix I). The conservation analysis of ND5 reveals the existence of several conserved regions. In mammals 33% of the whole protein is represented by invariant amino acids and 9 absolutely conserved regions, including a long stretch of 18 amino acids (236-253), can be identified. This stretch is also evident along vertebrates' alignment and invariant amino acids cover the 18% of the polypeptide chain. In eukaryotes, 22 amino acids are absolutely conserved (3.6%) and there are two zones with high local conservation (143-155 and 222-256), corresponding to helix I and extra-membrane loops DE and IJ (Fig. 22).

At least 7 non-synonymous variants in ND5 gene have been associated with LHON or LHON and other mitochondrial diseases, none of them reported on Mitomap as confirmed. All these variants hit extra-membrane loops on both sides of the membrane and define at least one region (loops DE and FG) with a possible functional role (Fig. 22B). Several haplogroups defining variants induce changes in the ND5 polypeptide chain, most of them concentrated in loops LM and MN.

***ND6 subunit***

Every hydropathy scale predicts clearly 5 TMHs for ND6 subunit with a clearly defined topology (Fig. 23). ND6 is the most divergent ND subunit but in mammals shows a hyper-conserved box (amino acids 59-70) in the helix C with 40 invariant residues (23% of the polypeptide chain). In vertebrates and eukaryotes this region is still highly conserved, with at least 4 absolutely conserved amino acids (Gly-61, Gly-62, Phe-67 and Tyr-69). Mutations associated with LHON are concentrated in helix B, a moderate conserved region with high conserved amino acids, in helix C, especially in the invariant box, and in the loop DE (Fig. 23B). Some non-synonymous polymorphisms have been accumulated in ND6 in general population (T14307C/K2b, T14318C/C, C14365T/H4a and A14582G/H4a). These variants are located in helices B and D and in loop DE and they correspond to poorly conserved positions.

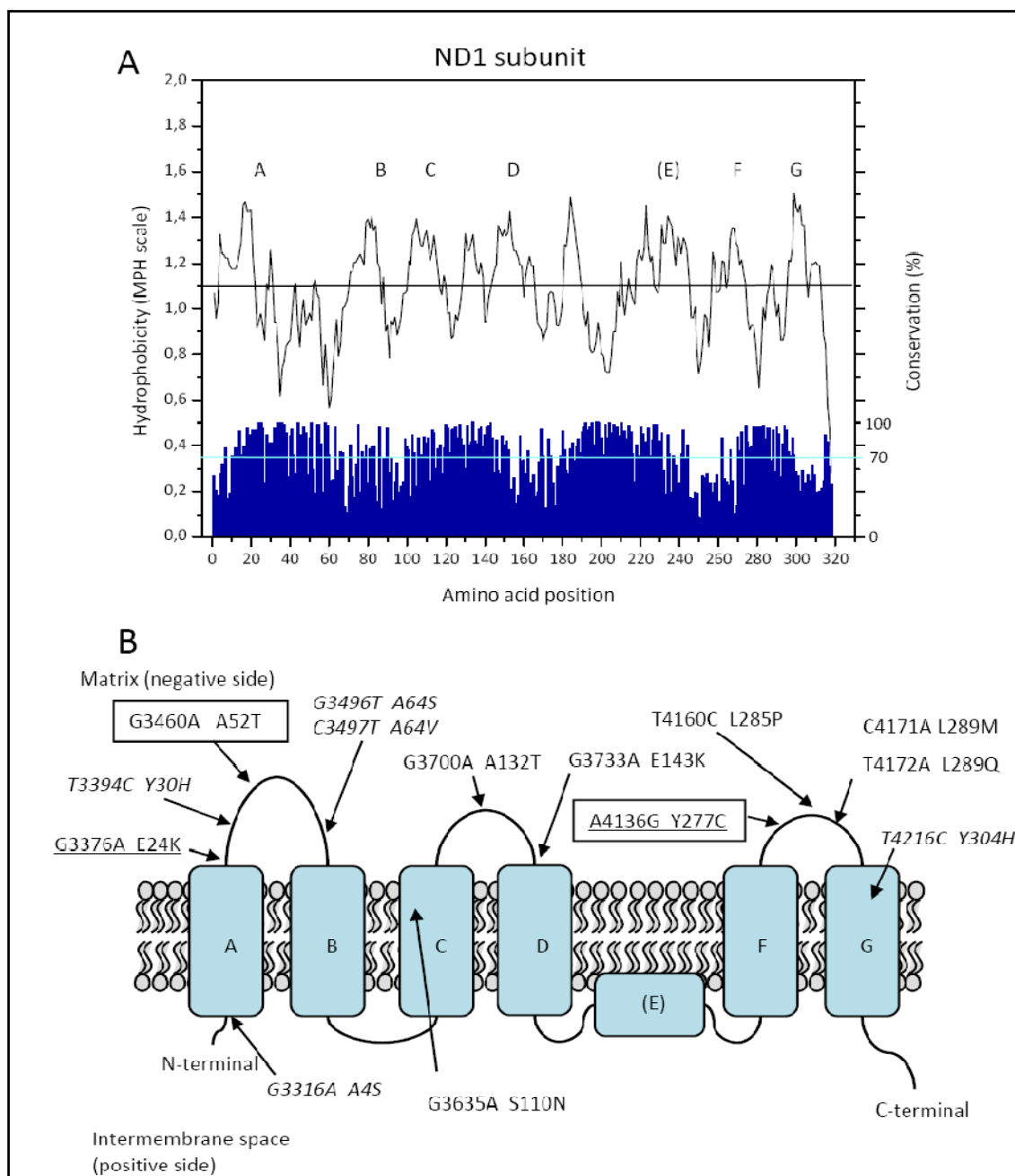


**Fig. 17** Hydrophathy plot, conservation analysis and protein model of ND1 subunit. A) Hydrophobicity profile of consensus sequence with MPH scale and percentage of conservation (blue bars) of each amino acid residue along the alignment of eukaryotic sequences. The conservation threshold of 70% is indicated with the light blue line. B) Structural model of ND1 subunit with corresponding nucleotide changes reported in Mitomap as associated with LHON. Possibly pathogenic mutations are in regular font, secondary and unclear variants are in italic, confirmed mutations are in the box and LHON plus or LHON/ other mitochondrial diseases overlap syndromes are underlined.

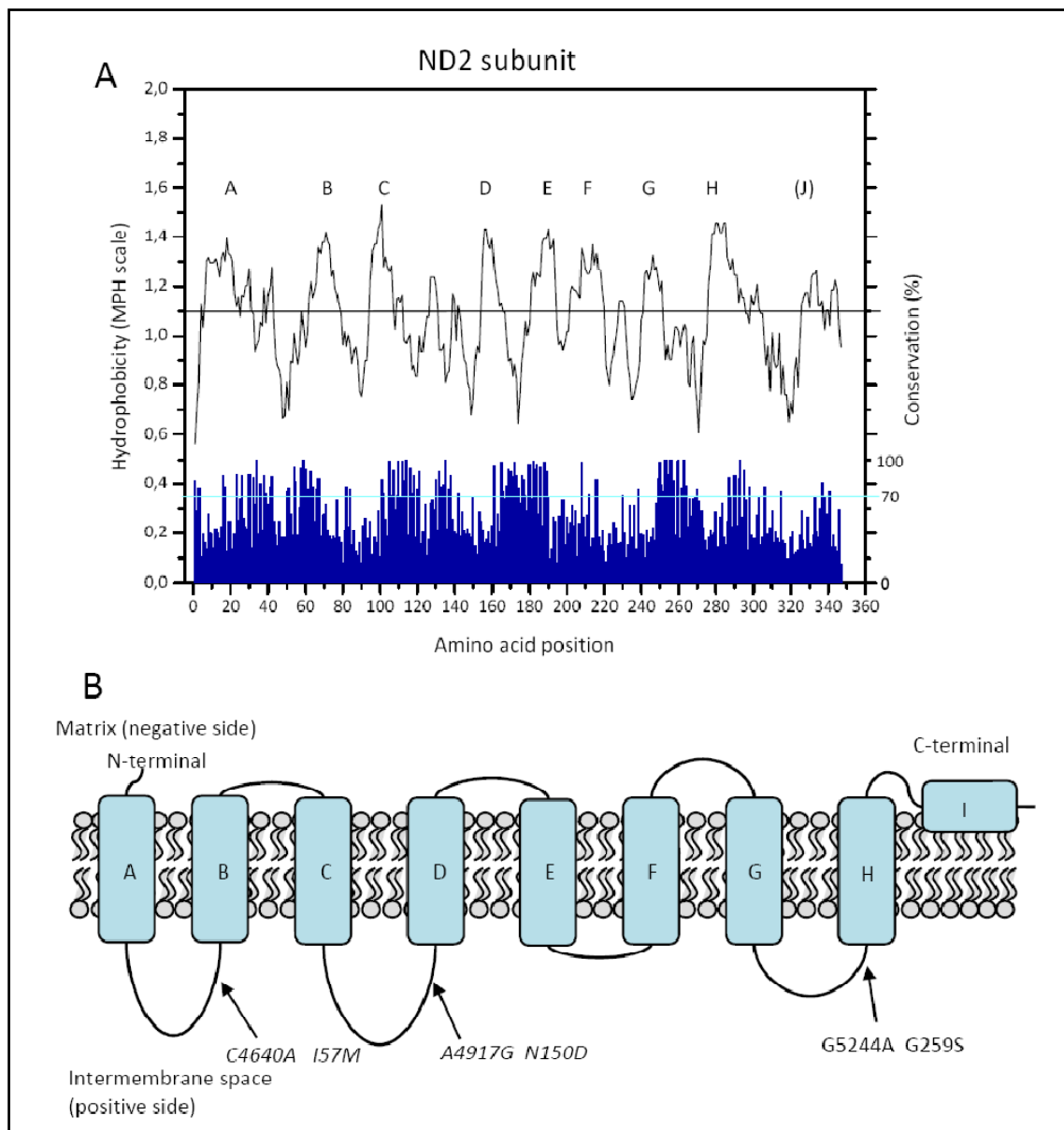


**Fig. 18** Hydrophathy plot, conservation analysis and protein model of ND2 subunit. A) Hydrophobicity profile of consensus sequence with MPH scale and percentage of conservation (blue bars) of each amino acid residue along the alignment of eukaryotic sequences. The conservation threshold of 70% is indicated with the light blue line. B) Structural model of ND2 subunit with corresponding nucleotide changes reported in Mitomap as associated with LHON. Possibly pathogenic mutations are in regular font, secondary and unclear variants are in italic, confirmed mutations are in the box and LHON plus or LHON/ other mitochondrial diseases overlap syndromes are underlined.

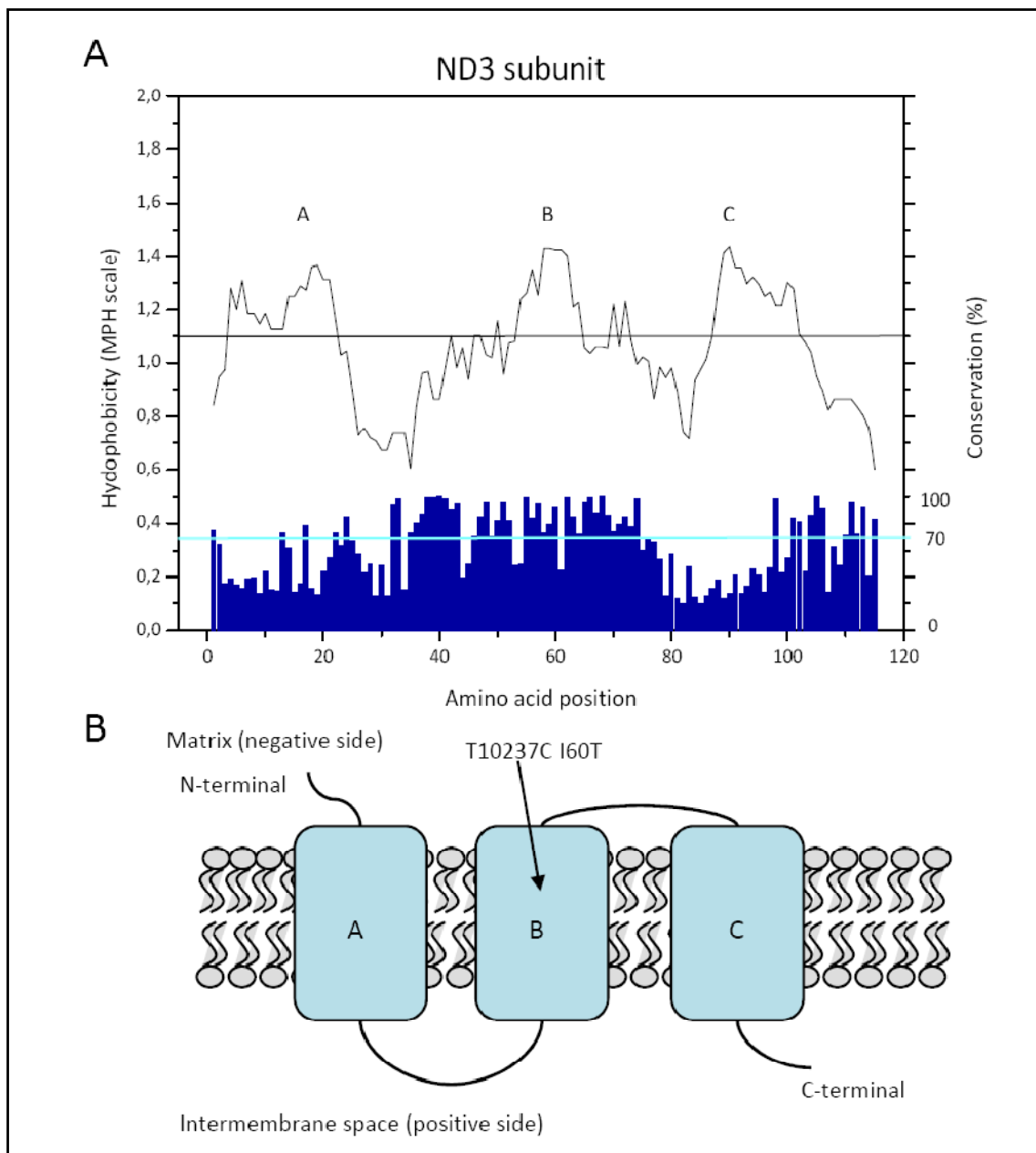


**Fig. 19** Hydropathy plot, conservation analysis and protein model of ND3 subunit. A) Hydropathy profile of consensus sequence with MPH scale and percentage of conservation (blue bars) of each amino acid residue along the alignment of eukaryotic sequences. The conservation threshold of 70% is indicated with the light blue line. B) Structural model of ND3 subunit with corresponding nucleotide changes reported in Mitomap as associated with LHON. Possibly pathogenic mutations are in regular font, secondary and unclear variants are in italic, confirmed mutations are in the box and LHON plus or LHON/ other mitochondrial diseases overlap syndromes are underlined.

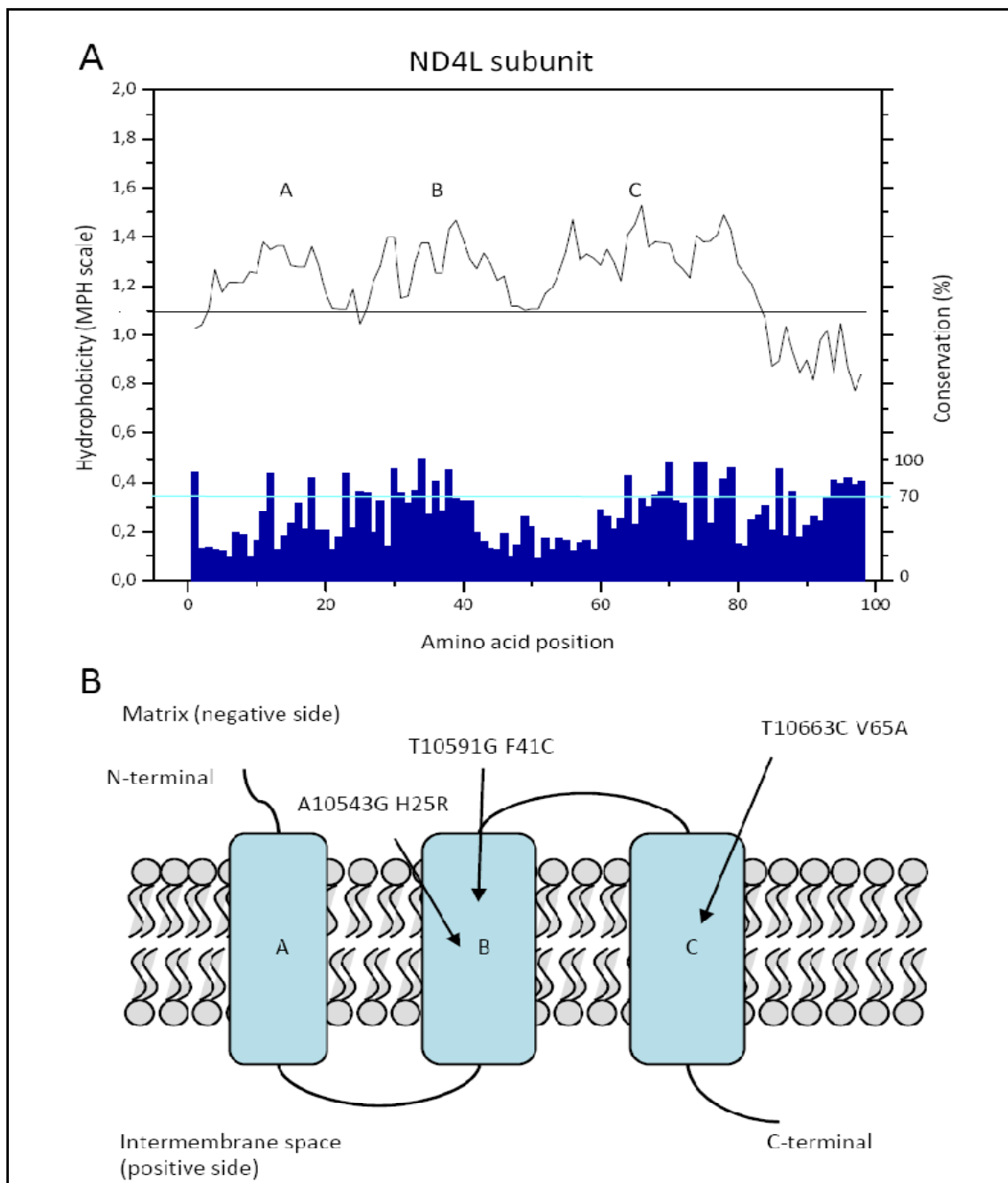


**Fig. 20** Hydrophathy plot, conservation analysis and protein model of ND4L subunit. A) Hydrophobicity profile of consensus sequence with MPH scale and percentage of conservation (blue bars) of each amino acid residue along the alignment of eukaryotic sequences. The conservation threshold of 70% is indicated with the light blue line. B) Structural model of ND4L subunit with corresponding nucleotide changes reported in Mitomap as associated with LHON. Possibly pathogenic mutations are in regular font, secondary and unclear variants are in italic, confirmed mutations are in the box and LHON plus or LHON/ other mitochondrial diseases overlap syndromes are underlined.

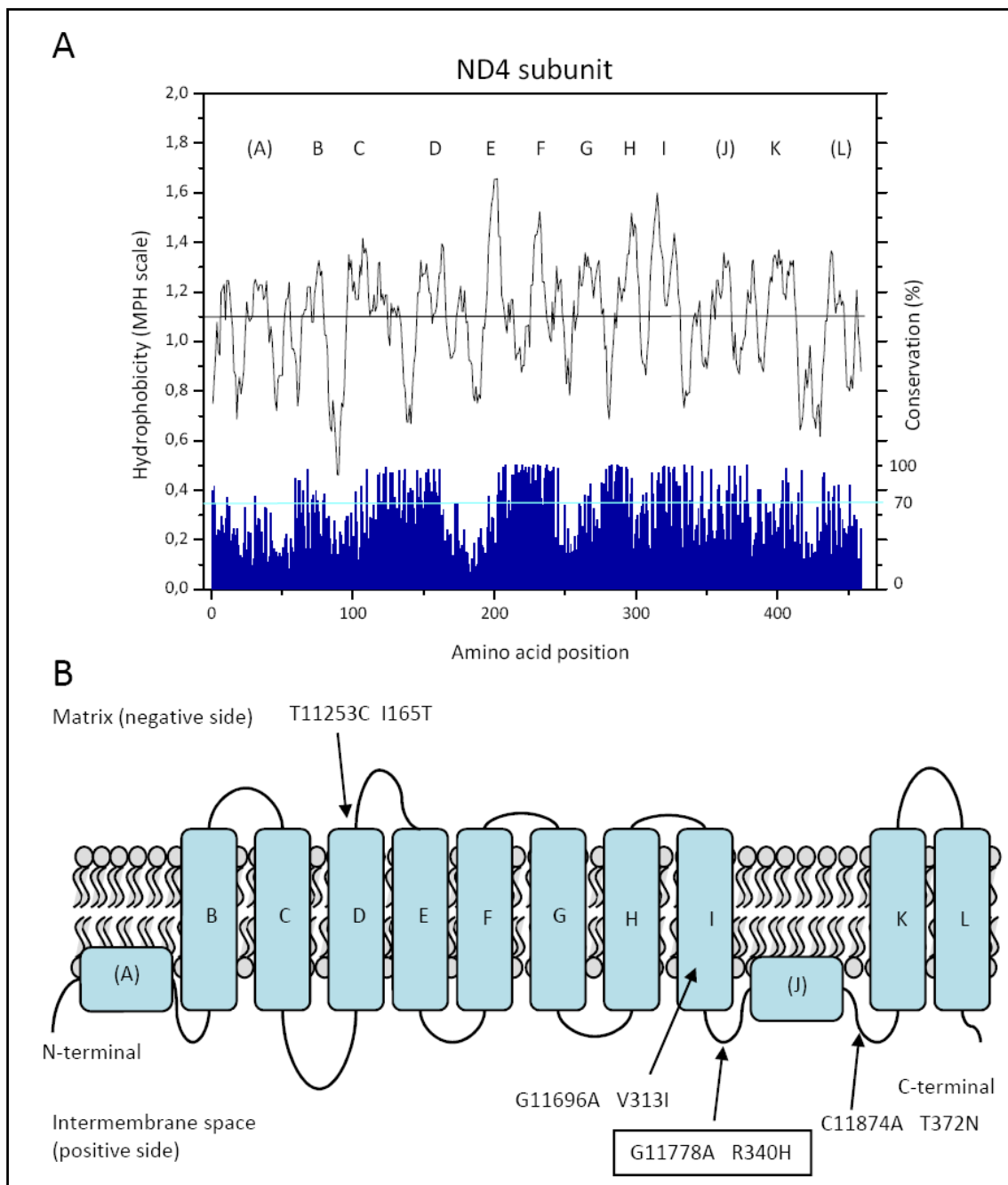


**Fig. 21** Hydrophathy plot, conservation analysis and protein model of ND4 subunit. A) Hydrophobicity profile of consensus sequence with MPH scale and percentage of conservation (blue bars) of each amino acid residue along the alignment of eukaryotic sequences. The conservation threshold of 70% is indicated with the light blue line. B) Structural model of ND4 subunit with corresponding nucleotide changes reported in Mitomap as associated with LHON. Possibly pathogenic mutations are in regular font, confirmed mutations are in the box and LHON plus or LHON/ other mitochondrial diseases overlap syndromes are underlined.

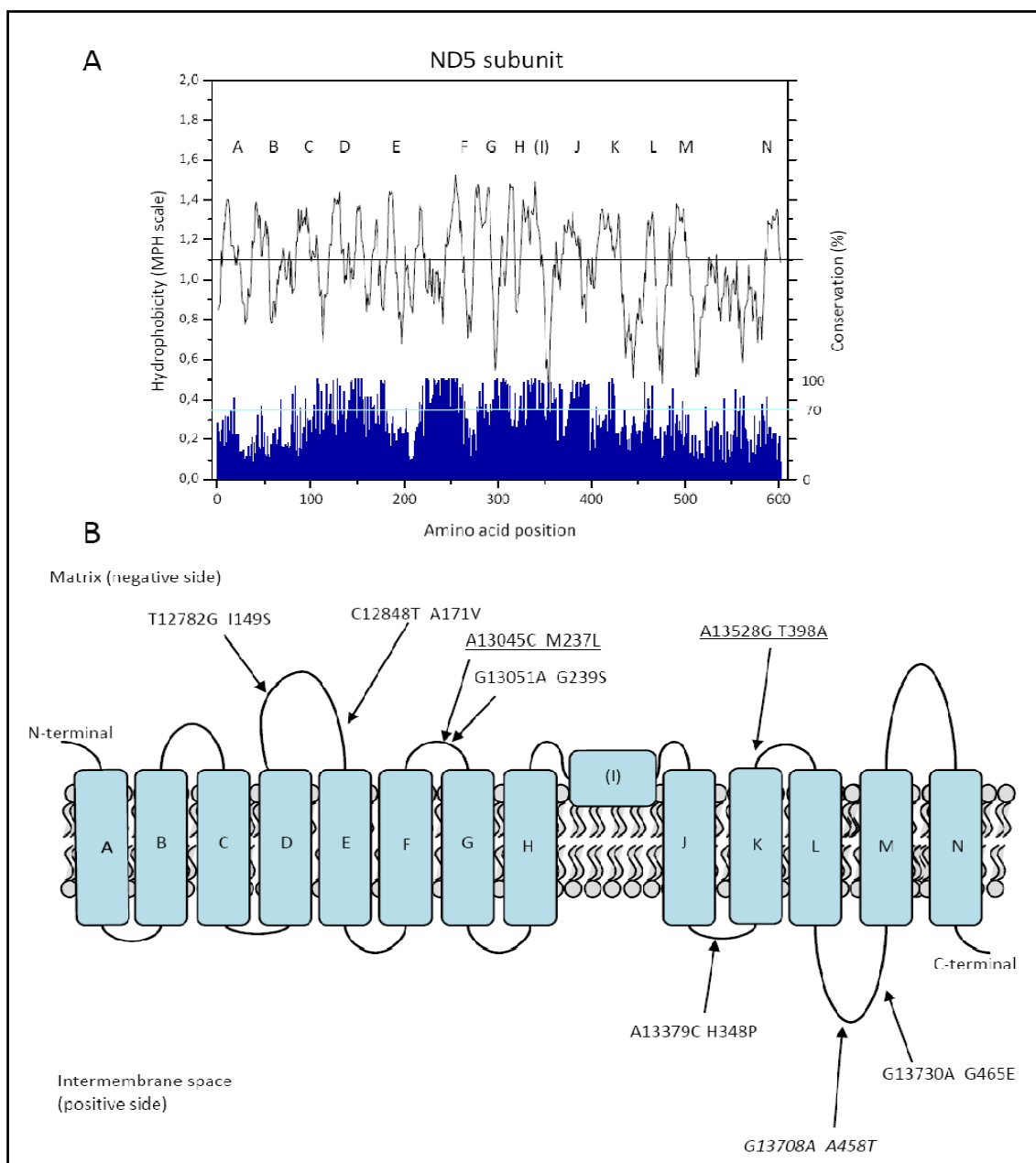


**Fig. 22** Hydrophathy plot, conservation analysis and protein model of ND5 subunit. A) Hydrophobicity profile of consensus sequence with MPH scale and percentage of conservation (blue bars) of each amino acid residue along the alignment of eukaryotic sequences. The conservation threshold of 70% is indicated with the light blue line. B) Structural model of ND5 subunit with corresponding nucleotide changes reported in Mitomap as associated with LHON. Possibly pathogenic mutations are in regular font, confirmed mutations are in the box and LHON plus or LHON/ other mitochondrial diseases overlap syndromes are underlined.

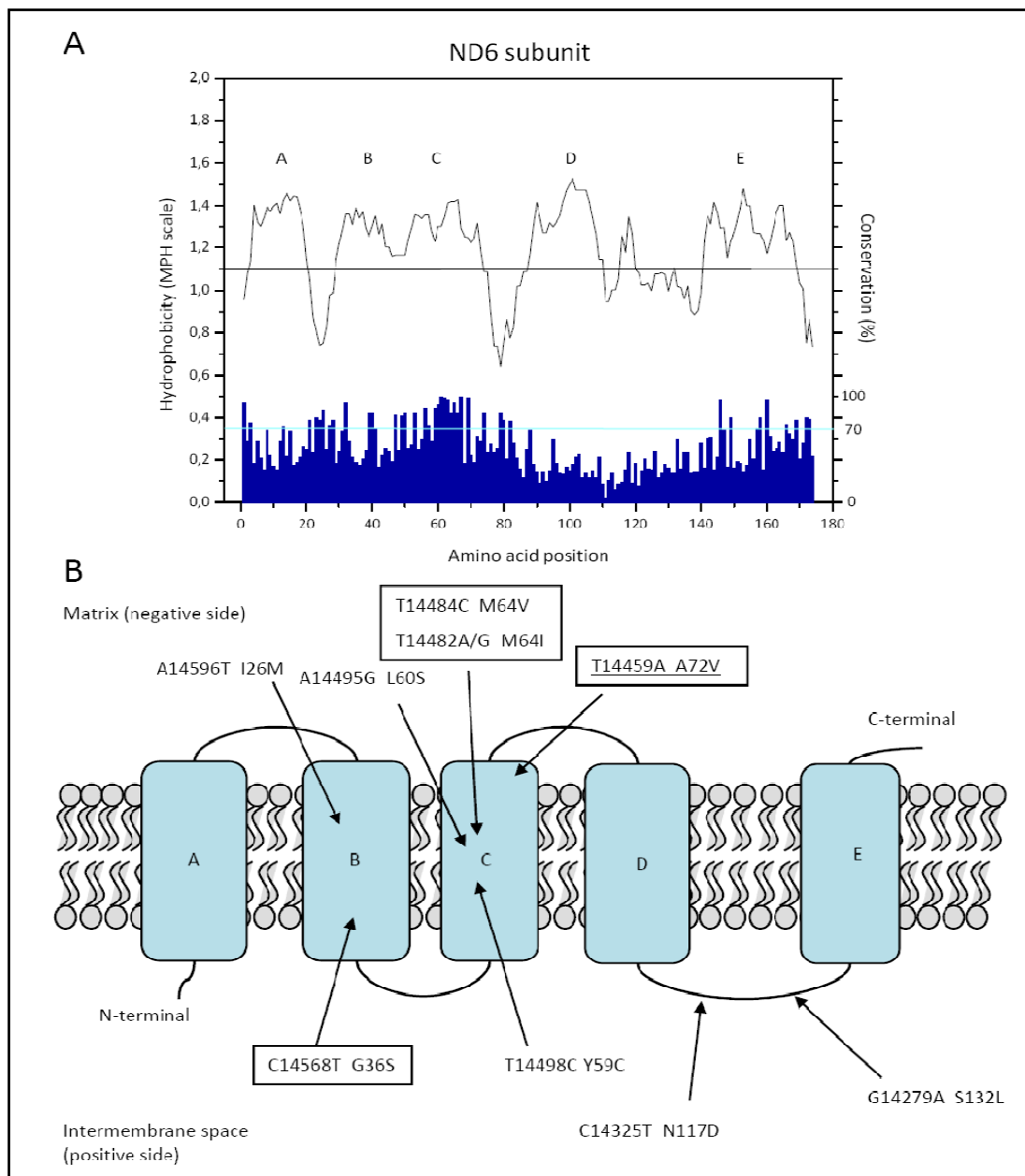


**Fig. 23** Hydropathy plot, conservation analysis and protein model of ND6 subunit. A) Hydrophobicity profile of consensus sequence with MPH scale and percentage of conservation (blue bars) of each amino acid residue along the alignment of eukaryotic sequences. The conservation threshold of 70% is indicated with the light blue line. B) Structural model of ND6 subunit with corresponding nucleotide changes reported in Mitomap as associated with LHON. Possibly pathogenic mutations are in regular font, confirmed mutations are in the box and LHON plus or LHON/ other mitochondrial diseases overlap syndromes are underlined.

### **Prediction of pathogenic potential of amino acid substitutions**

In this section we have analyzed the pathogenic potential of amino acid substitutions, due to mutations reported on Mitomap associated with LHON and with haplogroup related mtDNA polymorphisms. Conservation along alignments and three prediction tools available on-line (PolyPhen, SIFT and PMut) were used to assess the pathogenicity of these variants. Different predictions for each variant were obtained, depending on the selected method. If a variant is predicted as pathogenic at least by 3/4 methods, it is accepted as pathogenic, whereas if it is predicted by 2/4 methods it is considered uncertain. In tables 8 and 9 the analyzed variants with the corresponding pathogenicity prediction are reported.

Concerning the conservation analysis, 29/39 variants with potential pathogenic effects involve highly conserved positions along mammals (17 of those are invariants) and 27/39 along vertebrates (10 invariants). In eukaryotes only 22 variants affect a conserved amino acid and none of them invariant positions, underlining the extremely important role of these amino acids. Comparing the on-line prediction tools, PolyPhen results the most restrictive and predicts as possibly or probably pathogenic only 19/39 amino acid substitution with putative pathogenic role. SIFT predicts as non tolerated 24/39 variants, whereas PMut predicts as pathogenic 31/39 variants.

Every mutation cited on Mitomap as confirmed is predicted pathogenic by this integrated approach, with the only exception of C14568T/ND6 that has to be considered uncertain. The possibly synergistic variant A4136G/ND1 results pathogenic, whereas secondary mutations and unclear variants are predicted neutral or uncertain. Mitomap cites as 'reported' 28 variants; our analysis reveals that 19 may have a potential pathogenic role, 2 are uncertain and 7 are neutral.

The same approach has been applied on common polymorphisms conserved in European mtDNA haplogroups. In this case all the polymorphisms were predicted as not pathogenic, in fact 83% are neutral and only 17% are uncertain, mainly due to the moderate conservation of the affected amino acids (Tab. 9).

Locus	Disease	Nucleotide change	Amino acid change	Mitomap status	Amino acid conservation (%)			PolyPhen	SIFT	Pmut
					Mammals	Vertebrates	Eukaryotes	PSIC score	Tol-Non Tol	Score
ND1	NIDDM/LHON/PEO	G3316A	A4T	Unclear	66,67	64,08	55,71	0,211	T	0,5433
<u>ND1</u>	<u>LHON MELAS</u>	<u>G3376A</u>	<u>E24K</u>	<u>Reported</u>	<u>100</u>	<u>100</u>	<u>99,3</u>	<u>1,252</u>	<u>NT</u>	<u>0,9289</u>
<i>ND1</i>	<i>LHON/NIDDM</i>	<i>T3394C</i>	<i>Y30H</i>	<i>Unclear</i>	<i>97,53</i>	<i>96,26</i>	<i>82,52</i>	<i>0,731</i>	<i>T</i>	<i>0,5604</i>
<b>ND1</b>	<b>LHON</b>	<b>G3460A</b>	<b>A52T</b>	<b>Cfrm</b>	<b>97,53</b>	<b>70,09</b>	<b>59,44</b>	<b>1,646</b>	<b>NT</b>	<b>0,7564</b>
ND1	LHON	G3496T	A64S	Rep/Sec	62,96	54,21	47,18	0,669	T	0,2135
ND1	LHON	C3497T	A64V	Rep/Sec	62,96	54,21	47,18	0,151	T	0,8911
<u>ND1</u>	<u>LHON</u>	<u>G3635A</u>	<u>S110N</u>	<u>Reported</u>	<u>81,48</u>	<u>84,11</u>	<u>82,52</u>	<u>1,000</u>	<u>NT</u>	<u>0,6912</u>
<u>ND1</u>	<u>LHON</u>	<u>G3700A</u>	<u>A132T</u>	<u>Reported</u>	<u>97,53</u>	<u>93,4</u>	<u>80</u>	<u>0,743</u>	<u>NT</u>	<u>0,8188</u>
<u>ND1</u>	<u>LHON</u>	<u>G3733A</u>	<u>E143K</u>	<u>Reported</u>	<u>98,77</u>	<u>99,06</u>	<u>99,29</u>	<u>1,005</u>	<u>NT</u>	<u>0,9067</u>
<u>ND1</u>	<u>LHON</u>	<u>A4136G</u>	<u>Y227C</u>	<u>Pos syn</u>	<u>98,77</u>	<u>99,06</u>	<u>79,14</u>	<u>0,999</u>	<u>NT</u>	<u>0,9253</u>
ND1	LHON	T4160C	L285P	Reported	100	100	95,71	2,672	NT	0,9604
ND1	LHON	C4171A	L289M	Reported	98,77	83,02	57,86	0,051	T	0,1240
ND2	LHON	C4640A	I57M	Reported	80,65	89,77	66,39	0,419	T	0,3084
<u>ND2</u>	<u>LHON</u>	<u>G5244A</u>	<u>G259S</u>	<u>Reported</u>	<u>100</u>	<u>100</u>	<u>95,8</u>	<u>2,340</u>	<u>T</u>	<u>0,9388</u>
<u>ND3</u>	<u>LHON</u>	<u>T10237C</u>	<u>I60T</u>	<u>Reported</u>	<u>100</u>	<u>98,88</u>	<u>90,51</u>	<u>2,372</u>	<u>NT</u>	<u>0,8372</u>
ND4L	LHON	A10543G	H25R	Reported	100	98,41	84,44	3,419	NT	0,9011
<u>ND4L</u>	<u>LHON</u>	<u>T10591G</u>	<u>F41C</u>	<u>Reported</u>	<u>98,18</u>	<u>92,06</u>	<u>76,67</u>	<u>2,998</u>	<u>NT</u>	<u>0,9436</u>
<i>ND4L</i>	<i>LHON</i>	<i>T10663C</i>	<i>V65A</i>	<i>Reported</i>	<i>100</i>	<i>73,02</i>	<i>56,67</i>	<i>0,273</i>	<i>T</i>	<i>0,6545</i>
ND4	LHON; PD	T11253C	I165T	Reported	52,63	43,14	38,64	0,454	T	0,7019
ND4	LHON	G11696A	V313I	Reported	81,58	60,78	36,36	0,599	T	0,1251
<b>ND4</b>	<b>LHON</b>	<b>G11778A</b>	<b>R340H</b>	<b>Cfrm</b>	<b>100</b>	<b>100</b>	<b>98,86</b>	<b>2,608</b>	<b>NT</b>	<b>0,9763</b>
<u>ND4</u>	<u>LHON</u>	<u>C11874A</u>	<u>T372N</u>	<u>Reported</u>	<u>76,32</u>	<u>56,86</u>	<u>55,68</u>	<u>1,855</u>	<u>NT</u>	<u>0,7424</u>
ND5	LHON	T12782G	I149S	Reported	100	98,04	64,58	2,688	NT	0,6875
ND5	LHON	C12848T	A171V	Reported	100	100	86,46	2,097	NT	0,6527
<u>ND5</u>	<u>MELAS/LHON/LS</u>	<u>A13045C</u>	<u>M237L</u>	<u>Reported</u>	<u>100</u>	<u>100</u>	<u>98,96</u>	<u>2,814</u>	<u>NT</u>	<u>0,2867</u>
<u>ND5</u>	<u>LHON</u>	<u>G13051A</u>	<u>G239S</u>	<u>Reported</u>	<u>100</u>	<u>100</u>	<u>85,42</u>	<u>1,479</u>	<u>NT</u>	<u>0,7641</u>
ND5	LHON	A13379C	H348P	Reported	100	98,04	95,83	3,802	NT	0,8281
ND5	LHON-like	A13528G	T398A	Reported	47,37	47,06	28,13	0,060	T	0,1595
<u>ND5</u>	<u>LHON</u>	<u>G13730A</u>	<u>G465E</u>	<u>Reported</u>	<u>100</u>	<u>100</u>	<u>74,19</u>	<u>2,598</u>	<u>NT</u>	<u>0,9508</u>
ND6	LHON	G14279A	S132L	Reported	58,54	42,67	37,21	0,017	T	0,5366
ND6	LHON	T14325C	N117D	Reported	28,57	32,26	31,25	0,274	T	0,1682
<b>ND6</b>	<b>LYDT/LS</b>	<b>G14459A</b>	<b>A72V</b>	<b>Cfrm</b>	<b>100</b>	<b>69,33</b>	<b>67,44</b>	<b>2,198</b>	<b>NT</b>	<b>0,9490</b>
<u>ND6</u>	<u>LHON</u>	<u>C14482A</u>	<u>M64I</u>	<u>Reported</u>	<u>58,54</u>	<u>82,67</u>	<u>84,88</u>	<u>1,851</u>	<u>NT</u>	<u>0,5602</u>
<b>ND6</b>	<b>LHON</b>	<b>C14482G</b>	<b>M64I</b>	<b>Cfrm</b>	<b>58,54</b>	<b>82,67</b>	<b>84,88</b>	<b>1,851</b>	<b>NT</b>	<b>0,5602</b>
<u>ND6</u>	<u>LHON</u>	<u>T14484C</u>	<u>M64V</u>	<u>Cfrm</u>	<u>58,54</u>	<u>82,67</u>	<u>84,88</u>	<u>2,434</u>	<u>NT</u>	<u>0,6107</u>
ND6	LHON	A14495G	L60S	Reported	100	100	95,35	1,875	NT	0,9203
ND6	LHON	T14498C	Y59C	Reported	100	100	93,02	3,545	NT	0,9598
<b>ND6</b>	<b>LHON</b>	<b>C14568T</b>	<b>G36S</b>	<b>Cfrm</b>	<b>100</b>	<b>46,67</b>	<b>40,7</b>	<b>0,042</b>	<b>T</b>	<b>0,8363</b>
<i>ND6</i>	<i>LHON</i>	<i>A14596T</i>	<i>I26M</i>	<i>Reported</i>	<i>82,93</i>	<i>52</i>	<i>50</i>	<i>1,769</i>	<i>T</i>	<i>0,3020</i>

**Tab. 8** Prediction of functional role of amino acid substitution in ND1-ND6 and ND4L subunits. Variants list is downloaded from Mitomap and for each variant is reported the conservation analysis and the prediction of PolyPhen, SIFT and PMut. Confirmed mutations are in bold, variants predicted to be pathogenic are underlined and uncertain variants are in italic. (Abbreviations Cfrm: confirmed, Pos syn: possibly synergistic, Rep: reported, Sec: secondary)

Locus	Haplogroup	Nucleotide change	Amino acid change	Amino acid conservation (%)			PolyPhen	SIFT	PMut
				Mammals	Vertebrates	Eukaryotes	PSIC score	Tol-Not Tol	Score
<i>ND1</i>	<i>j1c1</i>	<i>T3394C</i>	<i>Y30H</i>	97,53	96,26	82,52	0,731	<i>T</i>	0,5604
<i>ND1</i>	<i>W</i>	<i>A3505G</i>	<i>T67A</i>	86,42	92,52	73,43	0,378	<i>NT</i>	0,2424
<i>ND1</i>	H1b	A3796G	T164A	64,2	64,15	47,86	0,747	T	0,2246
<i>ND1</i>	H4	C3992T	T229M	65,43	67,92	63,57	0,583	T	0,6805
<i>ND1</i>	H4a	A4024G	T240A	54,32	58,49	48,91	0,654	T	0,1636
<i>ND1</i>	R2-JT	T4216C	Y304H	61,73	68,87	48,2	0,825	T	0,2674
<i>ND2</i>	K2a	T4561C	V31A	50	39,77	30,25	0,331	T	0,5530
<i>ND2</i>	V1	T4639C	I57T	80,65	89,77	66,39	0,551	T	0,2518
<i>ND2</i>	U3b-K1a5	C4640A	I57M	80,65	89,77	66,39	0,419	T	0,3084
<i>ND2</i>	<i>R1-T</i>	<i>A4917G</i>	<i>N150D</i>	93,55	87,5	74,58	0,521	<i>T</i>	0,7432
<i>ND2</i>	N1b	C4960T	A164V	45,16	46,59	45,38	0,894	T	0,7019
<i>ND2</i>	N2	G5046A	V193I	66,13	72,73	59,63	0,332	T	0,2533
<i>ND2</i>	V1a	C5263T	A265V	66,13	48,86	40,34	0,255	T	0,8420
<i>ND2</i>	W-J1b	G5460A	A331T	40,32	32,95	28,21	1,015	T	0,1824
<i>ND3</i>	<i>K1-N1a-L3-J</i>	<i>A10398G</i>	<i>T114A</i>	83,58	60,67	41,91	0,194	<i>T</i>	0,6577
<i>ND4L</i>	U3a	A10506G	T13A	43,64	31,75	23,33	0,559	T	0,2914
<i>ND4</i>	K2c	A11015G	S86G	65,79	54,9	37,65	1,440	T	0,2821
<i>ND4</i>	<i>K2c</i>	<i>A11172G</i>	<i>N138S</i>	97,37	96,08	56,82	1,055	<i>T</i>	0,8843
<i>ND5</i>	M1	C12403T	L23F	34,21	43,14	31,71	0,000	T	0,1637
<i>ND5</i>	K1a4b-V2	A13105G	I257V	55,26	60,78	56,25	0,359	T	0,0377
<i>ND5</i>	K2b	G13135A	A267T	52,63	58,82	31,58	0,837	T	0,3782
<i>ND5</i>	U8a	G13145A	S270N	92,11	92,16	53,13	1,067	T	0,0158
<i>ND5</i>	U5b2	A13637G	E434R	73,68	49,02	26,04	0,985	T	0,3976
<i>ND5</i>	X2b-X2d-J	G13708A	A458T	44,74	52,94	34,38	0,610	T	0,1092
<i>ND5</i>	H11	G13759A	A475T	52,63	41,13	21,74	0,816	T	0,3063
<i>ND5</i>	N1a-I	A13780G	I482V	81,58	98,04	54,17	0,783	T	0,0478
<i>ND5</i>	I1b	T13879C	S515P	23,68	22	16,84	0,263	T	0,1023
<i>ND5</i>	U3a	C13934T	T533M	52,63	37,25	22,92	1,085	T	0,2700
<i>ND5</i>	X	A13966G	T544A	55,26	35,29	28,13	0,525	T	0,0758
<i>ND5</i>	M1	T14110C	F592L	73,68	64,71	58,24	0,000	T	0,2398
<i>ND6</i>	K2b	T14307C	S123G	60,98	34,67	32,1	0,094	T	0,4370
<i>ND6</i>	C	T14318C	N119S	48,65	24,64	20,99	0,347	T	0,1745
<i>ND6</i>	H4a	C14365T	V103M	63,41	58,67	47,67	0,415	T	0,4955
<i>ND6</i>	<i>H4a</i>	<i>A14582G</i>	<i>V31A</i>	46,34	74,67	69,77	0,195	<i>T</i>	0,5272

**Tab. 9** Prediction of functional role of amino acid substitution in ND1-ND6 and ND4L subunits. Variants are common polymorphisms retrieved from the general population and associated with European mtDNA haplogroups. For each variant is reported the conservation analysis and the prediction of PolyPhen (PSIC score higher than 1.5 are considered possibly damaging), SIFT and PMut (scores higher than 0.5 are considered pathological). Variants predicted to be pathogenic are underlined and uncertain variants are in italic.

### Identification of rare and putative new LHON pathogenic mutations

In 90% of cases, LHON is caused by one of three mtDNA common mutations (11778/ND4, 3460/ND1, 14484/ND6 in complex I subunit genes). However, in many cases the molecular diagnosis results negative for these mutations, even if the patients show a full LHON clinical phenotype. In order to explain the molecular cause of some of these cases, we here investigate 6 LHON probands from 5 unrelated Italian families (for family trees see Appendix C). All these patients result negative at LHON common mutation screening. We completely sequenced the mtDNA from these patients and we found 4 rare LHON mutations, some of them reported only once, and 2 new nucleotide changes with pathogenic potential. The raw data of mtDNA sequencing are reported in Appendix D and the list of non-synonymous nucleotide changes is reported in table 10. Figure 24 shows the tree encompassing the complete mtDNA sequences observed in the investigated pedigrees.

Family	Locus	Nucleotide change	Amino acid position	Amino acid change	Homoplasmy/Heteroplasmy	mtDNA haplogroup
<b>Fam. 1</b>	<b>ND1</b>	<b>G3700A</b>	<b>132</b>	<b>Ala-Thr</b>	<b>Homoplasmic</b>	H
	ND5	G13759A	475	Ala-Thr	-	
<b>Fam. 2</b>	ND1	T4172A	289	Leu-Gln	Homoplasmic	U6a
	COII	G7805A	74	Val-Ile	-	
	<b>ND6</b>	<b>C14568T</b>	<b>36</b>	<b>Gly-Ser</b>	<b>Heteroplasmic</b>	
	Cyt b	G15221A	159	Asp-Asn	-	
<b>Fam. 3</b>	ND1	T4216C	304	Tyr-His	-	J1c
	ND3	A10398G	114	Thr-Ala	-	
	ND5	G13708A	458	Ala-Thr	-	
	ND5	C13934T	533	Thr-Met	-	
	<b>ND6</b>	<b>G14459A</b>	<b>72</b>	<b>Ala-Val</b>	<b>Homoplasmic</b>	
	Cyt b	T14798C	18	Phe-Leu	-	
	Cyt b	C15452A	236	Leu-Ile		
<b>Fam. 4</b>	<b>ND6</b>	<b>A14495G</b>	<b>60</b>	<b>Leu-Ser</b>	<b>Heteroplasmic</b>	H
<b>Fam. 5</b>	<b>ATP6</b>	<b>A8944G</b>	<b>140</b>	<b>Met-Val</b>	-	K1a
	ATP6	G9055A	177	Ala-Thr	-	
	ND3	A10398G	114	Thr-Ala	-	
	<b>ND6</b>	<b>G14258A</b>	<b>139</b>	<b>Pro-Leu</b>	<b>Homoplasmic</b>	
	ND6	A14582G	31	Val-Ala	-	
	Cyt b	T14798C	18	Phe-Leu	-	

**Tab. 10** Non-synonymous variants found in probands' mtDNA from investigated families with relative amino acid substitutions. Rare or putative pathogenic mutations are reported in bold.

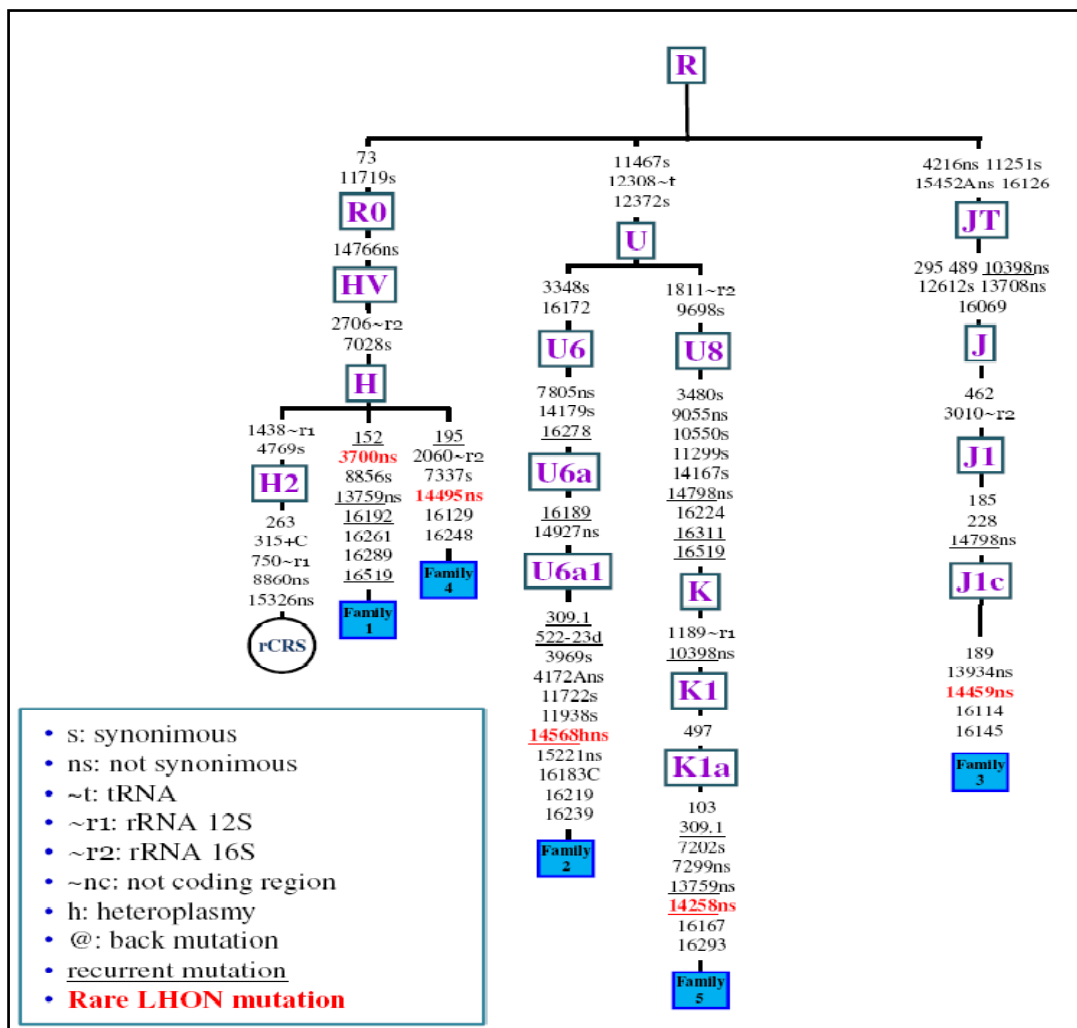


**Fig. 24** Tree encompassing the complete mtDNA sequences observed in the investigated families. Nucleotide variants are shown on the branches; they are transitions unless the base change is explicitly indicated. Insertions are suffixed with a plus sign“+” and the inserted nucleotide; underlining indicates recurrent polymorphisms; “s” indicates synonymous mutations whereas “ns” indicates non-synonymous mutations, “h” indicates heteroplasmic mutations. Pathogenic LHON mutations are shown in red.

**Family 1**

The mtDNA of II:1 from Family 1 has been completely sequenced and belongs to haplogroup H. Compared to revised Cambridge Reference Sequence (rCRS), only two non-synonymous nucleotide changes were found: G3700A/ND1 and G13759A/ND5. The ND1 variant cause the amino acid substitution Ala132Thr in ND1 protein sequence and has been previously reported as LHON pathogenic by Fauser and coll.<sup>316</sup>, whereas the ND5 nucleotide change is a common polymorphism reported in several haplogroups and diagnostic marker of haplogroup F1a1. The mutation load of G3700A/ND1 was assessed through a RFPL assay and the mutation resulted homoplasmic in DNA samples extracted from peripheral blood and urinary epithelium from II:1 (data not shown).

**Family 2**

The complete sequencing of mtDNA has been carried out on a DNA sample extracted from peripheral blood of IV:3 from Family 2. This mtDNA belongs to haplogroup U6a and harbors four non-synonymous nucleotide changes compared to rCRS. We found the heteroplasmic mutation C14568T/ND6, that induces an amino acid substitution in ND6 at position 36 (Gly36Ser), previously reported in literature as LHON causative.<sup>316-319</sup> Moreover, this mtDNA lineage is characterized by the variants T4172A/ND1, G7805A/COII and G15221A/*cytb*. The nucleotide change in COII gene defines the clade a of haplogroup U6, whereas the variant in *cytb* gene has been reported in association with five different haplogroups. Finally, nucleotide variant T4172A/ND1 has been reported only once in another mtDNA belonging to haplogroup U6a and probably is the marker of a specific subclade of this haplogroup. This polymorphism induces the amino acid substitution Leu289Gln in ND1 protein. Interestingly, the same amino acid is substituted (Leu289Met) in presence of the mutation C4171A/ND1, reported as LHON pathogenic.<sup>320</sup> In order to assess the mutational load of C14568T/ND6 mutation and its distribution on the maternal lineage, we performed an RFLP assay on DNA samples extracted from whole blood of several maternal relatives (III:2, III:3, III:4, IV:2, IV:5, IV:6, IV:7). In the investigated relatives only IV:5 harbor the LHON pathogenic mutation in heteroplasmic condition (Fig. 25B and C). Moreover, an analysis of heteroplasmy in DNA samples extracted from different tissues (whole

blood, platelets, skeletal muscle, and, when available urinary epithelium and hairs) has been performed (Fig. 25 A and C). In IV:3 mutant mtDNA reaches levels of about 90% in hairs, skeletal muscle and urinary epithelium, whereas in whole blood and platelet fraction is about 70%. In IV:5 mutated mtDNA is about 50% in peripheral blood and platelets and 70% in skeletal muscle.

The RFPL survey of all available DNA samples shows that the 4172/ND1 variant is homoplasmic in all maternal relatives and all available tissues from IV:3 and IV:5 individuals (data not shown).

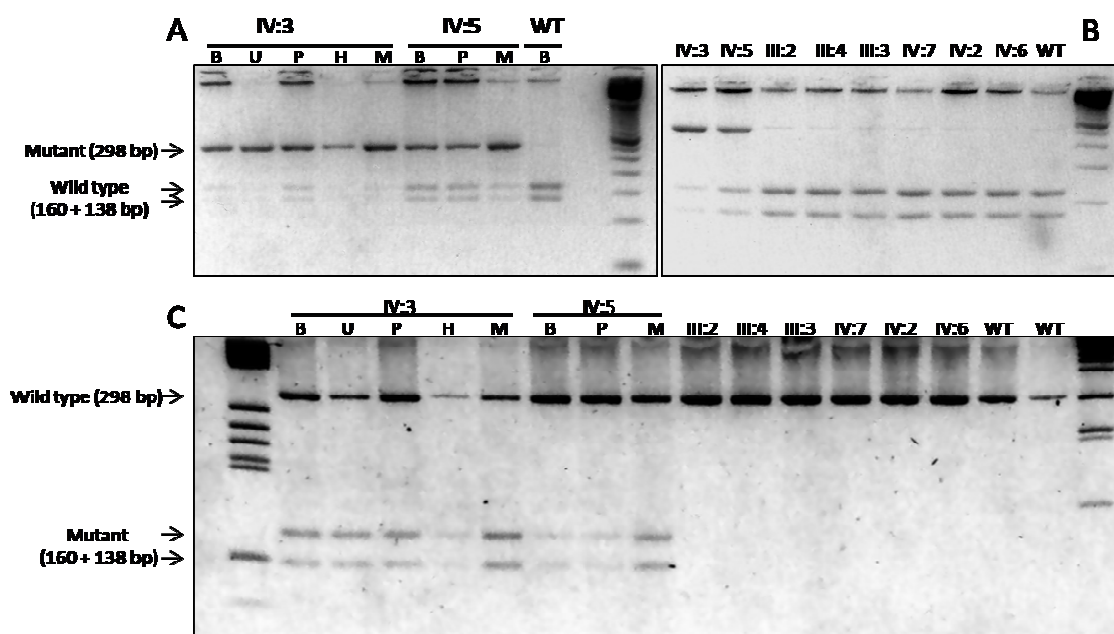


**Fig. 25** RFLP analysis of C14568T/ND6 within Family 2. In panel A and B is shown the RFLP using the restriction enzyme *AcI*: the allele T remains uncut (298 bp) whereas the *wild type* allele C is cut in two fragments. Panel A shows the RFLP assay in different tissues from individuals IV:3 and IV:5, panel B shows the same assay in DNA samples extracted from whole blood of all the available individuals of family 2. In panel C is shown the RFLP assay with the restriction enzyme *BcgI*: the allele C (*wild type*) remains uncut, whereas the allele T (mutant) is cut in two fragments. The assay in panel C has been carried out in all the available samples (different individuals and different tissues). Abbreviations: B whole blood, U urinary epithelium, P platelets, H hairs, M skeletal muscle.

### Family 3

We collected DNA samples from venous blood of seven individuals belonging to Family 3 (III:1, the proband, is a LHON patient, III:5 presents a complex disease characterized by spastic dystonia and bilateral striatal necrosis, all the others individuals are unaffected) and from skeletal muscle of III:5. The mtDNA of this family belongs to haplogroup J1c and is characterized by five variants in complex I genes (T4216C/ND1, A10398G/ND3, G13708A/ND5, C13934T/ND5 and G14459A/ND6), including the pathogenic mutation G14459A/ND6 and two variants in *cytb* gene (T14798C and C15452A). The pathogenic mutation in ND6 gene has been previously reported in some cases of LHON plus dystonia.<sup>238</sup> The polymorphisms in *cytb* and complex I genes, with the only exception of that in position 13934, are common markers of haplogroup J1c. Available samples were investigated with RFLP for the G14459A mutation (Fig. 26). The two affected individuals, III:1 and III:5, and one unaffected subject, III:2, harbored the homoplasmic mutation G14459A, whereas II:2 harbored the heteroplasmic mutation in venous blood (about 90-95% of mutant). All the other investigated individuals were *wild type*.

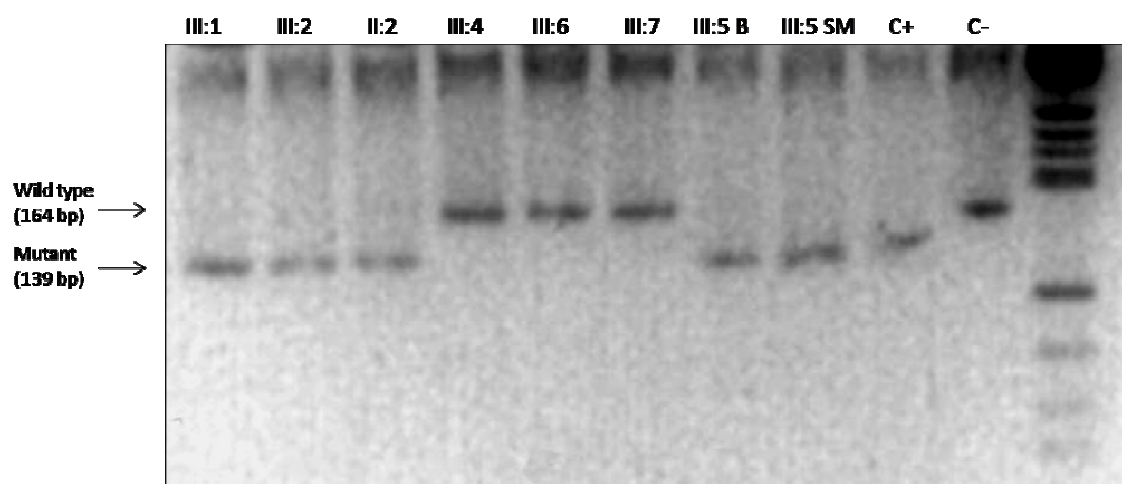


**Fig. 26** RFLP analysis of G14459A/ND6 in Family 3. The allele A generates a restriction site for the restriction enzyme MaeIII (139 and 25 bp), whereas the allele G remains uncut (164 bp). Abbreviations: B whole blood, SM skeletal muscle.

#### Family 4

Family 4 shows a low penetrance, being affected only four individuals along three generations. The only available sample is extracted from peripheral blood of III:4, the analyzed proband. The mtDNA of Family 4 belongs to haplogroup H and harbors a single nucleotide change compared to rCRS, the LHON pathogenic mutation A14495G/ND6, reported in literature by Chinnery et al.<sup>321</sup> The RFLP analysis reveal an heteroplasmic mutation, with about 50% of mutant molecules (Fig. 27).

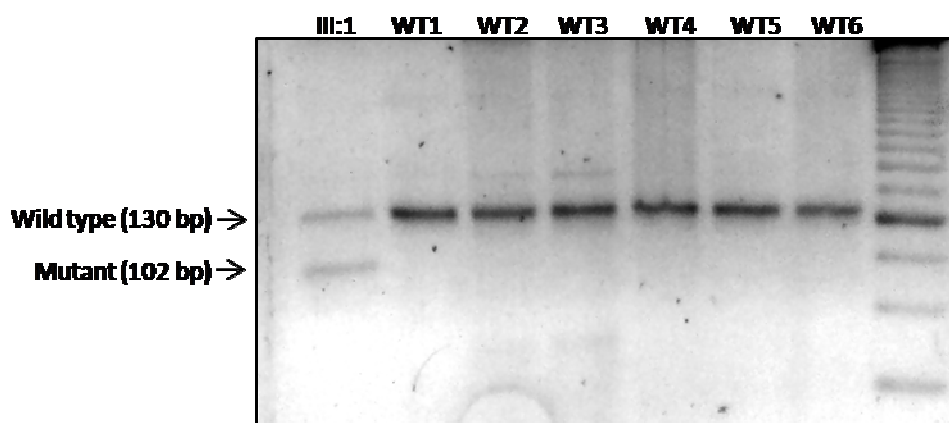


**Fig. 27** RFLP analysis of A14495G/ND6 in family III:1 from Family 4 and six different controls. The allele G generates a restriction site for NlaIII, whereas the *wild type* allele A remains uncut.

#### Family 5

Family 5 is composed of two related branches analyzed independently. The mtDNA sequencing in the two probands (IV:1 of branch a and IV:6 of branch b) revealed the presence of a common ancestor for both families and allowed their reconnection. The nucleotide variants present in the analyzed mtDNAs characterize haplogroup K1a. These polymorphisms are G9055A/ATPase6, A10938G/ND3 and T14798C/*cytb*. Furthermore, other three non-synonymous changes were detected, one in ATPase 6 gene (A8944G) and two in ND6 gene (G14258A and A14528G). The variant A14528G/ND6 is a common polymorphism associated with haplogroup H4 and reported also in other mtDNA backgrounds, such as haplogroup N9a, whereas the other two nucleotide changes are present only in two sequences over 3400 normal sequences of HmtDB ([www.hmtdb.uniba.it](http://www.hmtdb.uniba.it)) and may have role in the LHON pathogenesis of this family.<sup>322,323</sup> RFLP analysis of A14258G/ND6 shows a homoplasmic mutation in all samples investigated from both branches (data not shown).

### *Conservation analysis*

All the previously reported mtDNA nucleotide variants have been analyzed, in terms of amino acid position conservation in the three described data sets, and in terms of pathogenic potential, to establish whether they may have a functional effect. All the previously reported rare LHON mutations affect highly conserved amino acids, at least in mammals, being almost invariant. Furthermore, these amino acids are present in extremely conserved regions, suggesting a functional role for these domains (Fig. 28). In fact, G3700A/ND1 causes the substitution Ala-Thr in position 132 of ND1, very conserved from eukaryotes to mammals (from 80% to 93%), and is predicted to be pathogenic by SIFT and PMut (Tab. 10). This region in our ND1 model is located in the conserved loop CD, where another LHON putative mutation has been described in two unrelated pedigrees (G3733A/ND1).<sup>324</sup> The mutations C14568T, G14459A and A14495G of ND6 gene affect invariant position in the two very conserved regions in ND6 subunit (helices B and C). The G14459A and A14495G mutations are predicted as pathogenic or probably damaging by all the used prediction tools (Tab. 11), whereas the C14568T mutation is predicted pathogenic only by PMut (Tab. 10).

Interestingly, the polymorphism T4172A/ND1 of Family 2 affects the conserved amino acid Leu-289 (98.77% of conservation in mammals) in a very conserved region. The amino acid substitution induced by this variant (Leu289Glu) is predicted to be possibly pathogenic by the most restrictive prediction tool PolyPhen (PSIC score 1.899, Tab. 11). Moreover, the same position is affected by the LHON reported pathogenic mutation C4171A, but this latter mutation induces a Leu289Met substitution, considered by PolyPhen benign (PSIC score 0.052).

In the two branches of Family 5 we found two rare variants with a possible pathogenic potential (A8944G/ATPase6 and G14258A/ND6). The nucleotide change A8944G/ATPase6 affects amino acid Met-140, a position poorly conserved in vertebrates and eukaryotes, but invariant along mammals (Tab. 11). This amino acid resides in a very conserved region of ATPase a subunit, as shown in figure 28. Considering these features, this nucleotide change may have a functional role on ATP synthase activity and, consequently, a pathogenic potential in this family.

The mtDNA variant G14258A/ND6 affects a poorly conserved amino acid in a poorly conserved region (amino acid Pro-139, see Tab. 11 and Fig. 28), even if is adjacent to a

invariant residue Gly-141. PolyPhen predicts both amino acid substitutions as benign, but we cannot exclude a functional role for both these mtDNA variants, especially for the nucleotide change in ATPase6 that may have a strong impact on protein function, affecting an invariant amino acid.

Nucleotide change	Amino acid change	Conservation (%)			PolyPhen (PSIC score)	Family
		Mammals	Vertebrates	Eukaryotes		
<b>G3700A/ND1</b>	<b>A132T</b>	<b>97.53</b>	<b>93.4</b>	<b>80</b>	<b>Benign (0.741)</b>	Fam. 1
G13759A/ND5	A475T	52.63	41.18	21.74	Benign (0.816)	Fam.1
<u>T4172A/ND1</u>	<u>L289Q</u>	<u>98.77</u>	<u>83.02</u>	<u>57.86</u>	<u>Possibly damaging (1.899)</u>	Fam. 2
C4171A/ND1	L289M	98.77	83.02	57.86	Benign (0.052 )	
G7805A/COII	V74I	84.57	83.15	64.69	Benign (0.479)	Fam. 2
<b>C14568T/ND6</b>	<b>G36S</b>	<b>100</b>	<b>46.67</b>	<b>40.7</b>	<b>Benign (0.047)</b>	Fam. 2
G15221A/cyt b	D159N	38.00	44.00	42.00	Benign (0.140)	Fam. 2
T4216C/ND1	Y304H	61.73	68.87	48.2	Benign (0.825)	Fam. 3
A10398G/ND3	T114A	83.58	60.67	41.91	Benign (0.194)	Fam. 3
G13708A/ND5	A458T	44.74	52.94	34.38	Benign (0.610)	Fam. 3
C13934T/ND5	T533M	52.63	37.25	22.92	Benign (1.085)	Fam. 3
<b>G14459A/ND6</b>	<b>A72V</b>	<b>100</b>	<b>69.33</b>	<b>67.44</b>	<b>Probably damaging (2.197)</b>	Fam. 3
T14798C/cyt b	F18L	89.00	72.00	68.00	Benign (0.999)	Fam. 3
C15452A/cyt b	L236I	50.00	44.00	42.00	Benign (0.288)	Fam. 3
<b>A14495G/ND6</b>	<b>L60S</b>	<b>100</b>	<b>100</b>	<b>95.35</b>	<b>Probably damaging (2.788)</b>	Fam. 4
<b>A8944G/ATP6</b>	<b>M140V</b>	<b>100</b>	<b>65.52</b>	<b>36.08</b>	<b>Benign (1.023)</b>	Fam. 5
G9055A/ATP6	A177T	89.47	89.66	59.57	Benign (0.385)	Fam. 5
A10398G/ND3	T114A	83.58	60.67	41.91	Benign (0.194)	Fam. 5
<b>G14258A/ND6</b>	<b>P139L</b>	<b>34.15</b>	<b>36</b>	<b>32.56</b>	<b>Benign (0.037)</b>	Fam. 5
A14582G/ND6	V31A	46.34	74.67	69.77	Benign (0.195)	Fam. 5
T14798C/cyt b	F18L	89.00	72.00	68.00	Benign (0.999)	Fam. 5

**Tab. 11** Sequence analysis of amino acid substitutions identified in LHON families 1-5. In table are reported the amino acid conservation along the three alignments (mammals, vertebrates and eukaryotes) and the pathogenicity prediction obtained using PolyPhen, PSIC score is indicated inside brackets.

LHON G3700A/ND1	118	WSGWASNSNYLIGTLRAVAQ	139	LHON T4172A/ND1	272	WIRITAMPFRFRYDQLMLLWKNF	293
H.sapiens	118	WSGWASNSNYLIGTLRAVAQ	139	LHON C4171A/ND1	272	WIRITAMPFRFRYDQLMLLWKNF	293
P.troglodytes	118	WSGWASNSNYLIGTLRAVAQ	139	H.sapiens	272	WIRITAMPFRFRYDQLMLLWKNF	293
L.catta	118	WSGWASNSNYLIGTLRAVAQ	139	P.troglodytes	272	WIRITAMPFRFRYDQLMLLWKNF	293
M.musculus	118	WSGWASNSNYLIGTLRAVAQ	139	L.catta	272	WIRITAMPFRFRYDQLMLLWKNF	293
O.cuniculus	118	WSGWASNSNYLIGTLRAVAQ	139	M.musculus	272	WIRITAMPFRFRYDQLMLLWKNF	293
E.caballus	118	WSGWASNSNYLIGTLRAVAQ	139	O.cuniculus	272	WIRITAMPFRFRYDQLMLLWKNF	293
B.bovis	118	WSGWASNSNYLIGTLRAVAQ	139	E.caballus	272	WIRITAMPFRFRYDQLMLLWKNF	293
B.physalus	118	WSGWASNSNYLIGTLRAVAQ	139	B.bovis	272	WIRITAMPFRFRYDQLMLLWKNF	293
P.vitulina	118	WSGWASNSNYLIGTLRAVAQ	139	B.physalus	272	WIRITAMPFRFRYDQLMLLWKNF	293
F.catus	118	WSGWASNSNYLIGTLRAVAQ	139	P.vitulina	272	WIRITAMPFRFRYDQLMLLWKNF	293
O.anatinus	118	WSGWASNSNYLIGTLRAVAQ	139	F.catus	272	WIRITAMPFRFRYDQLMLLWKNF	293
				O.anatinus	272	WIRITAMPFRFRYDQLMLLWKNF	293
LHON G14258A/ND6	128	EGEGSLIREDDPICAGALYDYC	149	LHON A8944G/ATP6	130	PQCTPTEFLIPMIVITETSLIT	151
H.sapiens	128	EGEGSLIREDDPICAGALYDYC	149	H.sapiens	130	PQCTPTEFLIPMIVITETSLIT	151
P.troglodytes	128	EGEGSLIREDDPICAGALYDYC	149	P.troglodytes	130	PQCTPTEFLIPMIVITETSLIT	151
L.catta	127	ESKEGVIREDDSLGVASLYNKA	148	L.catta	130	PQCTPTEFLIPMIVITETSLIT	151
M.musculus	127	EVDVVVMLGGGICVAAVYSCA	148	M.musculus	130	PQCTPTEFLIPMIVITETSLIT	151
O.cuniculus	128	EGDEVGLIREDDSMVAALYSYC	149	O.cuniculus	130	PQCTPTEFLIPMIVITETSLIT	151
E.caballus	129	DTGDSAFSFEIIMCAALYSYC	150	E.caballus	130	PQCTPTEFLIPMIVITETSLIT	151
B.bovis	129	DTGDSFFSFEAMCITAAALYSYC	150	B.bovis	130	PQCTPTEFLIPMIVITETSLIT	151
B.physalus	129	DTGDSVFSFEATCITAAALYSYC	150	B.physalus	130	PQCTPTEFLIPMIVITETSLIT	151
P.vitulina	129	DTGDSFFSFEAMCITAAALYSYC	150	P.vitulina	130	PQCTPTEFLIPMIVITETSLIT	151
F.catus	129	DTGDSFFSFEAMCITAAALYSYC	150	F.catus	130	PQCTPTEFLIPMIVITETSLIT	151
O.anatinus	119	DLCCEVVLCCDYNEVSLISACC	140	O.anatinus	130	PQCTPTEFLIPMIVITETSLIT	151
LHON C14568T/ND6	25	PITYGGLVLIIVSGVVGCVIILNF	GGGYMGLIMVFLIYLGGMVVFVGYT	AMATE	76		
LHON A14495G/ND6	25	PITYGGLVLIIVSGVVGCVIILNF	GGGYMGLIMVFLIYLGGMVVFVGYT	AMATE	76		
LHON G14459A/ND6	25	PITYGGLVLIIVSGVVGCVIILNF	GGGYMGLIMVFLIYLGGMVVFVGYT	AMATE	76		
H.sapiens	25	PITYGGLVLIIVSGVVGCVIILNF	GGGYMGLIMVFLIYLGGMVVFVGYT	AMATE	76		
P.troglodytes	25	PITYGGLVLIIVSGVVGCVIILNF	GGGYMGLIMVFLIYLGGMVVFVGYT	AMATE	76		
L.catta	24	PITYGGLVLIIVSGVVGCVIILNF	GGGYMGLIMVFLIYLGGMVVFVGYT	AMATE	75		
M.musculus	25	PITYGGLVLIIVSGVVGCVIILNF	GGGYMGLIMVFLIYLGGMVVFVGYT	AMATE	76		
O.cuniculus	25	PITYGGLVLIIVSGVVGCVIILNF	GGGYMGLIMVFLIYLGGMVVFVGYT	AMATE	76		
E.caballus	26	PITYGGLVLIIVSGVVGCVIILNF	GGGYMGLIMVFLIYLGGMVVFVGYT	AMATE	77		
B.bovis	26	PITYGGLVLIIVSGVVGCVIILNF	GGGYMGLIMVFLIYLGGMVVFVGYT	AMATE	77		
B.physalus	26	PITYGGLVLIIVSGVVGCVIILNF	GGGYMGLIMVFLIYLGGMVVFVGYT	AMATE	77		
P.vitulina	26	PITYGGLVLIIVSGVVGCVIILNF	GGGYMGLIMVFLIYLGGMVVFVGYT	AMATE	77		
F.catus	26	PITYGGLVLIIVSGVVGCVIILNF	GGGYMGLIMVFLIYLGGMVVFVGYT	AMATE	77		
O.anatinus	25	PITYGGLVLIIVSGVVGCVIILNF	GGGYMGLIMVFLIYLGGMVVFVGYT	AMATE	76		

**Fig. 28** Global alignment of ND1, ND6 and ATPase6 protein sequences belonging to 11 different mammalian organisms. Amino acid residue with a percentage of conservation ranging between 70.0% and 79.9% are highlighted in light grey, those between 80.0% and 99.9% are highlighted in dark grey and those invariant (100%) are highlighted in black. Amino acid changes of interest are shown in bold.

### Determination of OXPHOS complexes activity

To verify the impact of the reported mutations on the respiratory complexes function, we measured the specific activity of complex I, complexes II+III, complex III and complex IV, by using conventional spectrophotometric assays, in platelet fractions of available individuals and of a control group. We studied the probands from Family 2 and Family 5a (respectively IV:3 and IV:1, see Appendix C) and two individuals from Family 3, III:1 (the LHON pure case) and III:5 (the LHON plus dystonia case).

The prediction for these patients carrying ND6 gene mutations (C14568T/Family 2, G14459A/Family 3 and G14258A/Family 5) would be a defective complex I activity.

Conversely, as shown in figure 29 A-B, the activities of respiratory chain complexes, and in particular complex I, measured in probands from Family 2 and Family 5 were not significantly different from controls. In the case of Family 2, this is probably due to the high percentage of *wild type* mtDNA in the platelet fraction (Fig. 25), whereas in the case of Family 5, the normal activity of complex I may be caused by a mild, not detectable, effect of this mtDNA variant on complex I activity, as for 14484/ND6,<sup>273</sup> or by the lack of functional effect on complex I, suggesting that this variant is only a polymorphism.

The two individuals from Family 3 showed a marked decrease of complex I activity (Fig. 29A), with a residual activity ranging from 35% in III:1 to 21% in III:5, demonstrating that the G14459A/ND6 mutation has indeed a severe effect on complex I activity. Moreover, in III:5 a strong increase of all the other complexes activities was observed (Fig. 29AB), suggesting a compensatory response of cells to the energetic impairment caused by the ND6 mutation.

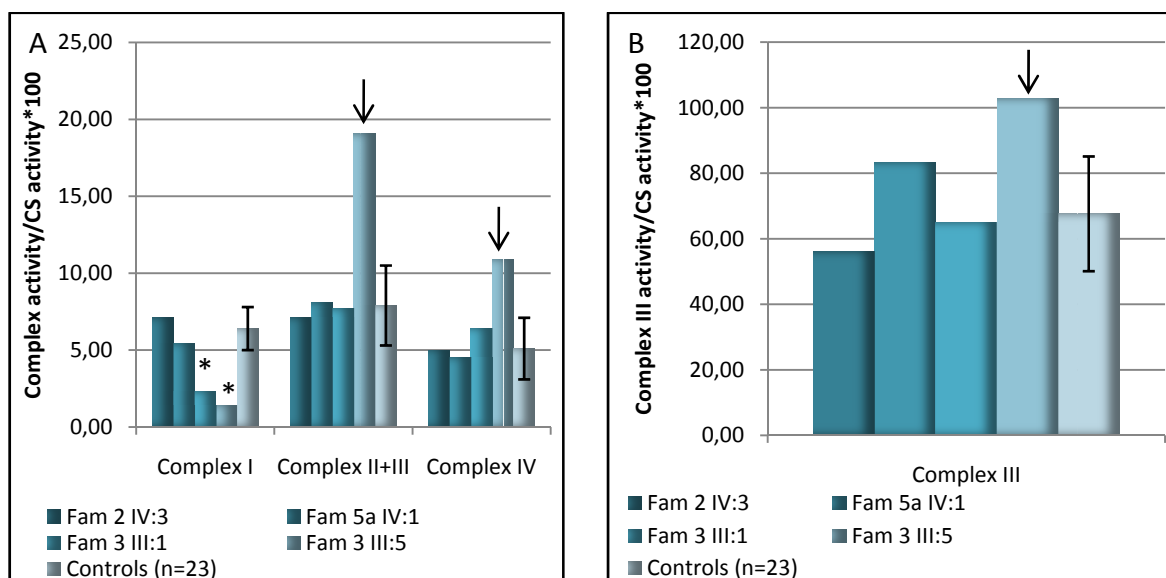


**Fig. 29** Complex I, II+III and IV activity (A) and complex III activity (B) in LHON individuals compared to control group. Data are reported as average±standard deviation. Asterisks indicate a reduction out of the control range, whereas arrows indicate an increase out of the control range.

---

### **Role of mtDNA polymorphisms in LHON plus myoclonus**

In order to investigate the occurrence of myoclonus in two LHON families, we studied five patients and one unaffected carrier. All six individuals had myoclonus, elevated serum lactic acid and accumulation of lactic acid in ventricles. The RFLP survey in all maternal relatives investigated showed the 11778/ND4 mutation in Family A and the 3460/ND1 mutation in Family B homoplasmic in blood, urinary epithelium, and skeletal muscle (data not shown). Based on the evidence of familial recurrence of myoclonus in these two families, which was strictly co-segregating with LHON on the maternal line in Family A, we sequenced the entire mtDNA extracted from skeletal muscle of individuals VI:15 from Family A and IV:2 from Family B (see Appendix C).

#### ***Family A***

The mtDNA from Family A belongs to haplogroup T2 and, in addition to the 11778/ND4 mutation, harbors five non-synonymous nucleotide changes commonly found in this haplogroup (Fig. 30). Three of the non-synonymous nucleotide changes (4136/ND1, 4216/ND1, and 4917/ND2) affect ND subunits of complex I, one (9139/ATPase6) the ATPase a subunit of complex V, and one (15452/*cytb*) the *cyt b* subunit of complex III. Those at nps 4216, 4917 and 15452 are ancient polymorphisms and characterize all haplogroup T mtDNAs. The two non-synonymous more recent variants of Family A (4136/ND1 and 9139/ATPase6) were surveyed by RFLP analysis in all available individuals and both were found homoplasmic in all tissues investigated. The rare 4136A>G/ND1 mutation has been previously found in three LHON families carrying an established primary mutation.<sup>242,325</sup> A further case has been reported on a haplogroup A mtDNA in a study investigating a cohort of patients with Alzheimer's disease of Japanese descent.<sup>326</sup> The 9139G>A/ATPase6 transition is also rare and probably define a branch within T2 haplogroup. It was found also on L2d and L3f1 haplogroups.

#### ***Family B***

The mtDNA of Family B is a member of haplogroup U4a (Fig. 30). In this sequence only two non-synonymous changes are present, and both affect the *cyt b* subunit (15693/*cytb*, 15773/*cytb*). Of the two, only the change at nucleotide position 15693 is an

ancient polymorphism that characterizes all haplogroup U4 mtDNAs. The more recent variant of Family B (15773 G>A/*cytb*) has been rarely observed on different haplogroups (C1, T2b, H and V2).

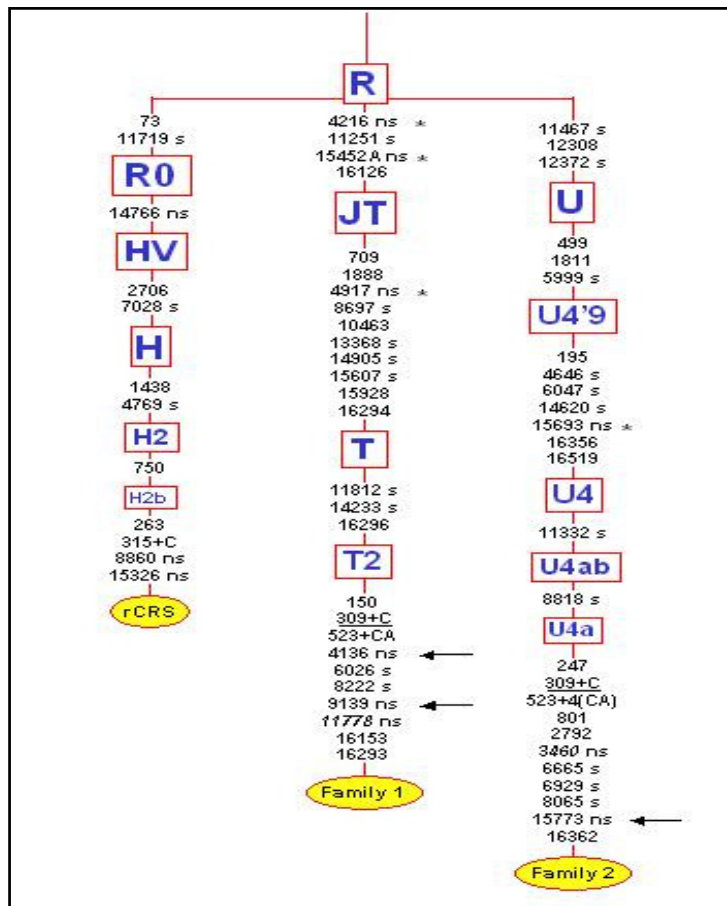


**Fig. 30** Tree encompassing the complete mtDNA sequences observed in the investigated families. Nucleotide variants are shown on the branches; they are transitions unless the base change is explicitly indicated. Insertions are suffixed with a plus sign “+” and the inserted nucleotide; underlining indicates recurrent polymorphisms; “s” indicates synonymous mutations whereas “ns” indicates non-synonymous mutations. Pathogenic LHON mutations are in italic and possibly synergistic polymorphisms are indicated by an arrow.

### *Conservation analysis*

To verify the possible functional significance of the non-synonymous changes found in the ND1, ND2, ATPase6 and *cyt b* genes, we analyzed their conservation and the prediction obtained with PolyPhen. The mammals alignments of the investigated

---

regions are reported in figure 31 and the percentages of conservation for each amino acid change are listed in table 12.

The two LHON pathogenic mutations at positions 3460/ND1 and 11778/ND4 show 59.4% and 99.2% of amino acid conservation in the alignment of eukaryotes, respectively, which increase to 97.5% and 100% (invariant position) when only mammals are considered. The position 277 of ND1 is highly conserved in both eukaryotes (78.6%) and mammals (98.7%). This feature – shared with the 11778/ND4 and 3460/ND1 mutations – neatly distinguishes the 4136/ND1 mutation from the ancient polymorphism 4216/ND1 whose amino acid conservation in the mammals is only 60.8%. The other ancient polymorphism 4917/ND2 shows, instead, a moderate-high conservation, ranging from 74.5% in eukaryotes to 93.5% in mammals. However, this amino acid resides in a poorly conserved region, probably with no functional role. The ATPase6 amino acid change A205T of Family A, due to the mutation at np 9139, despite being moderately conserved (76.0%) in eukaryotes, shows a conservation of 94.7% in mammals, but is located in a highly conserved region.

For Family B, the *cyt b* amino acid change M316T (15693/*cytb*) affects a poorly conserved position in eukaryotes (55%), which increased to a moderate conservation in mammals (71.0%) within a poorly conserved region of the protein. In contrast, the *cyt b* amino acid change V343M (15773/*cytb*) is a highly conserved amino acid position within a relatively conserved domain (Fig. 31, in eukaryotes 96% of conservation and in mammals 99%).

The PolyPhen predictive analysis of pathogenicity defines as “probably damaging” the 11778/ND4 mutation and “possibly damaging” the 3460/ND1 mutation, both being well established as pathogenic for LHON. The only other amino acid change scored as “possibly damaging” is V343M (15773/*cytb*) with a PSIC score difference of 1,570.

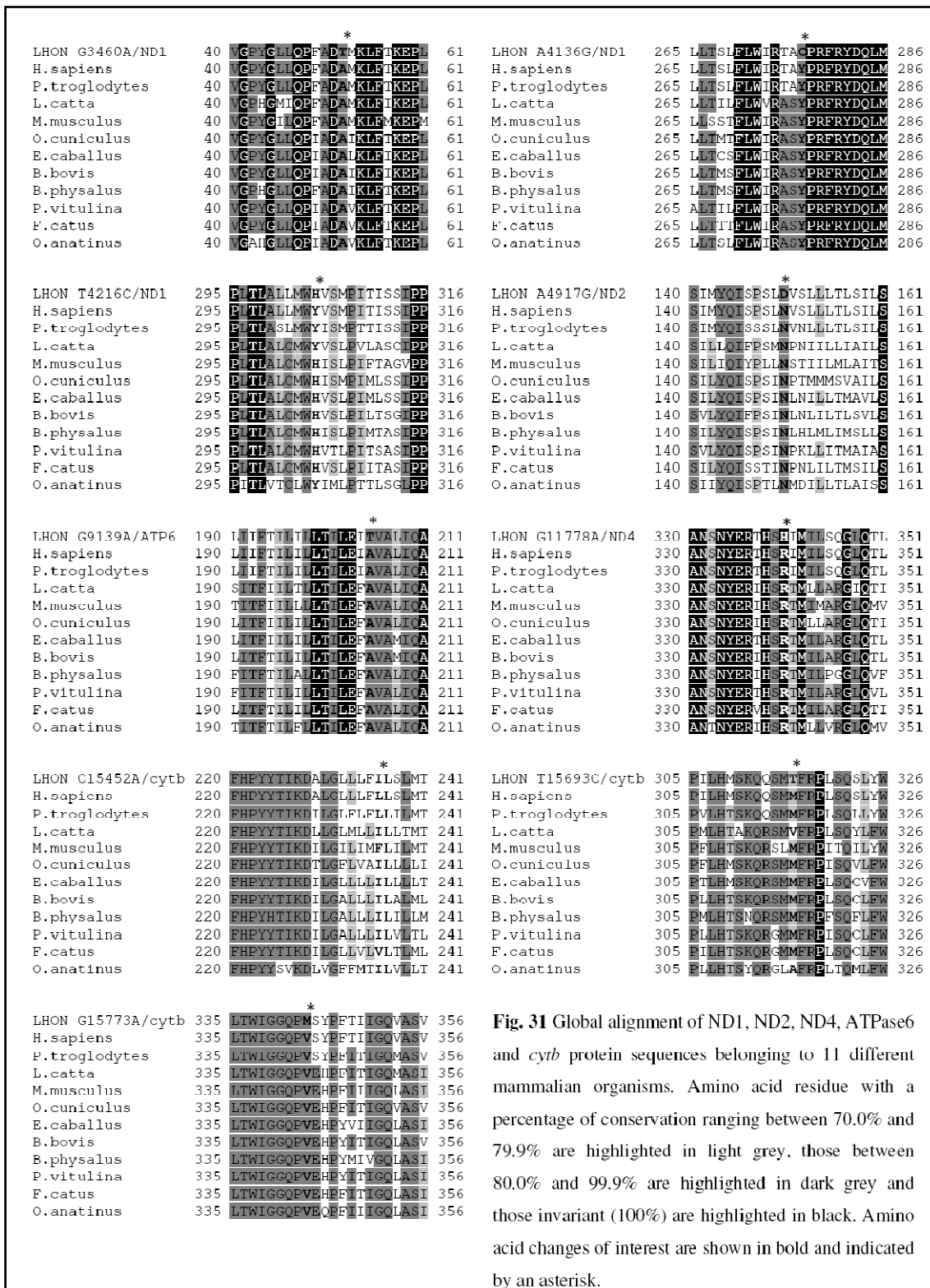


**Fig. 31** Global alignment of ND1, ND2, ND4, ATPase6 and *cytb* protein sequences belonging to 11 different mammalian organisms. Amino acid residue with a percentage of conservation ranging between 70.0% and 79.9% are highlighted in light grey, those between 80.0% and 99.9% are highlighted in dark grey and those invariant (100%) are highlighted in black. Amino acid changes of interest are shown in bold and indicated by an asterisk.

Nucleotide change	Amino acid change	Conservation (%)			PolyPhen prediction (PSIC score)	Family
		Mammals	Vertebrates	Eukaryotes		
<b>G11778A/ND4</b>	<b>R340H</b>	<b>100</b>	<b>100</b>	<b>99.2</b>	<b>Probably damaging (2.520)</b>	Fam. A
<u>A4136G/ND1</u> (possibly synergistic)	<u>Y277C</u>	<u>98.7</u>	<u>99.1</u>	<u>78.6</u>	<u>Benign</u>	Fam. A
T4216C/ND1	Y304H	60.8	68.9	48.2	Benign	Fam. A
A4917G/ND2	N150D	93.5	87.5	74.5	Benign	Fam. A
G9139A/ATP6 (possibly synergistic)	A205T	94.7	96.5	76.0	Benign	Fam. A
C15452A/ <i>cytb</i>	L236I	50.0	44.0	42.0	Benign	Fam. A
<b>G3460A/ND1</b>	<b>A52T</b>	<b>97.5</b>	<b>70.1</b>	<b>59.4</b>	<b>Possibly damaging (1.553)</b>	Fam. B
T15693C/ <i>cytb</i>	M316T	71.0	59.0	55.0	Benign	Fam. B
<u>G15773A/<i>cytb</i></u> (possibly synergistic)	<u>V343M</u>	<u>99.0</u>	<u>98.0</u>	<u>96.0</u>	<u>Possibly damaging (1.570)</u>	Fam. B

**Tab. 12** Sequence analysis of all amino acid substitutions identified in LHON plus families. In table are reported the amino acid conservation along the three alignments (mammals, vertebrates and eukaryotes) and the pathogenicity prediction obtained using PolyPhen, PSIC score is indicated inside brackets.

## Part 2 - Modifying factors in LHON: the role of mitochondrial biogenesis in variable penetrance

### Molecular characterization of LHON mutations

In this study we have analyzed 179 individuals belonging to 57 different LHON Italian families and 64 individuals belonging to a single large Brazilian family of Italian ancestry (conventionally named SOA-BR).<sup>327</sup> The family tree of SOA-BR is shown in Appendix C. Each individual has been previously investigated by RFLP analysis and characterized for LHON common mutations (11778/ND4, 14484/ND6 and 3460/ND1). Based on the clinical phenotype all subjects have been categorized in affected and carriers. In SOA-BR family, carrying the 11778/ND4 homoplasmic mutation, 25 individuals were considered affected and 39 carriers (Tab. 13). Moreover, molecular characterization of Italian families, summarized in table 13, reveals that 123 individuals harbored the 11778/ND4 LHON mutation (58 affected and 65 carriers), 20 individuals had the 14484/ND6 mutation (10 affected and 10 carriers) and 36 individuals had the 3460/ND1 mutation (19 affected and 17 carriers).

Family	Mutation	Affected	Carriers	Total
Brazilian (SOA-BR)	11778/ND4	25	39	64
Italian	11778/ND4	58	65	123
	14484/ND6	10	10	20
	3460/ND1	19	17	36

**Tab. 13** LHON individuals investigated in this study: total number and differentiation in affected and carriers.

DNA samples extracted from peripheral blood of these individuals have been analyzed and mtDNA haplogroups have been previously characterized. SOA-BR family belongs to haplogroup J, whereas the haplogroup distribution of Italian families is reported in table 14.

Haplogroup	11778 (n=37)	14484 (n=7)	3460 (n=13)
<b>H</b>	24.32	0.00	53.85
<b>HV</b>	5.41	0.00	0.00
<b>V</b>	2.70	14.29	0.00
<b>U</b>	13.51	0.00	7.69
<b>K</b>	8.11	0.00	7.69
<b>J</b>	21.62	71.43	15.38
<b>T</b>	13.51	0.00	0.00
<b>Other</b>	10.81	14.29	15.38

**Tab. 14** Distribution of mtDNA haplogroup within LHON Italian families expressed as percentages.

### Determination of mtDNA content in LHON individuals

The mtDNA copy number evaluation has been carried out on DNA samples extracted from peripheral blood of SOA-BR family members and selected individuals from the Italian families. This analysis has been approached in two different ways. The SOA-BR is very large (see Appendix C) and allows investigations within the family. We analyzed 64 individuals, 25 LHON affected and 39 LHON carriers. The control group was composed of 70 unrelated Brazilian individuals. Considering the Italian families, we performed a correlation study in selected individuals with homoplasmic LHON mutations, choosing to compare one affected individual, usually the proband, and one asymptomatic carrier on the same maternal lineage. Thus, we analyze 39 affected individuals, and their corresponding 39 carriers, 21 harboring the 11778/ND4 mutation, 5 harboring the 11484/ND6 mutation and 13 harboring the 3460/ND1 mutation. In the last step of this study we also determined the mtDNA copy number in DNA samples extracted from skeletal muscle biopsies of 13 control and 31 LHON individuals (25 affected and 6 carriers).

In figure 32 we show the average values of mtDNA copy number/cell in DNA samples of peripheral blood of control individuals, LHON affected and carriers belonging to the SOA-BR Family. In the control group the average value of mtDNA copy number/cell is  $190 \pm 8$ , whereas SOA-BR family individuals show higher mtDNA/copy number values

(respectively affected  $372 \pm 24$  and carriers  $516 \pm 30$ ). These values are significantly different for comparisons between LHON and control group and between LHON affected and carriers individuals ( $p < 0.001$  in both cases).

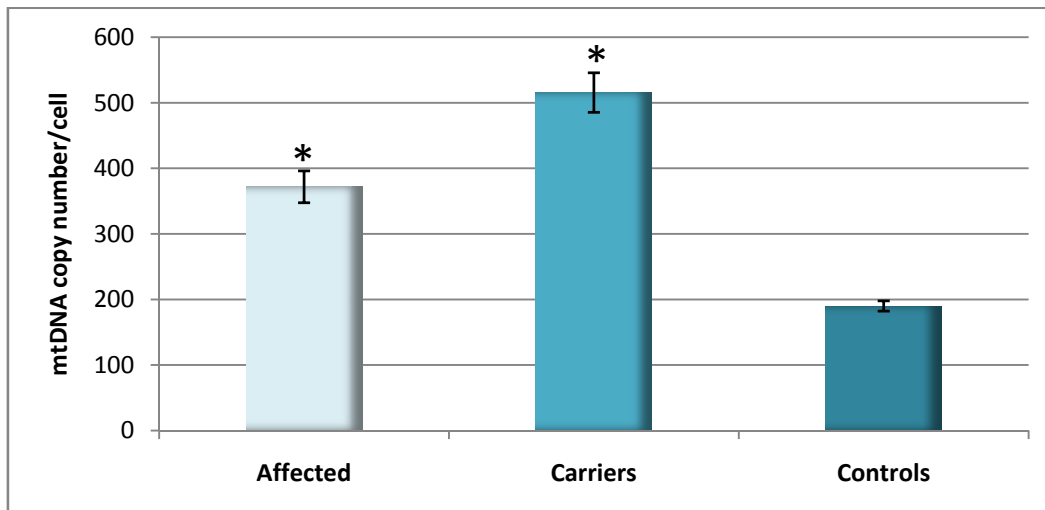


**Fig. 32** MtDNA copy number in controls and LHON affected and carriers belonging to the SOA-BR Family. Data are reported as average  $\pm$  SEM. Asterisks indicate statistical significance (at least  $p < 0.05$ ).

We then analyzed the distribution of mtDNA copy number within the three groups taking into consideration the age and sex, as factors possibly influencing this parameter (Fig. 33). The distribution of mtDNA copy number in controls and affected individuals resulted essentially normal, whereas in carriers two peaks can be easily distinguished (Fig. 33B). In control population no difference was found between males and females, being both normally distributed (Fig. 33F-I). In LHON affected individuals the distribution of mtDNA copy number is mainly due to males and the only two females available did not influence this distribution. On the contrary, the differential evaluation of mtDNA content in male and female carriers revealed that the two peaks are due to a divergent gender distribution of mtDNA copy number (Fig. 33E-H), being mtDNA content reduced in female carriers compared to males. In more than 83% of male carriers, mtDNA copy number was greater than 500, whereas it reached this value only in 37% of females. Thus, this mtDNA copy number value of 500 may be considered as a threshold for an efficient compensatory mechanism, but in females other factors

influencing penetrance have to be considered. Finally, no correlation between mtDNA copy number and age was found in these groups (data not shown).

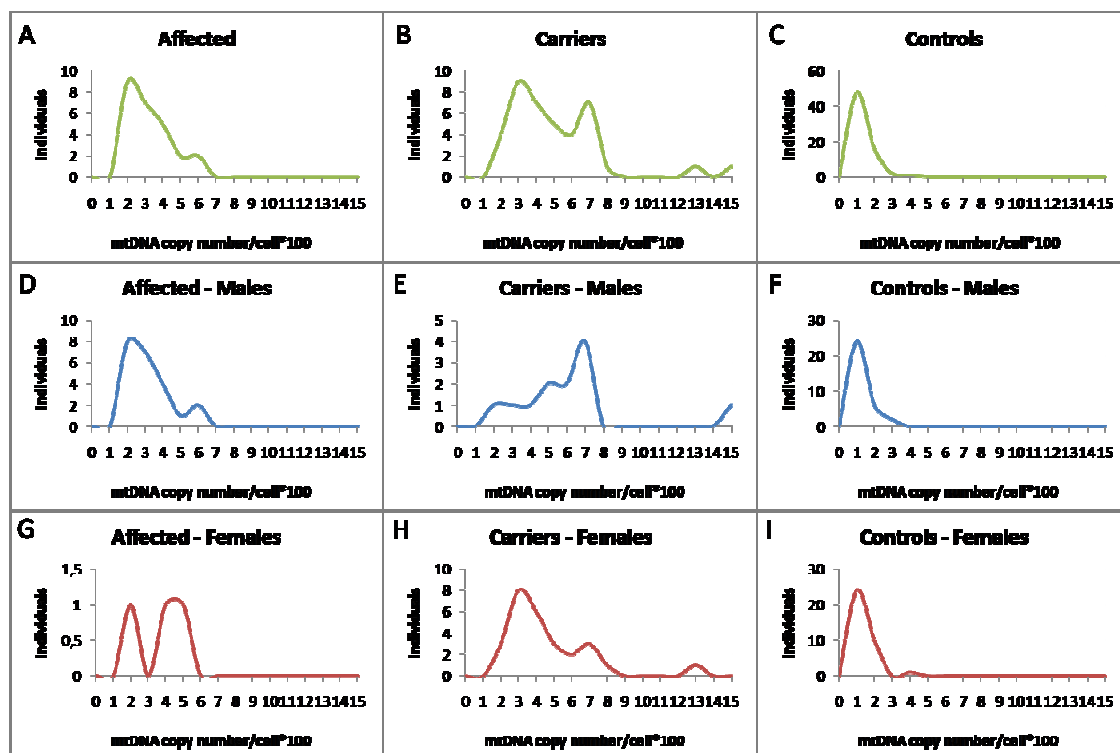


**Fig. 33** Distribution of mtDNA copy number in controls and LHON affected and carriers belonging to the SOA-BR family. In panel A, B and C is shown the general distribution, in panel D, E and F the distribution in males and in panel G, H and I the distribution in females.

Next, we carried out the analysis of mtDNA content in the DNA samples extracted from peripheral blood of LHON affected and carrier individuals belonging to 39 Italian families. Figure 34 shows the average values of mtDNA copy number/cell in LHON individuals, affected and carriers, with the most common mutations. As in the SOA-BR family, this analysis revealed an increased mtDNA content in LHON carriers compared to affected individuals, independent of LHON mutation. In affected individuals the average values of mtDNA copy number were  $305 \pm 14$  (11778/ND4),  $340 \pm 11$  (14484/ND6) and  $315 \pm 14$  (3460/ND1), whereas in LHON carriers were  $688 \pm 21$  (11778/ND4),  $660 \pm 77$  (14484/ND6) and  $583 \pm 41$  (3460/ND1). The absolute values of mtDNA copy number in affected and carriers resulted normally distributed and their

difference statistically significant ( $p < 0.001$  for 11778/ND4 and 3460/ND1 and  $p = 0.011$  for 14484/ND6).

We also analyzed the distribution of mtDNA copy number, considering age and sex, in Italian LHON affected and carriers. The general distribution of mtDNA copy number within these groups was essentially normal and no correlation with age has been found. In this population the difference between affected and carrier was more evident. In fact, only three carriers presented an mtDNA copy number below the value of 500 (results not shown). Thus, this value can be considered a threshold useful to discriminate affected from carrier individuals and may have a prognostic significance.

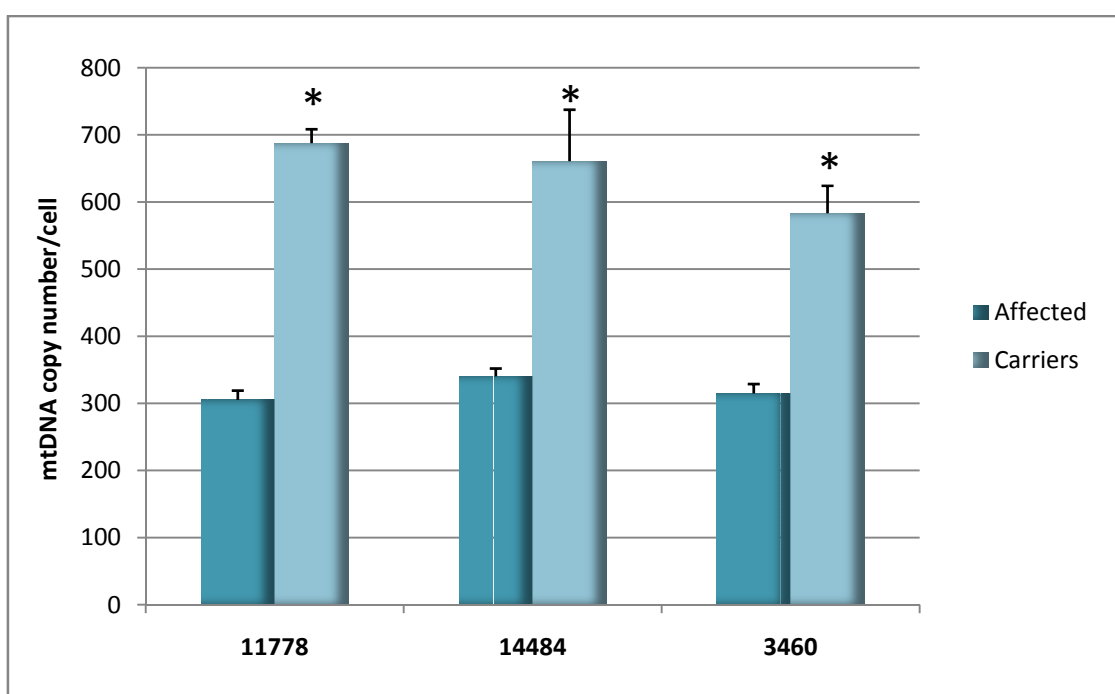


**Fig. 34** MtDNA content whole blood from LHON affected and carrier individuals belonging to Italian families. Values are reported as average  $\pm$  SEM. Asterisks indicate statistical significance ( $p < 0.05$ ).

The mtDNA quantification has been carried out also in skeletal muscle samples of LHON patients (affected and carriers) harboring the 11778/ND4 and 3460/ND1 mutations. These groups have been compared with a control group of 13 normal individuals. Also in this tissue, the mtDNA copy number of LHON individuals was significantly higher than controls (ANOVA Holm-Sidak test  $p = 0.020$ ), but the difference between LHON affected and carriers failed to reach a statistical significance

(t-test  $p=0.471$ ). In fact the average of mtDNA copy number in this study was  $5749\pm 443$  for controls,  $7461\pm 459$  for LHON affected and  $8271\pm 698$  for LHON carriers (Fig. 35). This result may reflect the high variability in mtDNA content in skeletal muscle, influenced by several factors such as life styles and training, or may be the consequence of a different metabolic adaptation of this tissue to the energetic failure due to LHON mutations. Moreover, another hypothesis is that this non significant increase is affected by the small number of investigated carriers, and consequently by the few experiments conducted.

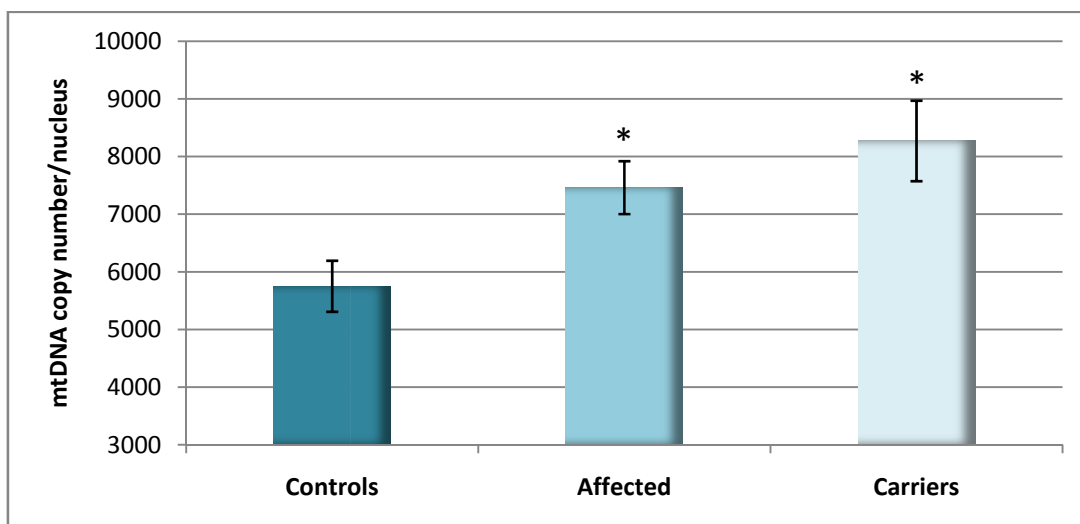


**Fig. 35** MtDNA content in skeletal muscle from controls and LHON individuals. Values are reported as average  $\pm$  SEM. Asterisks indicate values significantly different from controls ( $p<0.05$ ).

In conclusion, all together these data indicate that the energetic defect caused by LHON mutations is associated with induction of a compensatory mechanism triggering the mtDNA replication. Moreover, this mechanism seems particularly efficient in LHON carriers, suggesting its involvement in LHON penetrance.

### **Study of the G1444A polymorphism in PGC-1 $\alpha$ gene**

Based on the above results, we investigated the role of the functional polymorphism G1444A (Gly482Ser) in the PGC-1 $\alpha$  gene, which is the master regulator of mitochondrial biogenesis. According to the results of a recent study, the homozygous variant G (Gly/Gly) may influence the mtDNA content in cells, inducing a decrease in

mtDNA copy number.<sup>328</sup> Thus, this polymorphic variant may play an important role in the modulation of mitochondrial biogenesis, triggered as a compensatory mechanism by the energetic dysfunction. We have therefore analyzed the distribution of the G1444A polymorphism in the previously described SOA-BR family (25 affected and 39 carriers), in its control group and in all available individuals from Italian families (70 affected and 92 carriers). The genotyping was carried out on DNA samples extracted from peripheral blood. Moreover, the possible correlation between PGC-1 $\alpha$  genotype and mtDNA copy number has been tested. In table 15 the frequencies (expressed as percentages) of the three genotypes A/A, G/A and G/G are reported. Even if the “low copies” genotype G/G is under-represented in the carriers group, the three genotypes are not associated with the status of LHON affected or carrier, or to the status of LHON or control.

	Brazil			Italy		
	Affected	Carriers	Controls	Affected	Carriers	Controls (HapMap)
<b>A/A</b>	17%	23%	12%	15%	14%	20%
<b>G/A</b>	50%	66%	46%	37%	48%	33%
<b>G/G</b>	33%	11%	42%	48%	38%	47%

**Tab. 15** Distribution of genotypes of G1444A in PGC-1 $\alpha$  gene in the Brazilian and Italian groups.

Similar results have been obtained considering the frequencies of the alleles A or G within the investigated populations, or comparing the frequencies of the unfavorable genotype G/G to the other two (G/A plus A/A).

In order to verify if there was a correlation between the nucleotide variants in position 1444 of PGC-1 $\alpha$  gene and mtDNA content, we also compared the mtDNA copy number divided for the three possible genotypes in each studied population. As shown in figure 36 A and B, there is no association between mtDNA copy number and the PGC-1 $\alpha$  genotypes.

Taken together these data demonstrate that the G1444A polymorphism does not influence the cellular mtDNA content, at least in Italian and Brazilian population, and does not play a role in the variable penetrance in LHON.

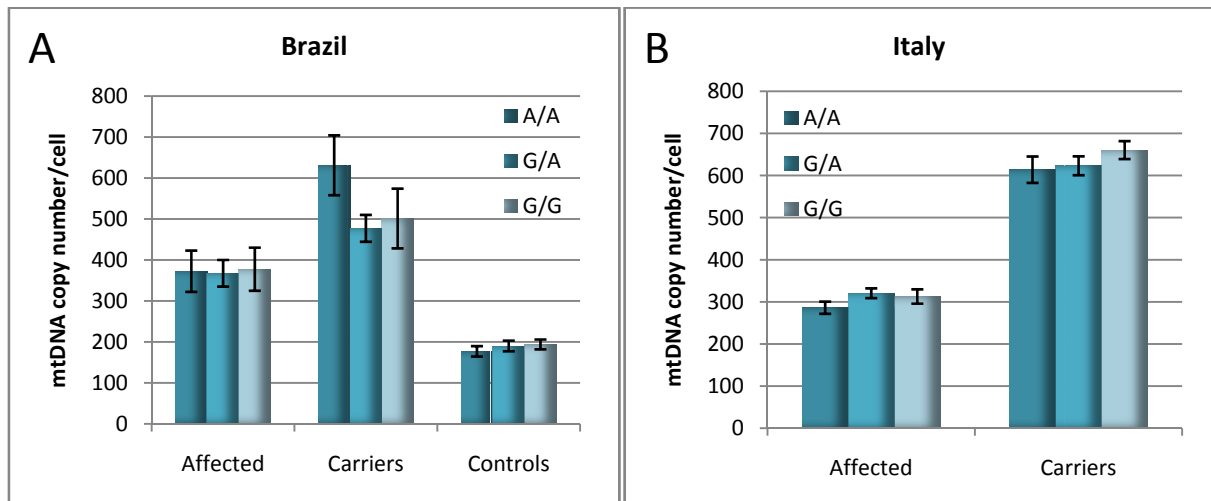


**Fig. 36** MtDNA copy number associated with the three genotypes of PGC-1 $\alpha$  in LHON (affected and carriers) and control individuals, from the two studied populations Brazilian (A) and Italian (B). Values are reported as average $\pm$ SEM.

### Gene expression assays for mitochondrial biogenesis regulators

Given the increased mtDNA copy number in LHON subjects, we decided to investigate the role of transcriptional coactivators belonging to the PGC-1 family (PGC-1 $\alpha$ , PGC-1 $\beta$  and PRC) and the mitochondrial transcription factor Tfam. In this assay we determined the relative gene expression of these genes in five LHON individuals (3 affected and 2 carriers), harboring the homoplasmic 11778/ND4 mutation, and 2 control individuals, using as reference gene  $\beta$ -actin (ACTB). The qRT-PCR assays were carried out on total RNA samples extracted from frozen skeletal muscle of these individuals. In figure 37, we show the results of comparison between LHON and control individuals. All the target genes were up-regulated in LHON samples compared to controls, but only PGC-1 $\beta$  and Tfam reached a statistical significance ( $p=0.006$ , whereas for PGC-1 $\alpha$  and PRC  $p=0.063$ ). The highest up-regulation was reached by PGC-1 $\alpha$  and PGC-1 $\beta$  ( $4.5\pm 0.9$  and  $6.7\pm 1.7$  fold increase, respectively), whereas PRC and Tfam were overexpressed about 3.5 fold. The increased mRNA levels of the mitochondrial

biogenesis regulators may therefore explain the raise of mtDNA observed in skeletal muscle of LHON subjects compared to controls (Fig. 35)

Figure 38 shows the relative gene expression of the same target genes in LHON affected and carriers individuals, obtained with the qRT-PCR assay, using actin B gene as a reference. No differences were detected in the selected genes between the two groups. These results may explain the findings reported in Fig. 34, where no statistically significant difference in mtDNA copy number was apparent in skeletal muscle of affected and carriers individuals.

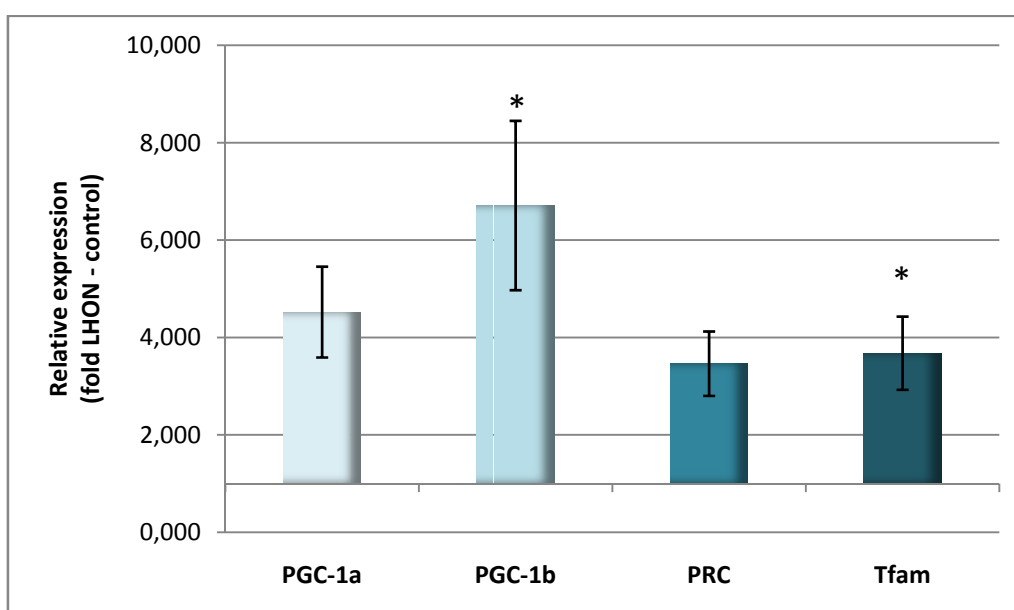


**Fig. 37** Relative gene expression of PGC-1 $\alpha$ , PGC-1 $\beta$ , PRC and Tfam in RNA samples extracted from skeletal muscle of LHON and control subjects, using  $\beta$ -actin (ACTB) as reference gene. Data are shown as fold of increase or decrease in LHON compared to control and are reported as average $\pm$ SEM. Asterisks indicate statistical significance ( $p < 0.005$ ).

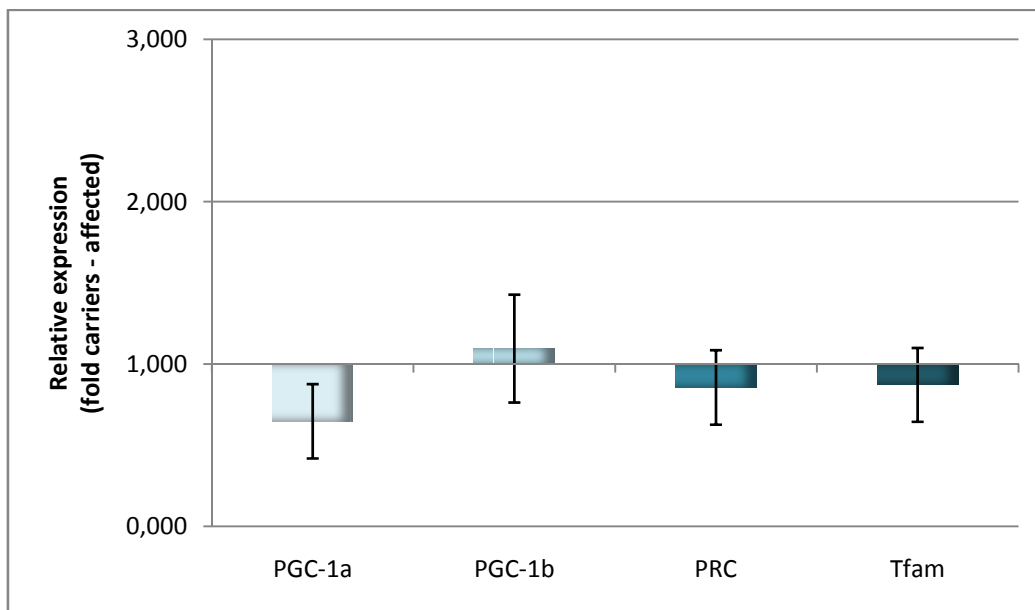


**Fig. 38** Relative gene expression of PGC-1 $\alpha$ , PGC-1 $\beta$ , PRC and Tfam in RNA samples extracted from skeletal muscle of LHON carriers and affected individuals, using  $\beta$ -actin (ACTB) as reference gene. Data are shown as fold of increase or decrease in LHON carriers compared to LHON affected and are reported as average $\pm$ SEM.

---

### **Part 3 – Activation of mitochondrial biogenesis as a therapeutic strategy for LHON**

According to the results reported above, induction of mitochondrial biogenesis might represent a compensatory mechanism activated in response to cellular energetic impairment caused by LHON mutations. A similar behavior has been previously reported for other mtDNA pathogenic mutations associated with more complex mitochondrial diseases (encephalomyopathies). To verify our hypothesis, we took advantage of cellular models of LHON (cybrids), to analyze the effect of the PPARs pan-activator bezafibrate, previously reported to induce mitochondrial biogenesis and to rescue mild and severe defects of the respiratory chain.<sup>329,330</sup> We have investigated six different cybrids cell lines, two *wild type*, two 11778/ND4, two 14484/ND6 and two 3460/ND1. Cybrid cell lines have the same nuclear background of osteosarcoma cell line 143B TK<sup>-</sup> and allow to test the effect of different mtDNA mutations. However, it has to be considered that these cell lines are immortalized and this may influence the cellular response to certain stimuli. We first assessed the biochemical defect discriminating LHON and *wild type* cybrids, as a baseline reference for the following experiments.

#### **Cell viability and energetic competence of LHON cybrids**

Determination of cell viability in a medium devoid of glucose and supplemented with galactose (galactose medium) was carried out. This assay allows evaluation of the mitochondrial energetic efficiency, since galactose slows down the glycolytic rate and cells are forced to rely on the ATP produced almost exclusively through oxidative phosphorylation. Accordingly, cells with defective respiratory chain cannot survive under these growth conditions. As reported in figure 39, all LHON cell lines failed to survive after 72h incubation in galactose medium, whereas control cell lines were still growing.

These results are in agreement with previous reports, confirming the occurrence of a severe oxidative phosphorylation dysfunction in LHON cybrids.<sup>285-287</sup>

Moreover, the specific activity of NADH ubiquinone oxidoreductase (complex I) was measured by means of a spectrophotometric assay. Figure 40 shows that the 3460/ND1 mutation only caused a significant reduction (-40%) in complex I specific activity compared to controls, whereas no difference was detected in the 11778/ND4 and 14484/ND6 cell lines. This result is in agreement with previous data reporting that the effect of LHON mutations on complex I activity is undetectable, except for the 3460/ND1 mutation.<sup>273</sup>

We also performed a polarographic analysis on digitonin-permeabilized cells. In this assay respiration driven by complex I substrates (pyruvate and glutammate) of LHON cells results invariably lower than controls, without reaching statistical significance (data not shown). Conversely, complex II driven respiration in LHON cells resulted comparable to controls.

However, the rate of ATP synthesis, determined in digitonin-permeabilized cells and normalized for the citrate synthase activity, a marker of mitochondrial mass, was strongly reduced in LHON cybrids, when driven by the complex I substrates, malate and pyruvate. This reduction was 39% in 3460/ND1 cells, 51% in 11778/ND4 cells and 71% in 14484/ND6 cells, respectively (Fig. 41). Conversely, we did not observe differences in ATP synthesis rate between LHON and *wild type* cybrids using the complex II substrate succinate plus rotenone (Fig. 41). These results clearly indicate a selective impairment in complex I in LHON cybrids. In conclusion, the assays of mitochondrial ATP synthesis and viability in galactose medium represent the most reliable outcome measures to evaluate the energetic deficit of LHON cybrids.

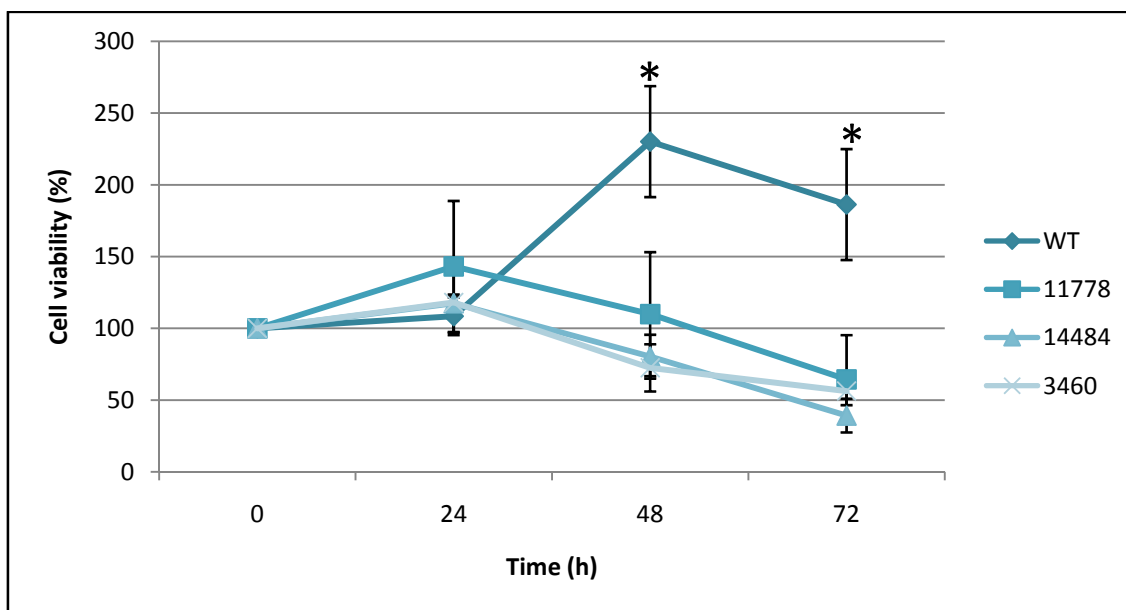


**Fig. 39** Effect of incubation in galactose medium on cell viability of LHON and control cybrids. Data are reported as average $\pm$ SEM. Asterisks indicate statistical significance ( $p < 0.005$ ).

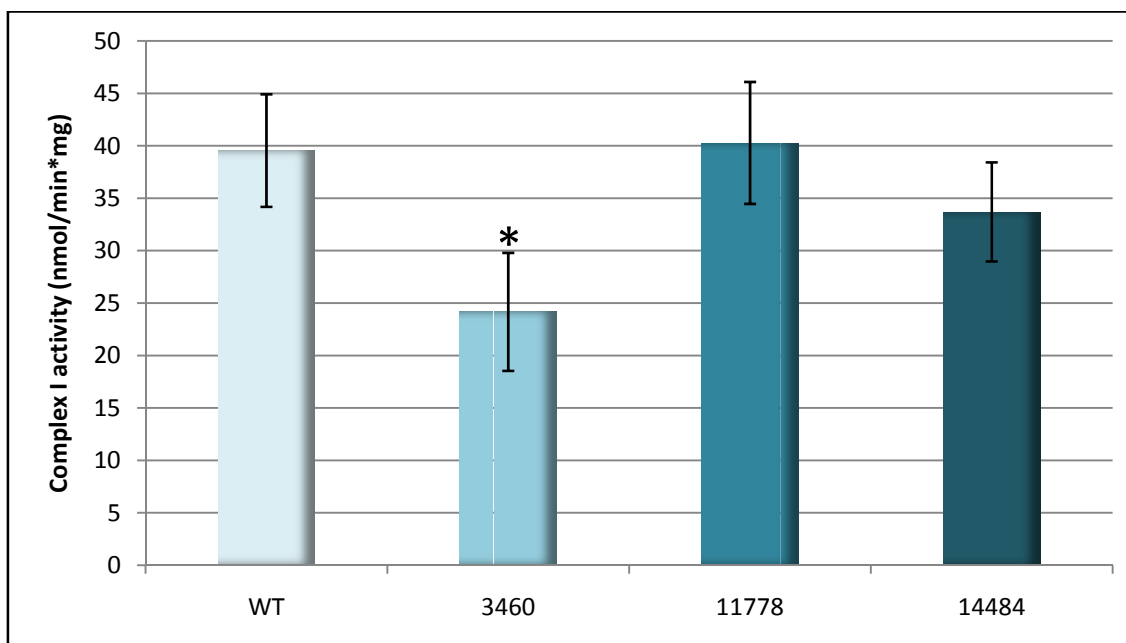


**Fig. 40** NADH ubiquinone oxidoreductase activity in LHON and control cybrids. Data are reported as average $\pm$ SEM. Asterisks indicate statistical significance ( $p < 0.005$ ).

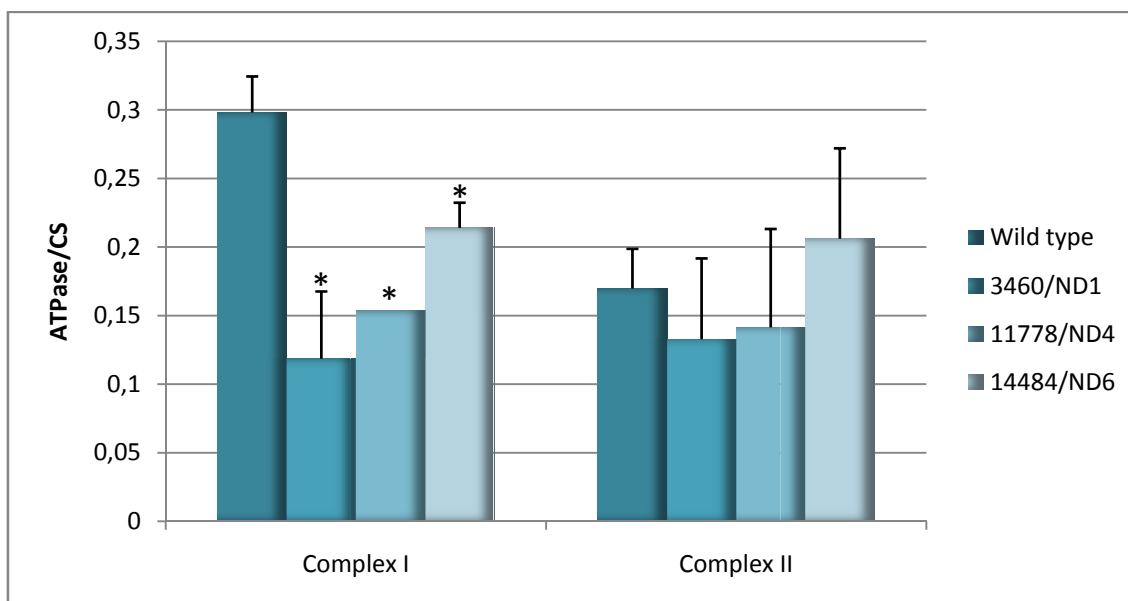


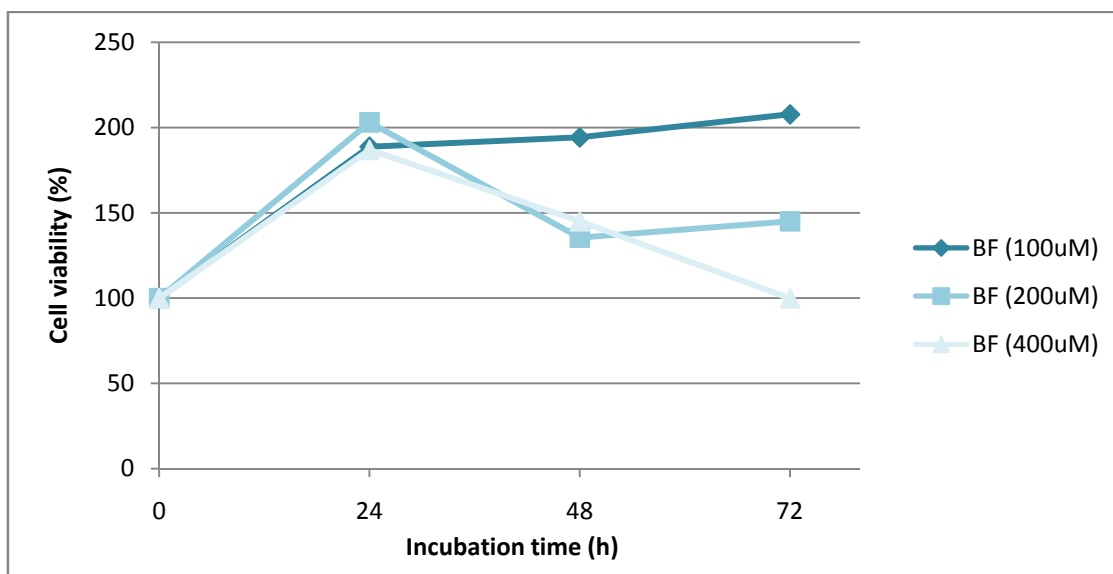
**Fig. 41** ATP synthesis rate normalized on citrate synthase activity, using complex I or complex II substrates, in permeabilized LHON and control cybrids. Data are reported as average $\pm$ SEM. Asterisks indicate statistical significance ( $p < 0.005$ ).

### Dose-response effect of bezafibrate

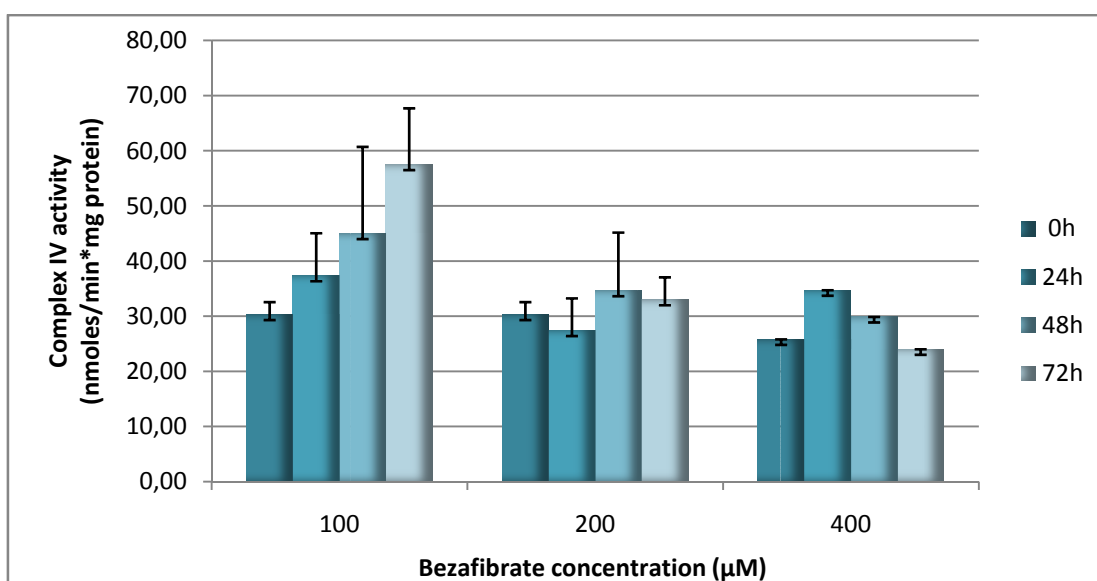
We then determined the concentration-dependent effect of bezafibrate in cybrid cells, by measuring cell viability and complex IV activity. *Wild type* cybrids were incubated with increasing concentrations of bezafibrate (from 100  $\mu$ M to 400  $\mu$ M) and with the corresponding DMSO volume, for different incubation times (0, 24, 48 and 72 hours).

Figure 42 shows the growth curve in complete medium supplemented with bezafibrate in different concentrations. After 48 and 72 hours of incubation, cells incubated with bezafibrate 200 $\mu$ M and 400 $\mu$ M are markedly reduced, whereas those incubated with bezafibrate 100 $\mu$ M still grow (until 215%), even if at low rate. Similar results were obtained with the same cells incubated with DMSO only (data not shown), suggesting a toxic effect of high DMSO concentration, particularly for long incubation time.

Figure 43, reveals that only 100  $\mu$ M bezafibrate was able to induce a time dependent increase in complex IV activity, whereas at higher concentrations bezafibrate had no effect. The increase in complex IV activity was due to bezafibrate, since treatment with DMSO only did not exert any effect (average  $24.24 \pm 3.3$  nmoles/min\*mg protein). Thus, we decided to incubate cells with 100  $\mu$ M bezafibrate for 72 hours in the following experiments.



**Fig. 42** Effect of incubation in bezafibrate medium on cell viability of wild type cybrids.



**Fig. 43** Cytochrome c oxidase activity in wild type cybrids incubated with increasing concentration of bezafibrate for different times. Data are reported as average±SEM.

### Effect of bezafibrate on mitochondrial biogenesis

We first tested the effect of bezafibrate on mitochondrial biogenesis activation. The mtDNA copy number/cell was evaluated in cells treated with bezafibrate and with DMSO. As shown in figure 44A, no effect on mtDNA content was determined after bezafibrate treatment, both in wild type and mutants. In fact the mtDNA copy number

of treated cells ranged from 83% to 93% of DMSO-treated cybrids. We also analyzed the relative gene expression of PGC-1 $\alpha/\beta$  and Tfam with a qRT-PCR assay. The relative mRNA levels of target genes were similar in treated and untreated samples (Fig. 44B). Furthermore, we performed a western blot analysis of several respiratory complexes subunits, nuclear or mitochondrial encoded, and of two structural proteins as control. These were three complex I subunits (NDUFA9, NDUFS3 and ND6), one complex II subunit (SDHA), three complex IV subunits (COX XI, COX IV and COX VIc) and one complex V subunit (ATPase a). The structural proteins actin and tubulin were used as controls for the densitometric analysis. As shown in figure 45, the levels of all analyzed proteins were not changed by bezafibrate treatment in all cell lines. Taken together, these data demonstrate that despite the effect on cell viability and complex IV activity, bezafibrate does not induce mitochondrial biogenesis and mtDNA replication or transcription in cybrid cells.

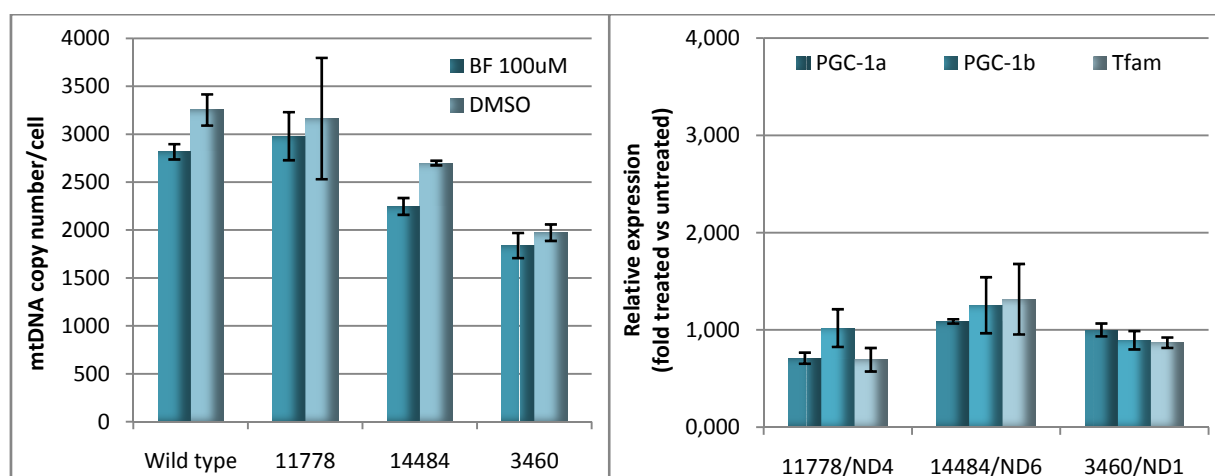


**Fig. 44** A) MtDNA copy number in LHON and control cybrids treated with bezafibrate 100  $\mu$ M for 72 hours or with equal volumes of DMSO for 72 hours. Data are reported as average $\pm$ SEM. B) Relative gene expression of PGC-1 $\alpha$ , PGC-1 $\beta$  and Tfam in RNA samples extracted from LHON cybrids treated with bezafibrate 100  $\mu$ M for 72 hours or with equal volumes of DMSO for 72 hours. Data are reported as average $\pm$ SEM.

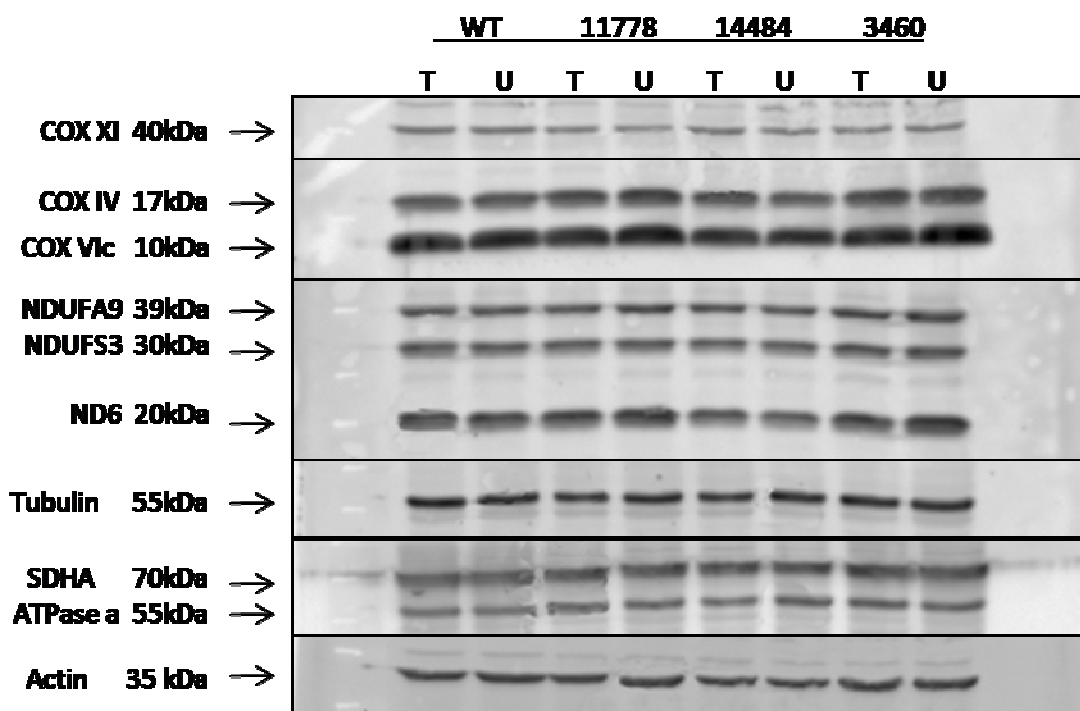


**Fig. 45** Western blot analysis of several respiratory chain proteins in LHON and control cybrids treated with bezafibrate 100  $\mu$ M for 72 hours or with equal volumes of DMSO for 72 hours. Actin and tubulin were used as loading control in densitometric analysis.

Bezafibrate has been reported as a pan-activator of PPARs and should consequently induce mitochondrial biogenesis through the PGC-1 pathway.<sup>329,330</sup> However, it is possible that bezafibrate might improve the respiratory chain activity, with a mechanism independent of mitochondrial biogenesis. To verify this hypothesis we evaluated whether bezafibrate could ameliorate the rate of mitochondrial ATP synthesis in LHON cybrids. Indeed, a slight increase in complex I-driven ATP synthesis, corrected for the citrate synthase activity, was apparent in bezafibrate-treated 11778/ND4 and 14484/ND6 cybrids, as shown in figure 46. This increase, however, was not statistically significant and was not observed in the 3460/ND1 LHON cybrids (Fig. 46 panel A). Complex II-mediated ATP synthesis was also unaffected by incubation with bezafibrate (Fig. 46 panel B).

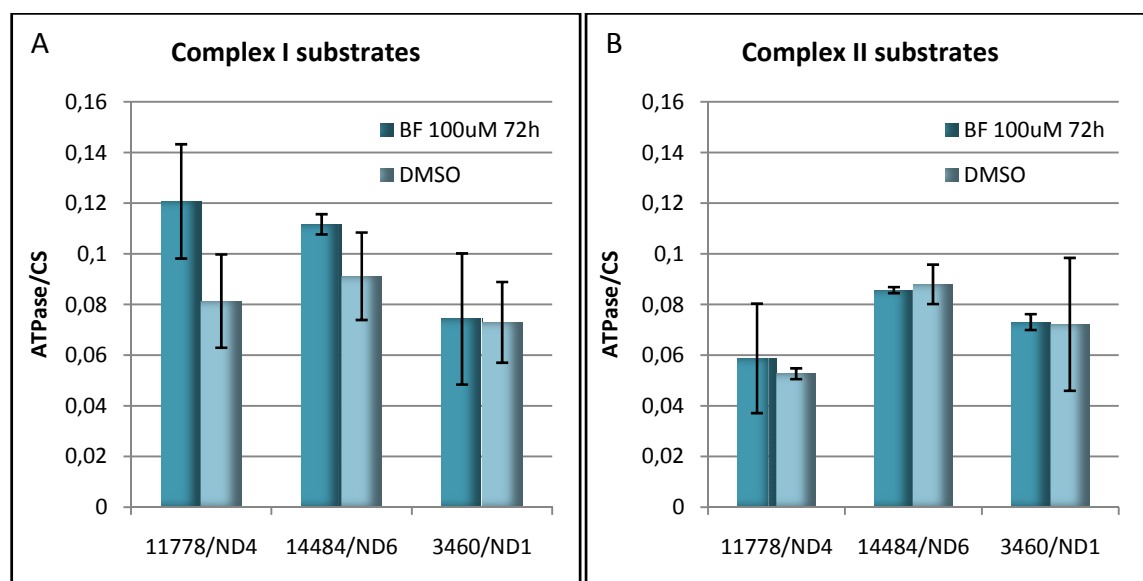


**Fig. 46** ATP synthesis rate normalized on citrate synthase activity, using complex I or complex II substrates, in permeabilized LHON cybrids treated with bezafibrate 100  $\mu$ M or with equal volume of DMSO for 72 hours. Data are reported as average  $\pm$  SEM.

Finally, we assessed the effect of bezafibrate on LHON and control cybrids growth in galactose medium. Cell viability was determined by means of the SRB assay. As shown in figure 47A, wild type cybrids viability was not influenced by the presence of bezafibrate or vehicle. The bezafibrate treatment was also ineffective in LHON cybrids when compared to DMSO, with the only exception of a transient, weak and not statistically significant effect after 48 hours of incubation in galactose (Fig. 47 panels B, C and D).

In conclusion, the data presented demonstrate that bezafibrate is unable to activate the signalling pathway for mitochondrial biogenesis induction and to trigger mtDNA replication or transcription, at least in the described experimental conditions. Moreover, bezafibrate does not exert any effect on mitochondrial ATP synthesis rate and fails to protect LHON cybrids from galactose-induced cell death. Thus, this drug is not able to influence the function or the activity of respiratory chain complexes in our cellular model.

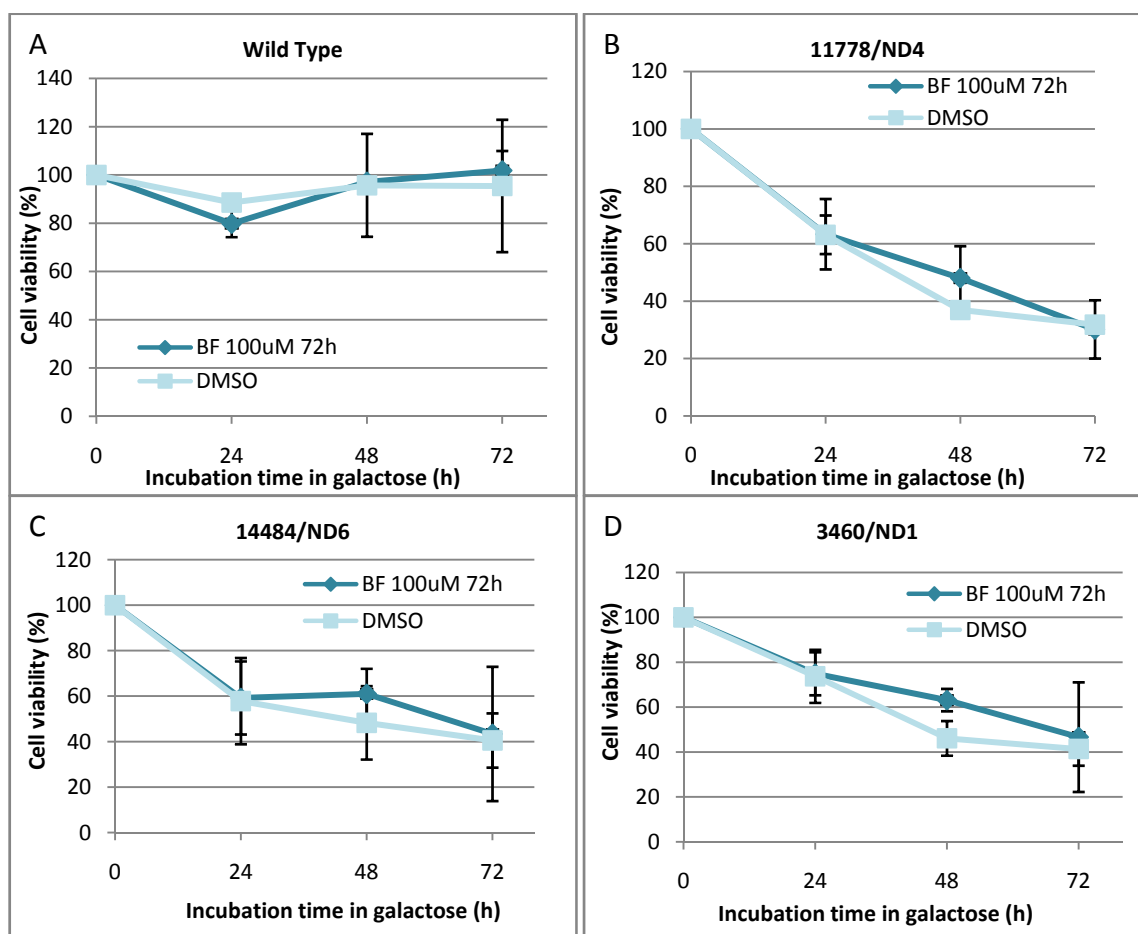


**Fig. 47** Effect of incubation in galactose medium, plus bezafibrate 100  $\mu$ M or equal volume of DMSO, on cell viability of control (panel A) and LHON cybrids (panels B, C and D). Data are reported as average  $\pm$  standard deviation.

# **Discussion**

Leber's hereditary optic neuropathy (LHON) is a usually monosymptomatic disease characterized by a bilateral acute or sub-acute loss of central vision, caused by the selective degeneration of RGCs, leading to optic atrophy. It is now clear that LHON is one of the most common mitochondrial diseases. However, many aspects of this pathology are still unclear, such as the male prevalence, the incomplete penetrance and the selective involvement of a single cell type. Moreover, several new pathogenic mutations have been reported in the last years increasing the range of mutations that have to be screened in the diagnostic protocols. Finally, the pathogenic mechanism is still debated and no effective therapies are available for LHON patients.

In this study we analyzed three aspects still unclear in LHON. At first, we investigated the role of rare mtDNA variants, mutations or polymorphisms, as causative or modifiers of LHON clinical phenotype. Second, we searched for a molecular feature able to distinguish affected and carrier subjects, within the same family or in different families, shedding light on the possible mechanism of variable penetrance. Lastly, we explored by a preliminary study, using the cellular model of LHON cybrids, the possibility of a pharmacologic therapeutic approach.

### **LHON pathogenic mutations are located in defined and conserved domains of mtDNA encoded complex I subunits**

Complex I is the first enzyme of the respiratory chain and catalyzes the transfer of two electrons from NADH to ubiquinone, coupled to pumping of 4 protons across the membrane. This protein complex presents an L-shaped global structure, with a hydrophobic arm embedded in the membrane and a hydrophilic peripheral arm protruding in the mitochondrial matrix.<sup>331,332</sup> Recently, the crystal structure of the hydrophilic arm has been solved, but currently there are only few data concerning the structural details of hydrophobic arm subunits.<sup>43</sup> We here propose new structural models for ND1-ND4 and ND4L complex I subunits, based on the analysis of hydropathy profiles generated starting from a wide global alignments of virtually all the available complete protein sequences.

To date, the only exhaustive work predicting a structural model for each mitochondrial encoded complex I subunits has been published in 1992 by Fearnley and Walker.<sup>333</sup> Other structural models have been proposed for ND1, ND6 and ND4, in order to define

the possible role of newly identified pathogenic mutations or to explain the biochemical characterization of the common LHON pathogenic mutations.<sup>239,271,274,321,324</sup> However, none of those is based on the great number of sequences currently available on generic and specialized data banks. Moreover, we analyzed three different data sets, corresponding to eukaryotes, vertebrates and mammals, to define either the most conserved regions, but also those regions particularly conserved in mammals that may be crucial for protein function. All the sequences are characterized by long hydrophobic segments, generally of 20 or more amino acids, probably folded in membrane spanning regions. These TMHs are connected by short hydrophilic loops, although some of them may be organized in extra-membrane domains.

Our analysis on average conservation and fraction of conserved amino acids, confirms that ND1 is invariably the most conserved subunit and that ND6 is the most divergent, as previously reported by Fearnley and Walker.<sup>333</sup> However, the other ND subunits have a different overall conservation within the three data sets. Considering the single ND subunits, our analysis on ND3 and ND4L reveals that these very short proteins are extremely hydrophobic and are folded in three TMHs, as previously reported.<sup>333</sup> In previous works, ND6 subunit was predicted to have 5 or 6  $\alpha$ -helices.<sup>333,274,321</sup> We here propose for ND6 subunit a structural model with 5 TMHs, similar to Fearnley and Walker and to Carelli et al, 1999.<sup>333,274</sup> In fact, we do not predict as membrane embedded the short region from amino acid 116 to 120, being too short to be considered a transmembrane helix. For ND1 at least two different models have been proposed. The first one represents ND1 with 8 membrane spanning domains<sup>239,333</sup>, whereas Carelli et al., 1997, and Valentino et al., 2004, proposed a structural model characterized by only 5 transmembrane segments and an extra-membrane domain with an hydrophobic region (helix E).<sup>271,324</sup> The model here proposed for ND1 is very similar to that one, with the only exception of the C-terminal, where we recognized another transmembrane domain. In fact, our model maintains 5 TMHs and one hydrophobic extra-membrane domain, probably an amphipatic helix on the positive side of the membrane, but presents another TMH (helix G in our model) in the C-terminal of the polypeptide chain. The structure of the ND4 subunit has been also predicted with 11 or 12 TMHs.<sup>333,271</sup> Our new model predicts 10 clearly defined TMHs and 2 additional helices that can be either transmembrane or located in extra-membrane domains. Furthermore, the topology of

ND4 across the membrane cannot be clearly defined, being the net charge on the two sides of the protein positive and very similar. Finally we proposed for ND2 a structural model with 8 TMHs and one uncertain helix and for ND5 a model with 13 TMHs and one unclear helix, whereas Fearnley and Walker predicted 10 and 15  $\alpha$ -helices for ND2 and ND5, respectively.<sup>333</sup>

The differences between the proposed models may be due to different approach or hydrophathy scales. In fact, models can be derived from a sequence from a single organism or from alignments of several sequences from different organisms. Moreover, the number of sequences and their divergence may influence the overall hydrophathy, if the model is generated on the average hydrophobicity along the alignment, or the generation of a consensus sequence (see results). The choice of the hydrophathy scale and the hydrophobicity threshold may also influence the structural models, when the template structure is unknown. As suggested by Degli Esposti et al., in several integral proteins the hydrophobicity scales based on statistical analysis correlate better than those based on transmembrane distribution of the residues, in several integral proteins.<sup>309,334</sup> Thus, commonly used hydrophathy scales, such as that of Kyte and Doolittle, may lead to wrong predictions for the folding of transmembrane proteins folding, even if their performance on globular protein are optimal.<sup>334,335</sup> Furthermore, an integration of different and appropriate predictive methods is recommended, since every single method is prone to errors.<sup>309</sup>

Prediction methods based exclusively on hydrophathy scales can be now combined with up to date methods based on different parameters, such as sequence profile analysis using amino acid properties, neural network (NN) and Hidden Markov Models (HMM) trained on transmembrane proteins with known structure (for reviews see Punta et al., 2007, and Simon et al., 2001).<sup>336,337</sup> Thus, in a future step we will use different prediction tools to ND1-ND6 and ND4L protein sequences, to generate an “ensemble” prediction of the protein structures. This approach, recently applied in different papers, for example Martelli et al., 2003, combining a NN and two different HMM predictors, is probably the best approach to *ab-initio* structure predictions.<sup>338,339</sup>

We used these models and some tools available on line for the prediction of pathogenicity to analyze the possible impact of mitochondrial mutations on the protein

function and to identify structural regions with a functional role and specific patterns for LHON pathogenic mutations.

Establishment of the pathogenic potential for an mtDNA mutation is still controversial. The classical criteria proposed by DiMauro and Schon are currently used to determine the pathogenic potential of a novel mtDNA nucleotide variant.<sup>340</sup> However, in 2006 a new score system has been introduced by Mitchell and coll.<sup>304</sup> This score system is based on a weighted analysis of the canonical criteria, the functional evidence of pathogenicity and the multiple and independent reports of pathogenicity of a mitochondrial mutation. Instead, our predictions represent an *in-silico* approach based exclusively on conservation analysis. Although our approach takes into account less parameters, it can be a “cheap and easy” tool for the initial screening of mitochondrial sequence variations, together with a careful search for the putative mutation in specialized data banks of mtDNA variation, such as HmtDB or Mitomap ([www.hmtdb.uniba.it](http://www.hmtdb.uniba.it), [www.mitomap.org](http://www.mitomap.org)).

Our analysis reveals that 25/39 nucleotide variants, reported on Mitomap as pathogenic for LHON, are predicted as probably damaging at least by 3/4 methods. All the mutations reported as “confirmed” on Mitomap are predicted as pathogenic by every used method, with the only exception of 14568/ND6 mutation that is predicted as unclear. Similar results were obtained applying the score system that predicts as probably or possibly pathogenic all these mutations, whereas 14568/ND6 was still considered neutral. Other 19 nucleotide variants, cited on Mitomap as “reported”, are predicted as pathogenic, whereas 2 are uncertain, being predicted as pathogenic by 2/4 methods. Instead, the score system recognizes as probably or possibly pathogenic 12 of the reported mutations. Thus, our approach probably is more prone to recognize some unclear variant as probably pathogenic, but none of the common non-synonymous polymorphisms, associated in the general population with mtDNA haplogroups, is predicted as pathogenic.

We also analyzed the position of the reported “primary” mutations and of some polymorphisms on the previously generated structural model of ND1-ND6 and ND4L subunits. This approach allows us to define some protein regions, usually characterized by local high conservation, with probable functional roles for these proteins. ND1 is a mutational hot spot of LHON and all the pathogenic (predicted or confirmed) mutations

are located in extra-membrane loops protruding in the mitochondrial matrix. Interestingly, these loops are the most conserved zones of the ND1 polypeptide and probably define a functional domain, as previously suggested by our group.<sup>271,324</sup> In ND4 only two mutations are considered pathogenic (G11778A and C11874A) and both are located in the loops facing the positive side of the membrane in the boundaries of the helix J, predicted as amphipatic. Concerning ND5, two regions particularly affected by pathogenic mutations can be defined. Similar to ND1 and ND4, extra-membrane loops are affected; the first region is defined by the loops DE and FG on the matrix side of the membrane, whereas the second is located on the positive side of the membrane (intermembrane space) and involves the loops JK and LM. The other hot spot for LHON pathogenic mutations is ND6 and the structural model here proposed clearly defines that only the helices B and C are affected by pathogenic LHON mutations.

### **Confirmation of pathogenic LHON rare mutations**

Five unrelated Italian families have been investigated. All of them fulfilled the clinical criteria to be diagnosed as LHON, but they were negative at the screening for the three LHON common mutations. Thus, complete sequencing of mtDNA has been carried out in DNA samples from the probands and we found four rare LHON mutations, previously reported, and two rare mtDNA variants with pathogenic potential (for discussion of these see next paragraph). We found one mutation in ND1 gene (G3700A) and three mutations in ND6 gene (C14568T, G14459A and A14495G), all of them previously reported at least once.

The mutation G3700A/ND1 was reported in a single case of LHON in 2002 by Fauser and coll., in a screening of 14 LHON patients negative for common mutations.<sup>316</sup> In that case the authors suggested that this mutation may have a pathogenic role for LHON within the family, but could not confirm this hypothesis because the mutation was found only in a single family. Our findings support that initial results, confirming that G3700A change is a rare primary LHON mutation, now identified in two LHON unrelated families and not present in over 3400 control sequences of HmtDB data bank. Our conservation analysis reveals that the amino acid substitution Ala132Thr affects a very conserved residue within a conserved extra-membrane loop of ND1, with possibly implicated in the quinone binding. Furthermore, the Ala to Thr change is non-

conservative, with a switch from a neutral and hydrophobic to polar and hydrophilic amino acid and an increase in steric volume. The pathogenicity of G3700A/ND1 mutation is also supported by the identification of another pathogenic mutation located in the same loop (G3733A, Glu143Lys) in two unrelated families by Valentino et al., 2004.<sup>324</sup>

In Family 2 we identified the heteroplasmic rare transition C14568T/ND6. This mutation induces the amino acid substitution Gly36Ser in the ND6 subunit and was previously found in two unrelated families in homoplasmic condition.<sup>316-319</sup> In our family the mutation was heteroplasmic, at different loads, in all the investigated tissues from two siblings (IV:3 and IV:5). Another sibling (IV:2) and the mother (III:2) were virtually *wild type*; however, in particular for the mother, it is possible that the percentage of mutant mtDNA was under the detection threshold for a standard RFLP analysis. Thus, a more sensitive approach, such as hot last cycle PCR or cloning and sequencing of the PCR fragment, have to be applied in these cases. The conservation analysis shows that Gly-36 is a divergent amino acid in eukaryotes and vertebrates, but reaches an absolute conservation within mammals. The Gly-Ser substitution is a non-conservative change in terms of hydrophobicity but does not affect the steric volume, being both amino acids are very small. Notwithstanding, glycine is hydrophobic and neutral, whereas serine is hydrophilic and polar. This amino acid resides in helix B of ND6, one of the best conserved regions of the protein probably involved in the quinone binding site. Furthermore, this mtDNA lineage harbors also the homoplasmic nucleotide variant T4172A/ND1. This nucleotide substitution has been reported once and probably is the marker of a specific subclade of haplogroup U6a. This polymorphism induces the amino acid substitution Leu289Gln in the ND1 protein. Interestingly, the same amino acid is substituted (Leu289Met) in presence of the mutation C4171A/ND1, reported as pathogenic for LHON.<sup>320</sup> In fact, Kim et al., 2002, reported this mutation in two unrelated LHON families belonging to haplogroup A (Korean ancestry), with a good visual prognosis and a high frequency of visual recovery. The amino acid position 289 in the ND1 subunit is well conserved in vertebrates and mammals and affects a conserved extra-membrane loop protruding on the matrix side. Surprisingly, the pathogenic change Leu289Met is predicted benign by all the used tools (PolyPhen, SIFT and PMut), whereas the polymorphic change Leu289Gln is predicted as

pathogenic. This may be explained by the substitution type. In fact, the substitution Leu289Met is conservative, being both leucine and methionine large, hydrophobic and neutral amino acids, whereas the Leu289Gln is non-conservative, being glutamine smaller and polar. Thus, the latter may have a stronger impact on ND1 function. Moreover, the biochemical effect of both variants on complex I activity is not evident in respiratory chain complexes activity assays. This could be explained by the high percentage of *wild type* mtDNA in the platelet fraction or by a mild effect on complex I activity, similar to the 14484/ND6 mutation.<sup>273</sup>

Taken singularly, the homoplasmic 14568/ND6 and 4171/ND1 mutations are usually associated with LHON phenotypes with good visual prognosis. Our family also shows a partial recovery of visual acuity, but it is characterized by a heteroplasmic mutation. However, the presence of the 4172/ND1 variant may modulate the pathogenicity of the 14568/ND6 mutation.

The 14459/ND6 mutation, found in Family 3, has been frequently reported in literature often associated with a variable clinical phenotype ranging from LHON, to LHON plus spastic dystonia, to Leigh syndrome.<sup>234,238,341-346</sup> This variability is also evident in our family, where the mutation was homoplasmic at least in three of the investigated subjects, being one unaffected carrier (III:2), one LHON affected (III:1) and one affected with spastic dystonia only (III:5). The fact that these three individuals were all homoplasmic, but discordant for their clinical expression, strongly suggests the influence of nuclear/environmental factors as modifiers. This nucleotide change induces the Ala72Val substitution. Along eukaryotes and vertebrates alignments, this position is very divergent, whereas in mammals is invariant and is located in the extremely conserved helix C of the ND6 subunit. This amino acid change is conservative, being alanine and valine very similar. Biochemical evaluations confirm a severe impairment of complex I. Interestingly, the subject with the most severe phenotype (III:5) shows an increase in complex II, complex III and complex IV activities, probably due to a compensatory mitochondrial proliferation. Even if this mutation is often associated to LHON plus spastic dystonia, our cases demonstrate that the mutational screening has to be carried out also in patients with pure LHON phenotype, negative for the common mutations.

We also identified the third LHON case associated with the heteroplasmic A14495G/ND6 mutation. The analysis of the complete mtDNA sequence revealed that this family is unrelated to the families reported by Chinnery et al., 2001, even if they all belong to haplogroup H.<sup>321</sup> We found this mutation with a heteroplasmic load of about 50% in peripheral blood. The same heteroplasmic load was found in one affected individual in the British family previously reported.<sup>321</sup> The authors proposed that mutational load may be higher in other tissues, or that some environmental factors may enhance the pathogenicity of the mutation or that the threshold level for this particular mutation may be lower than for the others. The A14495G mutation induces the amino acid change Leu60Ser. This amino acid position is extremely conserved and is part of the hyper-conserved helix C of ND6. Moreover, the amino acid substitution is non-conservative; in fact, leucine is a hydrophobic large amino acid, whereas serine is small, polar and usually exposed on the protein surface.

In conclusion, we here confirm the pathogenicity of four rare LHON mutations (G3700A/ND1, C14568T/ND6, G14459A/ND6 and A14495G/ND6) and suggest their inclusion in the diagnostic protocols. Furthermore, we also confirm that ND1 and ND6, in particular some hyper-conserved regions, are common hot spots for LHON mutations.

### **Novel putative pathogenic LHON mutations**

We here report two branches of a single family independently investigated and then reconnected through their mtDNA lineage. The two probands showed a typical LHON clinical phenotype but RFLP survey for LHON common mutations resulted negative. Thus, we sequenced the entire mtDNA molecule and we found two rare variants with pathogenic potential. This mtDNA lineage belongs to haplogroup K1a and harbors, in addition to haplogroup specific polymorphisms, the nucleotide variants A8944G/ATPase6 and G14258A/ND6.

All the confirmed LHON mutations affect mitochondrial encoded complex I subunit genes (see Mitomap), thus at our first analysis the variant 14258/ND6 seemed to be the most probable pathogenic mutation. However, conservation analysis, pathogenicity prediction and localization of the affected amino acid all suggest that this variant should not interfere with complex I function or assembly. In fact, the amino acid substitution

Pro139Leu affects a very divergent residue in a poorly conserved ND6 region (the extra-membrane loop DE). Two other putative mutations have been previously reported in the same loop.<sup>256,347</sup> The mutation T14325C was found in a Dutch pedigree, negative for LHON common mutations, with a single affected individual and hits the amino acid position Asn-117 (change to Asp). The authors proposed this variant as a candidate mutation but suggested further studies to prove its real pathogenicity. In the same loop is also located the mutation G14279A that induces the amino acid substitution Ser132Leu. Both these changes affect poorly conserved residues of ND6 and are predicted as neutral at least by PolyPhen and SIFT. Moreover, no biochemical assessments of complex I function have been carried out on patients or cell models harboring these mutations. Similarly, the 14258/ND6 variant is predicted as neutral by PolyPhen and SIFT and pathogenic by PMut, but with a low score and a low reliability. The measurement of complex I activity on platelet fraction shows a specific activity comparable to controls. This result may suggest that this variant is a polymorphism that does not influence complex I activity or it may be explained by considering that mild mutations often do not cause a detectable complex I impairment.<sup>273</sup> We also analyzed the presence of this variant in the general population. In HmtDB this variant is present only once in one mtDNA sequence belonging to haplogroup H and it was also reported in five individuals, from India and Nepal, by Semino et al., 1991.<sup>323,348</sup> Moreover, we also found this nucleotide variant in heteroplasmic condition in an LHON patient harboring the 14484/ND6 mutation on haplogroup L2.<sup>349</sup> However, it is still reasonable that 14258/ND6 change is a mild pathogenic mutation; in fact, no clinical details were provided on the individuals identified by the population studies of Herrnstadt et al., 2002, and Semino et al., 1991, and a mild mutation might have only subclinical effects.<sup>323,348</sup>

The other nucleotide change with a pathogenic potential is A8944G/ATPase6 and induce the amino acid substitution Met140Val. Our analysis reveals that the affected position is invariant in mammals and is predicted as pathogenic with high score by PMut. The affected region is extremely conserved in mammals and may play a role in ATP synthase function. Moreover, the A8944G variant has been reported only once on a L3 haplogroup background.<sup>322</sup> ATPase6 gene is usually a hot spot for Leigh syndrome, but some mutations have been reported in this gene in LHON pedigrees.

Abu-Amero and Bosley reported the nucleotide changes G8950A in a LHON plus dystonia patient, with a decrease in mitochondrial respiratory activity. However, no other details about that patient were provided.<sup>350</sup> The same authors identified the A8836G mutation, predicted as pathogenic by PolyPhen, but assessment of mitochondrial respiratory activity for this case was not available.<sup>351</sup> Moreover, in this study the increase of mtDNA content is suggested as a marker of pathogenicity, but in the sample characterized by A8836G mutation the relative mtDNA content was lower than the proposed threshold (1.27 versus 1.76 of threshold).<sup>351</sup> The heteroplasmic mutation A9016G was found in a LHON pedigree harboring the primary 14484/ND6 mutation. The authors defined the A9016G a secondary mutation able to induce a complete penetrance of the primary mutation in males.<sup>352</sup> However, the sequences reported in this study contain many errors as shown by successive analysis.<sup>353</sup> Quoting Bandelt et al., 2007, “it is still an open question whether the heteroplasmic mutation A9016G is real and (...) could be blamed for the high penetrance of LHON in that family”.<sup>353</sup> Another variant reported in ATPase6 gene is T9101C and causes a reduction in ATP synthase activity, even if the affected amino acid is poorly conserved.<sup>354</sup> Thus, the role of these mutations is still unclear and debated. We also found in an LHON pedigree, negative for common mutation and belonging to haplogroup C, the rare variant T8555C/ATPase6 (data not shown, analysis still in progress). This mutation may affect an important functional domain of ATPase a subunit, being predicted by PolyPhen as possibly damaging (classified as “improper substitution in the transmembrane region”), and also by PMut, despite it affects a poorly conserved amino acid.

In conclusion, we here propose for Family 5 two candidate pathogenic mutations (A8944G/ATPase6 and G14258A/ND6), but further studies are necessary, in particular biochemical investigations aimed to determine their real role on complex I and ATP synthase function.

### **Rare mtDNA variants are associated to LHON plus myoclonus**

We here report the recurrence of myoclonus in two Italian LHON families as a feature of central nervous system involvement besides the optic nerve. Since myoclonus was strictly maternally inherited in Family A, we sequenced the entire mtDNA and found

that there was an accumulation of non-synonymous variants in both families, similar to what was recently reported for the modifying effect of haplogroup J on LHON penetrance.<sup>327</sup> Occurrence of myoclonus in association with LHON has been previously reported in a few cases.<sup>355-357</sup> In our families, myoclonus seemed to be a feature independent from optic neuropathy, being present also in one individual not visually affected. The complete mtDNA sequencing, in conjunction with the conservation analysis of the observed variants, provided new clues to explain myoclonus in these two LHON families. The 4136/ND1 mutation in Family A is of particular interest because it was previously reported only four times, of which three were LHON families carrying one of the primary mutations (the QLD1 family from Australia and two Italian families).<sup>242,325</sup> The QLD1 family showed the co-occurrence, within the same maternal genealogy, of classical cases with LHON, cases of infantile encephalopathy with early deaths and features resembling Leigh syndrome, and cases of LHON and late onset of “spastic dystonia”.<sup>358</sup> This mtDNA was a member of haplogroup U4 and carried the 14484/ND6 LHON mutation, in conjunction with the 4160/ND1 mutation, which affects a very conserved amino acid position, the latter being implicated as responsible for the “plus” clinical features.<sup>242</sup> In the QLD1 family the 4136/ND1 mutation characterized only a branch of the maternal lineage and was thus considered a *de novo* event. In contrast, the two 4136/ND1 LHON families from Italy harbored the 11778/ND4 LHON mutation.<sup>325</sup> Similar to our Family A, their mtDNAs were members of haplogroup T2. Furthermore, they were characterized by a control-region motif (16126-16153-16293-16294-16296-16519-73-150) identical to that seen in our Family A.<sup>327</sup> The shared regional origin (Apulia) of the three Italian LHON families, and the fact that they also share a rare control-region motif (seen in only 1 out of 3087 Italian controls) indicate that the three T2 families are indeed related and share both the 11778/ND4 and the 4136/ND1 mutations by descent from a common maternal ancestor. This scenario is further supported by the finding that the single mtDNA with an identical control-region motif found in the control subjects is also a member of haplogroup T2, but does not harbor either the 4136/ND1 or the 11778/ND4 mutations. The fact that the 11778/ND4 mutation in one of the three LHON families was still heteroplasmic, while all samples investigated from Family 1 (10 individuals), as well as the other two haplogroup T2 LHON probands were homoplasmic mutant for the

4136/ND1 mutation, reveals that the 4136/ND1 mutational event predated the 11778/ND4 mutation.

Thus, the 4136/ND1 mutation has the potential for a functional relevance and a deleterious effect on complex I activity. Its conservation and recurrent association with LHON pedigrees strongly indicate that its co-occurrence with the canonical 11778/ND4 mutation may act synergistically to further impair complex I function, leading to a LHON “plus” phenotype. Furthermore, the same scenario applies to the 9139/ATPase6 variant in Family A, which also shows similar features of conservation and could synergistically affect mitochondrial function.

Sequence analysis in Family B revealed a novel combination of known non-synonymous *cytb* amino acid changes. In particular, the 15773/*cytb* variant showed a remarkable conservation in mammals, and was predicted as “possibly damaging” by PolyPhen. Thus, it can be envisioned that in the presence of the 3460/ND1 mutation, the 15773/*cytb* variant alone or the combination 15693/*cytb*+15773/*cytb* contribute to the clinical expression of the LHON “plus” phenotype – an effect analogous to that played by the *cytb* amino acid changes of haplogroup J in LHON patients in combination with the 11778/ND4 and 14484/ND6 mutations.<sup>327</sup> The rationale for this functional effect is that complex I co-assembles with complex III to form a supercomplex, and accumulation of amino acid changes induced by non-synonymous polymorphisms may affect this process. Obviously, we cannot exclude at this time that further genetic variability in the nuclear genome may contribute to the “plus” phenotype in these patients. However, the co-segregation of myoclonus and other adjunctive features in Family A along the maternal line more consistently suggests a major role for mtDNA.

### **Increased mtDNA content as a compensatory mechanism in LHON**

The increase of mtDNA content has been considered a compensatory response to the impaired function of the respiratory chain in aging and in some mitochondrial diseases. Several authors hypothesized that a reduced activity of the respiratory chain and the consequent ATP deficit, due to aging or mtDNA mutations, can induce a retrograde signaling pathway that results in increased mtDNA content to compensate the decreased cellular ATP levels. This hypothesis is supported by the increase of mtDNA copy number reported in different tissues of aged individuals, such as brain, skeletal muscle

or lung.<sup>359-361</sup> Moreover, it has been shown that NRF-1 and Tfam, two major players in mtDNA transcription, are up-regulated at least in skeletal muscle of aged subjects.<sup>362</sup> In MELAS and MERRF affected individuals it has been shown that the mtDNA copy number is significantly increased in leukocytes of young subjects compared to controls, whereas it is lower in old affected individuals.<sup>363</sup> The compensatory mechanism in these diseases is also evident by the presence of RRFs in the skeletal muscle, generated by the subsarcolemmal accumulation of aberrant mitochondria.

Conversely, skeletal muscle biopsies from LHON affected patients failed to reveal the presence of RRFs, even if in LHON/MELAS overlap syndromes they may be present.<sup>364</sup> However, some signs of mitochondrial proliferation are apparent in skeletal muscle biopsies from LHON patients, for example the increased subsarcolemmal SDH activity.<sup>324,365</sup> In LHON patients with the 11778/ND4 mutation, an increased succinate-cytochrome c reductase activity, with normal complex III activity, has been reported in blood cells mitochondria, suggesting the occurrence of a nuclear compensatory effect for defective respiratory chain.<sup>366</sup> Moreover, an increased mtDNA copy number in blood cells of LHON affected and asymptomatic carrier individuals harboring the 11778/ND4 and 14484/ND6 mutations, has also been reported.<sup>367,368</sup>

We analyzed the mtDNA content in peripheral blood cells and skeletal muscles of LHON affected and asymptomatic carriers belonging to the large 11778/ND4 Brazilian pedigree and to 39 Italian families harboring homoplasmic 11778/ND4, 14484/ND6 and 3460/ND1 mutations. In the SOA-BR family we found a significant increase of blood cells mtDNA copy number in LHON individuals, both affected and carriers. Interestingly, asymptomatic carriers showed a significantly higher mtDNA copy number also compared to the affected. This result has also been confirmed by analysis of mtDNA content in Italian LHON blood samples, comparing affected to carrier individuals. In skeletal muscle we found an increase of mtDNA in both LHON affected and carriers compared to controls, but no differences were found between the two LHON groups. In fact, LHON carriers presented a higher mtDNA copy number compared to controls, but this difference was not statistically significant. We believe that the increased mtDNA copy number may vary in different LHON individuals, being influenced by genetic and/or environmental unknown factors. The subjects with an efficient compensatory response have a high mtDNA copy number and may not develop

the disease (asymptomatic carriers), whereas those characterized by a lower mtDNA copy number cannot completely compensate for the energy defect and will be more prone to develop LHON (affected). We can neatly differentiate the LHON affected from asymptomatic carriers, setting a threshold for mtDNA copy number, and this parameter may now be considered a prognostic factor for developing LHON.

We did not find any correlation between mtDNA content and age or sex. However, within the carrier group we found a different distribution of mtDNA copy number between males and females. In fact, female asymptomatic carriers show a lower mtDNA copy number compared to males. This effect can be explained if the compensatory response is assumed as a multifactorial mechanism, in which mtDNA copy number operates in conjunction with other factors. In this model, the mtDNA content threshold could be lower in females, but the compensatory mechanism could still remain efficient due to the involvement of other stimuli or factors, for example estrogens.

Mitochondrial biogenesis is a complex and finely tuned process characterized by the coordinated expression of mitochondrial and nuclear genes. Several transcription factors are involved in this process, such as Tfam, NRF-1, NRF-2 and ERR $\alpha$  and the master regulators PGC-1 $\alpha/\beta$  and PRC.<sup>129-131</sup> In particular PGC-1 $\alpha$  is the most studied and the best known transcriptional coactivator of this pathway. The polymorphism Gly482Ser has been associated to a variety of pathologies, such as hypertension, diabetes mellitus and insulin resistance. A recent study demonstrates that PGC-1 $\alpha$  variant with Gly/Gly at 482<sup>nd</sup> amino acid impairs Tfam transcription, thus lowering mtDNA replication.<sup>328</sup> In particular, Choi et al., 2006, analyzed the mtDNA copy number of leukocytes from patients affected by diabetes mellitus and control individuals, reporting a 20% decrease of mtDNA in the homozygous variant G (Gly/Gly) of this polymorphism compared to the Ser/Ser variant.<sup>328</sup> Thus, this polymorphic variant may influence mitochondrial biogenesis triggered as a compensatory mechanism by the energetic dysfunction in LHON. We performed a genotyping analysis on DNA samples from blood cells of all the available individuals (LHON and controls) and we evaluated the distribution of the G1444A (Gly482Ser) polymorphism and its possible correlation with mtDNA copy number. The Gly482Ser polymorphism was equally distributed in the different groups (LHON affected, LHON carriers and controls) and was not associated to differences in mtDNA copy number. Therefore, in our hands this variant does not influence the

mtDNA content in the analyzed populations and is not involved in the variable penetrance in LHON.

The relative mRNA levels of PGC-1 $\alpha/\beta$ , PRC and Tfam in skeletal muscle were also investigated. All these genes were upregulated in LHON skeletal muscle compared to controls, suggesting their involvement in the mitochondrial biogenesis induction in LHON subjects. Conversely, no differences in mRNA levels were found between LHON affected individuals and asymptomatic carriers. These results may simply reflect the lack of significant difference in mtDNA content between affected and carriers in skeletal muscle. They may also suggest an alternative mechanism in the increase of mtDNA content in asymptomatic carriers, for example an increase in Tfam or POL $\gamma$  activity that may induce mtDNA replication also without the complex activation of PGC-1 dependent mitochondrial biogenesis. Thus, further investigations are necessary to understand the molecular mechanism that underlies the activation of mitochondrial biogenesis. In particular, a systematic analysis of mitochondrial proteome, transcriptome and functional studies in affected and carrier LHON subjects, may reveal new clues on LHON pathogenesis.

### **Bezafibrate does not improve the energetic function of LHON cybrids**

Recently, several studies demonstrate that PGC-1 coactivators have a major role in mitochondrial biogenesis regulation, both in physiological and pathological conditions. Srivastava et al., 2007, demonstrated that PGC-1 $\alpha/\beta$  overexpression can induce mitochondrial biogenesis, stimulates OXPHOS activity and mitochondrial respiration in cells harboring ND5 and COI nonsense mutations, suggesting a possible role of this pathway for an alternative therapeutic approach in respiratory chain deficiencies.<sup>369</sup> Moreover, PGC-1 $\alpha$  overexpression in cell lines stimulates mitochondrial respiration, ATP production and mitochondrial mass, and, after the exposure to oxidant injury, accelerates the recovery of mitochondrial function.<sup>370</sup> The overexpression of PGC-1 $\alpha$ , induced by transgenic expression in skeletal muscle, stimulates the mitochondrial proliferation and prevents the energetic failure in a mouse model of myopathy.<sup>329</sup> The authors demonstrate that induction of mitochondrial biogenesis successfully stimulates the respiratory chain function and ATP production, improving the mitochondrial myopathy phenotype, in terms of delayed onset and prolonged lifespan.<sup>329</sup> Interestingly,

similar results have been obtained by oral administration of bezafibrate, a commercially available drug currently used in the pharmacological treatment of metabolic disorders.<sup>329</sup> Bezafibrate is a PPARs pan-activator shown to induce PGC-1 $\alpha$  expression, via PPAR $\delta$ , at least in skeletal muscle (in cell lines and mice).<sup>371</sup> Furthermore, bezafibrate-induced mitochondrial biogenesis compensates moderate respiratory chain defects in fibroblasts and myoblasts derived from patients with different respiratory chain dysfunction caused by mutations in nuclear genes (enzyme subunits or assembly factors).<sup>330</sup>

However, bezafibrate effects on the respiratory chain are still debated; in a cell model and at high concentration (1 mM), this drug exhibits cytotoxic effects, induces lactate and acetate production and inhibits *in vitro* complex I activity.<sup>372</sup> This latter result has also been confirmed at lower concentration of bezafibrate, but in this case the drug does not influence cellular oxygen consumption and has milder effects on respiratory chain, compared to other fibrates or thiazolidinediones.<sup>373</sup> Conversely, Brunmair et al., 2004, showed that bezafibrate did not reduce complex I activity in skeletal muscle and liver homogenates.<sup>374</sup>

We here characterized the bioenergetic function of LHON mutant cybrids and their response to bezafibrate treatment. In our model, bezafibrate was not able to induce mitochondrial biogenesis, in terms of mtDNA replication or steady-state respiratory chain protein levels, and did not influence the ATP synthesis rate or protect LHON cybrids from galactose induced apoptosis. This result may be due to the tumoral nature of cybrid cell lines, which are derived from the 143B TK- osteosarcoma parental cell line, and, furthermore, to the continuous passages and selection in culture of these cells. Parental osteosarcoma or cybrid cell lines may accumulate chromosomal rearrangements (deletions, duplications or inversions) and consequently some assets in gene expression (for example genes belonging to the PGC-1 pathway) may be modified. Moreover, it has been demonstrated that multidrug resistance, mediated by ABC transporters, is present in several osteosarcoma cell lines, including 143B.<sup>375</sup> This phenomenon may cause a lower uptake of bezafibrate or the efflux of the drug from the treated cells. Primary cell lines from LHON patients, such as fibroblasts or myoblasts, may therefore represent a better model for these studies.

# **Conclusions**

Since 1988, when the first mtDNA mutation has been demonstrated to be the cause of Leber's hereditary optic neuropathy, this pathology has been intensively studied, even though to date many questions are still open. In fact, main features of LHON, such as male prevalence, variable penetrance and tissue selectivity, are still under investigation and the underlying pathogenic mechanisms are still unknown.

The results here reported contributed to the definition of new pathogenic LHON mutations and tried to clarify some aspects of the still unknown question of variable penetrance. The main concluding remarks of this thesis can be summarized as follows:

- Novel structural models for ND1-ND4 and ND4L complex I subunits have been generated and conservation analysis and pathogenicity prediction have been carried out for all LHON reported mutations (confirmed and candidates). This *in-silico* approach allowed us to locate LHON pathogenic mutations in defined and conserved protein domains, in particular for ND1, ND4, ND5 and ND6. Moreover, this approach can be a useful tool in the analysis of novel mtDNA variants with unclear pathogenic/functional role.
- Four rare LHON pathogenic mutations, two reported only once, have been identified. This study confirms that the ND1 and ND6 genes are mutational hot spots for LHON. All mutations were previously described at least once and we validated their pathogenic role, suggesting the need for their screening in LHON cases negative for the common mutations. Moreover, two novel mtDNA variants with a possible pathogenic role have been identified in two independent branches of a large pedigree. Functional studies are necessary to define their contribution to LHON in this family.
- The combination of mtDNA rare polymorphic variants in complex I, ATP synthase or cytochrome b genes, has been shown to be relevant in determining the maternal recurrence of myoclonus in unrelated LHON pedigrees. Thus, we suggest that particular mtDNA backgrounds and /or the presence of specific rare mutations may increase the pathogenic potential of the primary LHON mutations, thereby giving rise to the extraocular clinical features characteristic of the LHON "plus" phenotype.

- We identify the first molecular parameter that clearly discriminates LHON affected individuals from LHON asymptomatic carriers, the mtDNA copy number. This provides a valuable mechanism for future investigations on variable penetrance in LHON. However, the increased mtDNA content in LHON individuals was not correlated to the functional polymorphism G1444A of PGC-1 $\alpha$ , the master regulator of mitochondrial biogenesis, but may be due to gene expression of genes involved in this signaling pathway, such as PGC-1 $\alpha/\beta$  and Tfam.

Future studies will be necessary to identify the biochemical effects of rare pathogenic mutations and to validate the novel candidate mutations here described, in terms of cellular bioenergetic characterization of these variants. Moreover, we were not able to induce mitochondrial biogenesis in cybrids cell lines using bezafibrate. However, other cell line models are available, such as fibroblasts harboring LHON mutations, or other approaches can be used to trigger the mitochondrial biogenesis. For example, we showed that virus-mediated PGC-1 $\alpha/\beta$  overexpression, can improve OXPHOS defects caused by mutations in nuclear genes or mtDNA (Srivastava S et al., Hum Mol Genet, in press).

---

## References

1. DiMauro S, Schon EA. Mitochondrial respiratory-chain diseases. *N Engl J Med*. 2003; 348:2656-2668.
2. Wallace DC. A mitochondrial paradigm of metabolic and degenerative diseases, aging, and cancer: a dawn for evolutionary medicine. *Annu Rev Genet*. 2005; 39:359-407.
3. Margulis L. Symbiotic theory of the origin of eukaryotic organelles; criteria for proof. *Symp Soc Exp Biol*. 1975; 29:21-38.
4. Frey TG, Mannella CA. The internal structure of mitochondria. *Trends Biochem Sci*. 2000; 25:319-324.
5. Cereghetti GM, Scorrano L. The many shapes of mitochondrial death. *Oncogene*. 2006; 25:4717-4724.
6. Shaw JM, Nunnari J. Mitochondrial dynamics and division in budding yeast. *Trends Cell Biol*. 2002; 12:178-184.
7. Scorrano L. Proteins that fuse and fragment mitochondria in apoptosis: con-fissing a deadly con-fusion? *J Bioenerg Biomembr*. 2005; 37:165-170.
8. Fritz S, Rapaport D, Klanner E, et al. Connection of the mitochondrial outer and inner membranes by Fzo1 is critical for organellar fusion. *J Cell Biol*. 2001; 152:683-692.
9. Rapaport D, Brunner M, Neupert W, et al. Fzo1p is a mitochondrial outer membrane protein essential for the biogenesis of functional mitochondria in *Saccharomyces cerevisiae*. *J Biol Chem*. 1998; 273:20150-20155.
10. Rojo M, Legros F, Chateau D, Lombès A. Membrane topology and mitochondrial targeting of mitofusins, ubiquitous mammalian homologs of the transmembrane GTPase Fzo. *J Cell Sci*. 2002; 115:1663-1674.
11. Santel A, Fuller MT. Control of mitochondrial morphology by a human mitofusin. *J Cell Sci*. 2001; 114:867-874.
12. Kijima K, Numakura C, Izumino H, et al. Mitochondrial GTPase mitofusin 2 mutation in Charcot-Marie-Tooth neuropathy type 2A. *Hum Genet*. 2005; 116:23-27.
13. Lawson VH, Graham BV, Flanigan KM. Clinical and electrophysiologic features of CMT2A with mutations in the mitofusin 2 gene. *Neurology*. 2005; 65:197-204.
14. Züchner S, De Jonghe P, Jordanova A, et al. Axonal neuropathy with optic atrophy is caused by mutations in mitofusin 2. *Ann Neurol*. 2006; 59:276-281.
15. Alexander C, Votruba M, Pesch UEA, et al. OPA1, encoding a dynamin-related GTPase, is mutated in autosomal dominant optic atrophy linked to chromosome 3q28. *Nat. Genet*. 2000; 26:211-215.
16. Delettre C, Lenaers G, Griffoin JM, et al. Nuclear gene OPA1, encoding a mitochondrial dynamin-related protein, is mutated in dominant optic atrophy. *Nat Genet*. 2000; 26:207-210.
17. Amati-Bonneau P, Valentino ML, Reynier P, et al. OPA1 mutations induce mitochondrial DNA instability and optic atrophy 'plus' phenotypes. *Brain*. 2008; 131:338-351.

18. Hudson G, Amati-Bonneau P, Blakely EL, et al. Mutation of OPA1 causes dominant optic atrophy with external ophthalmoplegia, ataxia, deafness and multiple mitochondrial DNA deletions: a novel disorder of mtDNA maintenance. *Brain*. 2008; 131:329-237.
19. James DI, Parone PA, Mattenberger Y, Martinou JC. hFis1, a novel component of the mammalian mitochondrial fission machinery. *J Biol Chem*. 2003; 278:36373-36379.
20. Labrousse AM, Zappaterra MD, Rube DA, van der Bliek AM. *C. elegans* dynamin-related protein DRP-1 controls severing of the mitochondrial outer membrane. *Mol Cell*. 1999; 4:815-826.
21. Karbowski M, Jeong SY, Youle RJ. Endophilin B1 is required for the maintenance of mitochondrial morphology. *J Cell Biol*. 2004; 166:1027-1039.
22. Smirnova E, Griparic L, Shurland DL, van der Bliek AM. Dynamin-related protein Drp1 is required for mitochondrial division in mammalian cells. *Mol Biol Cell*. 2001; 12:2245-2256.
23. Grafstein B. Axonal transport: function and mechanisms. In: Waxman SG, Kocsis JD, Stys PK (Eds). *The axon: structure, function and pathophysiology*. Oxford University Press, Oxford. 1995; pp. 185-199.
24. Hollenbeck PJ. The pattern and mechanism of mitochondrial transport in axons. *Front Biosci*. 1996; 1:d91-d102.
25. Morris RL, Hollenbeck PJ. Axonal transport of mitochondria along microtubules and F-actin in living vertebrate neurons. *J Cell Biol*. 1995; 131:1315-1326.
26. Ochs S, Hollingsworth D. Dependence of fast axoplasmic transport in nerve on oxidative metabolism. *J Neurochem*. 1971; 18:107-114.
27. Sabri MI, Ochs S. Relation of ATP and creatine phosphate to fast axoplasmic transport in mammalian nerve. *J Neurochem*. 1972; 19:2821-2828.
28. Walker JE. The NADH:ubiquinone oxidoreductase (complex I) of respiratory chain. *Q Rev Biophys*. 1992; 25:253-324.
29. Carroll J, Shannon RJ, Fearnley IM, et al. Definition of the nuclear encoded protein composition of bovine heart mitochondrial complex I. Identification of two new subunits. *J Biol Chem*. 2002; 277:50311-50317.
30. Rustin P, Rotig A. Inborn errors of complex II - unusual human mitochondrial diseases. *Biochim Biophys Acta*. 2002; 1553:117-122.
31. Berry EA, Guergova-Kuras M, Huang LS, et al. Structure and function of cytochrome bc complexes. *Annu Rev Biochem*. 2000; 69:1005-1075.
32. Zeviani M, Spinazzola A, Carelli V, Nuclear genes in mitochondrial disorders. *Curr Opin Genet Dev*. 2003; 13:1-9.
33. Shoubridge EA. Cytochrome c oxidase deficiency. *Am J Med Genet*. 2001; 106:46-52.
34. Mitchell P. Coupling of phosphorylation to electron and hydrogen transfer by chemiosmotic type of mechanism. *Nature*. 1961; 191:144-148.

35. Abrahams JP, Leslie AG, Lutter R, et al. Structure at 2.8 Å resolution of F<sub>1</sub>-ATPase from bovine heart mitochondria. *Nature*. 1994; 370:621-628.
36. Galkin AS, Grivennikova VG, Vinogradov AV.  $\rightarrow$ H<sup>+</sup>/2e<sup>-</sup> stoichiometry in NADH-quinone reductase reactions catalyzed by bovine heart submitochondrial particles. *FEBS Lett*. 1999; 451:157-161.
37. Galkin A, Drose S, Brandt U. The proton pumping stoichiometry of purified mitochondrial complex I reconstituted into proteoliposomes, *Biochim Biophys Acta*. 2006; 1757:1575-1581.
38. Vogel RO, Smeitink JAM, Nijtmans LGJ. Human mitochondrial complex I assembly: A dynamic and versatile process. *Biochim Biophys Acta*. 2007; 1767:1215-1227.
39. Leonard K, Haiker H, Weiss H, Three-dimensional structure of NADH: Ubiquinone reductase (Complex I) from *Neurospora* mitochondria determined by electron microscopy of membrane crystals. *J Mol Biol*. 1987; 194:277-286.
40. Hofhaus G, Weiss H, Leonard K. Electron microscopic analysis of the peripheral and membrane parts of mitochondrial NADH dehydrogenase (Complex I). *J Mol Biol*. 1991; 221:1027-1043.
41. Guenebaut V, Vincentelli R, Mills D, et al. Three dimensional structure of NADH-dehydrogenase from *Neurospora crassa* by electron microscopy and conical tilt reconstruction. *J Mol Biol*. 1997; 265:409-418.
42. Hinchliffe P, Sazanov LA. Organization of iron–sulfur clusters in respiratory complex I. *Science*. 2005; 309:771-774.
43. Sazanov LA, Hinchliffe P. Structure of the hydrophilic domain of respiratory complex I from *Thermus thermophilus*. *Science*. 2006; 311:1430-1436.
44. Leif H, Weidner U, Berger A, et al. *Escherichia coli* NADH dehydrogenase I, a minimal form of the mitochondrial complex. *Biochem Soc Trans*. 1993; 21:998-1001.
45. Antonicka H, Ogilvie I, Taivassalo T, et al. Identification and characterization of a common set of complex I assembly intermediates in mitochondria from patients with complex I deficiency. *J Biol Chem*. 2003; 278:43081-43088.
46. Ugalde C, Vogel R, Huijbens R, et al. Human mitochondrial complex I assembles through the combination of evolutionary conserved modules: a framework to interpret complex I deficiencies. *Hum Mol Genet*. 2004; 13:2461-2472.
47. Vogel RO, Dieteren CE, van den Heuvel LP, et al. Identification of mitochondrial complex I assembly intermediates by tracing tagged NDUFS3 demonstrates the entry point of mitochondrial subunits. *J Biol Chem*. 2007; 282:7582-7590.
48. Lazarou M, McKenzie M, Ohtake A, et al. Analysis of the assembly profiles for mitochondrial and nuclear encoded subunits into complex I. *Mol Cell Biol*. 2007; 27:4228-4237.
49. Ogilvie I, Kennaway NG, Shoubridge EA. A molecular chaperone for mitochondrial complex I assembly is mutated in a progressive encephalopathy. *J Clin Invest*. 2005; 115:2784–2792.
50. Vahsen N, Cande C, Briere JJ, et al. AIF deficiency compromises oxidative phosphorylation. *EMBO J*. 2004; 23:4679-4689.

- 
51. Joza N, Oudit GY, Brown D, et al. Muscle-specific loss of apoptosis inducing factor leads to mitochondrial dysfunction, skeletal muscle atrophy, and dilated cardiomyopathy. *Mol Cell Biol.* 2005; 25:10261-10272.
  52. Chance B, Sies H, Boveris A. Hydroperoxide metabolism in mammalian organs. *Physiol Rev.* 1979; 59:527-605.
  53. Halliwell B, Gutteridge JM, Cross CE. Free radicals, antioxidants, and human disease: where are we now? *J Lab Clin Med.* 1992; 119:598-620.
  54. Cross CE, Halliwell B, Borish ET, et al. Oxygen radicals and human disease. *Ann Intern Med.* 1987; 107:526-545.
  55. Rhee SG. Cell signaling. H<sub>2</sub>O<sub>2</sub>, a necessary evil for cell signaling. *Science.* 2006; 312:1882-1883.
  56. Bohr VA. Repair of oxidative DNA damage in nuclear and mitochondrial DNA, and some changes with aging in mammalian cells. *Free Radic Biol Med.* 2002; 32:804-812.
  57. Linnane AW, Kios M, Vitetta L. The essential requirement for superoxide radical and nitric oxide formation for normal physiological function and healthy aging. *Mitochondrion.* 2007; 7:1-5.
  58. Rotig A, de Lonlay P, Chretien D, et al. Aconitase and mitochondrial iron-sulphur protein deficiency in Friedreich ataxia. *Nat Genet.* 1997; 17: 215-217.
  59. Melov S, Coskun P, Patel M, et al. Mitochondrial disease in superoxide dismutase 2 mutant mice. *Proc Natl Acad Sci USA.* 1999; 96:846-851.
  60. Riobo NA, Clementi E, Melani M, et al. Nitric oxide inhibits mitochondrial NADH:ubiquinone reductase activity through peroxynitrite formation. *Biochem J.* 2001; 359:139-45.
  61. Yamamoto T, Maruyama W, Kato Y, et al. Selective nitration of mitochondrial complex I by peroxynitrite: involvement in mitochondria dysfunction and cell death of dopaminergic SH-SY5Y cells. *J Neural Transm.* 2002; 109:1-13.
  62. Yamakura F, Taka H, Fujimura T, et al. Inactivation of human manganese-superoxide dismutase by peroxynitrite is caused by exclusive nitration of tyrosine 34 to 3-nitrotyrosine. *J Biol Chem.* 1998; 273:14085-14089.
  63. Clementi E, Brown GC, Feelisch M, et al. Persistent inhibition of cell respiration by nitric oxide: crucial role of S-nitrosylation of mitochondrial complex I and protective action of glutathione. *Proc Natl Acad Sci USA.* 1998; 95:7631-7636.
  64. Zhang Y, Marcillat O, Giulivi C, et al. The oxidative inactivation of mitochondrial electron transport chain components and ATPase. *J Biol Chem.* 1990; 265:16330-16336.
  65. Albano E, Bellomo G, Parola M, et al. Stimulation of lipid peroxidation increases the intracellular calcium content of isolated hepatocytes. *Biochim Biophys Acta.* 1991; 1091:310-316.
  66. Bacon BR, O'Neill R, Britton RS. Hepatic mitochondrial energy production in rats with chronic iron overload. *Gastroenterology.* 1993; 105:1134-1140.

- 
67. Zimmermann KC, Bonzon C, Green DR. The machinery of programmed cell death. *Pharmacol Ther.* 2001; 92:57-70.
68. Kerr JF, Wyllie AH, Currie AR. Apoptosis: a basic biological phenomenon with wide-ranging implications in tissue kinetics. *Br J Cancer.* 1972; 26:239-257.
69. Martin SJ, Reutelingsperger CP, McGahon AJ, et al. Early redistribution of plasma membrane phosphatidylserine is a general feature of apoptosis regardless of the initiating stimulus: inhibition by overexpression of Bcl-2 and Abl. *J Exp Med.* 1995; 182:1545-1556.
70. Martin SJ, Green DR. Protease activation during apoptosis: death by a thousand cuts? *Cell.* 1995; 82:349-352.
71. Raff M. Cell suicide for beginners. *Nature.* 1998; 396:119-122.
72. Adams JM, Cory S. The Bcl-2 protein family: arbiters of cell survival. *Science.* 1998; 281:1322-1326.
73. Eskes R, Desagher S, Antonsson B, et al. Bid induces the oligomerization and insertion of Bax into the outer mitochondrial membrane. *Mol Cell Biol.* 2000; 20:929-935.
74. Suzuki M, Youle RJ, Tjandra N. Structure of Bax: coregulation of dimer formation and intracellular localization. *Cell.* 2000; 103:645-654.
75. van Gurp M, Festjens N, van Loo G, et al. Mitochondrial intermembrane proteins in cell death. *Biochem Biophys Res Commun.* 2003; 304:487-497.
76. Zamzami N, Kroemer G. The mitochondrion in apoptosis: how Pandora's box opens. *Nat Rev Mol Cell Biol.* 2001; 2:67-71.
77. Acehan D, Jiang X, Morgan DG, et al. Three-dimensional structure of the apoptosome: implications for assembly, procaspase-9 binding, and activation. *Mol Cell.* 2002; 9:423-432.
78. Susin SA, Lorenzo HK, Zamzami N, et al. Molecular characterization of mitochondrial apoptosis-inducing factor. *Nature.* 1999; 397:441-446.
79. Miramar MD, Costantini P, Ravagnan L, et al. NADH oxidase activity of mitochondrial apoptosis-inducing factor. *J Biol Chem.* 2001; 276:16391-16398.
80. Wang X, Yang C, Chai J, et al. Mechanisms of AIF-mediated apoptotic DNA degradation in *Caenorhabditis elegans*. *Science.* 2002; 298:1587-1592.
81. Du C, Fang M, Li Y, et al. Smac, a mitochondrial protein that promotes cytochrome c-dependent caspase activation by eliminating IAP inhibition. *Cell.* 2000; 102:33-42.
82. Verhagen AM, Ekert PG, Pakusch M, et al. Identification of DIABLO, a mammalian protein that promotes apoptosis by binding to and antagonizing IAP proteins. *Cell.* 2000; 102:43-53.
83. Ekert PG, Silke J, Hawkins CJ, et al. DIABLO promotes apoptosis by removing MIHA/XIAP from processed caspase 9. *J Cell Biol.* 2001; 152:483-90.
84. Gray CW, Ward RV, Karran E, et al. Characterization of human HtrA2, a novel serine protease involved in the mammalian cellular stress response. *Eur J Biochem.* 2000; 267:5699-5710.
-

- 
85. Faccio L, Fusco C, Chen A, et al. Characterization of a novel human serine protease that has extensive homology to bacterial heat shock endoprotease HtrA and is regulated by kidney ischemia. *J Biol Chem.* 2000; 275:2581-2588.
  86. Suzuki Y, Imai Y, Nakayama H, et al. A serine protease, HtrA2, is released from the mitochondria and interacts with XIAP, inducing cell death. *Mol Cell.* 2001; 8:613-621.
  87. Thornberry N, Lazebnik Y. Caspases: enemies within. *Science.* 1998; 281:1312-1316.
  88. Cryns V, Yuan Y. Proteases to die for. *Genes Dev.* 1999; 12:1551-1570.
  89. Salvesen GS, Dixit VM. Caspases: intracellular signaling by proteolysis. *Cell.* 1997; 91:443-446.
  90. Reed JC. Apoptosis-regulating proteins as targets for drug discovery. *TRENDS Mol Med.* 2001; 7:314-319.
  91. Taylor RC, Cullen SP, Martin SJ. Apoptosis: controlled demolition at the cellular level. *Nat Rev Mol Cell Biol.* 2008; 9:231-241.
  92. Anderson S, Bankier AT, Barrell BG, et al. Sequence and organization of the human mitochondrial genome. *Nature.* 1981; 290:457-465.
  93. Clayton DA. Vertebrate mitochondrial DNA: a circle of surprises. *Exp Cell Res.* 2000; 255:4-9.
  94. Scarpulla RC. Transcriptional paradigms in mammalian mitochondrial biogenesis and function. *Physiol Rev.* 2008; 88:611-638.
  95. DiMauro S, Schon EA. The mitochondrial respiratory chain and its disorders. In *Mitochondrial medicine*. Ed. Informa healthcare. 2006. pp. 7-26.
  96. Sutovsky P, Moreno RD, Ramalho-Santos J, et al. Ubiquitin tag for sperm mitochondria. *Nature.* 1999; 402:371-372.
  97. Sutovsky P, Moreno RD, Ramalho-Santos J, et al. Ubiquitinated sperm mitochondria, selective proteolysis, and the regulation of mitochondrial inheritance in mammalian embryos. *Biol Reprod.* 2000; 63:582-590.
  98. Marchington DR, Macaulay V, Hartshorne GM, et al. Evidence from human oocytes for a genetic bottleneck in an mtDNA disease. *Am J Hum Genet.* 1998; 63:769-775.
  99. Falkenberg M, Larsson NG, Gustafsson CM. DNA replication and transcription in mammalian mitochondria. *Annu Rev Biochem.* 2007; 76:679-699.
  100. Garrido N, Griparic L, Jokitalo E, et al. Composition and dynamics of human mitochondrial nucleoids. *Mol Biol Cell.* 2003; 14:1583-1596.
  101. Torroni A, Schurr TG, Cabell MF, et al. Asian affinities and continental radiation of the four founding Native American mtDNAs. *Am J Hum Genet.* 1993; 53:563-590.
  102. Graven L, Passarino G, Semino O, et al. Evolutionary correlation between control region sequence and restriction polymorphisms in the mitochondrial genome of a large Senegalese Mandenka sample. *Mol Biol Evol.* 1995; 12:334-345.

103. Chen YS, Torroni A, Excoffier L, et al. Analysis of mtDNA variation in African populations reveals the most ancient of all human continent-specific haplogroups. *Am J Hum Genet.* 1995; 57:133-149.
104. Torroni A, Chen YS, Semino O, et al. mtDNA and Y-chromosome polymorphisms in four Native American populations from southern Mexico. *Am J Hum Genet.* 1994; 54:303-318.
105. Torroni A, Lott MT, Cabell MF, et al. mtDNA and the origin of Caucasians: identification of ancient Caucasian-specific haplogroups, one of which is prone to a recurrent somatic duplication in the D-loop region. *Am J Hum Genet.* 1994; 55:760-776.
106. Torroni A, Huoponen K, Francalacci P, et al. Classification of European mtDNAs from an analysis of three European populations. *Genetics.* 1996; 144:1835–1850.
107. Bogenhagen DF, Clayton DA. The mitochondrial DNA replication bubble has not burst. *Trends Biochem Sci.* 2003; 28:357–360.
108. Clayton DA. Mitochondrial DNA replication: what we know. *IUBMB Life.* 2003; 55:213–217.
109. Fridlender B, Fry M, Bolden A, et al. A new synthetic RNA-dependent DNA polymerase from human tissue culture cells (HeLa-fibroblast-synthetic oligonucleotides-template-purified enzymes). *Proc Natl Acad Sci U S A.* 1972; 69:452-455.
110. Gray H, Wong TW. Purification and identification of subunit structure of the human mitochondrial DNA polymerase. *J Biol Chem.* 1992; 267:5835-5841.
111. Pinz KG, Bogenhagen DF. Efficient repair of abasic sites in DNA by mitochondrial enzymes. *Mol Cell Biol.* 1998; 18:1257-1265.
112. Kaguni LS. DNA polymerase gamma, the mitochondrial replicase. *Annu Rev Biochem.* 2004; 73:293-320.
113. Pinz KG, Bogenhagen DF. Characterization of a catalytically slow AP lyase activity in DNA polymerase gamma and other family A DNA polymerases. *J Biol Chem.* 2000; 275:12509-12514.
114. Clayton DA. Replication and transcription of vertebrate mitochondrial DNA. *Annu Rev Cell Biol.* 1991; 7:453-478.
115. Holt IJ, Lorimer HE, Jacobs HT. Coupled leading- and lagging-strand synthesis of mammalian mitochondrial DNA. *Cell.* 2000; 100:515-524.
116. Yang MY, Bowmaker M, Reyes A, et al. Biased incorporation of ribonucleotides on the mitochondrial L-strand accounts for apparent strand-asymmetric DNA replication. *Cell.* 2002; 111:495-505.
117. Bowmaker M, Yang MY, Yasukawa T, et al. Mammalian mitochondrial DNA replicates bidirectionally from an initiation zone. *J Biol Chem.* 2003; 278:50961-50969.
118. Fish J, Raule N, Attardi G. Discovery of a major D-loop replication origin reveals two modes of human mtDNA synthesis. *Science.* 2004; 306:2098-2101.
119. Montoya J, López-Pérez MJ, Ruiz-Pesini E. Mitochondrial DNA transcription and diseases: past, present and future. *Biochim Biophys Acta.* 2006; 1757:1179-1189.

120. Montoya J, Gaines GL, Attardi G. The pattern of transcription of the human mitochondrial rRNA genes reveals two overlapping transcription units. *Cell*. 1983; 34:151–159.
121. Ojala D, Montoya J, Attardi G. tRNA punctuation model of RNA processing in human mitochondria. *Nature*. 1981; 290:470–474.
122. Masters BS, Stohl LL, Clayton DA. Yeast mitochondrial RNA polymerase is homologous to those encoded by bacteriophages T3 and T7. *Cell*. 1987;51:89-99.
123. Fisher RP, Clayton DA. Purification and characterization of human mitochondrial transcription factor 1. *Mol Cell Biol*. 1988; 8:3496–3509.
124. Parisi MA, Clayton DA. Similarity of human mitochondrial transcription factor 1 to high mobility group proteins. *Science*. 1991; 252:965–969.
125. Fisher RP, Lisowsky T, Parisi MA, Clayton DA. DNA wrapping and bending by a mitochondrial high mobility group-like transcriptional activator protein. *J Biol Chem*. 1992; 267:3358–3367.
126. Fisher RP, Parisi MA, Clayton DA. Flexible recognition of rapidly evolving promoter sequences by mitochondrial transcription factor 1. *Genes Dev*. 1989; 3:2202-2217.
127. Zeviani M, Antozzi C. Mitochondrial disorders. *Mol Hum Repr*. 1997; 3:133-148.
128. Diaz F, Moraes CT. Mitochondrial biogenesis and turnover. *Cell Calcium*. 2008; 4:24-35.
129. Virbasius CA, Virbasius JV, Scarpulla RC. NRF-1, an activator involved in nuclear-mitochondrial interactions, utilizes a new DNA-binding domain conserved in a family of developmental regulators. *Genes Dev*. 1993; 7:2431-2445.
130. Virbasius JV, Virbasius CA, Scarpulla RC. Identity of GABP with NRF-2, a multisubunit activator of cytochrome oxidase expression, reveals a cellular role for an ETS domain activator of viral promoters. *Genes Dev*. 1993; 7:380-392.
131. Scarpulla RC. Transcriptional activators and coactivators in the nuclear control of mitochondrial function in mammalian cells, *Gene*. 2002; 286:81-89.
132. Lin J, Tarr PT, Yang R, et al. PGC-1beta in the regulation of hepatic glucose and energy metabolism. *J Biol Chem*. 2003; 278:30843-30848.
133. Ling C, Poulsen P, Carlsson E, et al. Multiple environmental and genetic factors influence skeletal muscle PGC-1alpha and PGC-1beta gene expression in twins. *J Clin Invest*. 2004; 114:1518-1526.
134. Puigserver P, Spiegelman BM. Peroxisome Proliferator-Activated Receptor- $\gamma$  Coactivator 1 $\alpha$  (PGC-1 $\alpha$ ): transcriptional coactivator and metabolic regulator. *Endocrinol Rev*. 2003; 24:78-90.
135. Puigserver P, Wu Z, Park CW, et al. A cold-inducible coactivator of nuclear receptors linked to adaptive thermogenesis. *Cell*. 1998; 92:829-839.
136. Heery DM, Kalkhoven E, Hoare S, et al. A signature motif in transcriptional co-activators mediates binding to nuclear receptors. *Nature*. 1997; 387:733–736.
137. Puigserver P, Adelmant G, Wu Z, et al. Activation of PPAR $\gamma$  coactivator-1 through transcription factor docking. *Science*. 1999; 286:1368-1371.

138. Wallberg AE, Yamamura S, Malik S, et al. Coordination of p300-mediated chromatin remodeling and TRAP/mediator function through coactivator PGC-1 $\alpha$ . *Mol Cell*. 2003; 12:1137-1149.
139. Yuryev A, Patturajan M, Litingtung Y, et al. The C-terminal domain of the largest subunit of RNA polymerase II interacts with a novel set of serine/arginine rich proteins. *Proc Natl Acad Sci USA*. 1996; 93:6975-6980.
140. Baar K, Wende AR, Jones TE, et al. Adaptations of skeletal muscle to exercise: rapid increase in the transcriptional coactivator PGC-1. *FASEB J*. 2002; 16:1879-1886.
141. Norrbom J, Sundberg CJ, Ameln H, et al. PGC-1 $\alpha$  mRNA expression is influenced by metabolic perturbation in exercising human skeletal muscle. *J Appl Physiol*. 2004; 96:189-194.
142. Wu Z, Puigserver P, Andersson U, et al. Mechanism controlling mitochondrial biogenesis and function through the thermogenic activator PGC-1. *Cell*. 1999; 98:115-124.
143. Mootha VK, Lindgren CM, Eriksson KF, et al. PGC-1 $\alpha$ -responsive genes involved in oxidative phosphorylation are coordinately downregulated in human diabetes. *Nat Genet*. 2003; 34:267-273.
144. Vega RB, Huss JM, Kelly DP. The coactivator PGC-1 cooperates with peroxisome proliferator-activated receptor  $\alpha$  in transcriptional control of nuclear genes encoding mitochondrial fatty acid oxidation enzymes. *Mol Cell Biol*. 2000; 20:1868-1876.
145. Puigserver P, Rhee J, Donovan J, et al. Insulin-regulated hepatic gluconeogenesis through FOXO1-PGC-1 $\alpha$  interaction. *Nature*. 2003; 423:550-555.
146. Rhee J, Inoue Y, Yoon JC, et al. Regulation of hepatic fasting response by PPAR $\gamma$  coactivator-1 $\alpha$  (PGC-1): requirement for hepatocyte nuclear factor 4 $\alpha$  in gluconeogenesis. *Proc Natl Acad Sci USA*. 2003; 100:4012-4017.
147. Michael LF, Wu Z, Cheatham RB, et al. Restoration of insulin-sensitive glucose transporter (GLUT4) gene expression in muscle cells by the transcriptional coactivator PGC-1. *Proc Natl Acad Sci USA*. 2001; 98:3820-3825.
148. Lin J, Yang R, Tarr PT, et al. Hyperlipidemic effects of dietary saturated fats mediated through PGC-1 $\beta$  coactivation of SREBP. *Cell*. 2005; 120:261-273.
149. Kawakami Y, Tsuda M, Takahashi S, et al. Transcriptional coactivator PGC-1 $\alpha$  regulates chondrogenesis via association with Sox9. *Proc Natl Acad Sci USA*. 2005; 102:2414-2419.
150. Yoon JC, Puigserver P, Chen GX, et al. Control of hepatic gluconeogenesis through the transcriptional coactivator PGC-1. *Nature*. 2001; 413:131-138.
151. Zong H, Ren JM, Young LH, et al. AMP kinase is required for mitochondrial biogenesis in skeletal muscle in response to chronic energy deprivation. *Proc Natl Acad Sci USA*. 2002; 99:15983-15987.
152. Handschin C, Rhee J, Lin J, et al. An autoregulatory loop controls peroxisome proliferator-activated receptor  $\gamma$  coactivator 1 $\alpha$  expression in muscle. *Proc Natl Acad Sci USA*. 2003; 100:7111-7116.
153. Nisoli E, Carruba MO. Nitric oxide and mitochondrial biogenesis. *J Cell Sci*. 2006; 119:2855-2862.

- 
154. Nisoli E, Clementi E, Paolucci C, et al. Mitochondrial biogenesis in mammals: the role of endogenous nitric oxide. *Science*. 2003; 299:896-899.
  155. Lin J, Handschin C, Spiegelman BM. Metabolic control through the PGC-1 family of transcription coactivators. *Cell Metab*. 2005; 1:361-370.
  156. Puigserver P, Rhee J, Lin J, et al. Cytokine stimulation of energy expenditure through p38 MAP kinase activation of PPARgamma coactivator-1. *Mol Cell*. 2001; 8:971-982.
  157. Fan M, Rhee J, St-Pierre J, et al. Suppression of mitochondrial respiration through recruitment of p160 myb binding protein to PGC-1alpha: modulation by p38 MAPK. *Genes Dev*. 2004; 18:278-289.
  158. Rodgers JT, Lerin C, Haas W, et al. Nutrient control of glucose homeostasis through a complex of PGC-1alpha and SIRT1. *Nature*. 2005; 434:113-118.
  159. Li J, Puigserver P, Donovan J, et al. PGC-1 $\beta$ : a novel PGC-1-related transcription coactivator associated with host cell factor. *J Biol Chem*. 2002; 277:1645-1648.
  160. Meirhaeghe A, Crowley V, Lenaghan C, et al. Characterization of the human, mouse and rat PGC1 $\beta$  (peroxisome proliferator-activated receptor-gamma co-activator 1 $\beta$ ) gene invitro and in vivo. *Biochem J*. 2003; 373:155-165.
  161. Andersson U, Scarpulla RC. PGC-1-related coactivator, a novel, serum-inducible coactivator of nuclear respiratory factor 1-dependent transcription in mammalian cells. *Mol Cell Biol*. 2001; 21:3738-3749.
  162. Chau CA, Evans MJ, Scarpulla RC. Nuclear respiratory factor 1 activation sites in genes encoding the gamma-subunit of ATP synthase, eukaryotic initiation factor 2 $\alpha$ , tyrosine aminotransferase. Specific interaction of purified NRF-1 with multiple target genes. *J Biol Chem*. 1992; 267:6999-7006.
  163. Evans MJ, Scarpulla RC. NRF-1: a trans-activator of nuclearencoded respiratory genes in animal cells. *Genes Dev*. 1990; 4:1023-1034.
  164. Larsson NG, Wang JM, Wilhelmsson H, et al. Mitochondrial transcription factor A is necessary for mtDNA maintenance and embryogenesis in mice. *Nature Genet*. 1998; 18: 231-236.
  165. Rantanen A, Jansson M, Oldfors A, et al. Downregulation of Tfam and mtDNA copy number during mammalian spermatogenesis. *Mammalian Genome*. 2001; 12: 787-792.
  166. Falkenberg M, Gaspari M, Rantanen A, et al. Mitochondrial transcription factors B1 and B2 activate transcription of human mtDNA. *Nat Genet*; 2002; 31: 289-294.
  167. Alaynick WA. Nuclear receptors, mitochondria and lipid metabolism. *Mitochondrion*. 2008; 8:329-337.
  168. Mandard S, Muller M and Kersten S. Peroxisome proliferator-activated receptor  $\alpha$  target genes. *Cell Mol Life Sci*. 2004; 61:393-416.
  169. Kersten S, Desvergne B, Wahli W. Roles of PPARs in health and disease. *Nature*. 2000; 405:421-424.
  170. Nolte RT, Wisely GB, Westin S, et al. Ligand binding and co-activator assembly of the peroxisome proliferator-activated receptor-gamma. *Nature*. 1998; 395:137-143.
  171. Xu HE, Lambert MH, Montana VG, et al. Molecular recognition of fatty acids by peroxisome proliferator-activated receptors. *Mol Cell*. 1999; 3:397-403.

- 
172. Horowitz JF, Leone TC, Feng W, et al. Effect of endurance training on lipid metabolism in women: a potential role for PPAR $\alpha$  in the metabolic response to training. *Am J Physiol Endocrinol Metab.* 2000; 279:E348-E355.
  173. Lehman JJ and Kelly DP. Transcriptional activation of energy metabolic switches in the developing and hypertrophied heart. *Clin Exp Pharmacol Physiol.* 2002; 29:339-345.
  174. Villena JA, Kralli A. ERR $\alpha$ : a metabolic function for the oldest orphan. *Trends Endocrinol Metab.* 2008; 19:269-276.
  175. Greschik H, Wurtz JM, Sanglier S, et al. Structural and functional evidence for ligand-independent transcriptional activation by the estrogen-related receptor 3. *Mol Cell.* 2002; 9:303-313.
  176. Horard B, Vanacker JM. Estrogen receptor-related receptors: orphan receptors desperately seeking a ligand. *J Mol Endocrinol.* 2003; 31:349-357.
  177. Kallen J, Schlaeppli JM, Bitsch F, et al. Evidence for ligand-independent transcriptional activation of the human estrogen-related receptor alpha (ERR $\alpha$ ): crystal structure of ERR $\alpha$  ligand binding domain in complex with peroxisome proliferator-activated receptor coactivator-1 $\alpha$ . *J Biol Chem.* 2004; 279:49330-49337.
  178. Giguère V, Yang N, Segui P, et al. Identification of a new class of steroid hormone receptors. *Nature.* 1988; 331:91-94.
  179. Sladek R, Bader JA, Giguère V. The orphan nuclear receptor estrogen-related receptor alpha is a transcriptional regulator of the human medium-chain acyl coenzyme A dehydrogenase gene. *Mol Cell Biol.* 1997; 17:5400-5409.
  180. Bookout AL, Jeong Y, Downes M, et al. Anatomical profiling of nuclear receptor expression reveals a hierarchical transcriptional network. *Cell.* 2006; 126:789-799.
  181. Gofflot F, Chartoire N, Vasseur L, et al. Systematic gene expression mapping clusters nuclear receptors according to their function in the brain. *Cell.* 2007; 131:405-418.
  182. Laganière J, Tremblay GB, Dufour CR, et al. A polymorphic autoregulatory hormone response element in the human estrogen-related receptor alpha (ERR $\alpha$ ) promoter dictates peroxisome proliferator-activated receptor gamma coactivator-1 $\alpha$  control of ERR $\alpha$  expression. *J Biol Chem.* 2004 Apr 30; 279(18):18504-10. Epub 2004 Feb 20.
  183. Mootha VK, Handschin C, Arlow D, et al. Err $\alpha$  and Gabpa/b specify PGC-1 $\alpha$ -dependent oxidative phosphorylation gene expression that is altered in diabetic muscle. *Proc Natl Acad Sci USA.* 2004; 101:6570-6575.
  184. Liu D, Zhang Z, Teng CT. Estrogen-related receptor-gamma and peroxisome proliferator-activated receptor-gamma coactivator-1 $\alpha$  regulate estrogen-related receptor-alpha gene expression via a conserved multi-hormone response element. *J Mol Endocrinol.* 2005; 34:473-487.
  185. Luft R. The development of mitochondrial medicine. *Proc Natl Acad Sci USA.* 1994; 91:8731-8738.

186. Luft R, Ikkos D, Palmieri G, et al. A case of severe hypermetabolism of nonthyroid origin with a defect in the maintenance of mitochondrial respiratory control: a correlated clinical, biochemical, and morphological study. *J Clin Invest.* 1962; 41:1776-1804.
187. Wallace DC, Singh G, Lott MT, et al. Mitochondrial DNA mutation associated with Leber's hereditary optic neuropathy. *Science.* 1988; 242:1427-1430.
188. Holt IJ, Harding AE, Morgan-Hughes JA. Deletions of muscle mitochondrial DNA in patients with mitochondrial myopathies. *Nature.* 1988; 331:717-719.
189. DiMauro S and Schon EA. Mitochondrial disorders in the nervous system. *Annu Rev Neurosci.* 2008; 31:91-123.
190. Filosto M, Mancuso M. Mitochondrial diseases: a nosological update. *Acta Neurol Scand.* 2007; 115:211-221.
191. Hudson G, Carelli V, Spruijt L, et al. Clinical expression of Leber hereditary optic neuropathy is affected by the mitochondrial DNA-haplogroup background. *Am J Hum Genet.* 2007; 81:228-233.
192. Pello R, Martín MA, Carelli V, et al. Mitochondrial DNA background modulates the assembly kinetics of OXPHOS complexes in a cellular model of mitochondrial disease. *Hum Mol Genet.* 2008; 17:4001-4011.
193. Spinazzola A, Zeviani M. Disorders of nuclear-mitochondrial intergenomic signaling. *Gene.* 2005; 354:162-168.
194. Spinazzola A, Zeviani M. Disorders of nuclear-mitochondrial intergenomic communication. *Biosci Rep.* 2007; 27: 39-51.
195. Servidei S, Zeviani M, Manfredi G, et al. Dominantly inherited mitochondrial myopathy with multiple deletions of mitochondrial DNA: clinical, morphologic, and biochemical studies. *Neurology.* 1991; 41:1053-1059.
196. Hirano M, Marti R, Ferreiro-Barros C, et al. Defects of intergenomic communication: autosomal disorders that cause multiple deletions and depletion of mitochondrial DNA. *Semin Cell Dev Biol.* 2001; 12:417-427.
197. Kaukonen J, Juselius JK, Tiranti V, et al. Role of adenine nucleotide translocator 1 in mtDNA maintenance. *Science.* 2000; 289:782-785.
198. Spelbrink JN, Li FY, Tiranti V, et al. Human mitochondrial DNA deletions associated with mutations in the gene encoding Twinkle, a phage T7 gene 4-like protein localized in mitochondria. *Nat Genet.* 2001; 28:223-231.
199. Van Goethem G, Dermaut B, Löfgren A, et al. Mutation of POLG is associated with progressive external ophthalmoplegia characterized by mtDNA deletions. *Nat Genet.* 2001; 28:211-212.
200. Longley MJ, Clark S, Yu Wai Man C, et al. Mutant POLG2 disrupts DNA polymerase gamma subunits and causes progressive external ophthalmoplegia. *Am J Hum Genet.* 2006; 78:1026-1034.

- 
201. Ferraris S, Clark S, Garelli E, et al. Progressive external ophthalmoplegia and vision and hearing loss in a patient with mutations in POLG2 and OPA1. *Arch Neurol.* 2008; 65:125-131.
  202. Hirano M, Nishigaki Y, Martí R. Mitochondrial neurogastrointestinal encephalomyopathy (MNGIE): a disease of two genomes. *Neurologist.* 2004; 10:8-17.
  203. Nishino I, Spinazzola A, Hirano M. Thymidine phosphorylase gene mutations in MNGIE, a human mitochondrial disorder. *Science.* 1999 Jan; 283:689-692.
  204. Spinazzola A, Viscomi C, Fernandez-Vizarra E, et al. MPV17 encodes an inner mitochondrial membrane protein and is mutated in infantile hepatic mitochondrial DNA depletion. *Nat Genet.* 2006; 38:570-575.
  205. Elpeleg O, Miller C, Hershkovitz E, et al. Deficiency of the ADP-forming succinyl-CoA synthase activity is associated with encephalomyopathy and mitochondrial DNA depletion. *Am J Hum Genet.* 2005; 76:1081-1086.
  206. Bourdon A, Minai L, Serre V, et al. Mutation of RRM2B, encoding p53-controlled ribonucleotide reductase (p53R2), causes severe mitochondrial DNA depletion. *Nat Genet.* 2007; 39:776-780.
  207. Hirano M, Kaufmann, De Vivo D, et al. Mitochondrial neurology I: encephalopathies. In *Mitochondrial medicine*. Edited by DiMauro S, Hirano M and Schon EA, Informa Healthcare 2006. pp 27-44.
  208. MITOMAP: A Human Mitochondrial Genome Database. <http://www.mitomap.org>, 2008.
  209. Hirano M, Pavlakis SG. Mitochondrial myopathy, encephalopathy, lactic acidosis, and stroke-like episodes (MELAS): current concepts. *J Child Neurol.* 1994; 9:4-13.
  210. Yasukawa T, Suzuki T, Ueda T, et al. Modification defect at anticodon wobble nucleotide of mitochondrial tRNAs(Leu)(UUR) with pathogenic mutations of mitochondrial myopathy, encephalopathy, lactic acidosis, and stroke-like episodes. *J Biol Chem.* 2000; 275:4251-4257.
  211. Mancuso M, Filosto M, Mootha VK, et al. A novel mitochondrial tRNA<sup>Phe</sup> mutation causes MERRF syndrome. *Neurology.* 2004; 62:2119-2121.
  212. Holt IJ, Harding AE, Petty RK, et al. A new mitochondrial disease associated with mitochondrial DNA heteroplasmy. *Am J Hum Genet.* 1990; 46:428-433.
  213. Santorelli FM, Shanske S, Macaya A, et al. The mutation at nt 8993 of mitochondrial DNA is a common cause of Leigh's syndrome. *Ann Neurol.* 1993; 34:827-834.
  214. Bourgeron T, Rustin P, Chretien D, et al. Mutation of a nuclear succinate dehydrogenase gene results in mitochondrial respiratory chain deficiency. *Nat Genet.* 1995; 11:144-149.
  215. Ugalde C, Janssen RJ, van den Heuvel LP, et al. Differences in assembly or stability of complex I and other mitochondrial OXPHOS complexes in inherited complex I deficiency. *Hum Mol Genet.* 2004; 13:659-667.
  216. Tiranti V, Hoertnagel K, Carozzo R, et al. Mutations of SURF-1 in Leigh disease associated with cytochrome c oxidase deficiency. *Am J Hum Genet.* 1998; 63:1609-1621.

- 
217. Leber T. Ueber hereditaere und congenital angelegte Sehnervenleiden. *Graefes Arch Ophthal.* 1871; 17: 249-291.
218. Man PY, Griffiths PG, Brown DT, et al. The epidemiology of Leber hereditary optic neuropathy in the North East of England. *Am J Hum Genet.* 2003; 72:333-339.
219. Newman NJ. Leber's optic neuropathy. In Walsh and Hoyt's *Clinical Neuro-Ophthalmology*. Edited by Miller NR, Newman NJ. Williams & Wilkins. 1998; pp. 742-753.
220. Carelli V, Ross-Cisneros FN, Sadun AA. Mitochondrial dysfunction as a cause of optic neuropathies. *Prog Retin Eye Res.* 2004; 23:53-89.
221. Nikoskelainen E, Hoyt WF, Nummelin K. Ophthalmoscopic findings in Leber's hereditary optic neuropathy. II. The fundus findings in the affected family members. *Arch Ophthalmol.* 1983; 101:1059-1068.
222. Nikoskelainen E, Hoyt WF, Nummelin K, et al. Fundus findings in Leber's hereditary optic neuroretinopathy. III. Fluorescein angiographic studies. *Arch Ophthalmol.* 1984; 102:981-989.
223. Nikoskelainen E, Hoyt WF, Nummelin K. Ophthalmoscopic findings in Leber's hereditary optic neuropathy. I. Fundus findings in asymptomatic family members. *Arch Ophthalmol.* 1982; 100:1597-1602.
224. Stone EM, Newman NJ, Miller NR, et al. Visual recovery in patients with Leber's hereditary optic neuropathy and the 11778 mutation. *J Clin Neuroophthalmol.* 1992; 12:10-14.
225. Mackey D, Howell N. A variant of Leber hereditary optic neuropathy characterized by recovery of vision and by an unusual mitochondrial genetic etiology. *Am J Hum Genet.* 1992; 51:1218-1228.
226. Pezzi PP, De Negri AM, Sadun F, et al. Childhood Leber's hereditary optic neuropathy (ND1/3460) with visual recovery. *Pediatr Neurol.* 1998; 19:308-312.
227. Ortiz RG, Newman NJ, Manoukian SV, et al. Optic disk cupping and electrocardiographic abnormalities in an American pedigree with Leber's hereditary optic neuropathy. *Am J Ophthalmol.* 1992; 113:561-566.
228. Weiner NC, Newman NJ, Lessell S, et al. Atypical Leber's hereditary optic neuropathy with molecular confirmation. *Arch Neurol.* 1993; 50:470-473.
229. Mashima Y, Kimura I, Yamamoto Y, et al. Optic disc excavation in the atrophic stage of Leber's hereditary optic neuropathy: comparison with normal tension glaucoma. *Graefes Arch Clin Exp Ophthalmol.* 2003; 241:75-80.
230. do V F Ramos C, Bellusci C, Savini G, et al. Optic disc size is associated with development and prognosis of Leber's hereditary optic neuropathy. *Invest Ophthalmol Vis Sci.* 2008. [Epub ahead of print]
231. Newman NJ. Leber's hereditary optic neuropathy. New genetic considerations. *Arch Neurol.* 1993; 50:540-548.
-

- 
232. Nikoskelainen EK, Marttila RJ, Huoponen K, et al. Leber's "plus": neurological abnormalities in patients with Leber's hereditary optic neuropathy. *J Neurol Neurosurg Psychiatry*. 1995; 59:160-164.
233. Larson NG, Andersen O, Holme E, et al. Leber's hereditary optic neuropathy and complex I deficiency in muscle. *Ann Neurol*. 1991; 30:701-708.
234. Funalot B, Reynier P, Vighetto A, et al. Leigh-like encephalopathy complicating Leber's hereditary optic neuropathy. *Ann Neurol*. 2002; 52:374-377.
235. Funakawa I, Kato H, Terao A, et al. Cerebellar ataxia in patients with Leber's hereditary optic neuropathy. *J Neurol*. 1995; 242:75-77.
236. Cupini LM, Massa R, Floris R, et al. Migraine-like disorder segregating with mtDNA 14484 Leber hereditary optic neuropathy mutation. *Neurology*. 2003; 60:717-719.
237. Nikoskelainen E, Wanne O, Dahl M. Pre-excitation syndrome and Leber's hereditary optic neuroretinopathy. *Lancet*. 1985; 1:696.
238. Jun AS, Brown MD, Wallace DC. A mitochondrial DNA mutation at np 14459 of the ND6 gene associated with maternally inherited Leber's hereditary optic neuropathy and dystonia. *Proc Natl Acad Sci USA*. 1994; 91: 6206-6210.
239. Kirby DM, McFarland R, Ohtake A, et al. Mutations of the mitochondrial ND1 gene as a cause of MELAS. *J Med Genet*. 2004; 41:784-789.
240. Crimi M, Galbiati S, Moroni I, et al. A missense mutation in the mitochondrial ND5 gene associated with a Leigh-MELAS overlap syndrome. *Neurology*. 2003; 60:1857-1861.
241. Ugalde C, Triepels RH, Coenen MJ, et al. Impaired complex I assembly in a Leigh syndrome patient with a novel missense mutation in the ND6 gene. *Ann Neurol*. 2003; 54:665-669.
242. Howell N, Kubacka I, Xu M, et al. Leber hereditary optic neuropathy: involvement of the mitochondrial ND1 gene and evidence for an intragenic suppressor mutation. *Am J Hum Genet*. 1991; 48: 935-942.
243. De Vries DD, Went LN, Bruyn GW, et al. Genetic and biochemical impairment of mitochondrial complex I activity in a family with Leber hereditary optic neuropathy and hereditary spastic dystonia. *Am J Hum Genet*. 1996; 58:703-11.
244. Howell N, Miller NR, Mackey DA, et al. Lightning strikes twice: Leber hereditary optic neuropathy families with two pathogenic mtDNA mutations. *J Neuroophthalmol*. 2002; 22:262-269.
245. Carelli V, Barboni P, Sadun AA. Mitochondrial ophthalmology. In *Mitochondrial medicine*. Edited by DiMauro S, Hirano M, Schon EA. Informa healthcare. 2006. pp. 105-142.
246. Polyak SL. *The retina*. 1941. Ed. The University of Chicago Press.
247. Fine BS, Yanoff M. *Ocular histology. A text and atlas*. 1979. Ed. Harper & Row. pp 111-124.
248. Wang L, Dong J, Cull G, et al. Varicosities of intraretinal ganglion cell axons in human and nonhuman primates. *Invest Ophthalmol Vis Sci*. 2003; 44:2-9.
249. Glaser J, Sadun AA. *Anatomy of the visual sensory system in Neuro-Ophthalmology*. Ed. JB Lippincott Co. 1999; 3:75-94.
-

- 
250. Carelli V, Ross-Cisneros FN, Sadun AA. Optic nerve degeneration and mitochondrial dysfunction: genetic and acquired optic neuropathies. *Neurochem Int.* 2002; 40:573-584.
251. Sadun AA, Kashima Y, Wurdeman AE, et al. Morphological findings in the visual system in a case of Leber's hereditary optic neuropathy. *Clin Neurosci.* 1994; 2:165-172.
252. Sadun AA, Win PH, Ross-Cisneros FN, et al. Leber's hereditary optic neuropathy differentially affects smaller axons in the optic nerve. *Trans. Am. Ophthalmol. Soc.* 2000; 98:223-232.
253. Kerrison JB, Howell N, Miller NR, et al. Leber hereditary optic neuropathy. Electron microscopy and molecular genetic analysis of a case. *Ophthalmology.* 1995; 102:1509-1516.
254. Howell N. Human mitochondrial diseases: answering questions and questioning answers. *Int Rev Cytol.* 1999; 186:49-116.
255. Wallace DC. Mitochondrial diseases in man and mouse. *Science.* 1999; 283:1482-1488.
256. Howell N, Oostra RJ, Bolhuis PA, et al. Sequence analysis of the mitochondrial genomes from Dutch pedigrees with Leber hereditary optic neuropathy. *Am J Hum Genet.* 2003; 72:1460-1469.
257. Macmillan C, Johns TA, Fu K, et al. Predominance of the T14484C mutation in French-Canadian families with Leber hereditary optic neuropathy is due to a founder effect. *Am J Hum Genet.* 2000; 66:332-335.
258. Bu XD, Rotter JJ. X chromosome-linked and mitochondrial gene control of Leber hereditary optic neuropathy: evidence from segregation analysis for dependence on X chromosome inactivation. *Proc Natl Acad Sci USA.* 1991; 88:8198-8202.
259. Bu X, Rotter JJ. Leber hereditary optic neuropathy: estimation of number of embryonic precursor cells and disease threshold in heterozygous affected females at the X-linked locus. *Clin Genet.* 1992; 42:143-148.
260. Chen JD, Cox I, Denton MJ. Preliminary exclusion of an X-linked gene in Leber optic atrophy by linkage analysis. *Hum Genet.* 1989; 82:203-207.
261. Carvalho MR, Müller B, Rötzer E, et al. Leber's hereditary optic neuroretinopathy and the X-chromosomal susceptibility factor: no linkage to DXs7. *Hum Hered.* 1992; 42:316-320.
262. Chalmers RM, Davis MB, Sweeney MG, et al. Evidence against an X-linked visual loss susceptibility locus in Leber hereditary optic neuropathy. *Am J Hum Genet.* 1996; 59:103-108.
263. Pegoraro E, Carelli V, Zeviani M, et al. X-inactivation patterns in female Leber's hereditary optic neuropathy patients do not support a strong X-linked determinant. *Am J Med Genet.* 1996; 61:3563-62.
264. Oostra RJ, Kemp S, Bolhuis PA, et al. No evidence for 'skewed' inactivation of the X-chromosome as cause of Leber's hereditary optic neuropathy in female carriers. *Hum Genet.* 1996; 97:500-505.
265. Pegoraro E, Vettori A, Valentino ML, et al. X-inactivation pattern in multiple tissues from two Leber's hereditary optic neuropathy (LHON) patients. *Am J Med Genet A.* 2003; 119A:37-40.
266. Petruzzella V, Tessa A, Torraco A, et al. The NDUFB11 gene is not a modifier in Leber hereditary optic neuropathy. *Biochem Biophys Res Commun.* 2007; 355:181-187.
-

- 
267. Hudson G, Keers S, Yu Wai Man P, et al. Identification of an X-chromosomal locus and haplotype modulating the phenotype of a mitochondrial DNA disorder. *Am J Hum Genet.* 2005; 77:1086-1091.
268. Shankar SP, Fingert JH, Carelli V, et al. Evidence for a novel x-linked modifier locus for leber hereditary optic neuropathy. *Ophthalmic Genet.* 2008; 29:17-24.
269. Carelli V, Franceschini F, Venturi S, et al. Grand rounds: could occupational exposure to n-hexane and other solvents precipitate visual failure in leber hereditary optic neuropathy? *Environ Health Perspect.* 2007; 115:113-115.
270. Majander A, Huoponen K, Savontaus ML, et al. Electron transfer properties of NADH:ubiquinone reductase in the ND1/3460 and the ND4/11778 mutations of the Leber hereditary optic neuroretinopathy (LHON). *FEBS Lett.* 1991; 292:289-292.
271. Carelli V, Ghelli A, Ratta M, et al. Leber's hereditary optic neuropathy: biochemical effect of 11778/ND4 and 3460/ND1 mutations and correlation with the mitochondrial genotype. *Neurology.* 1997; 48:1623-1632.
272. Brown MD, Trounce IA, Jun AS, et al. Functional analysis of lymphoblast and cybrid mitochondria containing the 3460, 11778, or 14484 Leber's hereditary optic neuropathy mitochondrial DNA mutation. *J Biol Chem.* 2000; 275:39831-39381.
273. Degli Esposti M, Carelli V, Ghelli A, et al. Functional alterations of the mitochondrially encoded ND4 subunit associated with Leber's hereditary optic neuropathy. *FEBS Lett.* 1994; 352:375-379.
274. Carelli V, Ghelli A, Bucchi L, et al. Biochemical features of mtDNA 14484 (ND6/M64V) point mutation associated with Leber's hereditary optic neuropathy. *Ann Neurol.* 1999; 45:320-328.
275. Majander A, Finel M, Savontaus ML, et al. Catalytic activity of complex I in cell lines that possess replacement mutations in the ND genes in Leber's hereditary optic neuropathy. *Eur J Biochem.* 1996; 239:201-207.
276. King MP, Attardi G. Human cells lacking mtDNA: repopulation with exogenous mitochondria by complementation. *Science.* 1989; 246:500-503.
277. Baracca A, Solaini G, Sgarbi G, et al. Severe impairment of complex I-driven adenosine triphosphate synthesis in leber hereditary optic neuropathy cybrids. *Arch Neurol.* 2005; 62:730-736.
278. Lodi R, Taylor DJ, Tabrizi SJ, et al. In vivo skeletal muscle mitochondrial function in Leber's hereditary optic neuropathy assessed by <sup>31</sup>P magnetic resonance spectroscopy. *Ann Neurol.* 1997; 42:573-579.
279. Lodi R, Carelli V, Cortelli P, et al. Phosphorus MR spectroscopy shows a tissue specific in vivo distribution of biochemical expression of the G3460A mutation in Leber's hereditary optic neuropathy. *J Neurol Neurosurg Psychiatry.* 2002; 72:805-807.
280. Wong A, Cavalier L, Collins-Schramm HE, et al. Differentiation-specific effects of LHON mutations introduced into neuronal NT2 cells. *Hum Mol Genet.* 2002; 11:431-438.
281. Schoeler S, Winkler-Stuck K, Szibor R, et al. Glutathione depletion in antioxidant defense of differentiated NT2-LHON cybrids. *Neurobiol Dis.* 2007; 25:536-544.
-

- 
282. Beretta S, Mattavelli L, Sala G, et al. Leber hereditary optic neuropathy mtDNA mutations disrupt glutamate transport in cybrid cell lines. *Brain*. 2004; 127:2183-2192.
283. Carelli V, La Morgia C, Iommarini L, et al. Mitochondrial optic neuropathies: how two genomes may kill the same cell type? *Biosci Rep*. 2007; 27:173-184.
284. Floreani M, Napoli E, Martinuzzi A, et al. Antioxidant defences in cybrids harboring mtDNA mutations associated with Leber's hereditary optic neuropathy. *FEBS J*. 2005; 272:1124-1135.
285. Ghelli A, Zanna C, Porcelli AM, et al. Leber's hereditary optic neuropathy (LHON) pathogenic mutations induce mitochondrial-dependent apoptotic death in transmitochondrial cells incubated with galactose medium. *J Biol Chem*. 2003; 278:4145-4150.
286. Zanna C, Ghelli A, Porcelli AM, et al. Apoptotic cell death of cybrid cells bearing Leber's hereditary optic neuropathy mutations is caspase independent. *Ann N Y Acad Sci*. 2003; 1010:213-217.
287. Zanna C, Ghelli A, Porcelli AM, et al. Caspase-independent death of Leber's hereditary optic neuropathy cybrids is driven by energetic failure and mediated by AIF and Endonuclease G. *Apoptosis*. 2005; 10:997-1007.
288. Danielson SR, Wong A, Carelli V, et al. Cells bearing mutations causing Leber's hereditary optic neuropathy are sensitized to Fas-Induced apoptosis. *J Biol Chem*. 2002; 277:5810-5815.
289. Newman NJ, Biousse V, David R, et al. Prophylaxis for second eye involvement in leber hereditary optic neuropathy: an open-labeled, nonrandomized multicenter trial of topical brimonidine purite. *Am J Ophthalmol*. 2005; 140:407-415.
290. Mashima Y, Hiida Y, Oguchi Y. Remission of Leber's hereditary optic neuropathy with idebenone. *Lancet*. 1992; 340:368-369.
291. Mashima Y, Kigasawa K, Wakakura M, et al. Do idebenone and vitamin therapy shorten the time to achieve visual recovery in Leber hereditary optic neuropathy? *J Neuroophthalmol*. 2000; 20:166-170.
292. Manfredi G, Fu J, Ojaimi J, et al. Rescue of a deficiency in ATP synthesis by transfer of MTATP6, a mitochondrial DNA-encoded gene, to the nucleus. *Nat Genet*. 2002; 30:394-399.
293. Guy J, Qi X, Pallotti F, et al. Rescue of a mitochondrial deficiency causing Leber Hereditary Optic Neuropathy. *Ann Neurol*. 2002; 52:534-542.
294. Oca-Cossio J, Kenyon L, Hao H, et al. Limitations of allotopic expression of mitochondrial genes in mammalian cells. *Genetics*. 2003; 165:707-720.
295. Bokori-Brown M, Holt IJ. Expression of algal nuclear ATP synthase subunit 6 in human cells results in protein targeting to mitochondria but no assembly into ATP synthase. *Rejuvenation Res*. 2006; 9:455-469.
296. Bonnet C, Kaltimbacher V, Ellouze S, et al. Allotopic mRNA localization to the mitochondrial surface rescues respiratory chain defects in fibroblasts harboring mitochondrial DNA mutations affecting complex I or v subunits. *Rejuvenation Res*. 2007; 10:127-144.
-

- 
297. Bonnet C, Augustin S, Ellouze S, et al. The optimized allotopic expression of ND1 or ND4 genes restores respiratory chain complex I activity in fibroblasts harboring mutations in these genes. *Biochim Biophys Acta*. 2008; 1783:1707-1017.
  298. Ellouze S, Augustin S, Bouaita A, et al. Optimized allotopic expression of the human mitochondrial ND4 prevents blindness in a rat model of mitochondrial dysfunction. *Am J Hum Genet*. 2008; 83:373-387.
  299. Park JS, Li YF, Bai Y. Yeast NDI1 improves oxidative phosphorylation capacity and increases protection against oxidative stress and cell death in cells carrying a Leber's hereditary optic neuropathy mutation. *Biochim Biophys Acta*. 2007; 1772:533-542.
  300. Ghelli A, Porcelli AM, Zanna C, et al. Protection against oxidant-induced apoptosis by exogenous glutathione in Leber hereditary optic neuropathy cybrids. *Invest Ophthalmol Vis Sci*. 2008; 49:671-676.
  301. Qi X, Sun L, Hauswirth WW, et al. Use of mitochondrial antioxidant defenses for rescue of cells with a Leber hereditary optic neuropathy-causing mutation. *Arch Ophthalmol*. 2007; 125:268-272.
  302. Mitchell AL, Elson JL, Howell N, et al. Sequence variation in mitochondrial complex I genes: mutation or polymorphism? *J Med Genet*. 2006; 43:175-179.
  303. Thompson JD, Gibson TJ, Plewniak F, et al. The CLUSTAL X windows interface: flexible strategies for multiple sequence alignment aided by quality analysis tools. *Nucleic Acids Res* 1997; 25:4876-4882.
  304. Nicholas KB, Nicholas HB, Deerfield DW. GeneDoc: analysis and visualization of genetic variation EMBNEW NEWS. 1997; 4:14.
  305. Ramensky V, Bork P, Sunyaev S. Human non-synonymous SNPs: server and survey. *Nucleic Acids Res*. 2002; 30:3894-3900.
  306. Ng PC, Henikoff S. Accounting for human polymorphisms predicted to affect protein function. *Genome Res*. 2002; 12:436-446.
  307. Ferrer-Costa C, Orozco M, de la Cruz X. Sequence-based prediction of pathological mutations. *Proteins*. 2004; 57:811-819.
  308. Degli Esposti M, Ghelli A, Luchetti R, et al. New approaches to the prediction of the folding of membrane proteins with redox function. *Ital J Biochem*. 1989; 38:1-22.
  309. Degli Esposti M, Crimi M, Venturoli G. A critical evaluation of the hydropathy profile of membrane proteins. *Eur J Biochem*. 1990; 190:207-219.
  310. Bradford MM. A rapid and sensitive method for the quantitation of microgram quantities of protein utilizing the principle of protein-dye binding. *Anal Biochem*. 1976; 72:248-254.
  311. Bénit P, Goncalves S, Philippe Dassa E, et al. Three spectrophotometric assays for the measurement of the five respiratory chain complexes in minuscule biological samples. *Clin Chim Acta*. 2006; 374:81-86.

- 
312. Trounce IA, Kim YL, Jun AS, et al. Assessment of mitochondrial oxidative phosphorylation in patient muscle biopsies, lymphoblasts, and transmitochondrial cell lines. *Methods Enzymol.* 1996; 264:484-509.
313. Manfredi G, Yang L, Gajewski CD, et al. Measurements of ATP in mammalian cells. *Methods.* 2002; 26:317-326.
314. Achilli A, Rengo C, Magri C, et al. The molecular dissection of mtDNA haplogroup H confirms that the Franco-Cantabrian glacial refuge was a major source for the European gene pool. *Am J Hum Genet.* 2004; 75:910-918.
315. Cossarizza A, Riva A, Pinti M, et al. Increased mitochondrial DNA content in peripheral blood lymphocytes from HIV-infected patients with lipodystrophy. *Antivir Ther.* 2003; 8:315-321.
316. Fauser S, Lubrichs J, Besch D, et al. Sequence analysis of the complete mitochondrial genome in patients with Leber's hereditary optic neuropathy lacking the three most common pathogenic DNA mutations. *Biochem Biophys Res Com.* 2002; 295: 342-347.
317. Wissinger B, Besch D, Baumann B, et al. Mutation analysis of the ND6 gene in patients with Lebers hereditary optic neuropathy. *Biochem Biophys Res Com.* 1997; 234: 511-515.
318. Besch D, Leo-Kottler B, Zrenner E, et al. Leber's hereditary optic neuropathy: clinical and molecular genetic findings in a patient with a new mutation in the ND6 gene. *Graef Arch Clin Exper Ophthalmol.* 1999; 237: 745-752.
319. Fauser S, Leo-Kottler B, Besch D, et al. Confirmation of the 14568 mutation in the mitochondrial ND6 gene as causative in Leber's hereditary optic neuropathy. *Ophthalm Genet.* 2002; 23: 191-197.
320. Kim JY, Hwang JM, Park SS. Mitochondrial DNA C4171A/ND1 is a novel primary causative mutation of Leber's hereditary optic neuropathy with a good prognosis. *Ann Neurol.* 2002; 51: 630-634.
321. Chinnery PF, Brown DT, Andrews RM, et al. The mitochondrial ND6 gene is a hot spot for mutations that cause Leber's hereditary optic neuropathy. *Brain.* 2001; 124: 209-218.
322. Kivisild T, Shen P, Wall DP, et al. The role of selection in the evolution of human mitochondrial genomes. *Genetics.* 2006; 172:373-387.
323. Herrnstadt C, Elson JL, Fahy E, et al. Reduced-median-network analysis of complete mitochondrial DNA coding-region sequences for the major African, Asian, and European haplogroups. *Am J Hum Genet.* 2002; 70:1152-1171.
324. Valentino ML, Barboni P, Ghelli A, et al. The ND1 gene of complex I is a mutational hot spot for Leber's Hereditary Optic Neuropathy. *Ann Neurol.* 2004; 56:631-641.
325. Torroni A, Petrozzi M, D'Urbano L, et al. Haplotype and phylogenetic analyses suggest that one European-specific mtDNA background plays a role in the expression of Leber hereditary optic neuropathy by increasing the penetrance of the primary mutations 11778 and 14484. *Am J Hum Genet.* 1997; 60:1107-1121.
-

- 
326. Tanaka M, Cabrera VM, Gonzalez AM, et al. Mitochondrial genome variation in eastern Asia and the peopling of Japan. *Genome Res.* 2004;14:1832-1850.
327. Carelli V, Achilli A, Valentino ML, et al. Haplogroup effects and recombination of mitochondrial DNA: novel clues from the analysis of Leber hereditary optic neuropathy pedigrees. *Am J Hum Genet.* 2006;78:564-574.
328. Choi YS, Hong JM, Lim S, et al. Impaired coactivator activity of the Gly482 variant of peroxisome proliferator-activated receptor gamma coactivator-1alpha (PGC-1alpha) on mitochondrial transcription factor A (Tfam) promoter. *Biochem Biophys Res Commun.* 2006; 344:708-712.
329. Wenz T, Diaz F, Spiegelman BM, et al. Activation of the PPAR/PGC-1alpha pathway prevents a bioenergetic deficit and effectively improves a mitochondrial myopathy phenotype. *Cell Metab.* 2008; 8:249-256.
330. Bastin J, Aubey F, Rötig A, et al. Activation of peroxisome proliferator-activated receptor pathway stimulates the mitochondrial respiratory chain and can correct deficiencies in patients' cells lacking its components. *J Clin Endocrinol Metab.* 2008; 93:1433-1441.
331. Grigorieff N. Three-dimensional structure of bovine NADH:ubiquinone oxidoreductase (complex I) at 2.2 Å in ice. *J Mol Biol.* 1998; 277:1033-1046.
332. Peng G, Fritzsche G, Zickermann V, et al. Isolation, characterization and electron microscopic single particle analysis of the NADH:ubiquinone oxidoreductase (complex I) from the hyperthermophilic eubacterium *Aquifex aeolicus*. *Biochemistry.* 2003; 42:3032-3039.
333. Fearnley IM, Walker JE. Conservation of sequences of subunits of mitochondrial complex I and their relationships with other proteins. *Biochim Biophys Acta.* 1992; 1140:105-134.
334. Crimi M, Degli Esposti M. Structural predictions for membrane proteins: the dilemma of hydrophobicity scales. *Trends Biochem Sci.* 1991; 16:119.
335. Kyte J, Doolittle RF. A simple method for displaying the hydropathic character of a protein. *J Mol Biol.* 1982; 157:105-132.
336. Punta M, Forrest LR, Bigelow H, et al. Membrane protein prediction methods. *Methods.* 2007; 41:460-474.
337. Simon I, Fiser A, Tusnády GE. Predicting protein conformation by statistical methods. *Biochim Biophys Acta.* 2001; 1549:123-136.
338. Martelli PL, Fariselli P, Casadio R. An ENSEMBLE machine learning approach for the prediction of all-alpha membrane proteins. *Bioinformatics.* 2003; 19 Suppl 1:i205-211.
339. Taylor PD, Attwood TK, Flower DR. BPROMPT: A consensus server for membrane protein prediction. *Nucleic Acids Res.* 2003; 31:3698-3700.
340. DiMauro S, Schon EA. Mitochondrial DNA mutations in human diseases. *Am J Med Genet.* 2001; 106:18-26.
-

- 
341. Shoffner JM, Brown MD, Stugard C, et al. Leber's hereditary optic neuropathy plus dystonia is caused by a mitochondrial DNA point mutation. *Ann Neurol.* 1995; 38:163-169.
342. Jun AS, Trounce IA, Brown MD, et al. Use of transmitochondrial cybrids to assign a complex I defect to the mitochondrial DNA-encoded NADH dehydrogenase subunit 6 gene mutation at nucleotide pair 14459 that causes Leber hereditary optic neuropathy and dystonia. *Mol Cell Biol.* 1996; 16:771-777.
343. Kirby DM, Kahler SG, Freckmann ML, et al. Leigh disease caused by the mitochondrial DNA G14459A mutation in unrelated families. *Ann Neurol.* 2000; 48:102-104.
344. Houshmand M, Sharifpanah F, Tabasi A, et al. Leber's hereditary optic neuropathy: the spectrum of mitochondrial DNA mutations in Iranian patients. *Ann N Y Acad Sci.* 2004; 1011:345-349.
345. Tarnopolsky MA, Baker SK, Myint T, et al. Clinical variability in maternally inherited leber hereditary optic neuropathy with the G14459A mutation. *Am J Med Genet A.* 2004; 124A:372-376.
346. Gropman A, Chen TJ, Perng CL, et al. Variable clinical manifestation of homoplasmic G14459A mitochondrial DNA mutation. *Am J Med Genet A.* 2004; 124A:377-382.
347. Zhadanov SI, Atamanov VV, Zhadanov NI, et al. A novel mtDNA ND6 gene mutation associated with LHON in a Caucasian family. *Biochem Biophys Res Commun.* 2005; 332:1115-1121.
348. Semino O, Torroni A, Scozzari R, et al. Mitochondrial DNA polymorphisms among Hindus: a comparison with the Tharus of Nepal. *Ann Hum Genet.* 1991; 55:123-136.
349. Torroni A, Carelli V, Petrozzi M, et al. Detection of the mtDNA 14484 mutation on an African-specific haplotype: implications about its role in causing Leber hereditary optic neuropathy. *Am J Hum Genet.* 1996; 59:248-252.
350. Abu-Amero KK, Bosley TM. Detection of mitochondrial respiratory dysfunction in circulating lymphocytes using resazurin. *Arch Pathol Lab Med.* 2005; 129:1295-1298.
351. Abu-Amero KK, Bosley TM. Mitochondrial abnormalities in patients with LHON-like optic neuropathies. *Invest Ophthalmol Vis Sci.* 2006; 47:4211-4220.
352. Povalko N, Zakharova E, Rudenskaia G, et al. A new sequence variant in mitochondrial DNA associated with high penetrance of Russian Leber hereditary optic neuropathy. *Mitochondrion.* 2005; 5:194-199.
353. Bandelt HJ, Yao YG, Salas A, et al. High penetrance of sequencing errors and interpretative shortcomings in mtDNA sequence analysis of LHON patients. *Biochem Biophys Res Commun.* 2007; 352:283-291.
354. Lamminen T, Majander A, Juvonen V, et al. A mitochondrial mutation at nt 9101 in the ATP synthase 6 gene associated with deficient oxidative phosphorylation in a family with Leber hereditary optic neuroretinopathy. *Am J Hum Genet.* 1995; 56:1238-1240.
355. Diehl GE, Wilmes E. Etiology and clinical aspects of palatal myoclonus. *Laryngorhinootologie* 1990;69:369-372.
-

- 
356. Paulus W, Straube A, Bauer W, Harding AE. Central nervous system involvement in Leber's optic neuropathy. *J Neurol* 1993;240:251-253.
357. Carelli V, Valentino ML, Liguori R, et al. Leber's hereditary optic neuropathy (LHON/11778) with myoclonus: report of two cases. *J Neurol Neurosurg Psychiatry* 2001;71:813-816.
358. Wallace DC. A new manifestation of Leber's disease and a new explanation for the agency responsible for its unusual pattern of inheritance. *Brain* 1970;93:121-132.
359. Barrientos A, Casademont J, Cardellach F, et al. Reduced steady-state levels of mitochondrial RNA and increased mitochondrial DNA amount in human brain with aging. *Brain Res Mol Brain Res*. 1997; 52:284-289.
360. Lee HC, Lu CY, Fahn HJ, et al. Aging- and smoking-associated alteration in the relative content of mitochondrial DNA in human lung. *FEBS Lett*. 1998; 441:292-296.
361. Pesce V, Cormio A, Fracasso F, et al. Age-related mitochondrial genotypic and phenotypic alterations in human skeletal muscle. *Free Radic Biol Med*. 2001; 30:1223-1233.
362. Lezza AM, Pesce V, Cormio A, et al. Increased expression of mitochondrial transcription factor A and nuclear respiratory factor-1 in skeletal muscle from aged human subjects. *FEBS Lett*. 2001;501:74-78.
363. Liu CS, Cheng WL, Lee CF, et al. Alteration in the copy number of mitochondrial DNA in leukocytes of patients with mitochondrial encephalomyopathies. *Acta Neurol Scand*. 2006; 113:334-341.
364. Pulkes T, Eunson L, Patterson V, et al. The mitochondrial DNA G13513A transition in ND5 is associated with a LHON/MELAS overlap syndrome and may be a frequent cause of MELAS. *Ann Neurol*. 1999; 46:916-919.
365. Carelli V, Barboni P, Zacchini A, et al. Leber's Hereditary Optic Neuropathy (LHON) with 14484/ND6 mutation in a North African patient. *J Neurol Sci*. 1998; 160:183-188.
366. Yen MY, Lee HC, Liu JH, et al. Compensatory elevation of complex II activity in Leber's hereditary optic neuropathy. *Br J Ophthalmol*. 1996; 80:78-81.
367. Yen MY, Chen CS, Wang AG, et al. Increase of mitochondrial DNA in blood cells of patients with Leber's hereditary optic neuropathy with 11778 mutation. *Br J Ophthalmol*. 2002; 86:1027-1030.
368. Nishioka T, Soemantri A, Ishida T. mtDNA/nDNA ratio in 14484 LHON mitochondrial mutation carriers. *J Hum Genet*. 2004; 49:701-705.
369. Srivastava S, Barrett JN, Moraes CT. PGC-1alpha/beta upregulation is associated with improved oxidative phosphorylation in cells harboring nonsense mtDNA mutations. *Hum Mol Genet*. 2007; 16:993-1005.
370. Rasbach KA, Schnellmann RG. PGC-1alpha over-expression promotes recovery from mitochondrial dysfunction and cell injury. *Biochem Biophys Res Commun*. 2007; 355:734-739.
371. Hondares E, Pineda-Torra I, Iglesias R, et al. PPARdelta, but not PPARalpha, activates PGC-1alpha gene transcription in muscle. *Biochem Biophys Res Commun*. 2007; 354:1021-1027.
-

372. Scatena R, Bottoni P, Martorana GE, et al. Mitochondrial respiratory chain dysfunction, a non-receptor-mediated effect of synthetic PPAR-ligands: biochemical and pharmacological implications. *Biochem Biophys Res Commun.* 2004; 319:967-973.
373. Nadanaciva S, Dykens JA, Bernal A, et al. Mitochondrial impairment by PPAR agonists and statins identified via immunocaptured OXPHOS complex activities and respiration. *Toxicol Appl Pharmacol.* 2007; 223:277-287.
374. Brunmair B, Lest A, Staniek K, et al. Fenofibrate impairs rat mitochondrial function by inhibition of respiratory complex I. *J Pharmacol Exp Ther.* 2004; 311:109-114.
375. Gomes CM, van Paassen H, Romeo S, et al. Multidrug resistance mediated by ABC transporters in osteosarcoma cell lines: mRNA analysis and functional radiotracer studies. *Nucl Med Biol.* 2006; 33:831-840.

## Appendix A – Abbreviations (in alphabetical order)

ADP: adenosine diphosphate	Cyt <i>c</i> : cytochrome <i>c</i>
AIF: apoptosis inducing factor	DGUOK: deoxyguanosine kinase
AMP: adenosine monophosphate	DMEM: Dulbecco's modified Eagle medium
AMP07: average membrane preference	DMSO: dimethyl sulfoxide
AMPK: AMP activated protein kinase	DOA: Dominant Optic Atrophy
ANT: adenosine nucleotide translocator	DRIP: vitamin D receptor interacting proteins
Apaf1: apoptotic protease activating factor 1	Drp1: Dynamin-related protein
ATF2: activating transcription factor 2	EDTA: ethylenediaminetetraacetic acid
ATP: adenosine triphosphate	EGTA: ethylene glycol tetraacetic acid
B17.2L: NDUFA assembly factor 2	ER: estrogen receptor
BAT: brown adipose tissue	ERR: estrogen related receptor
Bcl-2: B cell lymphoma 2	ERRE: Estrogen related response element
BF: bezafibrate	FADH <sub>2</sub> : reduced <i>flavin</i> adenine dinucleotide
BH: Bcl-2 homology	FAK: focal adhesion kinase
BIR: baculovirus inhibitor repeats	FBS: Fetal bovine serum
BSA: bovine serum albumin	FMN: flavin mononucleotide
CAD/DFP: caspase activated DNase/DNA fragmentation factor	FoxO: forkhead box O
CamK: Ca <sup>2+</sup> /calmodulin dependent protein kinase	Fzo1p: fuzzy onion 1
CARD: caspase recruitment <i>domains</i>	GPx: glutathione peroxidase
CBP: CREB binding protein	HAT: histone acetyl transferase
cGMP: cyclic guanosine monophosphate	hFis1: human Fis
CMT2A: Charcot-Marie-Tooth type 2A	HMG: high mobility group
CoQ: coenzyme Q	HMM: Hidden Markov Models
CoQH <sub>2</sub> : reduced coenzyme Q	HNF4: hepatocyte nuclear factor 4
CPEO: Chronic Progressive External Ophthalmoplegia	IAP: inhibitors of apoptosis protein
CREB: cAMP response element binding protein	ICAD: inhibitor of caspase activated DNase
Cyt <i>b</i> : cytochrome <i>b</i>	IMM: inner mitochondrial membrane
	KSS: Kearns Sayre Syndrome
	LHON: Leber's hereditary optic neuropathy
	LRPPRC: Leucine-rich PPR-motif containing protein

---

MAC: mitochondrial apoptosis induced channel	NDUFA: NADH dehydrogenase (ubiquinone) 1 $\alpha$ subcomplex
MEF2: myocyte enhancer factor 2	NDUFB: NADH dehydrogenase (ubiquinone) 1 $\beta$ subcomplex
MELAS: Mitochondrial Encephalomyopathy Lactic Acidosis and Stroke-like episodes	NDUFS: NADH dehydrogenase (ubiquinone) Fe-S protein
MERRF: Myoclonus, Epilepsy and Ragged-Red Fibers	NDUFV: NADH dehydrogenase (ubiquinone) flavoprotein
Mfn1: mitofusin 1	NFL: Nerve Fiber Layer
Mfn2: mitofusin 2	NN: neural network
Mgm1p: mitochondrial genome maintenance	NRF: nuclear respiratory factor
MILS: Maternally Inherited Leigh Syndrome	Omi/HtrA2: HtrA serine peptidase 2
MNGIE: Mitochondrial NeuroGastroIntestinal Encephalomyopathy	OMM: outer mitochondrial membrane
MnSOD: Mn superoxide dismutase	Opa1: optic atrophy 1
MPH: membrane propensity for haemoproteins	OXPPOS: Oxidative Phosphorylation
MRI: Magnetic Resonance imaging	PBS: Phosphate buffered saline
MRS: Magnetic Resonance Spectroscopy	PCD: programmed cell death
MST1: mammalian sterile-20	PDCH: pyruvate dehydrogenase complex
MT: microtubules	PGC-1: peroxisome proliferator associated receptor $\gamma$ coactivator 1
mtDNA: mitochondrial DNA	PKA: protein kinase A
mTERF: mitochondrial termination factor	PMSF: phenyl methyl sulphonyl fluoride
mtRPOL: mitochondrial RNA polymerase	Poly: polymerase $\gamma$
mtSSB: mitochondrial single-stranded DNA binding protein	PPAR: peroxisome proliferator associated receptor
Myb: v-myb myeloblastosis viral oncogene homolog	PPRE: peroxisome proliferator associated receptor response element
NAD <sup>+</sup> : nicotinamide adenine dinucleotide	PRC: PGC-1 related coactivator
NADH: reduced nicotinamide adenine dinucleotide	PS: Pearson Syndrome
NARP: Neuropathy, ataxia, retinitis pigmentosa	PSIC: Position specific independent counts
nDNA: nuclear DNA	PTP: Permeability Transition Pore
	RAO-AR: Rao Argos
	rCRS: revised Cambridge reference sequence

---

RFLP: Restriction fragment length polymorphism	TRAIL: TNF related apoptosis inducing ligand
RGCs: Retinal Ganglion Cells	TRAP: TR-associated proteins
RMM: RNA recognition domain	TZD: thiazolidinedione
ROS: reactive oxygen species	UCP: uncoupling protein
RRF: Ragged Red Fiber	VEGF: vascular endothelial growth factor
RRM2B: ribonucleotide reductase M2 B (TP53 inducible)	YY1: YingYang1
RS: serine-arginine-rich domain	
RXR: retinoid acid X receptor	
SANDO: Sensory-Ataxia Neuropathy, Dysarthria and Ophthalmoplegia	
SC35: splicing component 35kDa	
SDH: succinyl dehydrogenase	
SDS: sodium dodecyl sulphate	
SOX9: sex determining region Y box 9	
SRB: sulforodhamine B	
SRBP1: sterol regulatory element binding protein	
SRC-1: steroid receptor coactivator 1	
SRp:Ser/Arg protein	
SUCLA2: succinylCoA synthetase	
TCA: trichloroacetic acid	
Tfam: mitochondrial transcription factor A	
TFB1M: mitochondrial transcription factor B1	
TFB2M: mitochondrial transcription factor B2	
TK2: Thymidine Kinase 2	
TMH: transmembrane helix	
TNF: tumor necrosis factor	
TP: thymidine phosphorylase	

**Appendix B – Primers sequences and PCR conditions**

LHON 11778		
Fw: 5'-GAATGTAGGAGTAATGATAAG-3'	Rv: 5'-ATTATCGAAAACTACTGAAC-3'	
1 cycle	25 cycles	1 cycle
94°C x 5'	94°C x 30" 55°C x 60" 72°C x 2'30"	72°C x 7'

LHON 14484		
Fw: 5'-ATCATATAGGTTTCTGTTGGT-3'	Rv: 5'-GGGACTGGGGGTACGGAGTC-3'	
1 cycle	25 cycles	1 cycle
94°C x 5'	94°C x 30" 49°C x 60" 72°C x 2'30"	72°C x 7'

LHON 3460		
Fw: 5'-AAGTGTTTCGCGGAAGGGGG-3'	Rv: 5'-GAGTAACATGGGTAAGATTA-3'	
1 cycle	30 cycles	1 cycle
94°C x 5'	94°C x 30" 55°C x 30" 72°C x 2'30"	72°C x 7'

LHON 14495		
Fw: 5'-AGTATATCCAAAGACAACCATCATCCCCAT-3'	Rv: 5'-ATGGGGGTTTAGTATTGATTGTTAGCGGTG-3'	
1 cycle	25 cycles	1 cycle
94°C x 5'	94°C x 30" 56°C x 30" 72°C x 30"	72°C x 7'

LHON 14459		
Fw: 5'-ATGCCTCAGGATACTCCTCAATAGCCGTC-3'	Rv: 5'-ATGGGGGTTTAGTATTGATTGTTAGCGGTG -3'	
1 cycle	25 cycles	1 cycle
94°C x 5'	94°C x 30" 56°C x 30" 72°C x 30"	72°C x 7'

LHON 3700		
Fw: 5'-TGAAGCCTGAGACTAGTTCGG-3'	Rv: 5'-ACTACAACCCTTCGCTGACG-3'	
1 cycle	32 cycles	1 cycle
96°C x 1'	94°C x 15" 56°C x 30" 72°C x 15"	72°C x 7'

LHON 14568		
Fw: 5'-CAAGACCTCAACCCCTGA-3'	Rv: 5'-CATTGGTCGTGGTTGTAGTCCGTGC-3'	
1 cycle	25 cycles	1 cycle
94°C x 5'	94°C x 30" 55°C x 60" 72°C x 2'30"	72°C x 7'

Candidate pathogenic mutation 14528		
Fw: 5'-CCTACTCCTAATCACATAACCTA-3'	Rv: 5'-CATTGGTCGTGGTTGTAGTCCGTGC-3'	
1 cycle	25 cycles	1 cycle
95°C x 5'	94°C x 30" 59°C x 60" 72°C x 2'30"	72°C x 7'

Candidate pathogenic mutation 4172		
Fw: 5'-ACGACCAACTCATACACCTG-3'	Rv: 5'-TTACTCTATCAAAGTAACTCT -3'	
1 cycle	25 cycles	1 cycle
94°C x 5'	94°C x 30" 56°C x 60" 72°C x 2'30"	72°C x 7'

mtDNA polymorphism 4136		
Fw: 5'-CCTGAACTCTACACAACA-3'	Rv: 5'-TTACTCTATCAAAGTAACTCT-3'	
1 cycle	25 cycles	1 cycle
94°C x 5'	94°C x 30" 56°C x 60" 72°C x 2'30"	72°C x 7'

mtDNA polymorphism 9319		
Fw: 5'-GCCTAACCGCTAACATTACT-3'	Rv: 5'-CTGGAGTGGTAAAAGGCTCA-3'	
1 cycle	25 cycles	1 cycle
94°C x 5'	94°C x 30" 56°C x 60" 72°C x 2'30"	72°C x 7'

mtDNA polymorphism 15773		
Fw: 5'-CAGAATAATAACACACCCGA-3'	Rv: 5'-GGAGTTGCAGTTGATGTGTG-3'	
1 cycle	25 cycles	1 cycle
94°C x 5'	94°C x 30" 56°C x 60" 72°C x 2'30"	72°C x 7'

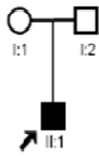
PGC-1 $\alpha$ polymorphism 1444		
Fw: 5'-TGCTACCTGAGAGAGACTTTG-3'	Rv: 5'-CTTTCATCTTCGCTGTCATC-3'	
1 cycle	30 cycles	1 cycle
94°C x 5'	94°C x 60" 60°C x 60" 72°C x 60"	72°C x 10'

Real Time PCR assays		
PGC-1 $\alpha$	Fw: 5'-ACACAGTCGCAGTCACAACAC-3'	Rv: 5'-GGAGTGGTGGGTGGAGTTAGG-3'
PGC-1 $\beta$	Fw: 5'-CAGACAGAACGCCAAGCATC-3'	Rv: 5'-TCGCACTCCTCAATCTCACC-3'
PRC	Fw: 5'-CAAGCAGAAACAGAAGAGAGAAG-3'	Rv: 5'-GGTGGGATGACAAGACAAGG-3'
Tfam	Fw: 5'-AACAACGAAAATATGGTGCTGAGG-3'	Rv: 5'-CAAGTATTATGCTGGCAGAAGTCC-3'
Actin B	Fw: 5'-ACTATGACTTAGTTGCGTTACCA -3'	Rv: 5'-GCCATGCCAATCTCATCTTG -3'
PREINCUBATION	AMPLIFICATION	MELTING CURVE
1 cycle	45 cycles	1 cycle
95°C x 10'	95°C x 30" 56°C x 20" 72°C x 25" Acquisition of fluorescence signal	95°C x 5' 65°C x 1' 65°C - 97°C (ramp rate 0.11°C/s) Acquisition of fluorescence in continuous

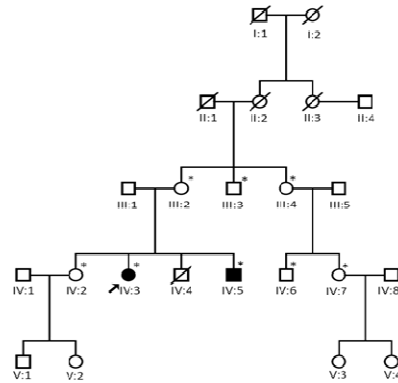
## Appendix C – Family trees of the investigated pedigrees

### 1. Rare LHON mutations pedigrees

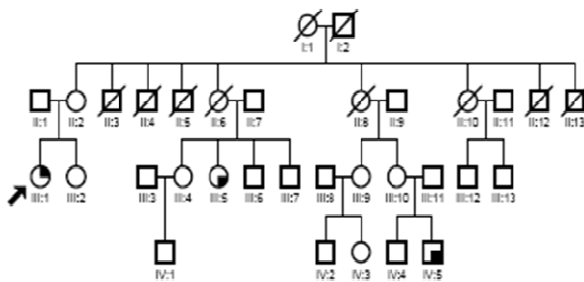
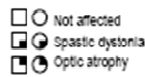
**Family 1 – Italy**  
**LBPV28 – G3700A/ND1**  
**Haplogroup H**



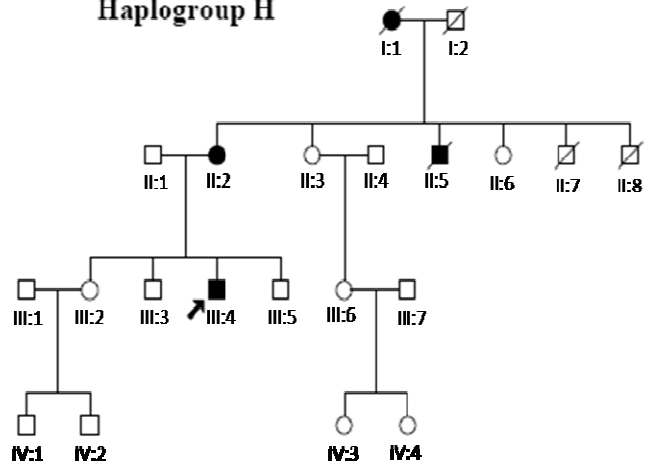
**Family 2 – Italy**  
**LBPV30bis – C14568T/ND6**  
**Haplogroup U6a (T4172A/ND1)**



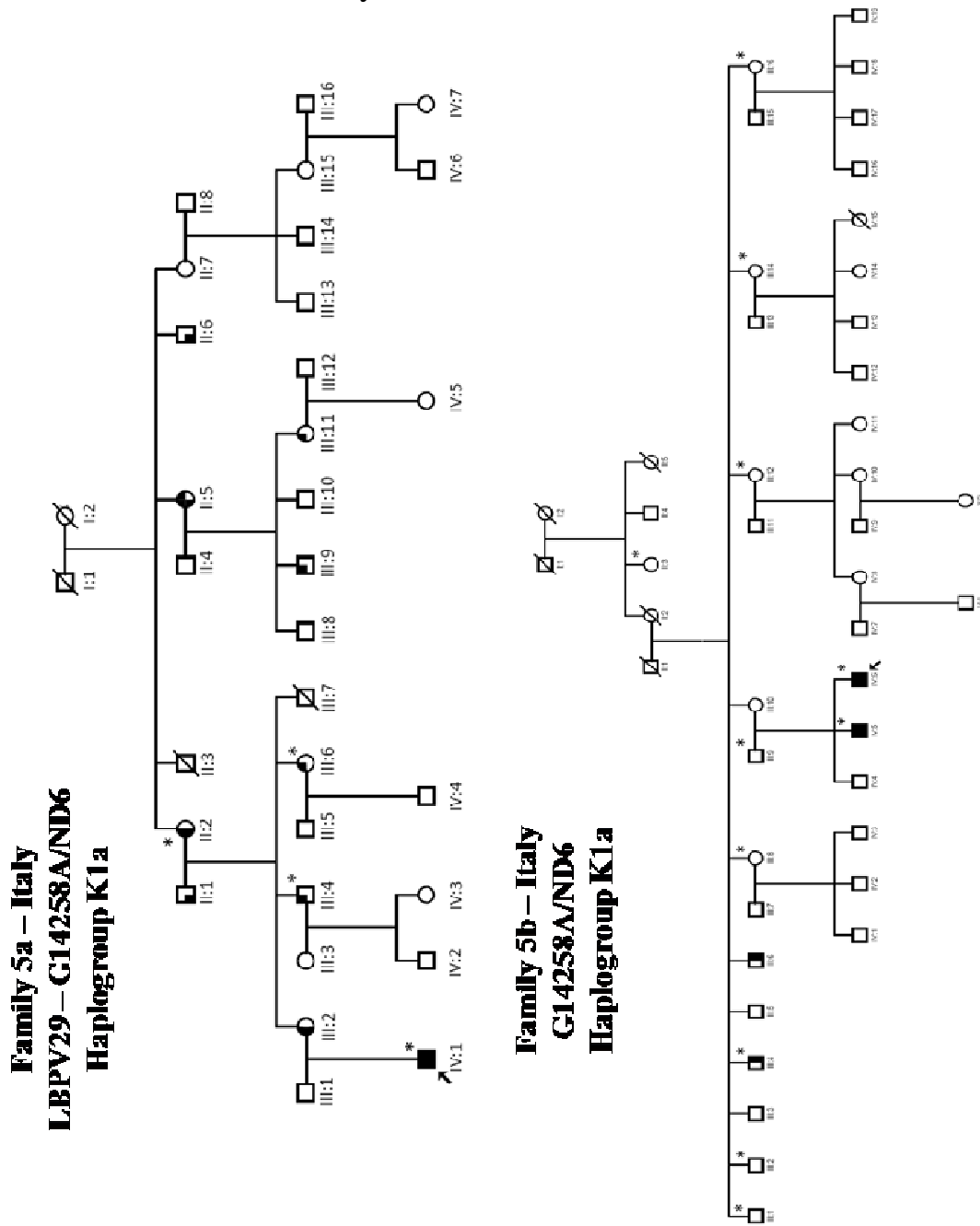
**Family 3 – Italy**  
**LBPV46 – G14459A/ND6**  
**Haplogroup J1c**



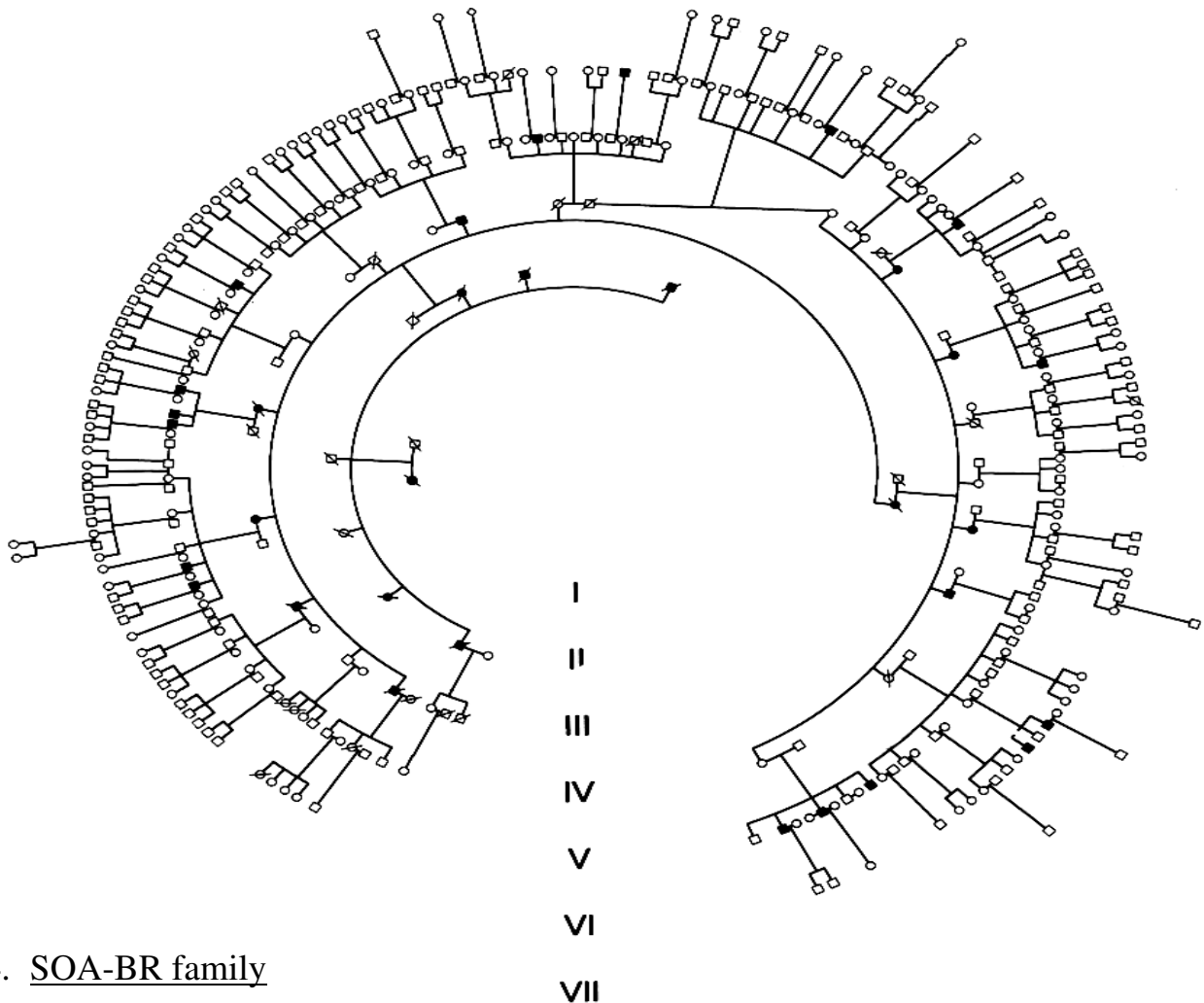
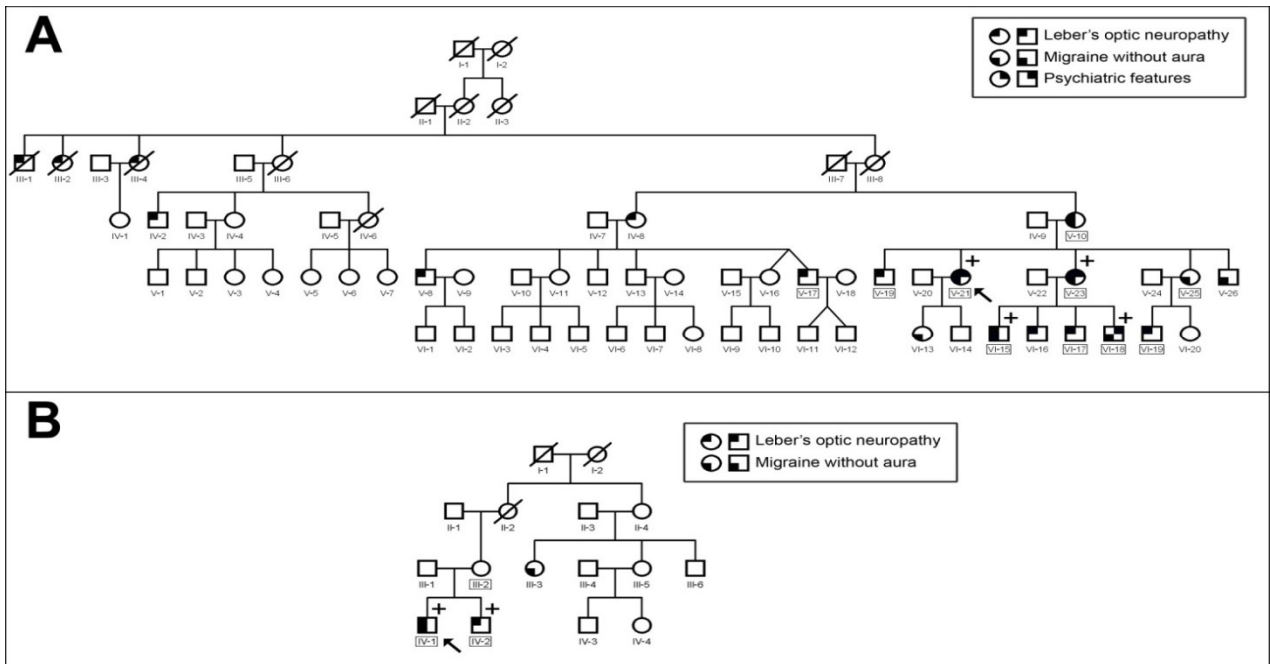
**Family 4 – Italy**  
**LBPV36 – A14495G/ND6**  
**Haplogroup H**



2. Novel LHON mutations family



### 3. Myoclonic Italian LHON pedigrees



### 4. SOA-BR family

## Appendix D – Raw data from complete mtDNA sequencing

<b>Family 1 - Haplogroup H</b>				
<b>Position</b>	<b>Map Locus</b>	<b>Nucleotide change relative to rCRS</b>	<b>Amino acid change</b>	<b>Notes</b>
150	D-loop	C to T	-	
263	D-loop	A to G	-	
315+C	D-loop	Insertion C	-	
750	12S rRNA	A to G	-	
1438	12S rRNA	A to G	-	
3107d	16S rRNA	Deletion C	-	
<b>3700</b>	<b>ND1</b>	<b>G to A</b>	<b>Ala to Thr</b>	
4769	ND2	A to G	Synonym	
8856	ATPase6	G to A	Synonym	
8860	ATPase6	A to G	Thr to Ala	+8858HhaI
13759	ND5	G to A	Ala to Thr	
15326	Cyt b	A to G	Thr to Ala	
16192	D-loop	C to T	-	
16261	D-loop	C to T	-	
16289	D-loop	A to G	-	
16519	D-loop	T to C	-	

<b>Family 2 - Haplogroup U6a</b>				
<b>Position</b>	<b>Locus</b>	<b>Nucleotide change relative to rCRS</b>	<b>Amino acid change</b>	<b>Notes</b>
73	D-loop	A to G	-	
263	D-loop	A to G	-	
309+C	D-loop	Insertion C	-	
315+C	D-loop	Insertion C	-	
523+CA	D-loop	Insertion CA	-	
750	12S rRNA	A to G	-	
1438	12S rRNA	A to G	-	
2706	16S rRNA	A to G	-	
3107d	16S rRNA	Deletion C	-	
3348	ND1	A to G	Synonym	
3369	ND1	G to A	Synonym	
<u>4172A</u>	<u>ND1</u>	<u>T to A Transversion</u>	Leu to Gln	
4769	ND2	A to G	Synonym	
7028	COI	C to T	Synonym	
7805	COII	G to A	Val to Ile	
8860	ATPase6	A to G	Thr to Ala	+8858HhaI
11467	ND4	A to G	Synonym	-11465MseI
11719	ND4	G to A	Synonym	-11718HaeIII
11722	ND4	T to C	Synonym	
11938	ND4	C to T	Synonym	
12308	tRNA Leu2	A to G	-	
12372	ND5	G to A	Synonym	
14179	ND6	A to G	Synonym	
<b>14568</b>	<b>ND6</b>	<b>C to T</b>	<b>Gly to Ser</b>	<b>heteroplasmic</b>
14766	Cyt b	C to T	Thr to Ile	+14766MseI
14926	Cytb	A to G	Synonym	
15221	Cytb	G to A	Asp to Asn	
15326	Cyt b	A to G	Thr to Ala	
16172	D-loop	C to T	-	
<u>16183C</u>	<u>D-loop</u>	<u>A to C Transversion</u>	-	
16189	D-loop	T to C	-	
16219	D-loop	A to G	-	

<b>Family 2 - Haplogroup U6a</b>				<b>(continue)</b>
<b>Position</b>	<b>Locus</b>	<b>Nucleotide change relative to rCRS</b>	<b>Amino acid change</b>	<b>Notes</b>
16239	D-loop	C to T	-	
16278	D-loop	C to T	-	

<b>Family 3 - Haplogroup J1c</b>				
<b>Position</b>	<b>Map Locus</b>	<b>Nucleotide change relative to rCRS</b>	<b>Amino acid change</b>	<b>Notes</b>
73	D-loop	A to G	-	
185	D-loop	G to A	-	
189	D-loop	A to G	-	
228	D-loop	G to A	-	
263	D-loop	A to G	-	
295	D-loop	C to T	-	
315+C	D-loop	Insertion C	-	
462	D-loop	C to T	-	
489	D-loop	T to C	-	
750	12S rRNA	A to G	-	
1438	12S rRNA	A to G	-	
2706	16S rRNA	A to G	-	
3010	16S rRNA	G to A	-	
3107d	16S rRNA	Deletion C	-	
4216	ND1	T to C	Tyr to His	+4216NlaIII
4769	ND2	A to G	Synonym	
7028	COI	C to T	Synonym	
8860	ATPase6	A to G	Thr to Ala	
10398	ND3	A to G	Thr to Ala	+10394Ddel
11251	ND4	A to G	Synonym	-11251Tsp509I
11719	ND4	G to A	Synonym	
12612	ND5	A to G	Synonym	
13708	ND5	G to A	Ala to Thr	-13704BstOI
13934	ND5	C to T	Thr to Met	
<b>14459</b>	<b>ND6</b>	<b>G to A</b>	<b>Ala to Thr</b>	
14766	Cyt b	C to T	Ile to Thr	
14798	Cyt b	T to C	Phe to Leu	
15326	Cyt b	A to G	Thr to Ala	
<u>15452A</u>	<u>Cyt b</u>	<u>C to A Transversion</u>	<u>Leu to Ile</u>	
16069	D-loop	C to T	-	
16114	D-loop	C to T	-	
16126	D-loop	T to C	-	

<b>Family 4 - Haplogroup H</b>				
<b>Position</b>	<b>Map Locus</b>	<b>Nucleotide change relative to rCRS</b>	<b>Amino acid change</b>	<b>Notes</b>
195	D-loop	T to C	-	
263	D-loop	A to G	-	
315+C	D-loop	Insertion C	-	
750	12S rRNA	A to G	-	
1438	12S rRNA	A to G	-	
2060	16S rRNA	A to G	-	
3107d	16S rRNA	Deletion C	-	
4769	ND2	A to G	Synonym	
7337	COI	G to A	Synonym	
8860	ATPase6	A to G	Thr to Ala	
<b>14495</b>	<b>ND6</b>	<b>A to G</b>	<b>Leu to Ser</b>	
15326	Cyt b	A to G	Thr to Ala	
16129	D-loop	G to A	-	
16248	D-loop	C to T	-	

<b>Family 5 – Haplogroup K1a</b>				
<b>Position</b>	<b>Map Locus</b>	<b>Nucleotide change relative to rCRS</b>	<b>Amino acid change</b>	<b>Notes</b>
73	D-loop	A to G	-	
263	D-loop	A to G	-	
315+C	D-loop	Insertion C	-	
497	D-loop	C to T	-	
750	12S rRNA	A to G	-	
1189	12S rRNA	T to C		
1438	12S rRNA	A to G	-	
1811	16S rRNA	A to G	-	
2281	16S rRNA	A to G	-	
2706	16S rRNA	A to G	-	
3107d	16S rRNA	Deletion C	-	
3480	ND1	A to G	Synonym	
4769	ND2	A to G	Synonym	
6137	COI	T to C	Synonym	
6329	COI	C to T	Synonym	
7028	COI	C to T	Synonym	+7025AluI
8860	ATPase6	A to G	Thr to Ala	+8858HhaI
<b>8944</b>	<b>ATPase6</b>	<b>A to G</b>	<b>Met to Val</b>	
9055	ATPase6	G to A	Ala to Thr	
9698	COIII	T to C	Synonym	
10398	ND3	A to G	Thr to Ala	
10550	ND4L	A to G	Synonym	
11038	ND4	A to G	Synonym	
11299	ND4	T to C	Synonym	
11467	ND4	A to G	Synonym	-11465MseI
11719	ND4	G to A	Synonym	-11718HaeIII
12308	tRNA Leu2	A to G	-	+12308Hinfl
12372	ND5	G to A	Synonym	
14167	ND6	C to T	Synonym	
<b>14258</b>	<b>ND6</b>	<b>G to A</b>	<b>Pro to Leu</b>	
14582	ND6	A to G	Val to Ala	
14766	Cyt b	C to T	Thr to Ile	+14766MseI
14798	Cyt b	T to C	Phe to Leu	
15253	Cyt b	A to G	Synonym	
15326	Cyt b	A to G	Thr to Ala	
16129	D-loop	G to A	-	
16224	D-loop	T to C	-	
16311	D-loop	T to C	-	
16519	D-loop	T to C	-	

<b>Family A – Haplogroup T2</b>				
<b>Position</b>	<b>Map Locus</b>	<b>Nucleotide change relative to rCRS</b>	<b>Amino acid change</b>	<b>Notes</b>
73	D-loop	A to G	-	
150	D-loop	C to T	-	
263	D-loop	A to G	-	
309+C	D-loop	Insertion C	-	
315+C	D-loop	Insertion C	-	
523+CA	D-loop	Insertion CA	-	
709	12S rRNA	G to A	-	
750	12S rRNA	A to G	-	
1438	12S rRNA	A to G	-	
1888	16S rRNA	G to A	-	

<b>Family A – Haplogroup T2</b>				<b>(continue)</b>
<b>Position</b>	<b>Map Locus</b>	<b>Nucleotide change relative to rCRS</b>	<b>Amino acid change</b>	<b>Notes</b>
2706	16S rRNA	A to G	-	
3107d	16S rRNA	Deletion C	-	
4136	ND1	A to G	Tyr to Cys	
4216	ND1	T to C	Tyr to His	+4216NlaIII
4769	ND2	A to G	Synonym	
4917	ND2	A to G	Asn to Asp	+4917Bfal
6026	COI	G to A	Synonym	
7028	COI	C to T	Synonym	+7025AluI
8222	COII	T to C	Synonym	
8697	ATPase6	G to A	Synonym	
8860	ATPase6	A to G	Thr to Ala	+8858HhaI
9139	ATPase6	G to A	Ala to Thr	
10463	tRNA Arg	T to C	-	
11251	ND4	A to G	Synonym	-11251Tsp509I
11719	ND4	G to A	Synonym	-11718HaeIII
<b>11778</b>	<b>ND4</b>	<b>G to A</b>	<b>Arg to His</b>	
11812	ND4	A to G	Synonym	
13368	ND5	G to A	Synonym	-11718HaeIII
14233	ND6	T to C	Synonym	-11718HaeIII
14766	Cyt b	C to T	Thr to Ile	+14766MseI
14905	Cyt b	G to A	Synonym	
15326	Cyt b	A to G	Thr to Ala	
15452A	Cyt b	C to A Transversion	Leu to Ile	
15607	Cyt b	A to G	Synonym	+15606AluI
15928	tRNA Thr	G to A	-	-15925MspI
16126	D-loop	T to C	-	
16153	D-loop	G to A	-	
16293	D-loop	A to G	-	
16294	D-loop	C to T	-	
16296	D-loop	C to T	-	

<b>Family B – Haplogroup U4a</b>				
<b>Position</b>	<b>Map Locus</b>	<b>Nucleotide change relative to rCRS</b>	<b>Amino acid change</b>	<b>Notes</b>
73	D-loop	A to G	-	
195	D-loop	T to C	-	
247	D-loop	G to A	-	
263	D-loop	A to G	-	
309+C	D-loop	Insertion C	-	
315+C	D-loop	Insertion C	-	
499	D-loop	G to A	-	
523+4CA	D-loop	insertion CACACACA	-	
750	12S rRNA	A to G	-	
801	12S rRNA	A to G		
1438	12S rRNA	A to G	-	
1811	16S rRNA	A to G	-	
2706	16S rRNA	A to G	-	
2792	16S rRNA	A to G	-	
3107d	16S rRNA	Deletion C	-	
<b>3460</b>	<b>ND1</b>	<b>G to A</b>	<b>Ala to Thr</b>	
4646	ND2	T to C	Synonym	
4769	ND2	A to G	Synonym	
5999	COI	T to C	Synonym	
6047	COI	A to G	Synonym	
6665	COI	C to T	Synonym	
6929	COI	A to G	Synonym	
7028	COI	C to T	Synonym	+7025AluI
8065	COII	G to A	Synonym	

<b>Family B – Haplogroup U4a</b>				<b>(continue)</b>
<b>Position</b>	<b>Map Locus</b>	<b>Nucleotide change relative to rCRS</b>	<b>Amino acid change</b>	<b>Notes</b>
8818	ATPase6	C to T	Synonym	
8860	ATPase6	A to G	Thr to Ala	+8858HhaI
11332	ND4	C to T	Synonym	
11467	ND4	A to G	Synonym	-11465MseI
11719	ND4	G to A	Synonym	-11718HaeIII
12308	tRNA Leu2	A to G	-	+12308HinfI
12372	ND5	G to A	Synonym	
14620	ND6	C to T	Synonym	
14766	Cyt b	C to T	Thr to Ile	+14766MseI
15326	Cyt b	A to G	Thr to Ala	
15693	Cyt b	T to C	Met to Thr	
15773	<i>Cytb</i>	<i>G to A</i>	<i>Val to Ala</i>	
16356	D-loop	T to C	-	
16362	D-loop	T to C	-	
16519	D-loop	T to C	-	

## **Candidate's publications 2005-2009**

do V F Ramos C, Bellusci C, Savini G, et al. Optic disc size is associated with development and prognosis of Leber's hereditary optic neuropathy. *Invest Ophthalmol Vis Sci*. 2008 Dec 20. (Epub ahead of print)

Gasparre G, Iommarini L, Porcelli AM, et al. An inherited mitochondrial DNA disruptive mutation shifts to homoplasmy in oncocytic tumor cells. *Hum Mutat*. 2009; 30:391-396.

Porcelli AM, Ghelli A, Iommarini L, et al. The antioxidant function of Bcl-2 preserves cytoskeletal stability of cells with defective respiratory complex I. *Cell Mol Life Sci*. 2008; 65:2943-2951.

La Morgia C, Achilli A, Iommarini L, et al. Rare mtDNA variants in Leber hereditary optic neuropathy families with recurrence of myoclonus. *Neurology*. 2008; 70:762-770.

Amati-Bonneau P, Valentino ML, Reynier P, et al. OPA1 mutations induce mitochondrial DNA instability and optic atrophy 'plus' phenotypes. *Brain*. 2008; 131:338-351.

Gasparre G, Porcelli AM, Bonora E, et al. Disruptive mitochondrial DNA mutations in complex I subunits are markers of oncocytic phenotype in thyroid tumors. *Proc Natl Acad Sci USA*. 2007; 104:9001-9006.

Carelli V, La Morgia C, Iommarini L, et al. Mitochondrial optic neuropathies: how two genomes may kill the same cell type? *Biosci Rep*. 2007; 27:173-184. Review.

### **In press or in preparation**

Srivastava S, Diaz F, Iommarini L, et al. PGC-1 $\alpha/\beta$  induced expression partially compensates for respiratory chain defects in cells from patients with mitochondrial disorders. (accepted *Human Molecular Genetics*)

Iommarini L, Valentino ML, Giordano C, et al. Mitochondrial DNA content in optic mitochondriopathies. (manuscript in preparation)

Iommarini L, Martelli PL, Ghelli A, et al. Modelling ND subunits of complex I: pathogenic mutation and non synonymous population variants in genotype-phenotype correlation. (manuscript in preparation)

Amati-Bonneau P, Achilli A, Reynier P, et al. Rare mtDNA point mutations pathogenic for Leber's hereditary optic neuropathy. (manuscript in preparation)

## Acknowledgements

This work has been supported by IRCCS Foundation “GB Bietti” for the study and the research in ophthalmology, Roma, and Programma Marco Polo, University of Bologna.

Thanks to

Prof. Michela Rugolo and Dr. Anna Maria Ghelli, Department of Evolutionistic Experimental Biology, University of Bologna, Italy

Dr. Valerio Carelli and Dr. Alessandra Maresca, Department of Neurological Sciences, University of Bologna, Italy

Prof. Carlos T. Moraes, Prof. Francisca Diaz, Dr. Tina Wenz and Dr. Alessandra Torraco, Department of Neurology, Miller School of Medicine, University of Miami, Miami, FL

Prof. Giulia d’Amati, Dr. Carla Giordano and Mariangela Sebastiani, Department of Experimental Medicine, University La Sapienza, Roma, Italy

Prof. Antonio Torroni and Dr. Alessandro Achilli, Department of Genetics and Microbiology, University of Pavia, Italy

E in via non ufficiale grazie mille a tutti voi...

...Andrea, mamma, papa', Silvia, Leo, Ale, Lucia, Anna, Anna Maria, Giuseppe, Claudia, Sara, Maria Antonietta, Robi, Youry, Alessandra, Panchi, Tinita, Sofia, Giorgia e Roberta.

Spero di non aver dimenticato nessuno.